

MICROWAVE ELECTRONICS

**APPLICATIONS OF FRACTAL BASED
STRUCTURES IN RADAR CROSS SECTION
REDUCTION**

A thesis submitted in partial fulfilment of the
requirements for the degree of
DOCTOR OF PHILOSOPHY

by

ANUPAM R. CHANDRAN

**Centre for Research in Electromagnetics and Antennas
Department of Electronics
Cochin University of Science and Technology
Cochin 682 022
India**

June 2007

*Dedicated
to
my parents*

CERTIFICATE

This is to certify that the thesis entitled "**Applications of Fractal Based Structures in Radar Cross Section Reduction**" is a bona fide record of the research work carried out by Mr. Anupam R. Chandran under my supervision in Department of Electronics, Cochin University of Science and Technology, India. The results embodied in this thesis or parts of it have not been presented for any other degree.

Cochin-22
28th JUNE 2007



Dr. C. K. Aanandan
(Supervising Guide)
Reader
Department of Electronics
Cochin University of Science & Technology
Cochin - 22

DECLARATION

I hereby declare that the work presented in this thesis entitled "**Applications of Fractal Based Structures in Radar Cross Section Reduction**" is based on the original work done by me under the supervision of Dr. C. K. Aanandan in the Department of Electronics, Cochin University of Science and Technology, India and that no part thereof has been presented for the award of any other degree.

Cochin-22
30th June 2007



Anupam R. Chandran

ACKNOWLEDGEMENT

I would like to express my deepest sense of gratitude to my supervising guide Dr. C.K. Aanandan, Reader, Department of Electronics, Cochin University of Science And Technology, for his excellent guidance, valuable suggestions and the constant support I received from him. It has been really a great privilege to work under his guidance.

I am extremely grateful to Dr. K. Vasudevan, Professor and Head, Department of Electronics, CUSAT, for his wholehearted support and interest shown in my work.

Let me express my deepest sense of gratitude to Prof. P. Mohanan for his invaluable suggestions and help.

I would like to express sincere thanks to Prof. K.T. Mathew, Prof. P.R.S. Pillai and Dr. Tessama Thomas for their support and co-operation.

I am indebted to Dr. T.K. Mathew for fruitful discussions, invaluable help and advice given to me for the successful completion of my work.

Special thanks are due to my colleague Mr. Gopikrisna for the timely help and co-operation.

It is with great pleasure I thank my colleagues Mr. Rohith K. Raj, Mr. Shynu S.V, now with Dublin Institute of Technology, Ireland, Ms. Deepti Das Krishna, Mr. Manoj Joseph, Ms. Suma MLN, Mr. Deepu V, Mrs. Sreedevi K. Menon, Mr. Gijo Augustin, Ms. Jitha, Ms. Shameena and all the other research scholars of CREMA lab for their valuable help and support.

The encouragement and support received from Mr. A.V. Praveen Kumar, Mr. Robin Augustine, Dr. Jaimon Yohannan, Mr. V. Hamsakutty, Mr. Anil Lonappan and Ms. Ullas of MTMR lab and all the research scholars of the Department of Electronics are gratefully acknowledged.

The encouragement I received from Dr. Joe Jacob, Senior lecturer, Newman College, Thodupuzha, kerala India, is greatly acknowledged.

I owe special thanks to Ms. Annie, Mr. Murali, Mr. Russel, Mr. Rajeev, Mr. Siraj, Mr. Ibrahim Kutty and all the other staff of the Department of Electronics for their whole hearted cooperation

I am also grateful to Mr. Suresh, Librarian, Department of Electronics and Dr. Beena, Librarian, Department of Physics for their help and co-operation.

During the tenure of my research, the research fellowship was supported by Cochin University of Science and Technology through University JRF. The financial support is gratefully acknowledged.

ANUPAM R. CHANDRAN

Contents

Chapter 1

INTRODUCTION	1
1.1 RADAR CROSS SECTION	2
1.2 RCS REDUCTION	5
1.3 FRACTAL	7
1.4 MOTIVATION	14
1.5 OUTLINE OF THE PRESENT WORK	15
1.6 ORGANISATION OF THE THESIS	18

Chapter 2

REVIEW OF THE PAST WORK	21
2.1 RADAR CROSS SECTION STUDIES	23
2.2 FRACTAL ELECTRODYNAMICS	48

Chapter 3

METHODOLOGY	55
3.1. OVERVIEW OF RCS MEASUREMENT SYSTEMS	57
3.2. MAJOR FACILITIES USED IN RCS MEASUREMENTS	59
3.2.1. Anechoic Chamber	59
3.2.2. Network Analyzer	60
3.2.3. Target Positioner And Controller	61
3.3 MEASUREMENT TECHNIQUES	61
3.3.1. Arch Method	63
3.4 DESIGN AND FABRICATION OF FRACTAL BASED METALLO-DIELECTRIC STRUCTURES	64

3.5 FLAT PLATES LOADED WITH METALLO-DIELECTRIC STRUCTURES	65
3.5.1 Metallo-Dielectric Structure Based on Various Iterated Stages of Sierpinski Carpet Fractal Geometry	66
3.5.2 Structures Based on the Third Iterated Stage of Sierpinski Carpet Fractal Geometry with Generators of Different Shapes	68
3.5.3 Sierpinski Gasket Based Metallisation	70
3.5.4 Sierpinski Carpet Fractal Geometries With Varying Lacunarity	71
3.5.5 Effect of Loading Superstrates	73
3.6 3D STRUCTURES	75
3.6.1 Cylinder	75
3.6.2 Dihedral corner reflector	76
3.6.3 Circular cone	77

Chapter 4

EXPERIMENTAL RESULTS	79
4.1 FLAT PLATES LOADED WITH FRACTAL BASED METALLO-DIELECTRIC STRUCTURES	82
4.1.1 Different Iterated Stages of Sierpinski Carpet Fractal Geometry	83
4.1.1 Sierpinski carpet with different patch shapes	89
4.1.2.1 Cross	89
4.1.2.2 Octagonal	91
4.1.2.3 Hexagonal	93
4.1.2.4 Circle	98
4.1.2.5 Diamond	101

4.1.2.6 Purina Square	103
4.1.2.7 Star	105
4.1.2.8 Cross bar fractal tree	108
4.1.2.9 Sierpinski carpet array	110
4.1.3 Sierpinski gasket based metallo-dielectric structure	112
4.2 EFFECT OF LOADING SUPERSTRATES	115
4.2.1 Superstrate loading on Sierpinski carpet fractal geometry	116
4.2.2 Superstrate loading on Sierpinski gasket fractal geometry	118
4.3 FRACTAL GEOMETRIES WITH VARYING LACUNARITY	120
4.4 RCS REDUCTION OF 3D STRUCTURES	125
4.4.1 Metallic Cylinder	125
4.4.2 Dihedral Corner Reflector	134
4.4.3 Circular Cone	163

Chapter 5

SIMULATION STUDIES AND ANALYSIS	167
5.1 BACKSCATTERING CHARACTERISTICS OF STRUCTURES WITH PATCHES OF DIFFERENT SHAPES	169
5.2 SIMULATED RESULTS	171
5.3 RCS ENHANCEMENT OF DIHEDRAL CORNER REFLECTOR	180
5.4 EFFECT OF SUPERSTRATE LOADING	186
5.5 EFFECT OF DIELECTRIC CONSTANT	187

Chapter 6

CONCLUSIONS	189
6.1 INFERENCES FROM EXPERIMENTAL INVESTIGATIONS	191
6.1.1 Fractal Based Metallo-Dielectric Structures Loaded Flat Plate	191

6.1.2 Experiments with 3D structures	193
6.2 CONCLUSIONS FROM SIMULATION STUDIES AND ANALYSIS	195
6.3 SCOPE FOR FURTHER WORK IN THIS FIELD	195
Appendix-1	197
DESIGN OF A BANDPASS FILTER USING CANTOR BAR BASED METALLO-DIELECTRIC STRUCTURE	
Appendix-2	209
DEVELOPMENT OF AN RCS MEASUREMENT FACILITY AND ITS AUTOMATION	
REFERENCES	217
INDEX	239
LIST OF PUBLICATIONS OF THE AUTHOR	242
RESUME OF THE AUTHOR	245

Chapter 1

INTRODUCTION

The history of radar dates back to the experiments of Heinrich Hertz in late 1880s, but the serious development of the radar equipment began in the middle 1930s simultaneously in several countries. The term RADAR stands for Radio Detection and Ranging and is coined during the World War II, when tremendous strides were made both in theory and practice of radar technology. Nowadays, radars are built in a wide range of sophistications, both in military and civilian applications.

Radar detects objects and locates them in range and angle, by transmitting electromagnetic waves of known waveform. These waves are reflected from the objects in space, and a portion of the wave energy comes back towards the radar. The radar reads this returned signal and analyzes it. This signal can be processed to determine many properties of the original object that the wave reflected off. Thus the location of the object (distance and angular position) as well as its velocity can be obtained by analyzing the returning signal.

A functional radar system consists of four basic elements. These are transmitter, antenna, receiver and an indicator. The transmitter produces radio frequency signals which are beamed towards the object using the antenna. The energy intercepted by the object is scattered in all directions. The scattered energy in a particular direction depends on the size, shape and composition of the obstacle as well as the frequency and

polarization of the incident wave. The energy scattered in the direction of the receiver is termed as 'echo' which is collected by the antenna and processed by the receiver. The target information is then displayed on the indicator.

In principle, a radar can operate in any frequency, but due to reasons like propagation effects, availability of components, target scattering characteristics, antenna size and angular resolution requirements, the frequency of operation is limited. Eventhough the electromagnetic spectrum in the frequency range of 3 MHz to 300 GHz is suitable for radar operation, the largest number of operational radars fall within the microwave frequency range.

1.1 RADAR CROSS SECTION

Radar cross section (RCS) is a measure of the target's ability to reflect the radar signals in the direction of the radar receiver. RCS is a characteristic of the particular target and is a measure of its size as seen by the radar. RCS is also a function of frequency, polarization, target configuration and orientation with respect to the incident field. The basis for the design and operation of dynamic RCS test ranges is the radar range equation. The radar range equation shows how the received power is influenced by the RCS of the target and other parameters. The radar equation for free space propagation is given by

$$P_r = \frac{P_t G_t G_r \lambda^2 \sigma}{(4\pi)^3 R^4}$$

Where

P_r = received power

P_t = transmitted power

G_t, G_r = transmitting and receiving antenna gains

λ = operating wavelength

R = range from radar to target

and σ = RCS of the target

The power reflected or scattered by a target is the product of its effective area and the incident power density. In general the 'area' is called scattering cross section of the target. For directions back towards the radar, it is called 'backscattering cross section' or the 'Radar Cross Section'. The scattering cross section is not a constant. It is an angular dependent property of the target. The far field RCS does not vary with changes in range. Although RCS is defined in terms of area, it has no general relationship with the physical area of the object. RCS can be expressed as

$$\sigma = 4\pi \lim_{R \rightarrow \infty} R^2 \frac{|E_s|^2}{|E_i|^2} = 4\pi \lim_{R \rightarrow \infty} R^2 \frac{|H_s|^2}{|H_i|^2}$$

Where E_s and H_s are the scattered electric and magnetic fields and E_i and H_i are the incident electric and magnetic fields respectively. The unit of cross section is usually given in square meters. Due to the large variation in RCS pattern from one aspect angle to another, it is convenient to display the RCS in logarithmic form. The unit commonly used is decibel over a square meter or dBsm i.e.

$$\text{RCS (dBsm)} = 10 \log_{10} \sigma$$

RCS of a target will have a wide variation, if the illuminating electromagnetic wave has got a wide range of frequencies. The variation of RCS with frequency is classified into three regions, depending on the size of the object. In the first region, the target dimensions are small compared to wavelength. This is called the Rayleigh region and RCS is proportional to the fourth power of frequency. In the second region, the target dimensions are approximately equal to the wavelength. This region is known as the resonance region. In the third region, the object dimensions are much larger than the wavelength. This region is called the optical region.

The knowledge of RCS characteristics of some simple targets is very important in RCS measurement and analysis of complex targets. Complex targets such as missiles, ships, aircrafts etc. can be described as collections of relatively simple shapes like spheres, flat plates, cylinders, cones and corner reflectors. In measuring the RCS of complicated objects, the measurements are often calibrated by comparing the echo levels of the test objects with those of the calibration target. As the echo strength of the calibration target must be known with high degree of accuracy, the calibration target is always a simple one.

A practical justification for RCS measurements is that it is an incentive to develop products that satisfy RCS requirements in addition to the more usual requirements of mission, range and payload. RCS measurements are necessary to verify anticipated performance as well as to

evaluate design approaches. In addition, these measurements are important for the evaluation of microwave absorbers.

The instrumentation for the measurement of RCS takes different forms. There are simple systems with continuous wave operation configured from conventional microwave components and standard receivers and transmitters. Modern network analyzers and frequency synthesizers have greatly expanded the RCS measurement facility. The transformation techniques like frequency domain to time domain available in most modern network analyzer systems further increased speed, accuracy and convenience. The study of Radar Cross Section and its reduction is of great importance in modern communication, and defense applications.

1.2 RCS REDUCTION

Reduction of Radar Cross Section is a method for increasing the survivability by reducing the detectability of objects of strategic importance like aeroplanes, rockets, missiles etc. There are four basic methods for reducing the RCS of a target. They are:

- shaping of targets
- use of radar absorbing materials
- passive cancellation
- active cancellation

Each of these techniques adopts different philosophic approaches and exploits different aspects of the encounter between radar and the object.

In the shaping technique, the target surfaces and edges are reoriented or reshaped to deflect the incident wave away from the radar. But this cannot be done for all viewing angles, since a reduction at one viewing angle is usually accompanied by an enhancement at another. For structures such as ships and ground vehicles, internal trihedral and dihedral corners can be avoided by bringing intersecting surfaces together at obtuse or acute angles. The disadvantage of shaping is that it can be made only at the engineering design phase of the target.

Radar absorbing material (RAM) reduces the energy reflected back to the radar by absorbing electromagnetic energy through a kind of Ohmic loss mechanism in which electromagnetic energy is converted to heat energy. At microwave frequencies, the loss is due to the finite conductivity of the material and the friction experienced by the molecules in attempting to follow the alternating fields of an impressed wave. Early absorbers used carbon as the basic material. But they are too bulky and fragile in operational environments. Magnetic absorbers are widely used for operational systems and the loss mechanism is due to a magnetic dipole moment. Magnetic absorbers offer the advantage of compactness even though they are heavy.

The basic concept of passive cancellation (also known as impedance loading) is to introduce an echo source whose amplitude and phase can be

adjusted so as to cancel the activity of another source. However the reduction caused for one frequency rapidly disappears as the frequency is changed. Consequently passive cancellation has been discarded as a useful RCS reduction technique.

In active cancellation method, electromagnetic waves of proper amplitude and phase are emitted from the target so as to cancel the reflected wave. For this, the target must sense the angle of arrival, intensity, frequency and waveform of the incident energy. This method is not widely used because of the complexity of the system design.

RCS reduction involves a lot of compromises, in which advantages are balanced against disadvantages. The requirement for reduced RCS conflicts with the conventional target structures. The final system design is a compromise which increases cost of the overall system. Reduced payload, added weight, and increased maintenance are other penalties of RCS reduction.

Reduction of radar cross section using fractal based structures is discussed in this thesis.

1.3 FRACTAL

Mandelbrot introduced the term 'fractal' (from the Latin *fractus*, meaning 'broken') in 1975, to characterize spatial or temporal phenomena that are continuous but not differentiable. Unlike more familiar Euclidean constructs, every attempt to split a fractal into smaller pieces results in the resolution of more structure.

A fractal is a rough or fragmented geometric shape that can be subdivided in parts, each of which is (at least approximately) a reduced-size copy of the whole. Fractal structures are of infinite complexity with a self-similar nature. What this means is that as the structure is zoomed in upon, the structure repeats. There never is a point where the fundamental building blocks are found. This is because the building blocks themselves have the same form as the original object with infinite complexity in each one. Euclidean structures have whole number dimensions, while fractal structures have fractional dimensions. Fractal geometries have been used previously to characterize unique occurrences in nature that were difficult to define with Euclidean geometries, including the length of coastlines, the density of clouds, and the branching of trees. Therefore, there arose a need for a geometry that handles these complex situations better than Euclidean geometry.

An example of fractal geometry found in nature can be seen in a fern, shown in the figure 1.



Figure 1 Fern, a fractal geometry found in nature

The entire frond has the same structure as each branch. If the individual branches are zoomed in upon, it is quite conceivable to imagine this as a completely separate frond with branches of its own.

Some of the deterministic fractal structures are Sierpinski gasket, Sierpinski carpet, cantor bar etc. For example, a Sierpinski gasket fractal is constructed by taking a filled equilateral triangle as the ‘initiator’ and an operation which excises an inverted equilateral triangle as the ‘generator’ which is the initiator inverted and scaled by one half. Each stage of fractal growth is found by applying the generator, or its scaled replica, to the initiator. The initiator governs the gross shape of the fractal structure while the generator provides the detailed structure and ensures self similarity and long range correlation. Repeated scaling and application of the generator yields a structure as shown in figure 2.

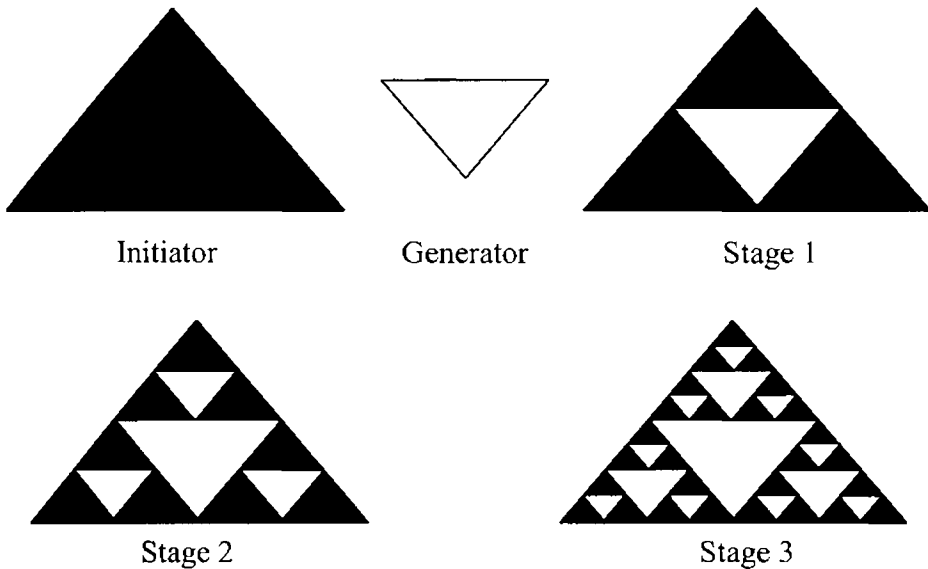


Figure 2 Various iterated stages of Sierpinski gasket fractal geometry

Different iterated stages of Sierpinski carpet are shown in figure 3 which is constructed using generator as a small filled square of size $1/3^{\text{rd}}$ of the initiator.

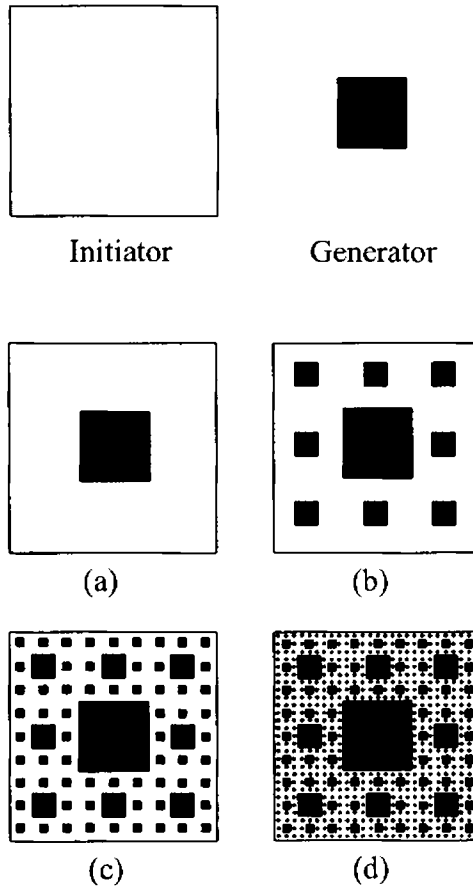


Figure 3 Different Iterated stages of Sierpinski carpet geometry (a) Stage 1 (b) Stage 2 (c) Stage 3 (d) Stage 4

Similarly, the Cantor bar is formed by a line segment whose $1/3^{\text{rd}}$ position from the middle is repeatedly removed. In this case the initiator is defined as a line segment of unit length and the generator is defined as excising line segment of length one-third. The bar is formed by repeated application of the generator and its scaled replica to the middle third of the

initiator or the previous stage of growth. When the thickness of the Cantor bar becomes vanishingly small, the resultant fractal becomes Cantor dust. The growth of Cantor bar fractal geometry is shown in figure 4.

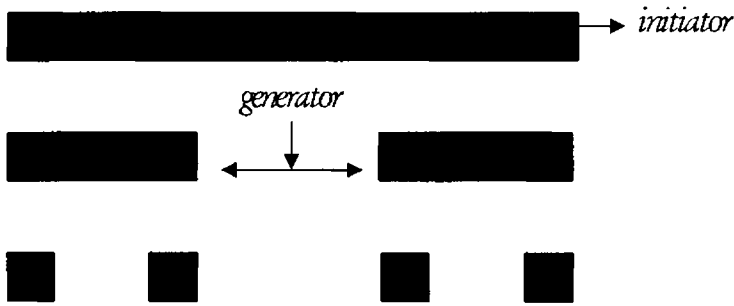


Figure 4 Growth of Cantor bar fractal

In fractal analysis, the Euclidean concept of 'length' is viewed as a process. This process is characterized by a constant parameter D known as the fractal (or fractional) dimension. The fractal dimension can be viewed as a relative measure of complexity, or as an index of the scale-dependency of a pattern. The fractal dimension is a summary statistic measuring overall 'complexity'.

Dimension of a geometry can be defined in several ways, most of these often lead to the same number, even though not necessarily. Some examples are topological dimension, Euclidean dimension, self-similarity dimension and Hausdorff dimension. Some of these are special forms of Mandelbrot's definition of the fractal dimension. However, the most easily understood definition is for self-similarity dimension. A self-similar set is one that consists of scaled down copies of itself. To obtain this value, the geometry is divided into scaled down, but identical copies of itself. If there

are n such copies of the original geometry scaled down by a fraction f , the similarity dimension D is defined as:

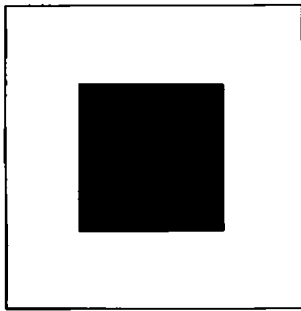
$$D = \frac{\log n}{\log\left(\frac{1}{f}\right)}$$

$D = \log(\text{number of self similar pieces}) / \log(\text{magnification factor})$

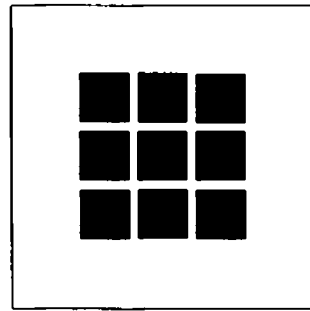
For example, a square can be divided into 4 copies of $\frac{1}{2}$ scale, 9 copies of $\frac{1}{3}$ scale, 16 copies of $\frac{1}{4}$ scale, or n^2 copies of $1/n$ scale. Substituting in the above formula, the dimension of the geometry is ascertained to be 2. Similarly we can decompose a cube into n^3 self similar pieces of $1/n$ with a dimension of 3. The same approach can be followed for determining the dimension of fractal geometries.

Another property associated with fractal geometries include lacunarity. Lacunarity is a term coined to express the nature of the area of the fractal having hollow spaces (“gappiness”) [151]. The concept of ‘lacunarity’ was introduced by Mandelbrot [150] as one of the geometric parameters to characterise fractal. A fractal is ‘lacunar’ if its gaps tend to be large, in the sense that they include large intervals, while fractals with small gaps have small lacunarity. Highly lacunar fractals are those which are very inhomogeneous and far from being translationally invariant, while fractals of low lacunarity are more homogenous and approach translational invariance. There can be several fractals with the same dimensionality but different lacunarities, reflecting that the eliminated areas are scattered differently. Lacunarity gives an idea of the way in which it is filled or the texture of the set while fractal dimension gives a measure of how much space is filled by the set [170].

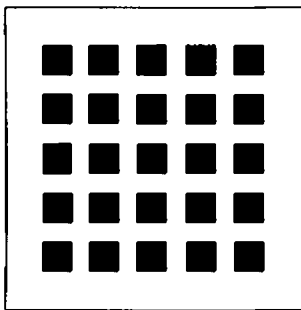
The structures shown in the figure 5 have the same fractal dimension but the distribution of the patches is different, keeping the area occupied constant



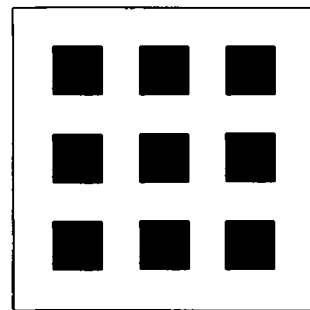
L1



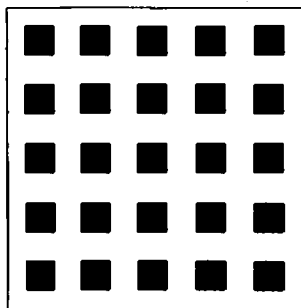
L2



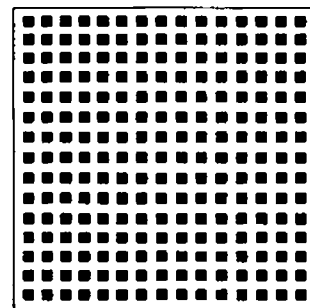
L3



L4



L5



L6

Figure 5 Sierpinski carpets with varying lacunarity with $D = 1.915$

1.4 MOTIVATION

A complex target can be represented as collection of basic target elements like flat plates, corner reflectors, cones and spheroids etc. It is convenient to isolate the dominant sources in target echo and fix our attention on a limited number of individual elements instead of composite target. Flat plates and corner reflectors are the major scattering centres in the complex target structures. RCS reduction of these scattering centres is the major concern to the design of targets invisible to radar's eye. The dominant scattering centers of the targets can be covered with fractal based metallo-dielectric structures with proper parameters, thereby reducing the RCS. These structures do not offer any air resistance because the metallisations is in the same plane as the dielectric sheet. Multipath interference from building surfaces is a problem familiar to urban TV reception. It is a serious problem for air traffic control systems at airports due to interference from hanger walls near airport runways. An approach to design hanger walls with these surfaces can eliminates unwanted reflections.

In this thesis, the effect of embedding fractal structures on flat plates, cylinders, dihedral corners and circular cones is investigated. It is observed that this technique offers a good amount of reduction in the RCS of these targets.

1.5 OUTLINE OF THE PRESENT WORK

The scattering property of a periodic structure depends on the frequency of the electromagnetic wave as well as the angle of incidence. By properly selecting the periodicity, one can achieve minimum reflection/transmission at certain frequencies and angles of incidence. Thus the structure becomes 'frequency selective'. By properly combining different layers of the periodic surfaces, it is possible to obtain the frequency selective property for a wide range of angles of incidence. These structures find applications in electromagnetics as frequency selective surfaces (FSS). They can be used as radomes, frequency scanned gratings, sub reflectors for multifrequency antenna systems.

An FSS backed by a ground plane can be used for reducing the RCS of a target. These structures which can give selective reflection can be used to reduce unwanted reflection which may interrupt other communication systems. Development of frequency selective surfaces has wide range of applications in communication and radar systems. For example, communication between the aircraft and the terminal buildings is affected by unwanted reflections from nearby structures such as walls of a building.

Specular reflections from conducting surfaces can be eliminated by corrugations of proper period and depth. These corrugations can be of any shape like saw tooth, rectangular or fin. Corrugations on a conducting surface with proper parameters can be applied to targets to divert the power of an incident electromagnetic wave away from the radar and

thereby reduce the RCS. However, corrugated surfaces on a metallic plate are heavy and bulky and its fabrication is a tedious and time consuming task. A strip grating, made by etching thin periodic metallic strips on a dielectric sheet (metallo-dielectric structure) placed over a conducting plane, shows similar effects of corrugated surface and is called as Simulated Corrugated Surface (SCS) [132]. Corrugations and SCS have the property of eliminating specular reflections obeying the principle of Bragg scattering. An important advantage of SCS over corrugations is in the ease of fabrication technique using the photolithographic technique.

The main disadvantage of strip gratings developed earlier is that eliminations of specular reflection is effective only for limited frequency range and limited angular range, which impose a constraint on its use in the design of reflection free surfaces. The use of SCS proved that the frequency bandwidth and angular range of suppression of specular reflection can be increased appreciably, when the period of the grating etched on a dielectric of appropriate thickness satisfies the Bragg condition, but the reduction in backscattered power obtained is only for a limited range of frequencies. Reduction of backscattered power is also not obtainable simultaneously for TE and TM polarizations of the incident wave using strip grating. Figure 6 shows the schematic diagram of a corrugated surface and a reflector backed strip grating.

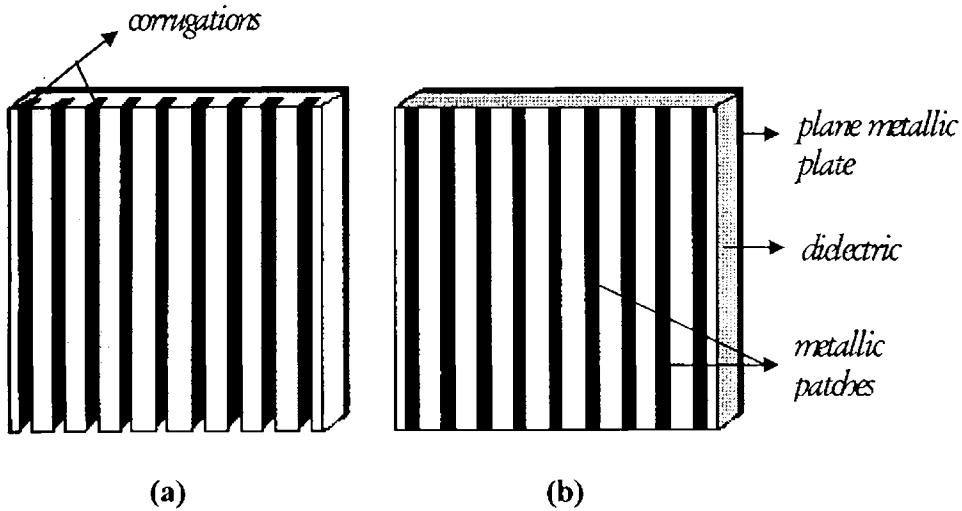


Figure 6 Schematic diagram of
 (a) Corrugated surface
 (b) Reflector backed strip grating

The present work aims at the reduction of RCS of targets using metallo-dielectric structures based on fractal geometry. The effect of loading these structures over a flat plate, cylinder, dihedral corner reflector and circular cone are investigated. Fractal structures have certain properties like self similarity and space filling property. So fractal based metallization on a dielectric substrate backed with a conducting surface can be useful in reducing the backscattered power simultaneously at different frequency bands and also with improved bandwidth. Also RCS reduction can be obtained for both TE and TM polarization of the incident field over a large bandwidth for structures that are symmetric.

1.6 ORGANISATION OF THE THESIS

The scheme of the work presented in this thesis is given below:

An exhaustive review of the work done in the field of Radar Cross Section studies and fractal electrodynamics is presented in chapter 2.

The methodology adopted for the work presented in this thesis is highlighted in chapter 3. The methods used for the measurements of monostatic and bistatic RCS are presented.

Chapter 4 highlights the experimental results of the investigations carried out on the scattering behaviour of flat plate, cylinder, dihedral corner reflector and circular cone loaded with fractal based metallo-dielectric structures. The effect of various parameters such as dielectric thickness, dielectric constant, Shape of metallizations and fractal geometry are investigated.

In chapter 5, the results of the experimental studies are validated by analyzing the structures using electromagnetic simulation softwares. The simulation and experimental results are compared for different cases. Comparisons of the backscattering properties of different structures are also presented for different frequency bands.

Conclusions drawn from the investigations are presented in chapter 6. The scope of future work in this field is also discussed.

Work done by the author in the related fields is presented in appendices I and II. The design of a band pass filter employing metallo - dielectric structure based on cantor bar fractal geometry is presented as appendix I. The development of an Arch method for RCS measurements and its automation is presented in appendix II.

REVIEW OF THE PAST WORK IN THE FIELD

Methods for reducing Radar Cross Section (RCS) of objects have been investigated by many researchers both experimentally and theoretically for the last so many years. This chapter presents a chronological review of important research in the fields of RCS studies, RCS reduction techniques and fractal based scattering and radiating structures. This chapter is divided into two sections. The first section presents a review of RCS studies, RCS reduction techniques and its measurement techniques and the studies of fractal electrodynamics are reviewed in the second section.

2.1 RADAR CROSS SECTION STUDIES

The history of investigations on Radar Cross Section dates back to the early part of twentieth century. The results of the investigations were not published until World War II. From the end of the World War II till the present time, the radar response of specific targets has continued to be an area of considerable interest to many researchers, and great deal of work has been reported in the field.

The analysis and measurements on RCS of various objects are available in open literature [1-4]. Hu [5] had measured the RCS of a dipole antenna in the VHF range with the input terminals of the dipole shorted. The experimental results were compared with theoretical values.

W. J. Bow et al [6] presented the computed radar cross section data for microstrip patch antenna arrays as a function of array size, incident signal frequency, and anisotropy.

E. H. Newman and Forria [7] presented a solution to the problem of plane wave scattering by a rectangular microstrip patch on a grounded dielectric substrate. The model does not include the microstrip feed, and thus does not include the so-called “antenna mode” component of the scattering. The solution begins by formulating an electric field integral equation for the surface current density on the microstrip patch.

D. Pozar [8] envisaged the problem of a rectangular microstrip antenna printed on a uniaxially anisotropic substrate. The effect of anisotropy on the resonant frequency and surface wave excitation of the antenna is considered, and the radar cross section (RCS) of the antenna is calculated. The RCS calculation includes the effect of the load impedance (antenna mode scattering). The derivation of the uniaxial Green’s function

in spectral form, the associated moment method analysis for the input impedance and scattering of the microstrip patch, and the expressions for the far-zone fields of a source on a uniaxial substrate are presented.

D. R. Jackson [9] proposed a general formula for an arbitrary resonant conductive body within a layered medium, which shows that the body radar cross section is directly related to the radiation efficiency of the body.

A. Taflove and K. Umashankar [10] presented two disparate approaches- FDTD and MoM, the analysis and modeling of realistic scattering problems using these two methods are summarized and compared. New results based on these two methods for induced surface currents and radar cross section are compared for the three dimensional canonical case of a conducting metal cube illuminated by a plane wave.

D. Colak et al [11] presented a dual series based solution for the scattering of an H-polarized plane wave from a silted infinite circular cylinder coated with absorbing material from inside or outside. For both cases, numerical results are presented for the radar cross section and comparisons are given for two different realistic absorbing materials.

C. -G. Park et al [12] investigated the problem of transverse magnetic plane wave scattering from a dihedral corner reflector. Using the mode matching technique, the transmitted and scattered fields are expressed in the angular spectral domain in terms of radial waveguide modes.

D. A. Edward et al [13] presented the application of variational techniques to the electromagnetic scattering problem. It has been shown that these techniques can deal effectively with distorted structures and the case of orthogonal and nonorthogonal distorted dihedrals in some detail.

Harrison and Heinz [14] had derived a formula for the RCS of a solid wire, tabular and strip chaff of finite conductivity approximating one half wavelengths or less in length.

In the RCS analysis of coated metal plate by Knop [15], the thickness of the plate and that of the coating were assumed to be thin, and the size of the plate was large, so that physical optics approximation could be used.

Blore [16] had made experimental investigation for the effect of nose on backscattering RCS of grooves, cone spheres, double backed cones, double rounded cones and cone spheres.

Rheinstein [17] had carried out several series of rigorous numerical calculations of the backscatter cross sections of a conducting sphere with a thin lossless dielectric coating.

Senior [18] reviewed the analytical techniques available for estimating the backscattering cross section of a metal target with classification given on the basis of wavelength to dimension of the targets.

Blacksmith et al. [19] reviewed the history of radar cross section measurement. Crispin and Maffet [20-21] reviewed the RCS measurement methods for simple and complex shapes, with special attention being devoted to results rather than derivations of formulae.

The conditions of RCS measurement in terms of variations in the amplitude and phase of the incident field at the target, were discussed by Kouyoumijian and Petits [22]. A number of minimum range conditions were listed and discussed. The theoretical and measured data pertaining to background levels which can be achieved with conventional target supports were presented by Freeny [23].

Leipa and Senior [24] investigated the scattering of plane electromagnetic wave by a metallic sphere loaded with a circumferential slot in a plane normal to the direction of incidence. The slot was assumed to be of small width and the field scattered in any direction is obtained by the superposition of the field diffracted by an unloaded sphere, and the field radiated by excited slot. Numerical and experimental results of backscattering were also presented.

Corriher and Pyron [25] have presented a bibliography of articles on radar reflectivity and related subjects. The design of an extremely high range resolution FM/CW X-band radar and RCS measurements were illustrated by Alongi et al. [26]. The primary design objective was to provide the capability to measure RCS of scaled models with a range resolution equal to a small fraction of the target length. Millin et al. [27] presented a numerical technique for the determination of scattering cross section of infinitely long cylinders of arbitrary cross section.

Radar cross section of a rectangular flat plat was investigated by Ross [28]. The simple physical optics theory was used for predicting the near specular values of RCS but failed to account for polarization dependence. The calculations based upon the geometrical theory of diffraction showed excellent agreement with measured data except on edge on aspects.

Miller et al. [29] presented the monostatic RCS results for straight wires having lengths of multiple wavelengths. The numerical RCS values obtained from solving the Pocklington's integral equation for induced current, fall within 1 dB of experimental measurements.

RCS of a perfectly conducting sphere coated with a spherically inhomogeneous dielectric was obtained using the geometrical theory of

diffraction by Alexopoulos [30]. The result was compared to the second order approximation obtained by asymptotic theory.

Miller and Morton [31] have studied the RCS of a metal plate with resonant slot. RCS of a thin plate for near grazing incidence was studied by Yu [32] with three higher order diffraction techniques.

Rahmat Samii and Mittra [33] employed a new integral equation to calculate the current distribution on a rectangular plate, when illuminated by a plane wave. Numerical results were also presented for the RCS of a plate for different angles of incidences and different dimensions of the plate.

Lin et al. [34] experimentally and numerically investigated the RCS of a conducting rectangular plate. The numerical example also included the edge on incidence where physical optics and geometric theory of diffraction have failed.

Wier et al. [35] developed a technique for making RCS measurements over wide frequency bands. The Hewlett-Packard (HP) automatic network analyzer, which measures the scattering parameters at discrete frequencies over a band, has been adapted to obtain RCS measurements. Typically the background clutter, antenna cross coupling and system errors in the absence of target were reduced by the system measurement techniques to an equivalent value of -45 dBsm.

Mautz and Harrington [36] presented the computation of radiation and scattering of electromagnetic fields by electrically large conducting cylinders using geometrical theory of diffraction for the transverse electric case. The computation accuracy was checked by comparing the results to corresponding ones computed by a moment method solution to the H-field integral equation.

An accurate mathematical model for the backscattering from a loaded dihedral corner has been developed by Corona et al. [37]. This model employed a generalization of physical optics to loaded surfaces which takes into account the lighting of each face by rays diffracted by edge of other one.

Griesser and Balanis [38] predicted the backscattered cross section of dihedral corner reflectors which have right, obtuse and acute interior angles, using the uniform theory of diffraction (UTD) plus an imposed edge diffraction extension. Multiple reflected and diffracted fields up to third order were included in the analysis, for both horizontal and vertical polarizations.

Arvas and Sarkar [39] have considered the problem of determining the RCS of two dimensional structures consisting of both dielectric and conducting cylinders of arbitrary cross section. Both transverse electric and transverse magnetic cases are considered. The problem is formulated in a set of coupled integral equations involving equivalent electric and magnetic surface currents, radiating in unbounded media.

The low RCS measurement requires careful cancellation of the background reflections. The large size of the target tends to upset the background cancellation balance obtained in the absence of the target. So, when the cross section of the target is large, the target to background cross section ratio can be made large.

RCS reduction of dihedral corners, which are major scattering centers in radar signatures of ship and military ground vehicles, was studied by Knott [40]. A criterion was developed that gives the required corner angle as a function of RCS reduction desired and electrical size of corner faces.

The broadside RCS of a rectangular box was studied by Tsai [41] using the integral equation technique. Jones and Shumpert [42] presented the electromagnetic scattering behaviour of a perfectly conducting infinitesimally thin, spherical shell with circular aperture. The problem was formulated in terms of E-field integral equation. The calculated values of surface currents and RCS were presented and discussed for several cases of interest.

A scheme is presented by J. L. Volakis et al [43] for reducing the RCS of patch antennas outside their operational band without compromising gain performance. This is achieved by placing a narrow resistive strip (distributed loading) around the periphery of the patch which has minimal effect at the operational frequency of the patch. Results are presented using a finite element-boundary integral code demonstrating the effectiveness of this scheme over the traditional method of using lumped loads.

Keen [44] presented the development of a numerical technique for calculation of the RCS of any regular shape of corner reflector consisting of three orthogonal plates. A simple and accurate formula to calculate the backscattered RCS of a perfectly conducting hollow, finite circular cylinder with closed termination was proposed by Huang [45]. The radiated field from the cavity region was evaluated via, the Kirchoff approximation and the reciprocity theorem.

Le Vine [46] presented a solution for the backscatter RCS of dielectric disks, of arbitrary shape, thickness and dielectric constant. The result was obtained by employing a Kirchoff type approximation, to obtain the field inside the disk.

The application of the uniform asymptotic theory of diffraction to obtain an expression for RCS of curved plate was presented by Sanyal and Bhattacharyya [47]. Comparison with experimental results shows good agreement even for different small and intermediate radii of curvature of the plate.

An asymptotic high frequency estimation of monostatic RCS of a finite planar metallic structure coated with a lossy dielectric was made and compared with experiments in X band, by Bhattacharyya and Tandon [48].

Rembold [49] reported the measurement of RCS of a long metallic rod using continuous wave Doppler radar at 60 GHz. The derived expression for RCS demonstrates good agreement with the measured data. A continuous wave RCS measurement facility in the X band was described by Bhattacharyya et al. [50]. The set up was capable of automatically measuring the monostatic RCS over aspect angle ranging from 0 to +or – 180° for both parallel and perpendicular polarizations. The typical value of effective isolation between transmitted and received signal was of the order of 60 dB and dynamic range of 35 dB.

Corona et al. [51] studied the radiation characteristic of a 90° dihedral corner reflector and showed that it can be conveniently used as a reference target in experimental determination of RCS. The numerical model developed using physical optics and image method, has been improved by taking into account the rays diffracted by corner edges.

In 1987, Dybdal [52] reviewed the fundamentals of RCS measurements. The wide bandwidth electronic and digital signals processing capabilities encouraged the earlier objective of determining the RCS and have extended to include the developing techniques to distinguish different types of targets and modifying the target scattering properties.

Achievable accuracy and those factors that limited the accuracy were **discussed**.

Lee and Lee [53] calculated the RCS of a circular waveguide **terminated** by a perfect electric conductor. Geometrical theory of **diffraction** was employed for the rim diffraction and physical optics was employed for the interior irradiation.

Anderson [54] used the method of physical optics to calculate the **magnitude** of the reduction of RCS, which result from modest departures from orthogonality. The theoretical results were compared with **experimental** measurements which are found to be in very good agreement.

Welsh and Link [55] developed two theoretical models for RCS measurements of large targets consisting of multiple independent point scatterers.

The history of bistatic RCS of complex objects was presented by Glaser [56]. Beginning with the first radars before World War II, the discussion proceeds with current experimental and analytical modeling methods. Data were presented from experiments on cylinders and missiles.

Youssef [57] presented a summary of developments and verifications of a computer code, for calculating the RCS of complex targets. It is based on physical optics, physical theory of diffraction, ray tracing, and semi-empirical formulations. Wu [58] evaluated the RCS of arbitrarily shaped homogeneous dielectric body of revolution by surface integral formulation. Accuracy of the method was verified by good agreement with the exact solutions for the RCS of a dielectric sphere.

Mitschang and Wang [59] described hybrid methods incorporating both numerical and high frequency asymptotic techniques for

electromagnetic scattering problems of complex objects. Sarkar and Arvas [60] have presented an E-field equation for the computation of RCS of finite composite conducting and lossy inhomogeneous dielectric bodies.

RCS patterns of lossy dihedral corner reflectors were calculated using a uniform geometrical theory of diffraction for impedance surfaces by Griesser and Balanis [61]. All terms upto third order reflections and diffractions were considered for patterns in the principal plane. The dihedral corners examined have right, obtuse, acute interior angles and patterns over the entire 360° azimuthal plane were calculated.

The problem of determination of the fields scattered by an infinite dielectric cylinder of arbitrary cross section, located at the interface between two semi-infinite dielectric media was presented by Marx [62]. The derivation of integral equations was given for transverse electric mode, for dielectric cylinder and for a perfectly conducting cylinder.

Pathak and Burkholder [63] have analysed the problem of high frequency electromagnetic scattering by open ended waveguide cavities with an interior termination, via three different approaches, modal, ray and beam techniques. Typically numerical results based on the different approaches were presented, and some pros and cons of these approaches were discussed.

The problem of electromagnetic scattering from a plate with rim loading for transverse electric (TE) and transverse magnetic (TM) polarizations was examined by Bhattacharyya [64], based on uniform geometrical theory of diffraction. An attempt was made to estimate the width of the coating around the edges which gives the same result as the plate of same size which is uniformly coated. Theoretical results were presented and discussed.

Penno et al. [65] examined the scattering from a perfectly conducting cube. The results presented were for a cube on the order of 1.5 – 3 wavelengths on edge, which is illuminated at broadside incidence. Hybrid iterative method was employed, which utilizes an initial approximation of the surface currents on the cube faces.

Tice [66] has presented an overview of RCS measurement techniques. In this review, the measurement radar was limited to ground based radar systems. Targets included operational full scale ships and aircrafts, full scale aircraft mounted on pylons and scale model of ships in water.

Choi et al. [67] have investigated the backscattering RCS of finite conducting cones using equivalent current concept based on uniform geometrical theory of diffraction. The discrete Fourier transform method was used to calculate the RCS of orthogonal and non-orthogonal dihedral corner reflectors by Shen [68]. The results obtained using the method compare favourably with measurements and predictions computed using the method of moments.

The RCS of a partially open rectangular box in the resonant region was investigated by Wang et al. [69]. Two dimensional numerical results were generated using the method of moment's solution to the electric field integral equation. The dependence of the resonant behaviour on the box dimension, aperture size and incident polarization were interpreted in terms of the field distribution inside the cavity. Experimental data for a three dimensional box were also presented. They were consistent with the two dimensional simulation.

Blejer [70] presented the polarization matrix for a cylinder on a circular disk using the physical optics approximation. Multiple scattering

between the cylinder and the circular disk ground plane was obtained by invoking the image theory, and was expressed as a bistatic return from the cylinder and its image, due to the image field. Theoretical values were compared with experimental results.

Goggans and Shumpert [71] presented the RCS of dielectric filled cavity backed apertures in two dimensional bodies for both TE and TM polarizations. The method of moment technique was employed to solve a set of combined field integral equations for equivalent induced electric and magnetic currents on the exterior of the scattering body and associated aperture.

Baldauf et al. [72] presented a general method for calculating the RCS of three dimensional targets. Following shooting and bouncing ray method, a dense grid of rays was launched from the incident direction towards the target. Each ray was traced according to geometrical optics theory including the effect of ray tube divergence, polarization and material reflection coefficient. At the point where the ray exits the target, a physical optics type integration is performed to obtain the scattered fields. The theoretical results were in good agreement with measured data.

Mongia et al. [73] reported the results of precise measurement of RCS of dielectric resonators of cylindrical and rectangular shape at resonance. The measured results were compared with those predicted by asymptotic theory.

The monostatic RCS spectra of rotating fan array, with tilted metal blades were investigated by Yang and Bor [74]. The high frequency theoretical treatment of slowly rotating and electrically large scatterer was based on the quasi-stationary method with the physical optics / physical

theory of diffraction technique. The agreement with the theoretical and experimental results was acceptable.

Trueman et al. [75] investigated the effect of wire antennas on the high frequency RCS of aircraft by comparing the RCS of strip, cylinder, and a rod with and without attached wire.

Mishra et al. [76] presented the precision measurements of RCS of simple rod and cylinder for all angles of incidence in a plane containing the long axis of the target. Fully automated RCS measurement setup used an HP series 9000, model 332 instrumentation controller for process control and data acquisition and processing. HP 8510 Network analyzer system with HP 8511A frequency converter as receiver front end was used to determine the scattered field amplitude and phase at many frequencies from 2 to 18 GHz. The extensive measured RCS data were used as a reference for validating numerical computations.

Rius et al. [77] presented a new and original approach for computing the RCS of complex radar targets, in real time 3-D graphics workstation. RCS of aircrafts were obtained through physical optics (PO), method of equivalent currents (MEC), physical theory of diffraction (PTD) and impedance boundary condition (IBC). A graphical processing approach of an image of the target at the workstation screen was used to identify the surface of the target visible from the radar viewpoint and obtain the unit normal at each point. The high frequency approximations to RCS prediction were then easily computed from the knowledge of the unit normal at illuminated surface of the target. This hybrid graphic electromagnetic computing results in real-time RCS prediction for complex targets.

RCS of rectangular microstrip patch on a lossy biased ferrite substrate was investigated by Yang et al. [78], based on a full wave integral equation formulation in conjunction with the method of moments. The RCS characteristics, especially the resonance behaviour of the patch, with various biasing conditions were studied and compared to the case of an unbiased ferrite.

Birtcher et al. [79] measured the RCS of a long bar (at X-band) and a scale model aircraft (at C-band) under the quasi plane wave illumination and cylindrical wave illumination and compared the results.

The RCS of a small circular loop made from YBCO high temperature superconductor were calculated as a function of applied magnetic field strength by Cook and Khamas [80]. It was shown that RCS is reduced as the magnetic field increases and that effect was more pronounced as the radiation distance decreases.

The RCS of several bodies proposed by the electromagnetic code consortium (EMCC) was calculated using transmission line matrix (TLM) method [81]. The results were in good agreement with experimental and moment method solutions, when TLM was used together with an appropriate boundary condition and a near to far zone transmission approach.

Grooves [82] have proposed an important class of boundary structures, having alternate areas of conducting and non-conducting materials, for control and direction of electromagnetic waves incident on them.

The solution for the problem of a plane wave incident obliquely on a parallel wire grid, which is backed by a plane conducting surface was

presented by Wait [83]. It was shown that, in certain cases, a resistive wire grid will absorb the entire incident wave.

The theoretical and experimental results for the reflection and transmission of uniform plane electromagnetic waves, normally incident on an ideal strip grating was presented by Primich [84]. The theory was based on the variational method, and measurements were made at normal incidence in a parallel plate region operating in 8 – 10 cm wavelength range.

Tadaka and Shiniji [85] presented a diffraction grating which was a new version of microwave passive repeater developed to improve the transmission qualities of links utilizing mountain diffraction. Principles and characteristics of diffraction gratings were given with test results.

Sigelmann [86] has studied the surface wave modes in a dielectric slab covered by a periodically slotted conducting plane. Sampling and variational methods were used to obtain surface wave modes.

Jacobson [87] described an analytical and experimental investigation of practical, two dimensional periodically modulated slow wave structures. The structure was a dielectric slab covered on one side by a perfectly conducting ground plane and the other side by perfectly conducting strips perpendicular to the direction of propagation.

Integral equations for currents induced on an infinite perfectly conducting grating for plane wave illumination were presented by Green [88]. These integral equations were approximated by matrix equations, which were readily solved for currents. From these currents the strengths of the grating modes were obtained.

A numerical solution for the problem of scattering of a plane wave by a dielectric sheet with an embedded periodic array of conducting strips

was presented by Lee [89]. The solution to the problem of scattering of plane wave by an infinite periodic array of thin conductors on a dielectric slab was formulated by Montgomery [90]. Numerical results were presented with experimental data.

Montgomery [91] analyzed the scattering of an infinite periodic array of microstrip disks on a dielectric sheet using Galerkin solution of vector integral equation. In 1979, he studied [92] the solutions of TE and TM scattering for an infinite array of multiple parallel strips. The solution was found using the perturbation form of modified residue calculus technique. Numerical results were presented and discussed.

By using microwave models of optical gratings, Tamir et al. [93-95] realized dielectric grating with asymmetric triangular or trapezoidal profiles that exhibit beam coupling efficiencies. The behaviour of leaky modes along microwave gratings show that, Bragg scattering approach provides simple design criteria for blazed dielectric gratings and broad band high efficient optical beam coupling devices.

Petit [96] presented the electromagnetic theory of plane grating, in which the integral methods and differential methods were studied in greater depth.

Kalhor and Ilyas [97] analyzed the problem of scattering of electromagnetic waves by periodic conducting cylinders embedded in a dielectric slab backed by a plane reflector using the integral equation technique. The results were compared with the limited numerical results available in the literature and indicate excellent agreement.

A method of analysis of strip gratings with more than one conducting strip per period was given by Archer [98] and that was then applied to a periodic twin strip grating with two unequal gaps.

Formulae for ideal and good grating system were given by Xu-Jeandong and Guorui [99]. Some applications of the strip grating systems such as frequency filter, polarization rotators and impedance transformers were introduced and the principle design considerations of impedance transformers were discussed.

Kobayashi [100] investigated the problem of diffraction by a thick strip grating with the aid of Wiener-Hopf technique. Kobayashi [101-102] considered periodic parallel plate grating with dielectric loading, and the problem was analyzed with the same technique. The Wiener-Hopf equation was solved by decomposition procedure and then the modified residue calculus technique (MRCT) was applied to increase the accuracy of the solution.

Jose and Nair [103] have showed that the gratings can be used to simulate the effect of rectangular corrugations in conducting surfaces. The perfect blazing of reflector backed thin strip gratings to $n = -1$ spectral order for both TE and TM polarizations were compared with corrugated reflection gratings.

A fast convergent integral equation solution to the scattering problem of TE/TM plane wave by a one dimensional periodic array of thin metal strips on a dielectric substrate was described by Wu [104].

The development of reflector backed strip gratings exhibiting the properties like the elimination of specular reflection from a conducting surface for normal and near normal incidence was reported by Jose et al. [105]. This was achieved by using self complimentary strip grating which were not possible using conventional rectangular metallic corrugations.

Kalhor [106] analyzed the scattering of electromagnetic waves from a dielectric slab loaded with periodic array of conducting strips, using

mode matching technique. The fields were expanded in term of a suitable propagating and evanescent modes in various regions. He presented the variation of energy of significant scattered modes with various structure parameters for both polarizations of incident wave.

Kildal [107] defined artificially soft and hard surfaces for electromagnetic waves. Transversely corrugated surfaces and other alternative surfaces form soft surfaces and longitudinally corrugated surfaces from hard surfaces.

Kalhor [108] analyzed the diffraction of e.m. waves by plane gratings of finite extent and the results were compared with that of infinite extent to determine the minimum structure sizes that should be used in experimental measurements to obtain meaningful results.

The scattering and guidance of electromagnetic waves from a two dimensionally periodic metal grating structure were investigated by Wu and Chen [109]. The numerical results obtained were useful for the design of new devices in 2-D periodic structure, particularly in millimeter wave frequency range, such as antennas, filters, couplers and distributed reflectors.

Jin and Volakis [110] have discussed the scattering characteristic of an infinite and truncated periodic array of perfectly conducting patches on a dielectric slab. An approximate solution was presented for truncated array scattering based on the exact solution for the corresponding infinite array. The result was obtained numerically by solving for the patch currents via, a conjugate gradient fast Fourier transform technique. The scattering pattern of the finite array was then computed approximately by integrating the infinite periodic array currents over the extent of the given finite array.

A new robust approach for the analysis of strip gratings both of finite and infinite conductivity, for both TE and TM cases, was described by Naqvi and Gallagher [111]. The field distributions in the plane of the grating were expanded in a Fourier series, whose coefficients were derived as the solution to an infinite dimensional system of linear equations.

Aas [112] presented the concepts of artificially soft and hard surfaces, interpreted in terms of plane wave reflection properties of the surfaces, in particular the reflection phase angles for two orthogonal polarizations. Numerical results for corrugated and strip loaded surfaces were presented. The results indicate that strip loaded surface is the most promising candidate for hard surface. The advantage of strip loaded surface is that, when properly designed it can have a larger bandwidth while at the same time being thinner than corrugated surface.

Gedney and Mittra [113] have analyzed the problem of diffraction by a thick, conducting grating situated in an inhomogeneous dielectric slab, using the generalized network formulation, which combines the method of moment and finite element method. The solutions were presented for both TE and TM polarization.

Borkar et al. [114] presented the design procedure of a millimeter wave twist reflector, which is a polarization sensitive device consisting of unidirectional planar metallic grating supported on a dielectric substrate. The loss factor of the dielectric material has been accounted for the prediction of twist reflector performance. With the introduction of these corrections, experimental results were found to be in close agreement with the theory.

Gimeno et al. [115] presented a numerical model to analyse a system formed by the cascade connection of slanted strip grating plates, to

rotate the polarization of a linearly polarized wave. General criteria of design were presented and four plates 60° polarizer was designed in the 7–8 GHz band. Good agreement was found between theoretical and measured results.

Jose et al. [116] presented a method for RCS reduction of metallic cylinders using strip grating technique. The RCS of a cylinder with periodic strip loaded dielectric surface was determined experimentally and it is compared with the reference target having the same dimensions. Typical reduction of 30-40 dB was reported. The RCS measurements were made using HP 8510B network analyzer along with test set. The measurement principle was based on the time gated signal which is differentiated according to their time of arrival. This signal was analyzed using the network analyzer, which is configured to make swept frequency RCS measurements in the time domain with required corrections.

Ajaikumar et al. [117] studied the effect of rectangular strips on a dielectric slab on the RCS of dihedral corner reflector for TE polarization. The strip grating technique was found to be more effective in the RCS reduction of corners for normal incidence. Typical reduction of 40 – 50 dB was achieved but only over narrow frequency range.

Hong and Zhu [118] presented a mixed technique for calculating the RCS characteristics of a dielectric coated conducting cylinder loaded with metallic strips, for TE wave incidence, the technique was based on the Spectral Domain Method (SDM), Conjugate Gradient Method (CGM) and Fast Fourier Transform (FFT). Numerical results were presented which shows the RCS can be effectively controlled by adjusting the period or spaces between the strips.

Kell and Pederson [119] compared RCS measurements in narrow band continuous wave system and on short pulse system. They also presented data for one model target.

Knott [120] had shown that the deformation of metallic flat plates into cylindrical segments reduces the large specular echo but does not necessarily reduce the mean cross section by more than 1 dB or so.

Ebbeson [121] has given the results of an analytical and numerical investigation of TM polarized plane wave scattering from an infinite fin-corrugated surface. The surface was composed of infinitely thin, perfectly conducting fins of spacing $\lambda/2 < a < \lambda$. Specular reflections from this ideal surface were completely converted to backscatter in a direction opposite to the incident wave when the fin period and height were properly chosen. A procedure for the design and performance prediction of a finite fin-corrugated surface composed of finitely thick fins were also described.

John et al. [122] described a bistatic RCS measurement technique. It used the variation of CW null balance approach, resulting in rapid measurement time. A network analyzer and process computer were incorporated into the existing image ground plane system to improve the bistatic capability and flexibility.

Jull and Ebbeson [123] proposed the use of corrugated surfaces to reduce interfering reflections from buildings. Numerical examination was made for infinite comb grating under H – polarized plane wave illumination with grating space between λ and $\lambda/2$. Model measurements at 35 GHz on finned surfaces of finite size under non plane wave illumination are given to verify whether the surfaces behave essentially as predicted for the infinite comb.

Jull et al [124] reported that perfect blazing of reflection gratings to the $n = -1$ spectral order for both TE and TM polarizations is possible with rectangular grooves with angle of incidence in the range 19.5° to 59.4° . Design dimensions were verified experimentally at 35 GHz.

Heath and Jull [125] described that corrugations could completely convert specular reflection from a conducting surface to backscatter. They showed that this was possible with rectangular groove surface profile for either TE or TM polarizations or for both simultaneously. Numerical and experimental results were illustrated for a surface, designed for plane wave incidence at 50° from the normal.

An experimental investigation of the scattering from crossed gratings of square pyramids was conducted by Cai et al. [126]. They have provided examples of the use of equivalent singly periodic grating surfaces as a guide to the design of crossed grating surfaces.

Jull et al [127] presented a numerical analysis of thin corrugated strips with rectangular groove profiles, dual blazed to $n = -1$ spectral order. It has shown that, high efficiency gratings remain efficient as the number of grating elements is reduced to as few as two, provided that incidence is not near grazing. Numerical results show that the main effect of reduced grating size is a broadening of the diffracted beam, which can be predicted from a simple formula.

The fundamental of radar cross section measurements was reviewed by Robert B. Dybdal [128]. Measurement facilities including the present research activities on compact range techniques are then described. Those factors that limit the accuracy of RCS measurements are discussed.

T. Mathew et al. [129] demonstrated a trapezoidal strip grating surface that eliminates specular reflection over almost the entire X-band frequency range for TM polarization.

D. S. Stephen et al. [130] reported the elimination of specular reflection over a wide range of aspect angles for TE polarization by a strip grating surface of two dimensional periodicity.

They also [131] proposed simultaneous elimination of specular reflection and backscattered power from a plane metallic surface by simulated corrugated surfaces of constant period and variable strip width for TM polarization.

T. Mathew et al. [132] developed a simulated corrugated surface that eliminates specular and backscattered power simultaneously for both TE and TM polarization.

The RCS of a finite-size ground plane with perforated triangular apertures has been characterized by Kathleen L. Virga [133]. The results of the monostatic RCS computed by the method of moments surface patch formulation for a plane wave incident on finite size plates with two widely spaced and two closely spaced apertures have been presented.

A modified mode matching technique that uses the segmentation method to analyse the scattering properties of a dual periodic strip grating is presented by D. S. Stephen et al [134].

Polarimetric radar cross sections were measured for two large Bruderhedrals at 35 and 93 GHz [135]. The overall spread in the measured RCS was 2 dB. It was found that the absolute RCS as well as the dependence of the RCS on elevation angle could be significantly altered by a slight misalignment of the Bruderhedral.

The transmission line modeling (TLM) method is applied to determine the radar cross section of very thin conducting targets under critical illumination that are included in a benchmark of thin plates proposed by the electromagnetic code consortium (EMCC) for validation of low-frequency electromagnetic computational codes [136].

S.Y. Wang and S. K. Jeng [137] proposed a compact closed-form formula for the RCS of a perfectly conducting right dihedral corner reflector at arbitrary aspect angles. M. O. White [138] presented an overview of radar cross section, measurements, prediction and control.

H. Mosallaei and Y. Rahmat-Samii [139] presented a modal/GA technique for RCS reduction in a wide-band frequency range for planar, cylindrical, and spherical conducting structures. Using the GA method, RCS of these structures is reduced more than 27dB by designing an optimized RAM coating. In addition, it is shown that the optimum RAM coating designed for a planar structure can also reduce the RCS of the cylindrical and spherical structures effectively.

A comparative study on target identification using RCS signature of an aircraft in both the frequency domain and the range domain is proposed by Chan [140].

Smith [141] demonstrated a technique for measuring the RCS of 2D diffracting sources. The measured and predicted diffraction RCS of a conducting halfplane edge and a gap in an otherwise infinite conducting plane are presented. The technique may be used to measure the diffraction coefficient of an impedance discontinuity.

P. Corona et al [142] analyzed the electromagnetic backscattering by a perfectly conducting dihedral corner reflector with sinusoidal profiles characterized by different periodicity values.

An application of the theory of open electromagnetic problems by **circuital analysis** is presented by Penaranda [143] for the reduction of radar **cross sections** of homogeneous cylinders without need for other dielectric **media**.

V. Losada et al [144] proposed Galerkin's method in the Hankel **transform domain (HTD)** to the determination of the RCS of unloaded **stacked** circular microstrip patch antennas fabricated on a two-layered **substrate** which may be made of a uniaxial anisotropic dielectric, a **magnetized ferrite** or a chiral material.

Richard Norland [145] showed how the assumption that specular **backscattered** reflection pattern of the flat plate reduces the induced **multipath** error is constrained by the radar wavelength, geometric **parameters** and by the plate dimension.

Misran et al [146] compared the performance of a concentric ring **reflectarray** element backed either by a solid metal ground plane or a **frequency-selective surface**. Simulated and measured results showed that **the 'in-band'** reflection phase response of the two structures is similar; however, the periodic surface reduces the **'out-of-band'** reflectivity of the **antenna** by more than 4 dB, thereby decreasing its RCS profile to these **signals**.

A. E. Serebryannikov and A. I. Nosich [147] developed a **generalized** model to study the TE-polarized plane wave scattering by coated and uncoated slotted circular cylinders of nonzero thickness and by a filled and empty circular cylinders with sectoral cuttings.

Peixoto et al [148] investigated the RCS reduction of dihedrals by **shaping** and by application of Radar Absorbing Material (RAM).

2.2 FRACTAL ELECTRODYNAMICS

The blend of fractal geometries and electromagnetics is called fractal electrodynamics. A good reference on the basics of fractal geometry, especially on how they pertain to the field of electrodynamics is described by D. L. Jaggard in [149]. Fractal geometry was first defined by Benoit Mandelbrot [150], to define many perplexing geometries found in nature. A very good reference for fractal antennas as elements and array can be found in [151] by D. H. Werner and R. Mittra.

J. Romeu and Y. Rahmat-Samii [152] proposed that the multiband properties of self-similar fractals can be advantageously exploited to design multiband frequency selective surfaces. It is shown that the self similarity of the Sierpinski dipole translates into a dual-band behaviour of a FSS made by arraying a two iteration Sierpinski dipole.

C. Puente-Baliarda et al [153] studied the multiband behaviour of the fractal Sierpinski antenna.

D. H. Werner et al. [154] discussed about the recent developments in the field of fractal antenna engineering, with particular emphasis placed on the theory and design of fractal arrays.

C. T. P. Song et al. [155] introduced a parallel feed staked fractal antenna using square Sierpinski and diamond Sierpinski carpet, which are suitable for applications in picocell environments for the operating bands of GSM, DECT and WLAN systems.

G. J. Walker and J. R. James [156] proposed the concept of fractal volume antenna in order to increase the degree of design freedom associated with fractal antenna elements and hence improve their input matching characteristics.

Z. Du et al [157] analysed the square microstrip fractal patch antenna in a Sierpinski carpet and the effects of its elements. They proposed that the multi-band frequency operation of the antenna resulted from the driven element and not from the parasitic fractal elements.

D. H. Werner and D. Lee [158] proposed a technique for the design of multiband and dual polarized frequency selective surfaces that is based on the use of fractal screen elements.

D. H. Werner and P. L. Werner [159] explained the fundamental relationship between self-similar, that is, fractal, arrays and their ability to generate radiation patterns which possess fractal features. The theoretical foundation and design procedures are developed for using fractal arrays to synthesize fractal radiation patterns having certain desired characteristics. A family of functions, known as generalized Weierstrass functions, are shown to play a pivotal role in the theory of fractal radiation pattern synthesis.

D. L. Jaggard and A. D. Jaggard [160] examined the radiation pattern from a new fractal array, the Cantor ring array. They also studied the case of thinned uniformly excited elements, and found that for large fractal dimension and low lacunarity, the Cantor ring array is considerably better than the periodic array, and appears to have lower sidelobes or a large visible range for a given sidelobe level than similar random arrays for number of elements less than or equal to hundred.

Y. Kim and D. L. Jaggard [161] presented a novel method of random array synthesis. It has been demonstrated that quasi-random arrays possess the ability to control the sidelobe of the radiation pattern.

Using Sierpinski gasket as an example A. Lakhtakia [162] showed that the paraxial Fraunhofer-zone diffracted field of a self-similar fractal screen exhibits self-similarity.

C. Peunte-Baliarda [163] described a novel approach to the design of frequency independent systems based on fractal structures. The effort has been focused in describing a technique to design low side-lobe and multiband arrays, which has always been difficult due to the sensitivity of most current design techniques to variations on the operating wavelength.

X. Sun and D. L. Jaggard [164] investigated the reflection and transmission properties of finely divided fractal layers. They observed the behaviour of electromagnetic or optical waves normally incident upon generalized Cantor bar fractal multilayers for various fractal dimensions and stages of growth.

D. H. Werner et al. [165] proposed a technique for generating sum and difference pattern using Sierpinski carpet based fractal subarrays.

M. Lehman and M. Garavaglia [166] obtained the input impedance and the reflectance for a multilayer structure with periodic and fractal distribution and demonstrated how it shows a self similar behaviour according to the type of the structure.

D. L. Jaggard and Y. Kim [167] introduced the concept of band limited fractals and used to describe the diffraction of electromagnetic and optical waves by irregular structures. They demonstrated it through the example of plane-wave diffraction by a fractal phase screen of finite extent.

D. L. Jaggard and X. Sun [168] considered the scattering of electromagnetic waves from perfectly conducting fractal surfaces. The surface was modeled by a multiscaled bandlimited continuous fractal function. They analytically developed a generalized Rayleigh solution for electromagnetic wave scattering from such fractal surfaces. After examining the convergence of Rayleigh systems, they numerically

calculated the coupling strengths and related the angular scattering energy distribution to the fractal descriptors of the surface.

E. Jakeman [169] investigated on the scattering by a corrugated random surface with fractal slope. Wu and Hu [170] studied the phase transitions on more complex Sierpinski carpets. Variations of the critical exponents with various geometric factors and the scaling of resistor networks are examined.

Reflection and transmission properties of polyadic fractal superlattices are formulated, solved analytically, and characterized for variations in fractal dimension, lacunarity, number of gaps, stage of growth, and angle of incidence by A. D. Jaggard and D. L. Jaggard [171].

D. L. Jaggard and X. Sun [172] investigated and characterized the reflection and transmission properties of finely divided fractal layers.

The surface impedance of two thin metallic films of different fractal structures realized on printed circuits have been measured in free-space over the frequency range 10 GHz to 20 GHz by E. Troncet et al [173]. A modeling scheme based on Maxwell's equations and Fresnel's diffraction theory is proposed.

C. Puente Baliarda et al. [174] presented a model that explains the behaviour of the Sierpinski fractal antenna. The model is applied to predict the behaviour of the Sierpinski fractal antenna when the flare angle is modified and its validity is assessed by comparing its predictions with measured data.

D. H. Werner and S. Ganguly [175] has presented a comprehensive overview of recent developments in the rapid growing field of fractal antenna engineering.

J. P. Gianvittorio et al [176] designed frequency selective surfaces using the iterative techniques of fractals which exhibit two or three stop bands depending on the number of iterations.

F. Chiadini et al [177] highlighted the self-similarity features of the frequency dependent reflection coefficient of a dielectric cantor prefractal obtained by applying cantor set construction to the optical layer lengths.

L Zhou et al [178] studied the reflective properties of a small dielectric plate covered with fractal like metallic pattern generated by a particular type of space filling curves. They observed both experimentally and theoretically that the plate could reflect electromagnetic waves in a multitude of frequencies, generated from a near field monopole antenna.

C. T. P. Song et al [179] demonstrated a novel method for designing a wideband quasi-log periodic monopole antenna based on the principles of the fractal Sierpinski gasket and circular disk monopole.

D. H. Werner et al [180] presented a novel method for designing reconfigurable multi-band linear and planar antenna arrays.

D. H. Werner et al [181] proposed a methodology for exploiting the self-similarity and symmetry in the geometrical structure of fractal arrays to develop fast algorithms for calculating the impedance matrix and driving point impedance.

From the above review of past work in the field, it is clear that many researchers have studied the scattering properties of strip gratings and to reduce RCS of targets using strip grating technique. No work has been reported for reducing RCS of a target using fractal based metallo-dielectric structure. This thesis is the outcome of the investigations carried out to reduce the RCS of targets by applying Metallo-Dielectric Structures

(MDS) based on fractal geometries on the target surfaces. The scattering characteristics of simple targets like flat plate, dihedral corner and cylinder loaded with MDS are investigated.

METHODOLOGY

This chapter highlights the methodology adopted for the work presented in this thesis. Description of the different types of targets investigated and their fabrication details are presented. The measurement techniques as well as the essential facilities used for the study are also described.

3.1 OVERVIEW OF RCS MEASUREMENT SYSTEMS

During the past several years, the increasing interest in the radar signature reduction techniques has induced the development of Radar Cross Section (RCS) measurement facilities. The demand for accurate measurements of radar reflectivity of targets has resulted in proliferation of RCS measurement systems. Technological advances in coherent waveform generation, along with high speed digital signal processing, have opened door for utilizing the radar for target identification and classification. In RCS measurements, the response of the target is analyzed by bouncing radar signals off the targets and picking up the returned signals with the receiving antenna.

An RCS measurement system has the following basic elements.

- An Instrumentation radar capable of launching and receiving a microwave signal of sufficient intensity
- Data processing and recording equipments
- A low reflection environment
- Target support fixture and turn table

Nowadays, there are numerous commercial and in-house radars that cover wide frequency range and bands centered at different frequencies in the microwave region. The various radar systems include continuous wave (CW), frequency modulated CW (FMCW), interrupted FMCW, pulsed, etc. Almost all systems in use today are coherent, that is, they are capable of measuring both amplitude and phase.

A low reflection environment is an outdoor test range or an indoor chamber whose walls are covered with absorbing materials to reduce reflection. The target is supported on a specially designed support fixture with low reflectivity. The target support is fixed on a turn table. For accurate measurements, the target must be at sufficiently long distance from the radar so that the incident electromagnetic wave is plane over the target.

To allow the selection of an appropriate RCS measurement system, the system performance required for a given application must be specified. Key performance criteria include frequency coverage, range of targets and measurement accuracy. Depending on the application, RCS may be measured as a function of target position, frequency, transmit-receive polarization or bistatic angle between the transmitter and receiver. The potential errors in RCS measurements can be reduced by means of careful instrumentation and facility design.

A linear relationship between the final processed amplitude or phase of a detected signal relative to the amplitude and phase of the input signal must be maintained over the operating dynamic range, when accurate measurements are to be made. The absolute accuracy of the RCS measurements is dependent on the validity of primary system calibration and system stability. The primary system calibration is generally accomplished by replacing the target with a reflector of known RCS.

In the present work, measurements are carried out using HP 8510C/ Rohde & Schwarz ZVB 20 vector network analyzer. The targets are fixed on a turn table kept inside an anechoic chamber.

3.2 MAJOR FACILITIES USED IN RCS MEASUREMENTS

3.2.1 ANECHOIC CHAMBER

In indoor antenna pattern and RCS measurements, the reflections from the surrounding walls, objects and external radiation may create errors. Proper care has to be taken to avoid such spurious reflections for better accuracy. Hence RCS measurements are conducted in a facility called “Anechoic chamber” for avoiding spurious reflections.

An anechoic chamber is an artificially simulated free space environment in which the electromagnetic wave propagation studies can be performed with good accuracy. This is a large room whose interior portions are covered with microwave absorbers, having good coefficient of absorption in the frequency range of interest. Instead of flat sheet absorbers, pyramidal and wedge shaped absorbers are used to reduce the reflections further. In the present chamber, commercially available polyurethane foam based microwave absorbing material is used for covering the inner walls and floor of the chamber. Electromagnetic interference shielding is provided by putting thin aluminium sheets between the absorbers and the walls of the room.

Monostatic RCS measurements of different targets were carried out in a tapered anechoic chamber. For bistatic measurements and to study the scattered power distribution, a new facility in an anechoic environment is designed and built up.

3.2.2 NETWORK ANALYSER

A network analyzer is an equipment incorporating swept-frequency measurements to characterize the complex network parameters of a device with high speed and accuracy. Network analysis is accomplished by creating data model of transfer and impedance characteristics of a linear network through stimulus response testing over the frequency band of interest. A vector network analyser measures both the magnitude and phase of the reflection and transmission coefficients.

The main components of a vector network analyzer are, a microwave source, an S-parameter or reflection/transmission test set, frequency converter, detector and a display unit. The sweep oscillator generates RF signal to stimulate the device under test. The transducer, which is the reflection/transmission test unit, is connected between the signal source and the receiver. It has a three fold function. The first is to split the incoming signal into reference and test signals. Secondly it is capable of extending the electrical length of reference channel, so that the distances traveled by the reference and test signals are equal. Finally it connects the system properly for transmission or reflection measurements. In the receiver, the harmonic converter mixes the RF signal with a local oscillator output and the resultant IF is given to the display unit.

An HP 8510C vector network analyzer is used for the monostatic RCS measurements of different targets described in this work. This is a fully computer controlled system capable of measuring transmission and reflection characteristics of passive and active networks in the form of

gain, S-parameters and normalized impedance in the range of 45 MHz to 20 GHz. This system uses HP 8341B sweep oscillator and HP 8514 S - parameter test set. Measurements can be done either in ramp or stepped sweep mode. The ramp sweep mode is fast enough to make real-time measurements. The stepped sweep mode is more accurate but slower as it synthesizes each measured frequency.

The measurement results can be displayed on one of the independent channels of the network analyzer. The channels can be displayed simultaneously with results presented in logarithmic/linear magnitude, phase or group delay format or polar coordinates. With time domain gating technique, undesired responses can be removed, thereby increasing the accuracy of measurement. The measured data is acquired and stored in a PC interfaced with the network analyser.

3.2.3 TARGET POSITIONER AND CONTROLLER

For measuring RCS pattern, the target is rotated about a vertical axis in the azimuth plane keeping the transmitter antenna stationary. A target positioner (turn table) which can be controlled using a PC is used for the pattern measurement. A stepper motor based turn table is used so as to rotate the target to the required angle and take the measurements.

3.3 MEASUREMENT TECHNIQUES

Monostatic measurements are done in a tapered anechoic chamber. The target is mounted on a target support which is a thin, cylindrical

column made of wood which is attached to the turn table, kept at the quiet zone of the chamber. The target alignment combines the use of laser beam reflections from the target and visual sighting techniques, depending on the target geometry. A set of wideband horn antennas is used to illuminate the target and measure the backscattered power. The two horn antennas are arranged with a small bistatic angle of 3° . The error incurred in RCS measurements by this bistatic angle is negligible. Microwave absorbing materials are interposed between two antennas to avoid leakage from transmitter to receiver. Schematic of the measurement setup is shown in figure 1.

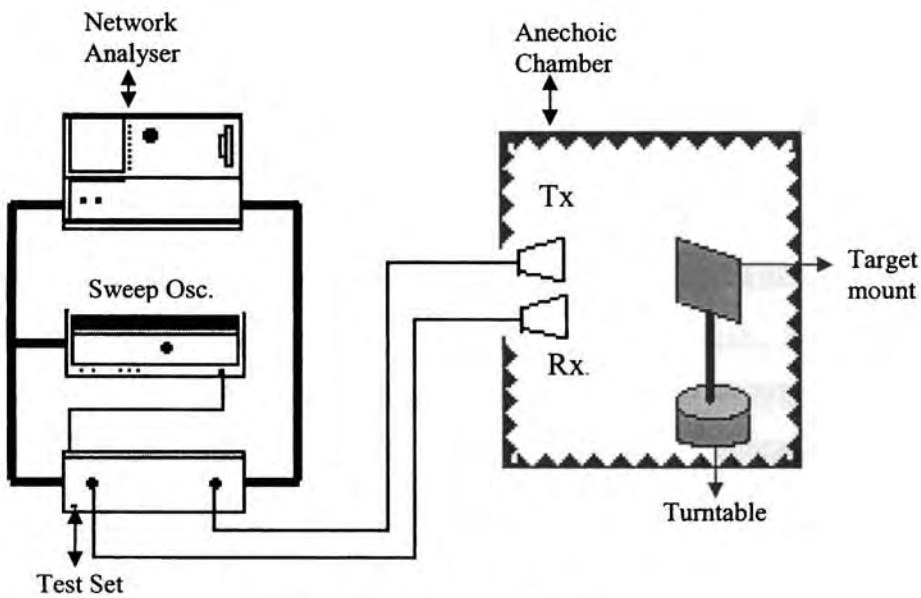


Figure 1 Measurement setup

The RCS measurement system uses a calibration technique which allows the internal error correction capabilities of HP 8510 C to calibrate the anechoic chamber without target. The transmission coefficient (S_{21}) of the anechoic chamber without target is first measured. Then the reference

target is placed and a THRU RESPONSE calibration is performed in the Network Analyser and stored in the CAL SET. The result of empty chamber and reference target measurements are used to generate calibration coefficients used in error correction of the system so that the background return is directly removed from the measurements.

For getting the RCS patterns, the positioner moves the target to the start angle of measurement. Network analyzer is triggered to take measurements and computer acquires the data for this position. After that, a control pulse is sent to the positioner to move through the next step angle and another pulse will be sent back to the computer for reading this data. Thus the data is acquired for each step angle of measurement. The measured data is stored in the computer which can be used for obtaining the RCS pattern at the desired frequency.

3.3.1 ARCH METHOD

The Arch method is used to study the distribution of scattered power around the target. The setup is indigenously fabricated in an anechoic environment. The Arch is a semicircular wooden frame that allows the transmitting and receiving antennas to be fixed at a constant distance from the centre of the test panel, for a variety of subtended angles. The transmitting antenna mounted on a wooden carriage is placed closed to the arch. The metallo-dielectric structure with proper metallic backing plate is placed on a turntable at the centre of the arch. The receiving antenna is moved on the arch for measuring the scattered power from the target of interest for an angle of 180° . For this, a stepper motor

driven by a microcontroller based unit, interfaced to a PC is used. The measurements are taken using a Rohde & Schwarz ZVB 20 network analyser interfaced to the PC. Photograph of the setup for the arch method is shown in figure 2.

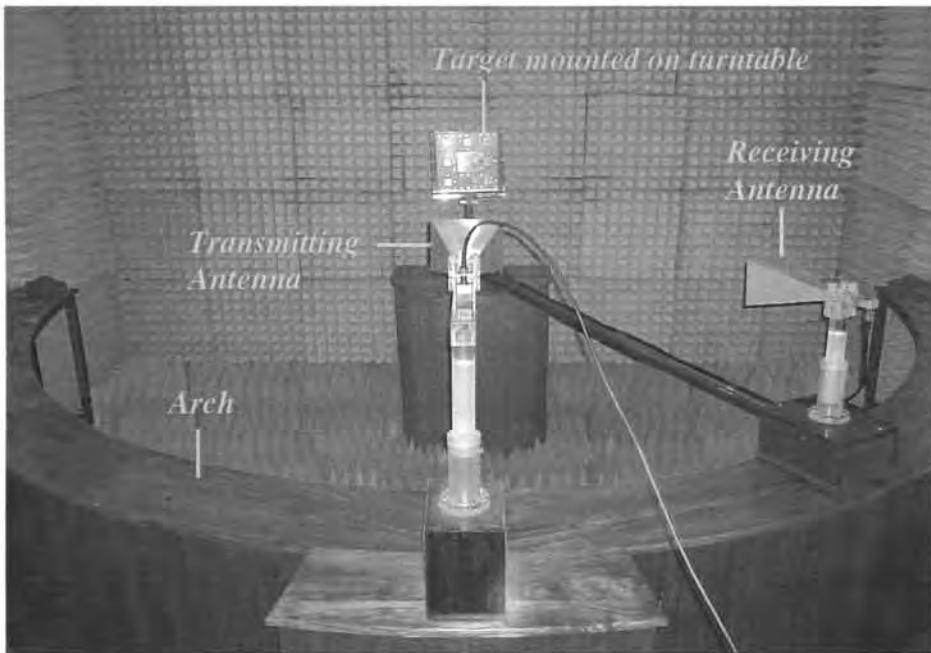


Figure 2 The Arch method

3.4 DESIGN AND FABRICATION OF FRACTAL BASED METALLO-DIELECTRIC STRUCTURES

The work presented in this thesis is on the reduction of backscattered power of metallic targets by loading frequency selective structures or metallo-dielectric structures based on fractal geometries. The

dimensions of the targets considered here are large compared to the wavelength so that the target RCS is in the optical region.

Complex target can be represented as collection of basic target elements like:

- Flat plate
- Cylinder
- Dihedral corner reflector
- Circular cone

Metallo-dielectric structures based on fractal geometries on a dielectric substrate are embedded on these targets so that the incident electromagnetic wave is scattered in the direction away from the radar.

3.5 FLAT PLATES LOADED WITH METALLO-DIELECTRIC STRUCTURES

Flat plate is a simple target characterized by its large RCS for normal incidence. In the present study backscattering reduction of a conducting flat plate of dimension 30 cm X 30 cm is investigated. The following types of metallo-dielectric structures are fabricated and studied.

- Different iterated stages of Sierpinski Carpet fractal geometry
- Different modified geometries of the third iterated stage of Sierpinski carpet fractal geometry
- Sierpinski gasket based metallo-dielectric structure
- Sierpinski carpet fractal geometries with varying lacunarity

➤ Effect of loading superstrates on:

(a) Sierpinski carpet fractal geometry

(b) Sierpinski gasket fractal geometry

3.5.1 METALLO-DIELECTRIC STRUCTURE BASED ON VARIOUS ITERATED STAGES OF SIERPINSKI CARPET FRACTAL GEOMETRY

Scattering measurements are carried out for different iterated stages of Sierpinski carpet on dielectric substrate of different thickness. Fabrication details of the targets are described below. Schematic diagram of reflector backed metallo- dielectric structure with fractal based metallization is shown in figure 3.

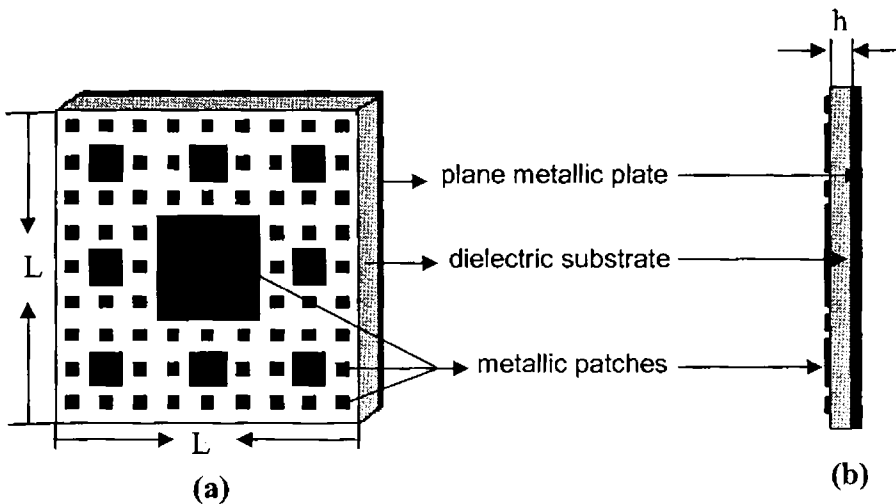


Figure 3 Schematic diagram of reflector backed fractal based metallo-dielectric structure, $L = 30$ cm, $h =$ substrate thickness
(a) Fractal based (b) Side view

A plane metallic (usually aluminium to reduce weight) plate of dimension 30 cm X 30 cm² is machined and polished to make it perfectly flat and reflective. A metal embedded, dielectric sheet of uniform thickness

(h) and dielectric constant $\epsilon_r = 2.56$ is loaded to one surface of the flat plate. Metallizations based on Sierpinski carpet fractal geometry are made over the dielectric sheet by conventional etching technique.

Various iterated stages of Sierpinski carpet fractal geometries fabricated for the study are shown in figure 4. The dimension of the Sierpinski carpet used is 1.89. Scattering measurements are done for each iterated stage by varying the dielectric thickness required for minimum backscattering is found.

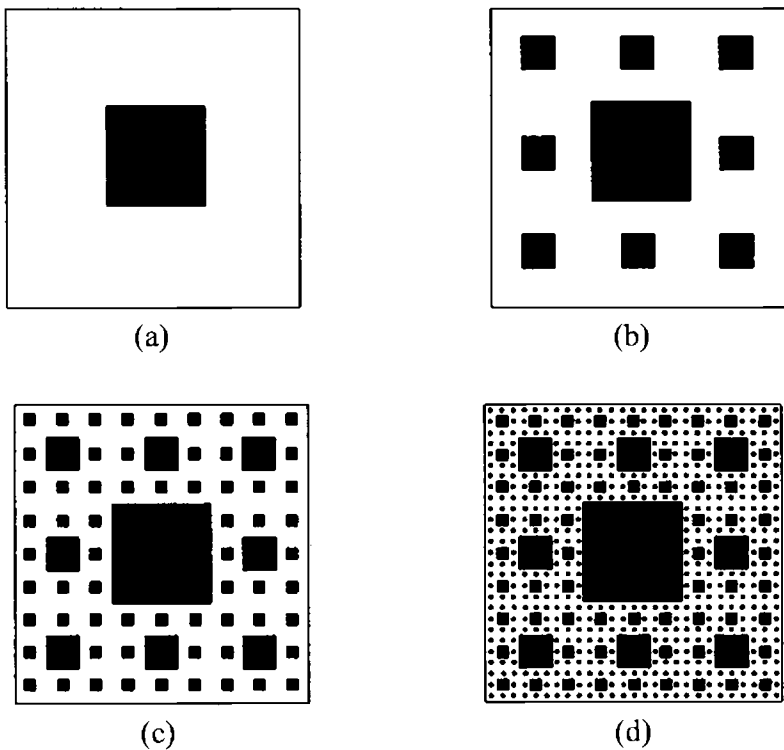
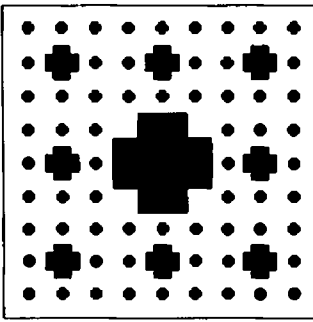


Figure 4 Iterated stages of Sierpinski carpet geometry, dimension $D = 1.89$

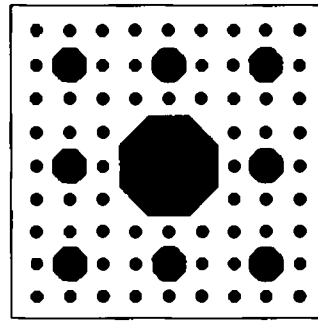
- (a) Stage 1 (b) Stage 2
(c) Stage 3 (d) Stage 4

3.5.2 STRUCTURES BASED ON THE THIRD ITERATED STAGE OF SIERPINSKI CARPET FRACTAL GEOMETRY WITH GENERATORS OF DIFFERENT SHAPES

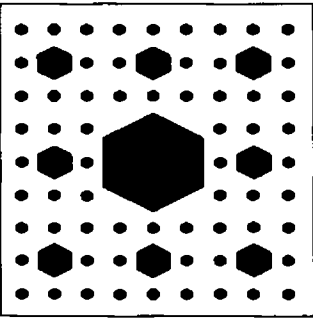
To study the effect of the shape of individual elements on backscattering, Sierpinski carpet fractal geometries with patches of different shapes are fabricated as shown in figure 5.



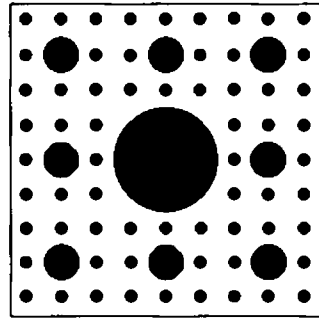
Cross



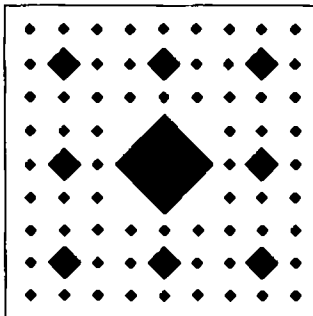
Octagon



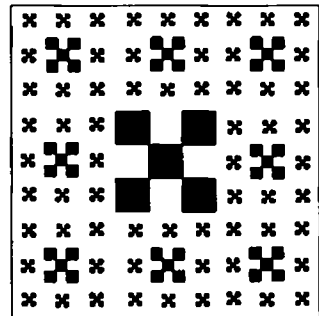
Hexagon



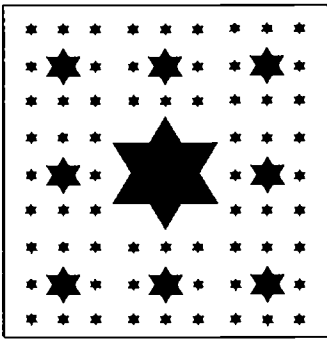
Circle



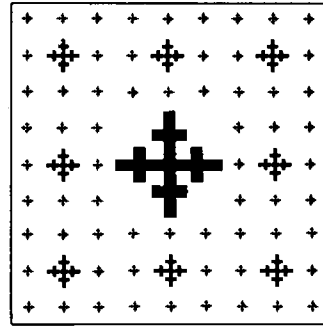
Diamond



Purina square



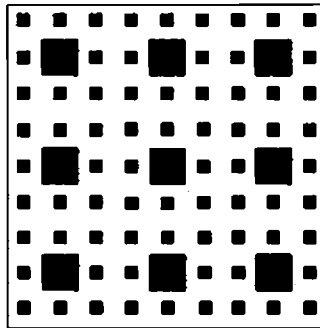
Star



Cross bar tree

Figure 5 Top view of the third iterated stage of Sierpinski carpet fractal geometries with patches of different shapes

All these fractals possess the same initiator but with generators of different shapes. Here also dielectric thickness is varied to get maximum reduction in backscattered power. Also, the scattering properties of an array of the second iterated stage of Sierpinski carpet fractal geometry shown in figure 6 is investigated.



Sierpinski carpet array

Figure 6 Top view of the array of second iterated stage of the Sierpinski carpet fractal geometry

3.5.3 SIERPINSKI GASKET BASED METALLISATION

The third iterated stage of the Sierpinski gasket fractal geometry with fractal dimension $D = 1.585$ is shown in Figure 7 (a). Four such structures are combined to form a square as shown in Figure 7 (b). The metallization is fabricated by photo etching on a dielectric substrate of size $30 \times 30 \text{ cm}^2$ and dielectric constant $\epsilon_r = 2.56$. Measurement is done for different dielectric thickness to find out the optimum value giving maximum reduction in backscattered power in a particular frequency band.

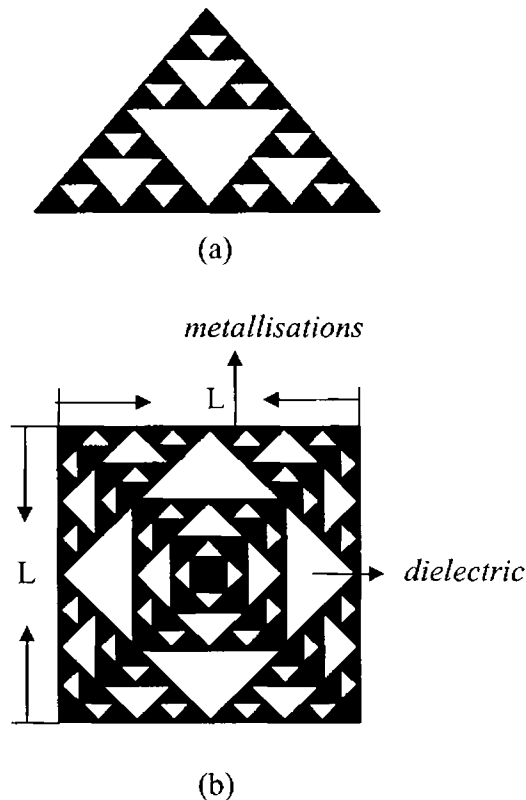


Figure 7 (a) Third iterated stage of Sierpinski gasket
 (b) Top view of metallo-dielectric structure
 $L = 30 \text{ cm}$

3.5.4 SIERPINSKI CARPET FRACTAL GEOMETRIES WITH VARYING LACUNARITY

Different fractals can be constructed that have the same dimension but that looks widely different because they have different lacunarity. Scattering characteristics of Sierpinski carpet with varying lacunarity is described.

The geometries having different lacunarities shown in figure 8 are generated by taking into account a Sierpinski carpet of length 'b' with a metallisation of length 'l'. Here the structure consisting of 'm' subsquares, which denotes the number of squares in a row or column each having length 'n' i.e. $l = m \times n$. As shown in the figure 'p' is the distance between neighboring subsquares, and 'q' is the distance between the square and the outermost subsquares. All the carpets have the same amount of total cut-out area and thus the same fractal dimensionality, but the total cut out has been divided into a different number of holes such that the lacunarity may be varied, while keeping the connectivity fixed. For all the six carpets $b = 30$ cm and $l = 15$ cm. Thus they all have the same $D = \ln(30^2 - 15^2) / \ln 30 = 1.915$. The figure 8 shows the structures L1–L6 in the increasing order of its lacunarity. The parameters of the different structures investigated are given in Table 1.

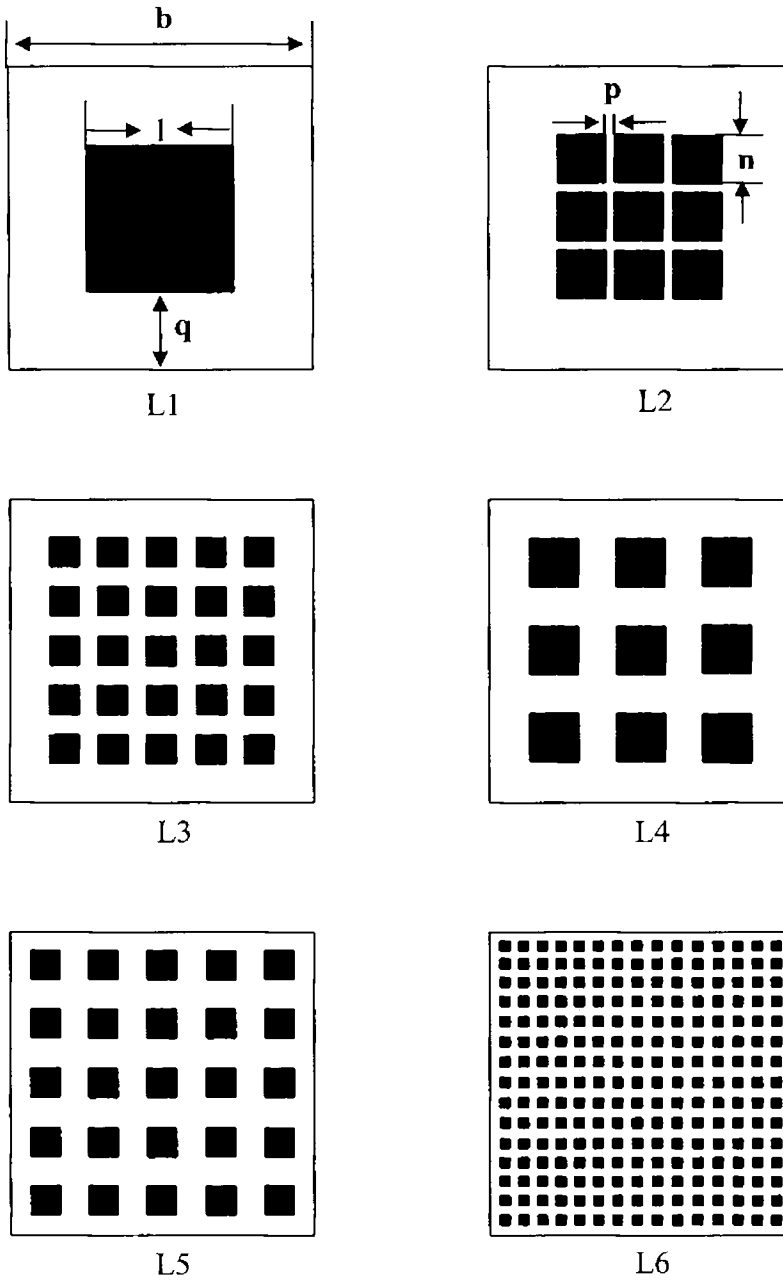


Figure 8 Sierpinski carpets with varying lacunarity with $D = 1.915$

TABLE 1 Parameters of the Sierpinski carpets ($D = 1.915$), $m \times n = 15$ cm

Sierpinski Carpets	n (cm)	m	p (cm)	q (cm)
L1	15	1	0	8
L2	5	3	1	7
L3	3	5	2	4
L4	5	3	4	4
L5	3	5	3	2
L6	1	15	1	1

3.5.5 EFFECT OF LOADING SUPERSTRATES

The frequency at which the minimum backscattering is obtained depends on the dielectric thickness of the metallo-dielectric structure. It has been observed that this frequency can be tuned by loading superstrates. Here the scattering behaviour of superstrates loaded on reflector backed metallo-dielectric structure of different geometries is studied.

Superstrates are loaded over the metallo-dielectric structures of fixed substrate thickness (h). The superstrate thickness (t) is varied and the backscattered power is measured. The experiment is repeated for the metallo-dielectric structures of different dielectric thickness and the backscattered power is compared with that from a plane metallic plate of

same dimension. Schematic of a superstrate loaded metallo-dielectric structure is shown in figure 9.

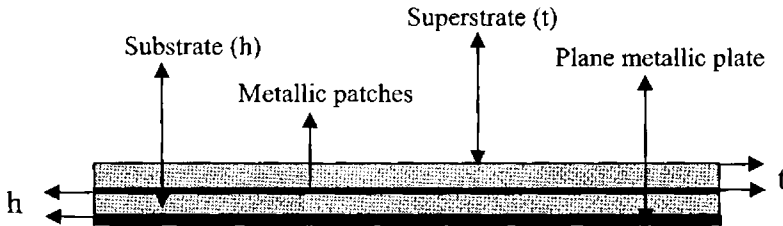


Figure 9 Cross-Sectional view of Superstrate loaded metallo-dielectric structure
 h = Substrate thickness
 t = Superstrate thickness

3.6 3D STRUCTURES

As mentioned earlier the RCS reduction of basic structures which form a complex target is investigated. Fractal based metallo-dielectric structures are applied on the three dimensional shapes such as cylinder, dihedral corner and circular cone and the scattering properties are studied.

3.6.1 Cylinder

The schematic of metallic cylinder loaded with metallo-dielectric structure based on Sierpinski carpet fractal geometry is shown in figure 10. The structure is illuminated using a horn antenna for both TE and TM polarizations and the backscattered power is measured using an identical horn antenna.

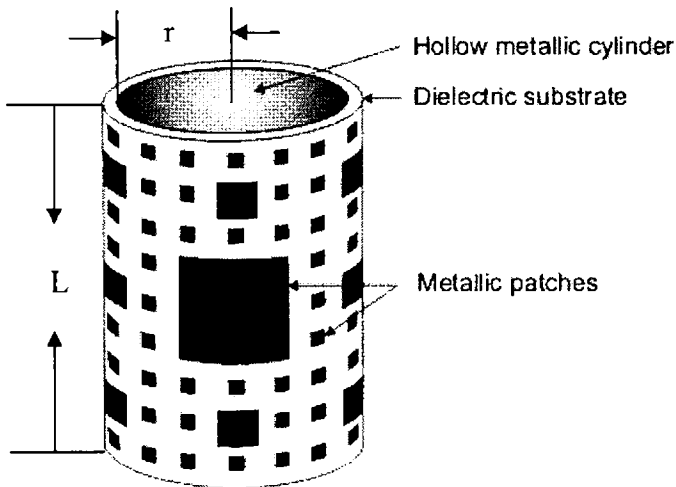


Figure 10 Schematic of metallic cylinder loaded with fractal based metallo-dielectric structure, $L = 30$ cm, $r = 9.55$ cm

Measurements are performed by varying the dielectric thickness for both TE and TM polarizations and the optimum dielectric thickness giving minimum backscattered power is found out. The backscattered power at various angles of incidence is measured by rotating the target. The backscattered power from these structures is compared with that of an unloaded plane metallic plate or cylinder of the same dimension.

3.6.2 Dihedral corner reflector

Right angled dihedral corner reflector provides a large radar cross section over a wide angular range in a plane normal to its wedge. The large echo which arises due to multiple reflections from the two mutually orthogonal flat surfaces dominates the backscattered pattern. The flat surfaces of the dihedral corner reflector are loaded with fractal structures and the backscattering is measured. This is repeated for different corner angles.

The dihedral corner reflector is formed by attaching two square metallic plates of side $L = 30$ cm on a hinge arrangement. The structure is specially designed so as to vary the corner angle precisely from 0 to 180° . The metallization based on Sierpinski carpet fractal geometry is fabricated on a dielectric substrate material of $\epsilon_r = 2.56$ and is inserted in the corner reflector as shown in figure 11. The target under test is mounted on a support which is attached to the turn table kept at the quiet zone of the anechoic chamber. A set of wide band horn antennas are used to illuminate the target and to measure the backscattered field. The measurements are performed for TE and TM polarizations for different

corner angles. Effect of dielectric thickness for each corner angle is studied. A metallic dihedral corner reflector of the same dimension is used as the reference target.

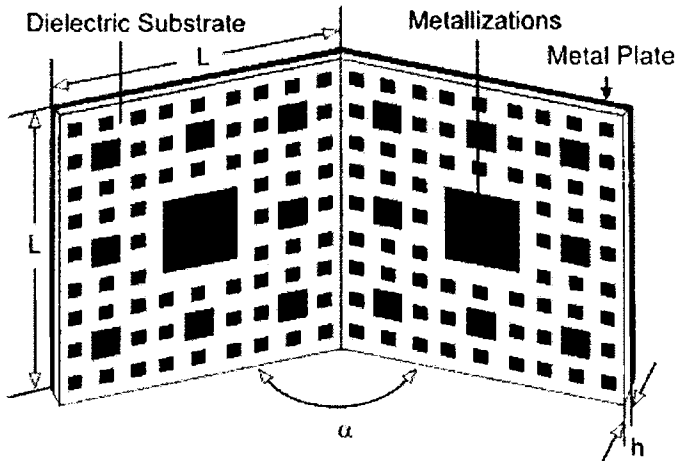


Figure 11 Dihedral corner reflector loaded with fractal based metallo-dielectric structure, $L = 30$ cm

3.6.3 Circular cone

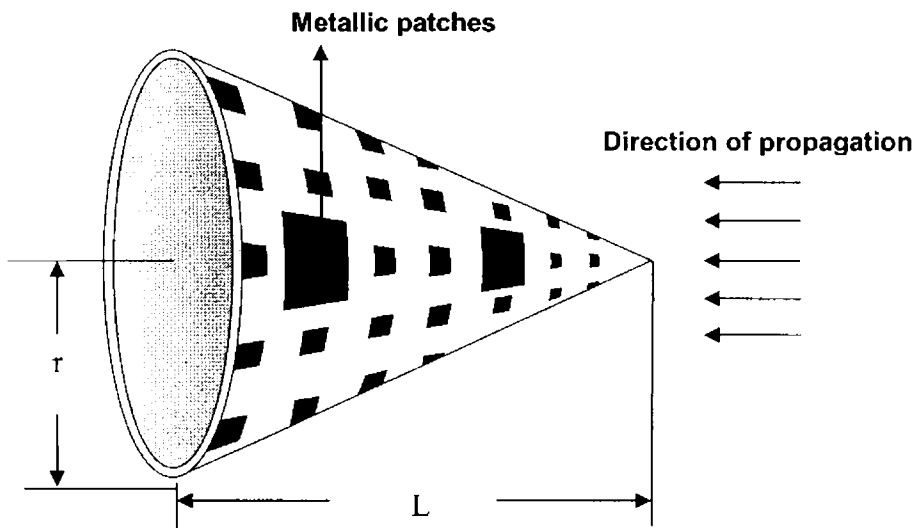


Figure 12 Metallic circular cone loaded with array of Sierpinski carpet fractal geometry, radius = 11 cm, $L = 22$ cm.

A metallic circular cone of outer radius $r = 11$ cm and length $L = 22$ cm is used in the present study. Fractal structure based on the array of Sierpinski carpet is fabricated on a dielectric substrate and is loaded over the metallic cone as shown in figure 12.

The direction of the incident wave is as indicated in the figure. The backscattered power is measured for the structure for different dielectric substrate thickness and is compared with a square metallic plate of same base area of 22 cm^2 . The optimum thickness giving minimum backscattering is found out. The variation of backscattered power for different angles of incidence is measured by rotating the structure on the turntable.

Chapter 4

EXPERIMENTAL RESULTS

This chapter highlights the results of the scattering measurements carried out on different targets such as flat plate cylinder, dihedral corner reflector and circular cone, loaded with metallo-dielectric structures based on fractal geometries. The scattering characteristics of the above targets with different parameters are measured for TE and TM polarizations in C, X and Ku frequency bands.

Reduction of Radar Cross Section (RCS) of targets is of great importance in the design of low detectable targets. The conventional methods of RCS reduction are shaping of targets, use of absorbing materials, passive cancellation and active cancellation. It is also possible to reduce the RCS of targets by modifying its scattering properties so that the scattered energy is diverted away from the radar. This can be achieved by loading dielectric backed metallisations (metallo-dielectric structures) on the target surface.

The results of the scattering measurements carried out on different targets loaded with metallo-dielectric structures based on fractal geometries are described in this chapter. The investigations were carried out in the frequency range 4.5 GHz – 16 GHz. As mentioned in the previous chapter, the following targets which form the basic building blocks of any complex target are investigated.

- Flat plate
- Cylinder
- Dihedral corner reflector
- Circular cone

Fractal based metallo-dielectric structures (MDS) etched on dielectric substrates of different thickness are loaded over these targets. The parameters of the MDS were optimized to produce large reduction in backscattering. The results of the backscattering measurements for TE and TM polarizations of the incident electromagnetic waves are presented and compared with that of the original target.

- TE – polarizations : Magnetic field perpendicular to the plane of incidence
- TM – polarizations : Electric field perpendicular to the plane of incidence

4.1 FLAT PLATES LOADED WITH FRACTAL BASED METALLO-DIELECTRIC STRUCTURES (MDS)

Measurement results of the flat plates loaded with fractal based MDS is presented in this section. The following types of fractal structures were investigated.

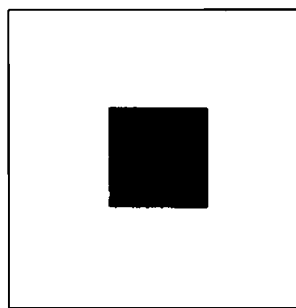
- Different iterated stages of Sierpinski carpet fractal geometry
- Sierpinski carpet fractal geometry with different patch shapes
- Sierpinski gasket based metallo-dielectric structure
- Fractal geometries with varying lacunarity

The scattering characteristics of the above targets were measured for TE and TM polarizations in C, X and Ku bands to study the following.

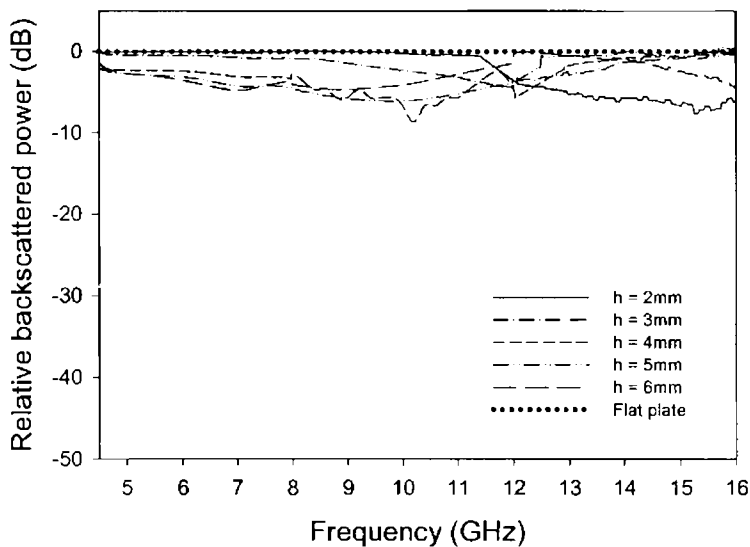
- Variation of backscattered power with frequency
- Variation of backscattered power with angle of incidence.
- Angular distribution of the scattered power
- Change in backscattered power with dielectric thickness, fractal geometry, patch shape and dielectric constant
- Effect of loading superstrates

4.1.1 Different Iterated Stages of Sierpinski Carpet Fractal Geometry

Here, the backscattering measurements were taken for both TE and TM polarized fields incident normally on the target. The first iterated stage of Sierpinski carpet fractal geometry and the scattered power measured for different dielectric thickness compared to that of flat plate of same dimension is shown in figure 4.1. Measured results for the second, third and fourth iterated stages are shown in figures 4.2-4.4.



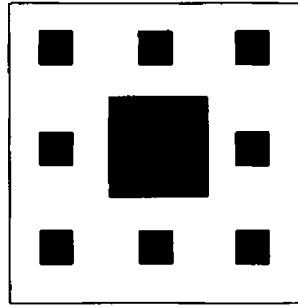
(a)



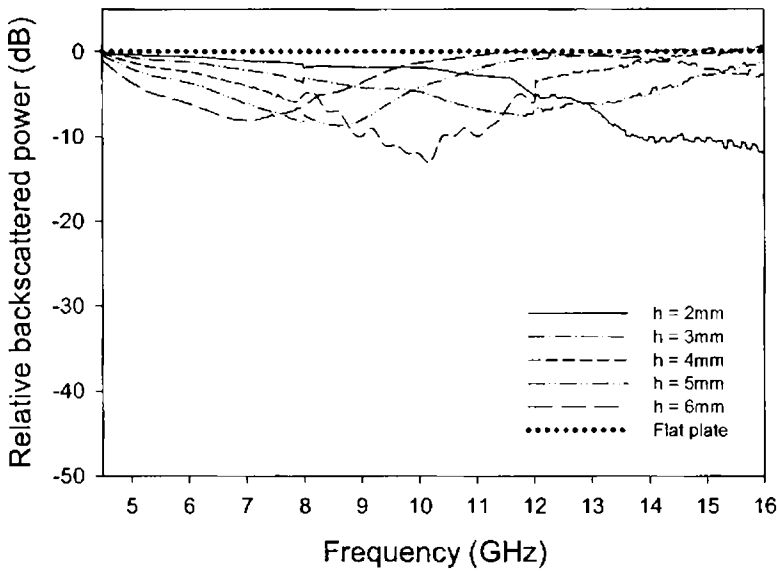
(b)

Figure 4.1 (a) First iterated stage of Sierpinski carpet fractal geometry
(b) Variation of backscattered power with frequency for different dielectric thickness (h)

The backscattered power is measured for normal incidence in the range of frequencies covering C, X and Ku bands. The measurement is repeated for different iterated stages of the Sierpinski carpet fractal geometry. The dielectric thickness is also varied in each case, and the results are shown in figures 4.1-4.4.

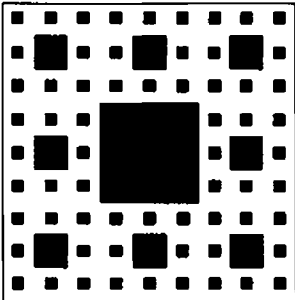


(a)

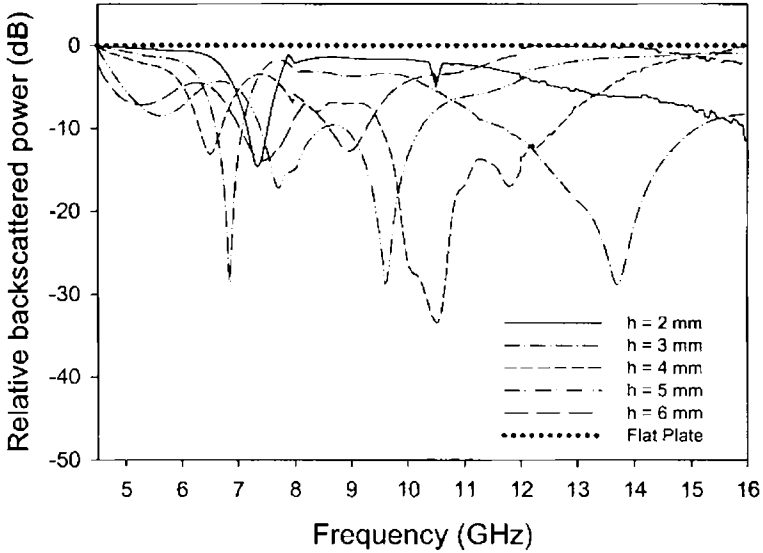


(b)

Figure 4.2 (a) Second iterated stage of Sierpinski carpet
 (b) Variation of backscattered power with frequency for different dielectric thickness (h)

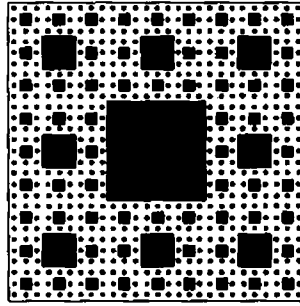


(a)

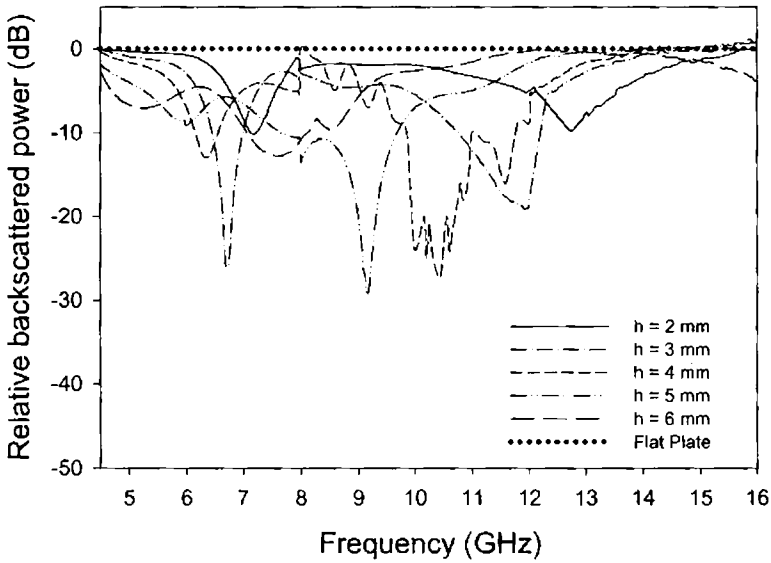


(b)

Figure 4.3 (a) Third iterated stage of Sierpinski carpet
(b) Variation of backscattered power with frequency for different dielectric thickness (h)



(a)



(b)

Figure 4.4 (a) Fourth iterated stage of Sierpinski carpet fractal geometry
 (b) Variation of backscattered power with frequency for different dielectric thickness (h)

It is found that there is no appreciable reduction in backscattered power for the first and second iterated stages. A maximum reduction in backscattered power of -32 dB is obtained at 10.5 GHz for the third iterated stage for a substrate of thickness $h = 4$ mm. It is clear from figure 4.4 that the backscattering obtained for the fourth iterated stage is less than that for the third stage.

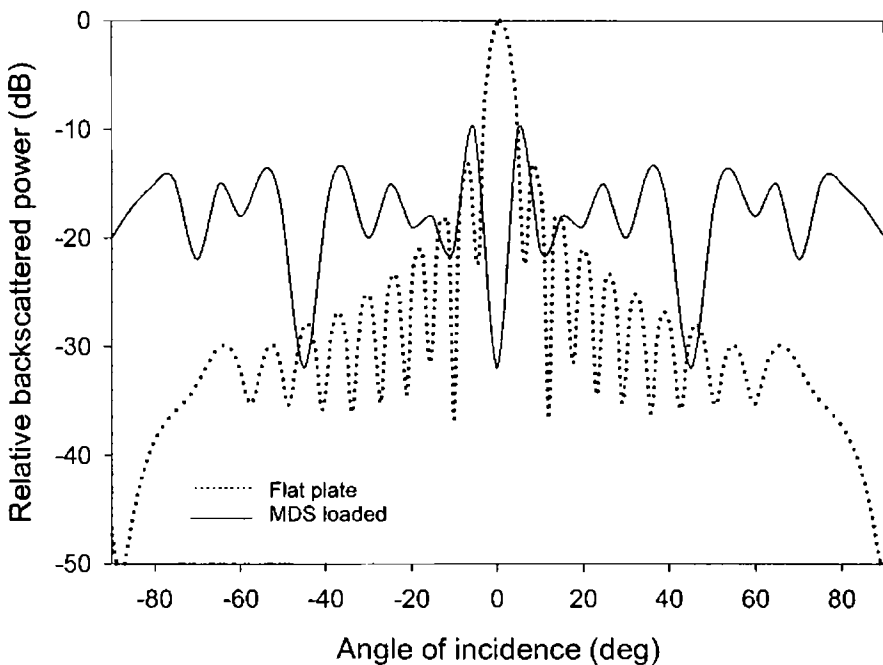


Figure 4.5 Backscattered power variations with angle of incidence for the third iterated stage, $h = 4$ mm, $f = 10.5$ GHz

Since the third iterated stage is giving maximum reduction in backscattered power, it is investigated further. Backscattering is measured for different angles of incidence by rotating the target keeping the transmitter and receiver antennas stationary. The result of this measurement is shown in figure 4.5. It is found that the backscattering is

minimum at normal incidence, for this particular thickness. Maximum backscattered power of -10 dB is obtained at an angle of incidence of 5° .

For a particular angle of incidence, backscattering reduction is obtained by the redistribution of scattered power in other directions. This angular distribution of the scattered power is measured for normal incidence by moving the receiver antenna around the target, keeping the transmitter antenna and target stationary. The power scattered from the structure at various angles is shown in figure 4.6. It is found that the scattered power is distributed symmetrically with respect to the normal in both the azimuth and elevation angular ranges, due to the symmetry in the structure of the target. Maximum backscattered power of -7 dB is obtained for a scattering angle of 10° .

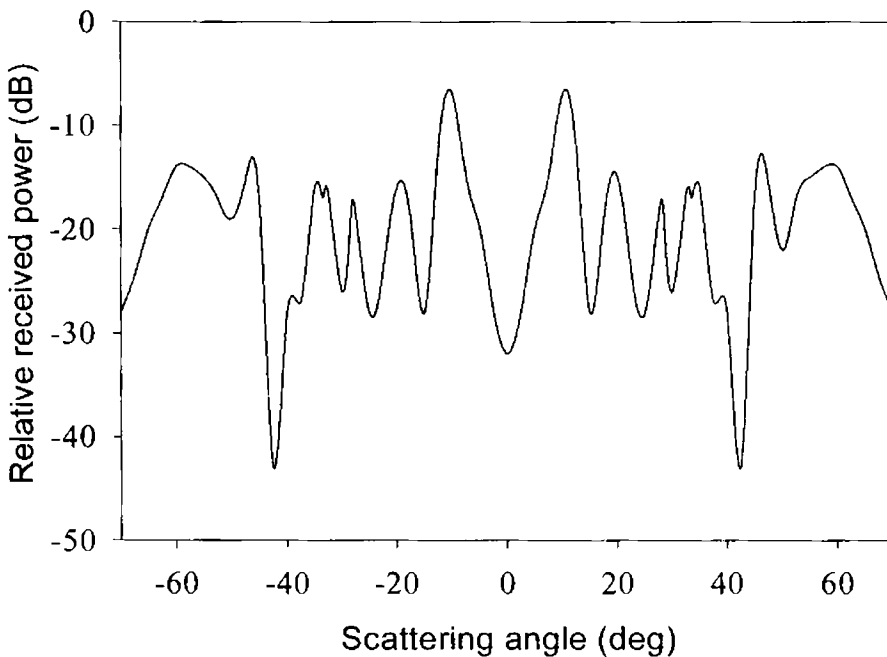


Figure 4.6 Distribution of scattered power along the azimuth for normal incidence for the third iterated stage, $h = 4$ mm, $f = 10.5$ GHz

4.1.2 Sierpinski carpet with different patch shapes

From the previous section it is concluded that the third iterated stage of the Sierpinski carpet fractal structure is giving maximum reduction in backscattered power over a considerable range of frequencies. Therefore this fractal geometry constructed with patches of different shapes as generator and is used for studying the scattering characteristics as described below.

4.1.2.1 Cross

Sierpinski carpet geometry with patches of the shape of Cross is shown in figure 4.7.

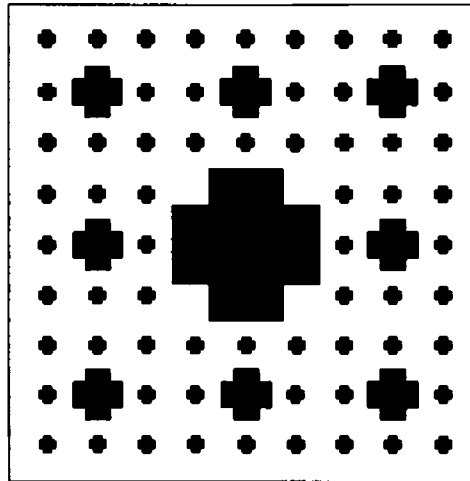
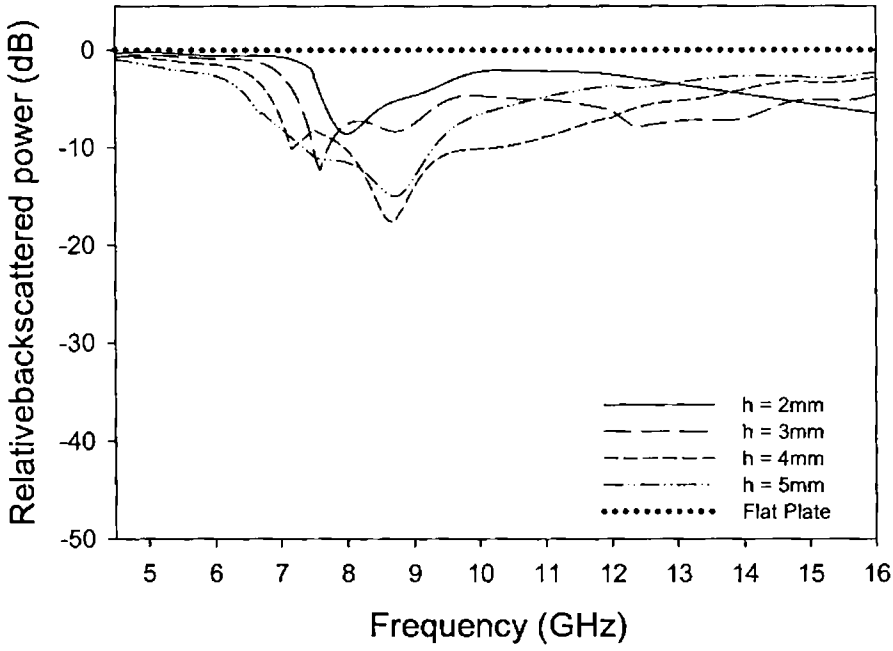
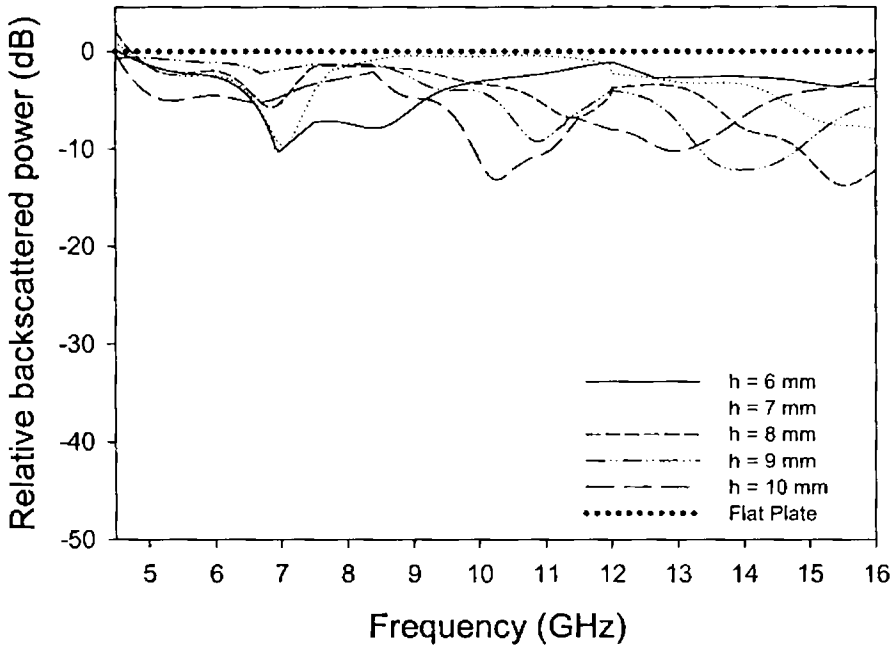


Figure 4.7 Third stage of the Sierpinski carpet fractal with Cross as the generator



(a)



(b)

Figure 4.8 (a) & (b) Backscattering characteristics with frequency for different substrate thickness for the structure with cross shaped generator

Backscattered power is measured in different frequency bands for this structure for different substrate thickness and the results are shown in figures 4.8 (a) and (b). A maximum reduction in backscattered power of -17.6 dB is obtained at 8.65 GHz, for a dielectric thickness $h = 4$ mm.

4.1.2.2 Octagon

Octagonal shaped patches are used to construct fractal based metallo-dielectric structure as shown in figure 4.9.

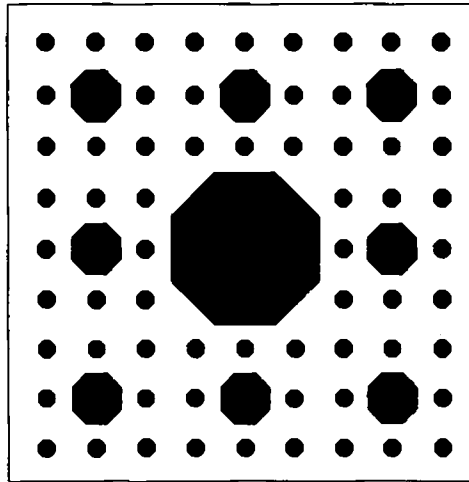


Figure 4.9 Sierpinski carpet with octagon as the generator

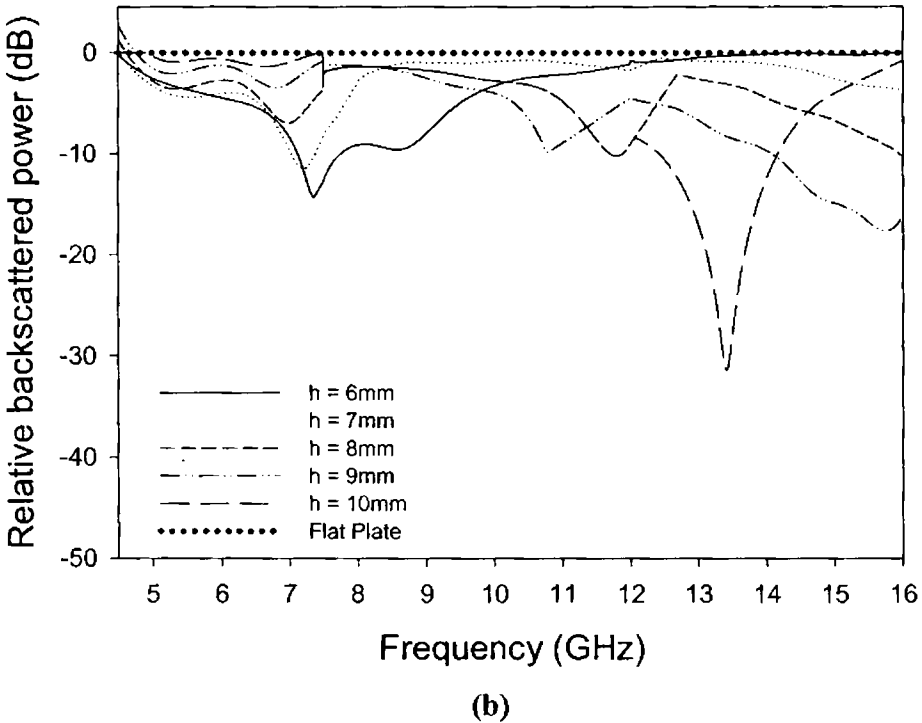
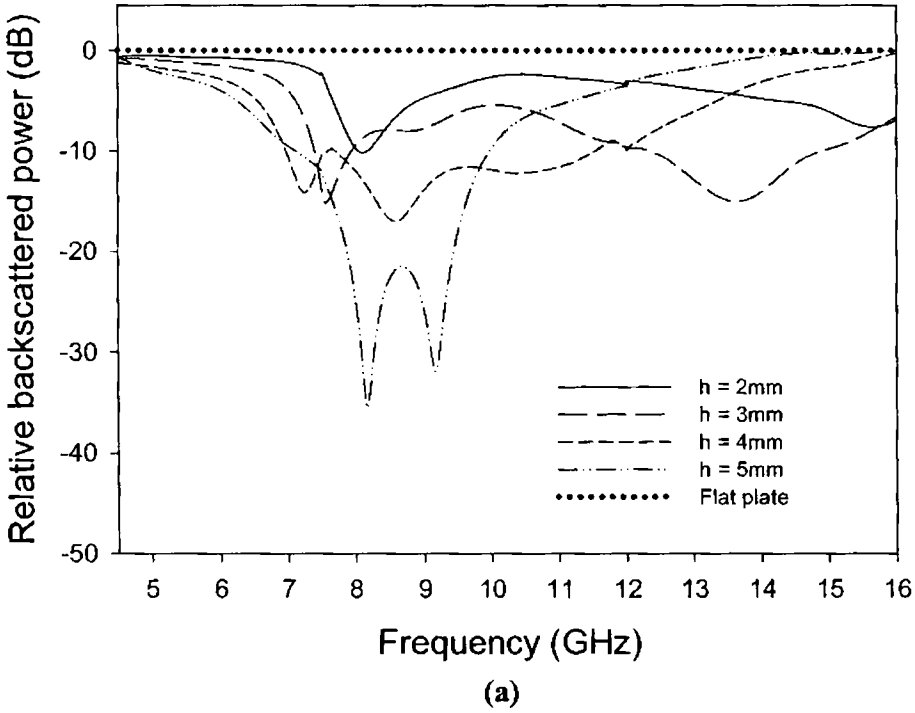


Figure 4.10 (a) & (b) Backscattered power variations with frequency for different substrate thickness for the structure with octagonal patches

Measurement results for the structure in figure 4.9 are shown in figures 4.10 (a) and (b). A maximum reduction in backscattered power of -35.5 dB is obtained at 8.15 GHz for a substrate thickness of 5 mm.

4.1.2.3 Hexagon

Metallo-dielectric structure constructed with hexagonal patches is shown in figure 4.11.

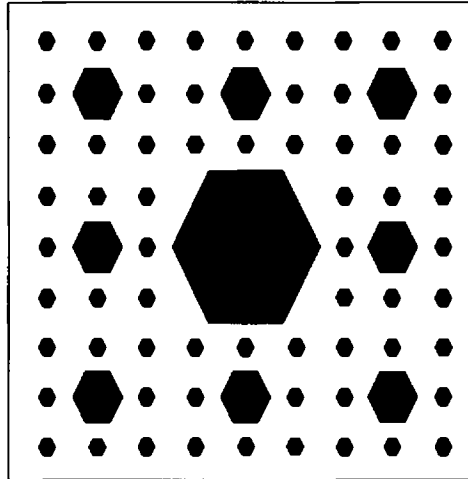
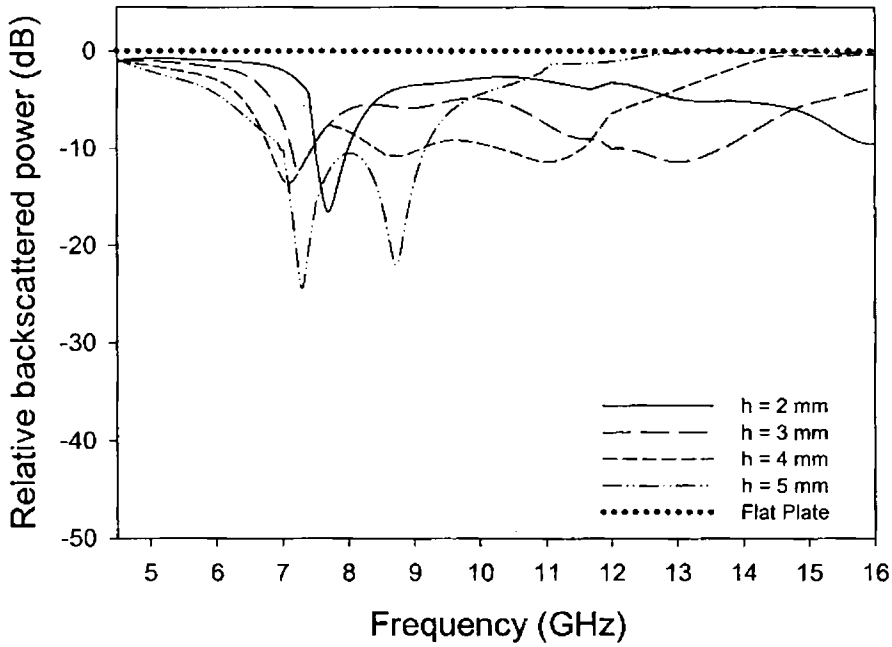
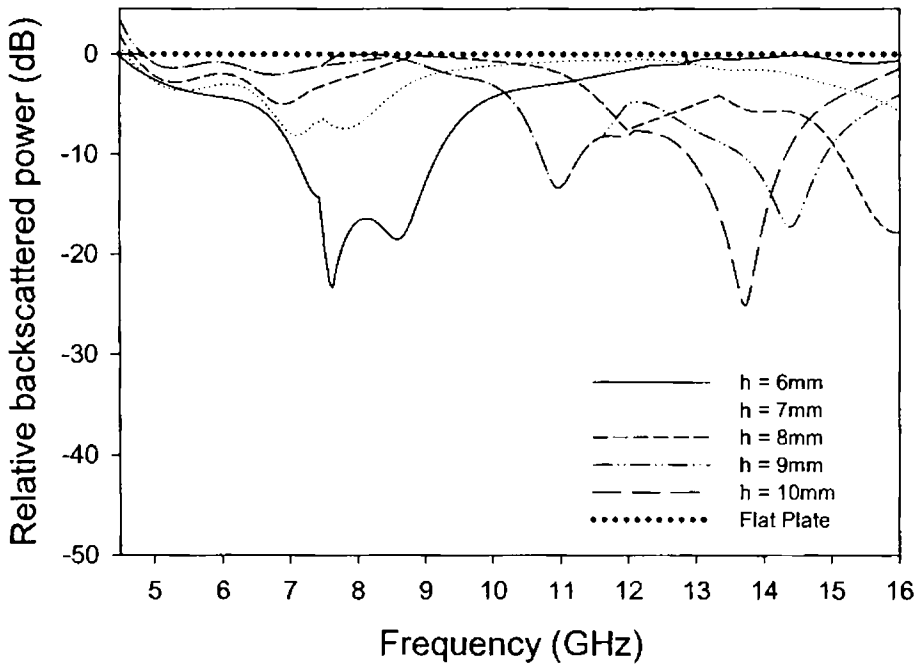


Figure 4.11 Sierpinski carpet with hexagon as the generator

Since the patch shape is not symmetric, scattering measurements are done for both TE and TM polarizations. The experiment is conducted for a large variation of substrate thickness and the measured results for TE polarization is shown in figure 4.12 (a) and (b). An appreciable reduction in backscattered power is obtained at 9.9 GHz for a dielectric thickness of $h=5$ mm. A bandwidth (- 10 dB) of 2.82 GHz is achieved.



(a)

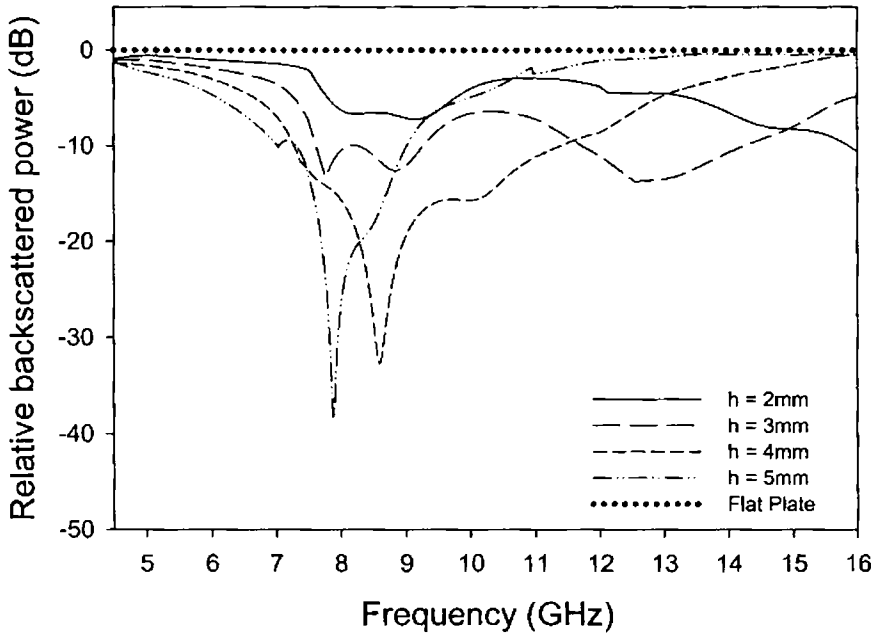


(b)

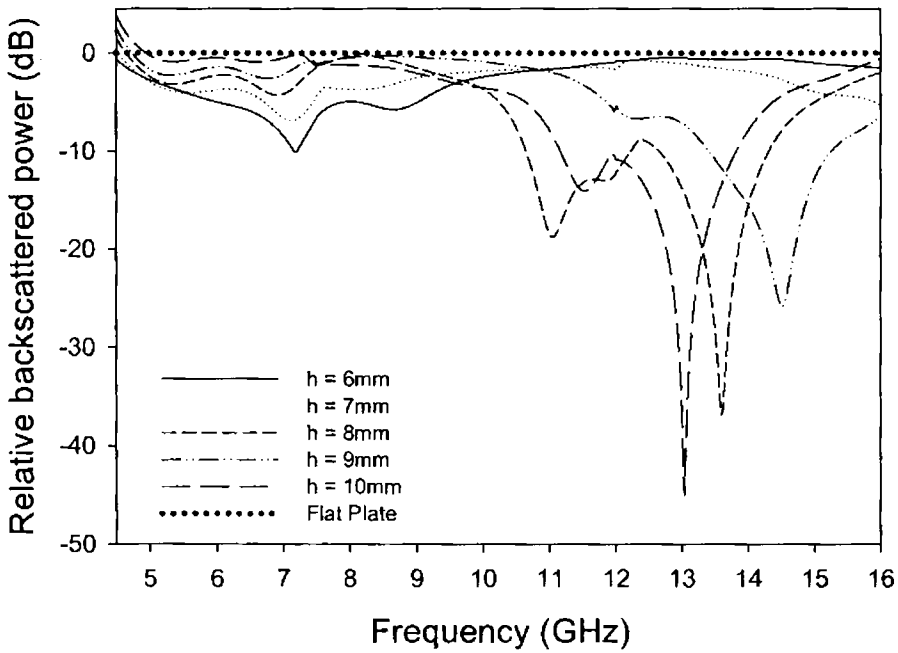
Figure 4.12 (a) & (b) Backscattered power variations with frequency for different substrate thickness for the structure with hexagonal patches for TE polarisation

TM polarization is also showing similar results with the maximum reduction obtained at a slightly different frequency. From figure 4.13 (a) and (b), a maximum reduction in backscattered power of -38 dB is obtained at 8.24 GHz for a substrate thickness of 5 mm. A bandwidth of 2.13 GHz below -10 dB is achieved. Also, this structure is giving a reduction in backscattered power over an appreciable range of frequencies in X-band.

From figure 4-13(b), it is observed that a reduction in backscattered power of about 45 dB is obtained at 13.04 GHz for a thickness $h = 10$ mm apart from the dip at 8.24 GHz. The observations indicate that the metallo-dielectric structure can be optimized to give minimum backscattering at a different frequency by varying the thickness of the substrate. The variation of backscattered power with angle of incidence for the hexagonal shaped fractal for the two frequencies giving minimum backscattering is shown in figure 4.14 (a) and (b).

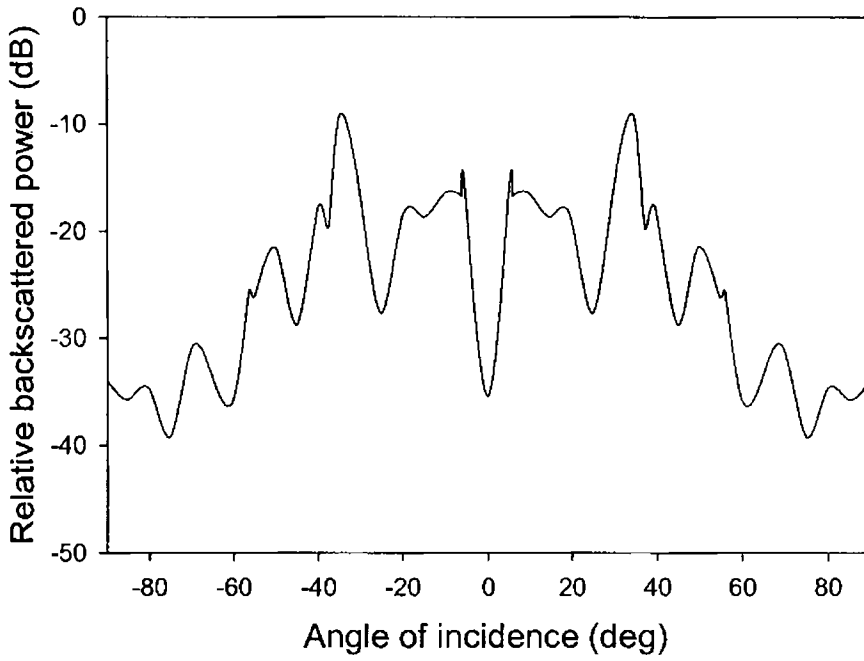


(a)

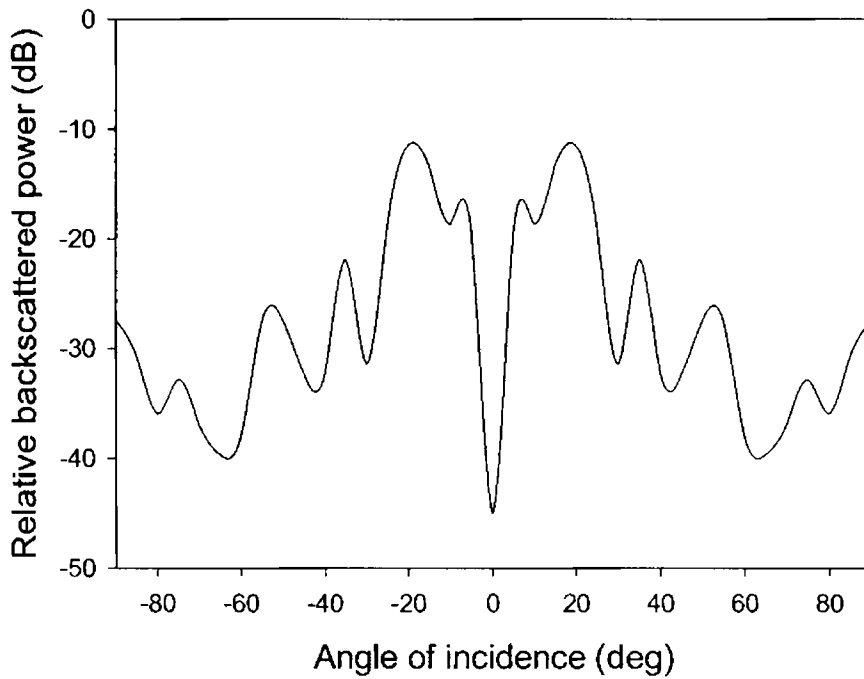


(b)

Figure 4.13 (a) & (b) Backscattered power variations with frequency for different substrate thickness for the structure with hexagonal patches for TM polarisation



(a)



(b)

Figure 4.14 (b) Variation of backscattered power with angle of incidence
(a) $f = 8.24$ GHz $h = 5$ mm
(b) $f = 13.04$ GHz $h = 10$ mm

4.1.2.4 Circle

Third iterated stage of the Sierpinski carpet structure with circular patches as the generator is shown in figure 4.15.

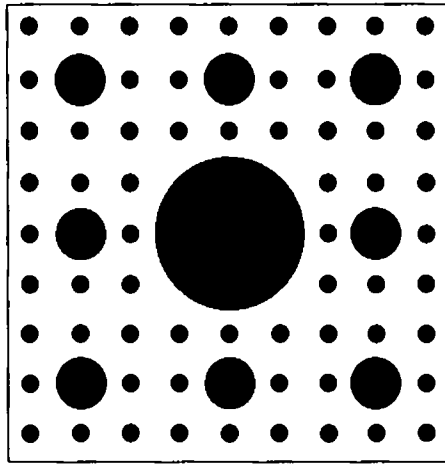
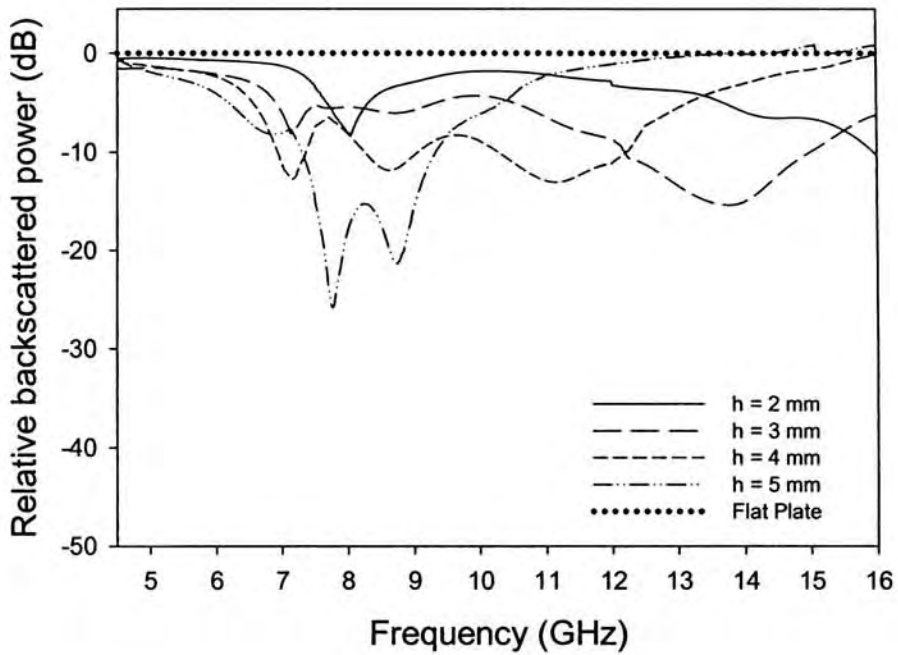
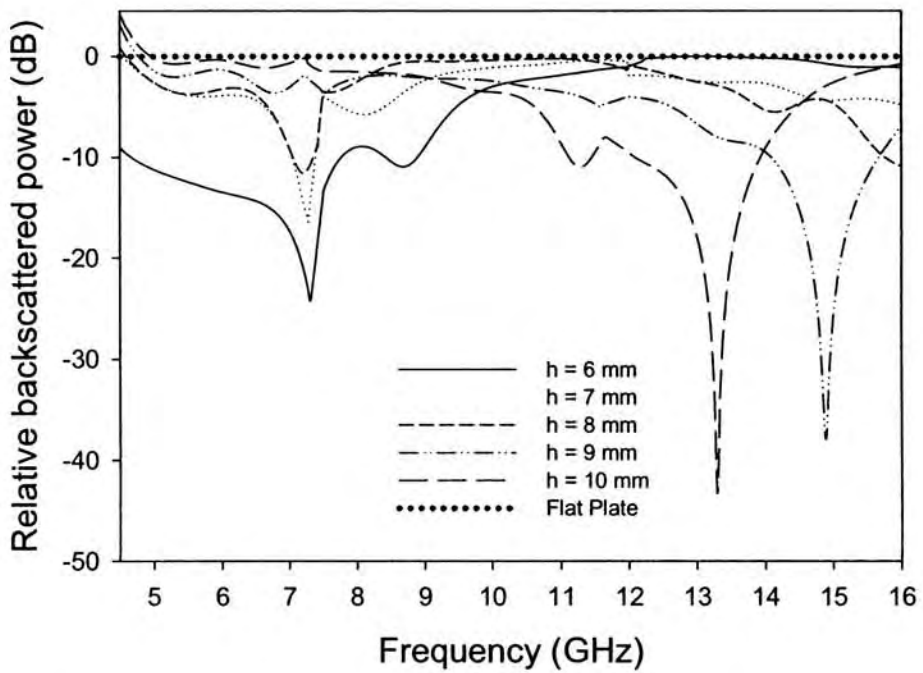


Figure 4.15 Sierpinski carpet with circle as the generator

The reduction in backscattered power with frequency for various substrate thickness for this case is shown in figures 4.16 (a) and (b). This structure is found to give backscattering reduction to an appreciable range of frequencies. The minimum thickness at which an appreciable reduction in backscattered power obtained is $h = 5$ mm. The frequency of minimum backscattering is 7.77 GHz. A bandwidth of 2.57 GHz below -10 dB is achieved for this structure.

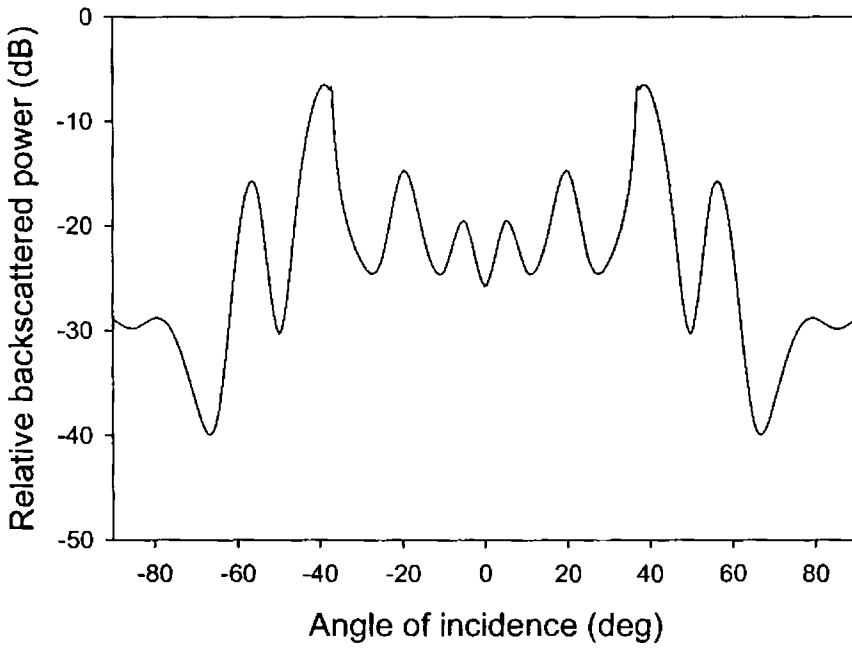


(a)

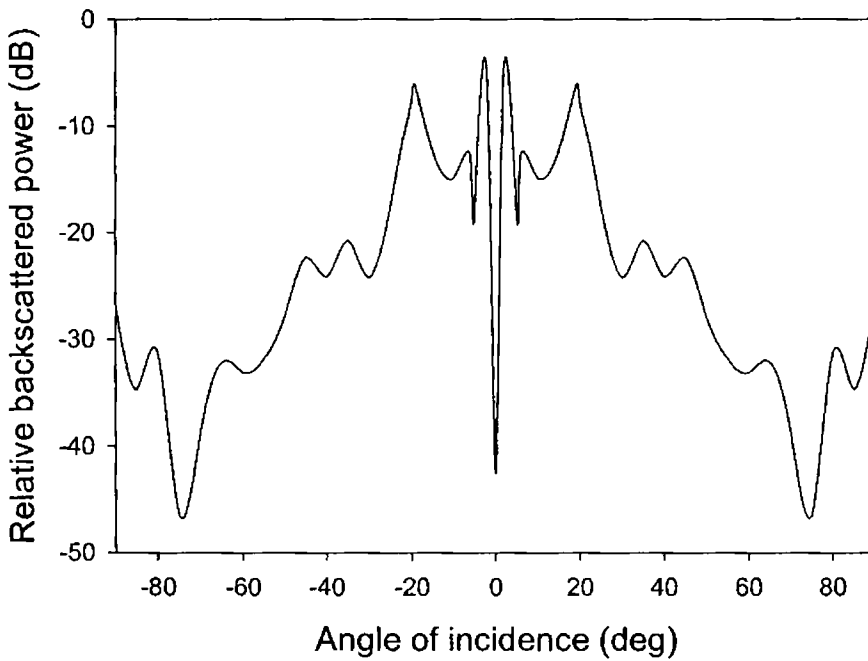


(b)

Figure 4.16 (a) & (b) Variation of backscattered power with frequency for the structure with circular patches



(a)



(b)

Figure 4.17 (b) Backscattered power variations with angle of incidence(a) $f = 7.77$ GHz $h = 5$ mm(b) $f = 13.28$ GHz $h = 10$ mm

Effect of the angle of incidence on the backscattering for this structure at the two frequencies of minimum backscattering are plotted in figures 4.17 (a) and (b).

4.1.2.5 *Diamond*

In this case, diamond shaped patches are used as generator to construct the metallo-dielectric structure and the geometry is shown in figure 4.18.

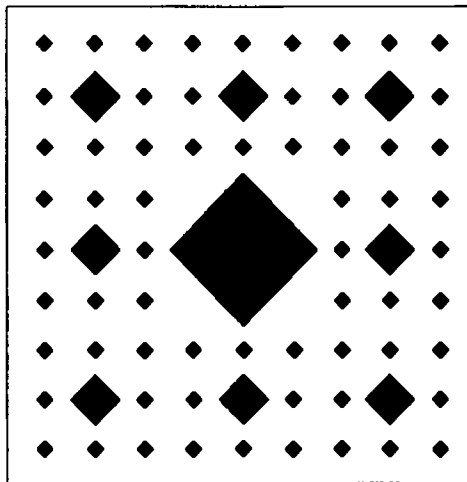
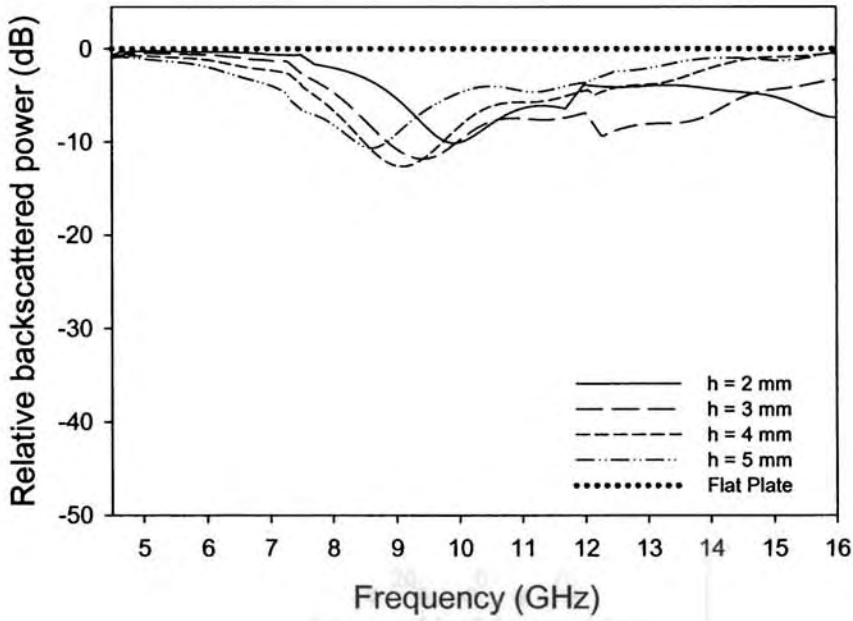
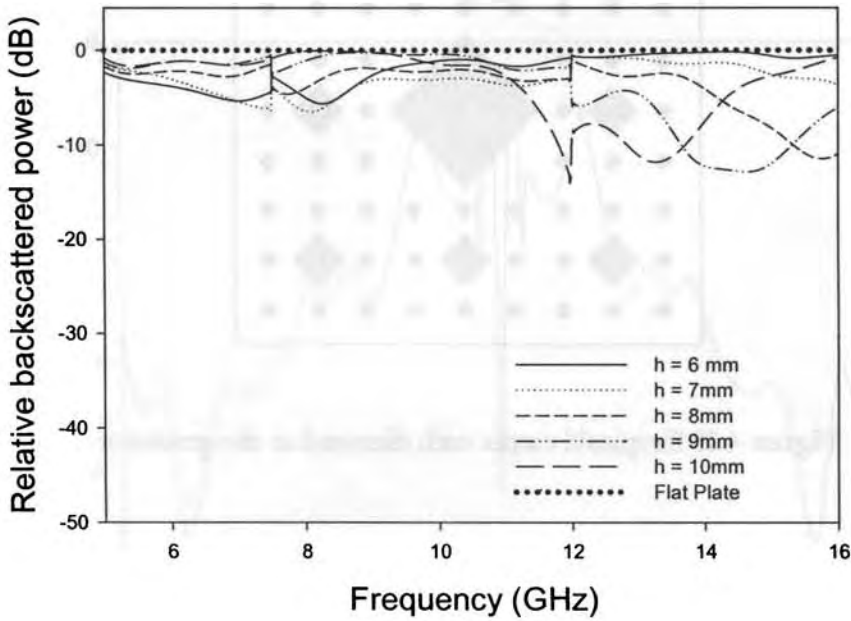


Figure 4.18 Sierpinski carpet with diamond as the generator



(a)



(b)

Figure 4.19 (a) & (b) Backscattered power variations with frequency for different substrate thickness for the structure with diamond shaped patches.

The backscattered power measured at different frequencies for different substrate thickness is shown in figure 4.19 (a) and (b). It is observed that, no considerable reduction in the backscattered power is obtained for this structure.

4.1.2.6 Purina square

Sierpinski carpet with patches of the shape Purina square is shown in figure 4.20. Figure 4.21 (a) and (b) shows the variation of backscattered power with frequency for substrates of various thickness.

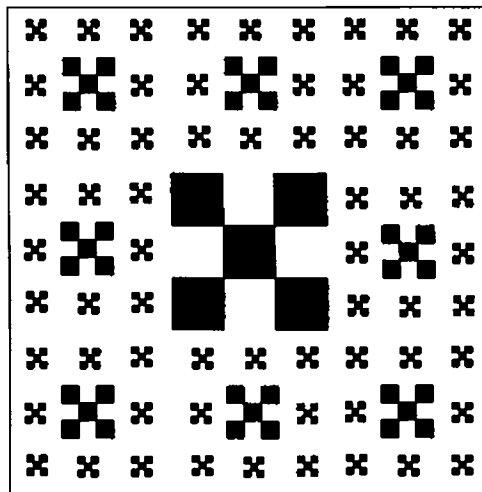
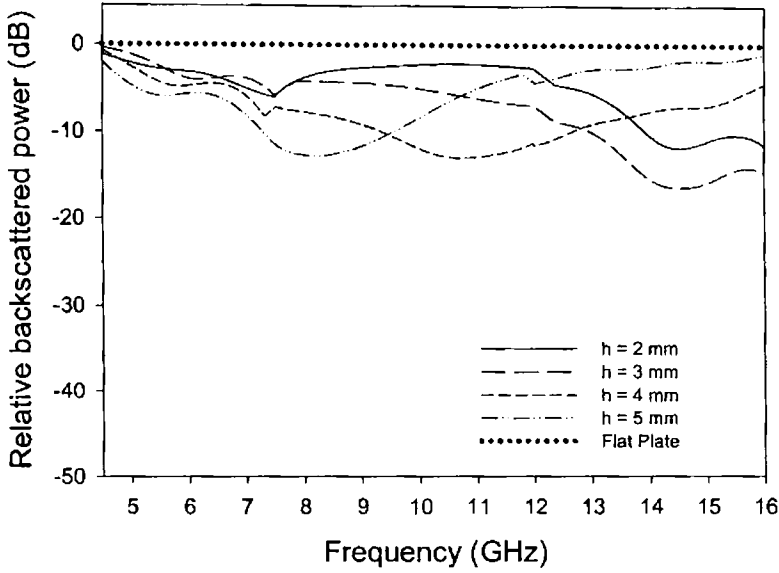
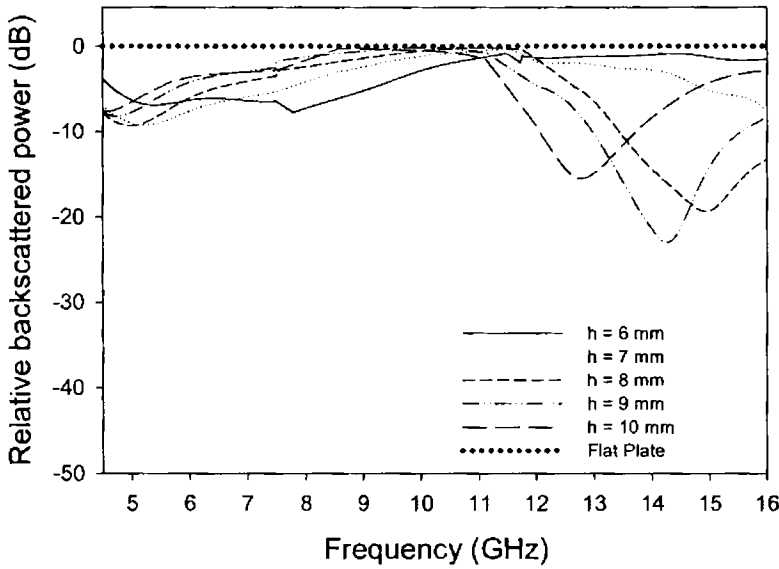


Figure 4.20 Sierpinski carpet with Purina square as the generator

The observations indicate that a maximum reduction in backscattered power of -23 dB is obtained at 14.26 GHz for a dielectric thickness of height, $h = 9$ mm.



(a)



(b)

Figure 4.21 (a) & (b) Variation of backscattered power with frequency for the structure with patches of the shape Purina square

4.1.2.7 Star

The third iterated stage of the Sierpinski carpet fractal geometry with patches of the Star shape is shown in figure 4.22.

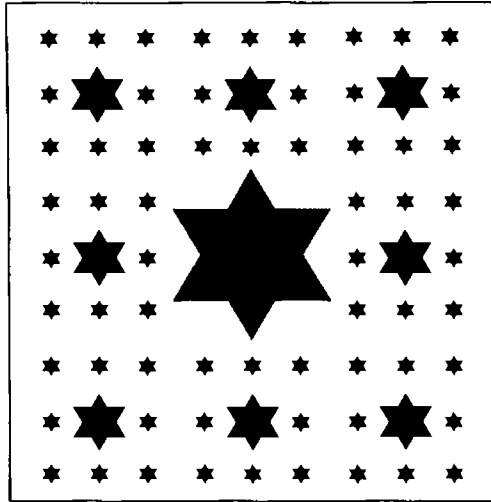
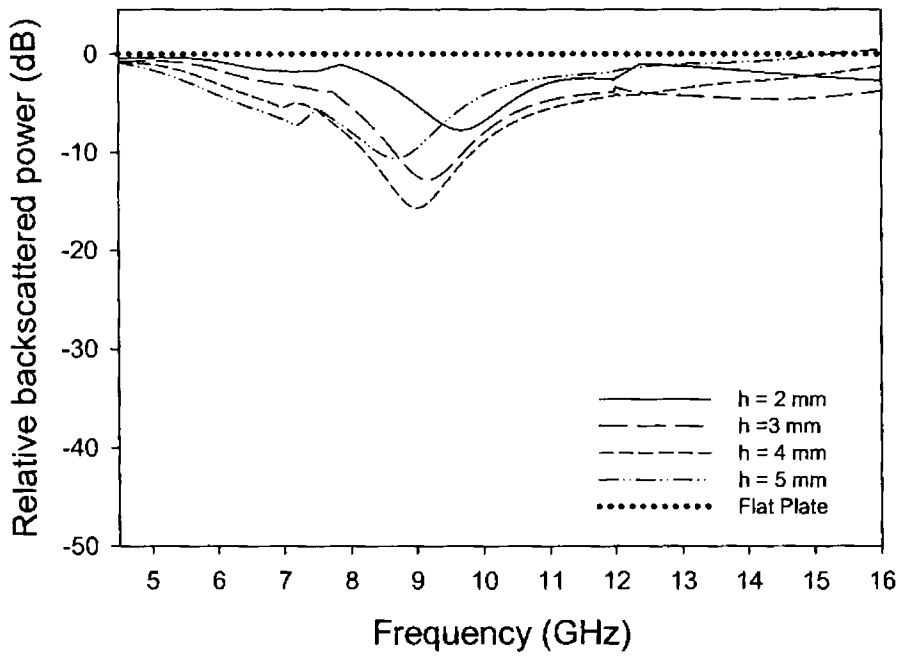


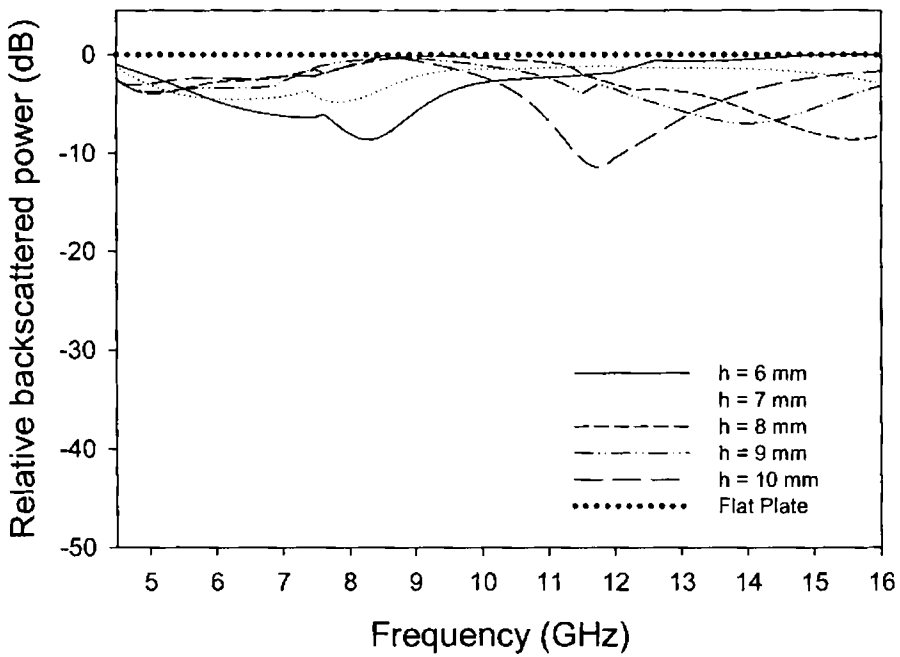
Figure 4.22 Sierpinski carpet with star as the generator

Since this the structure is not symmetric, the measurements are taken for TE and TM polarization of the incident field. The results are shown in figures 4.23 (a) and (b).

It is observed that for both cases, the maximum reduction in backscattered power is obtained for a dielectric thickness of 4 mm. Variations of backscattered power with frequency is almost identical for both polarizations.

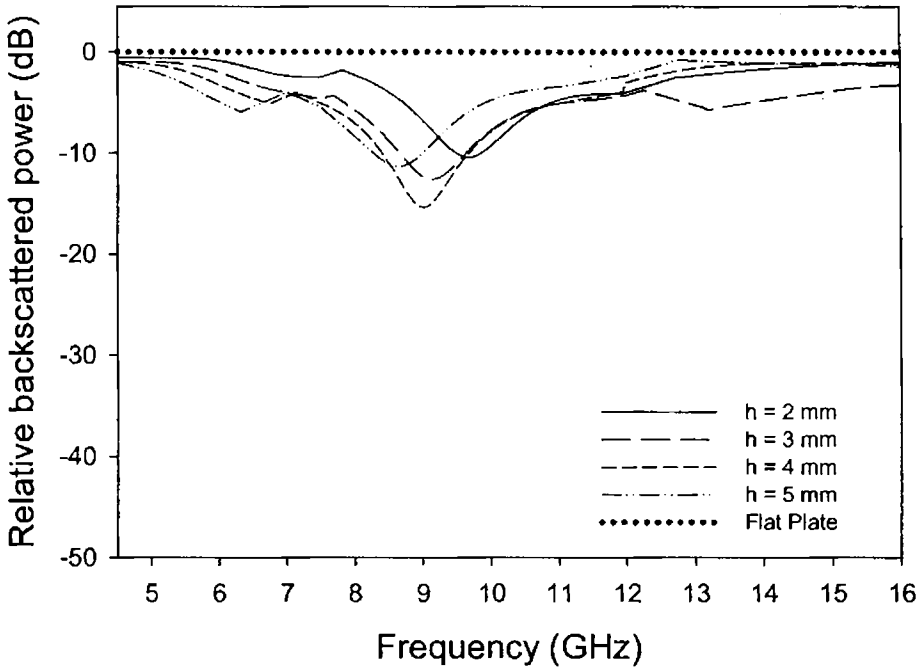


(a)

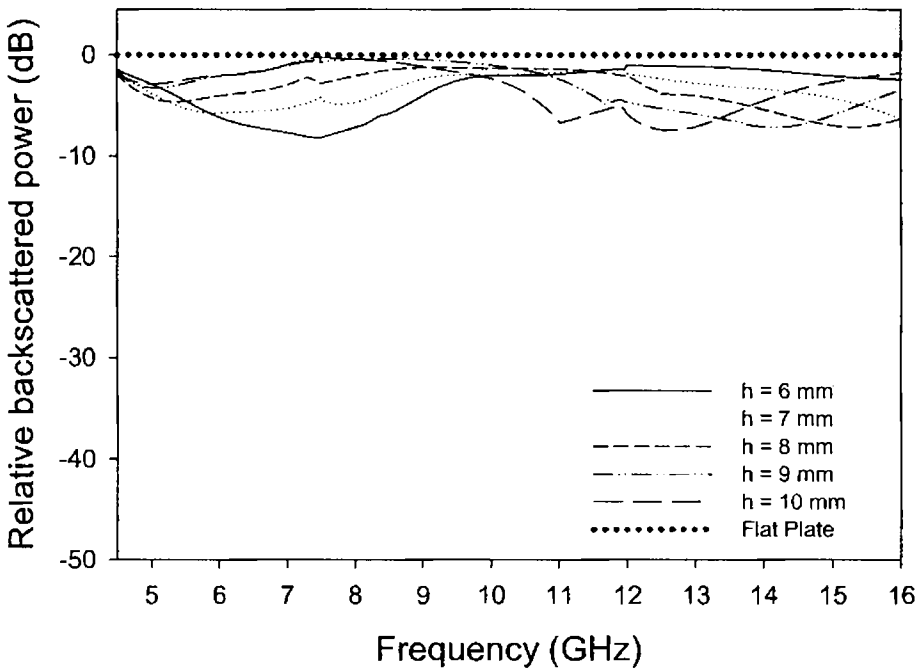


(b)

Figure 4.23 (a) & (b) Variation of backscattered power with frequency (TE - Polarization) for the structure with Star shaped patches



(a)



(b)

Figure 4.24 (a) & (b) Variation of backscattered power with frequency (TM – Polarization) for the structure with Star shaped patches

4.1.2.8 *Cross bar fractal tree*

Figure 4.25 shows the metallo-dielectric structure based on the Sierpinski carpet geometry with crossed bar fractal tree shaped patches.

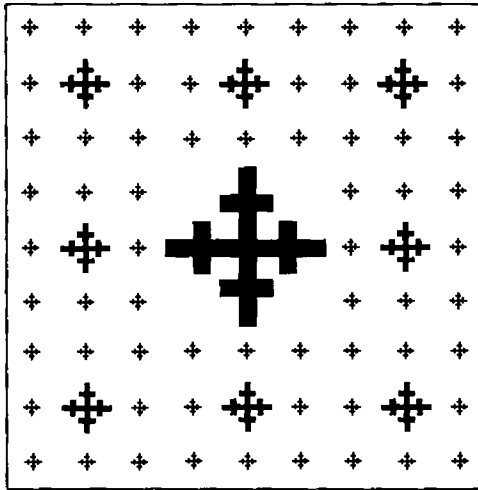


Figure 4.25 Sierpinski carpet with Crossed bar fractal tree as the generator

From the experimental results shown in figures 4.26 (a) and (b) it is observed that this structure is not giving appreciable reduction in the backscattered power.

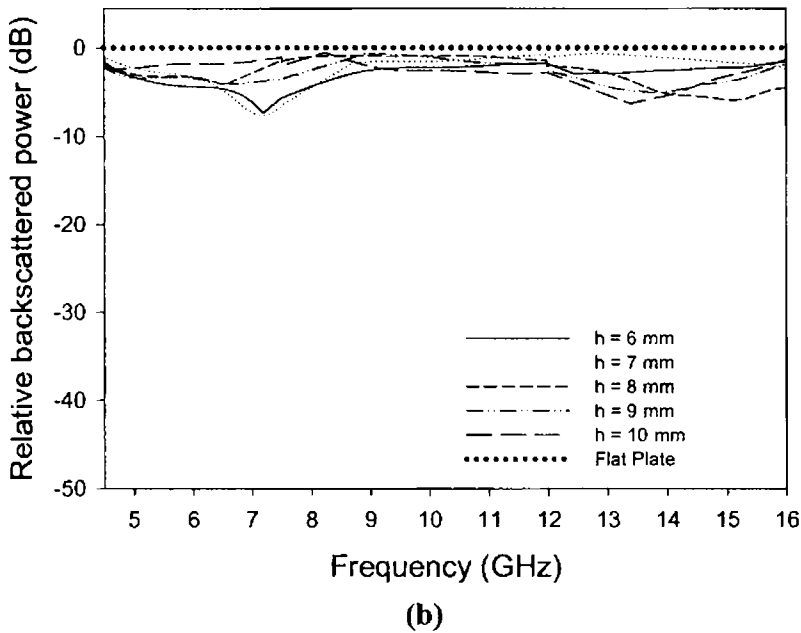
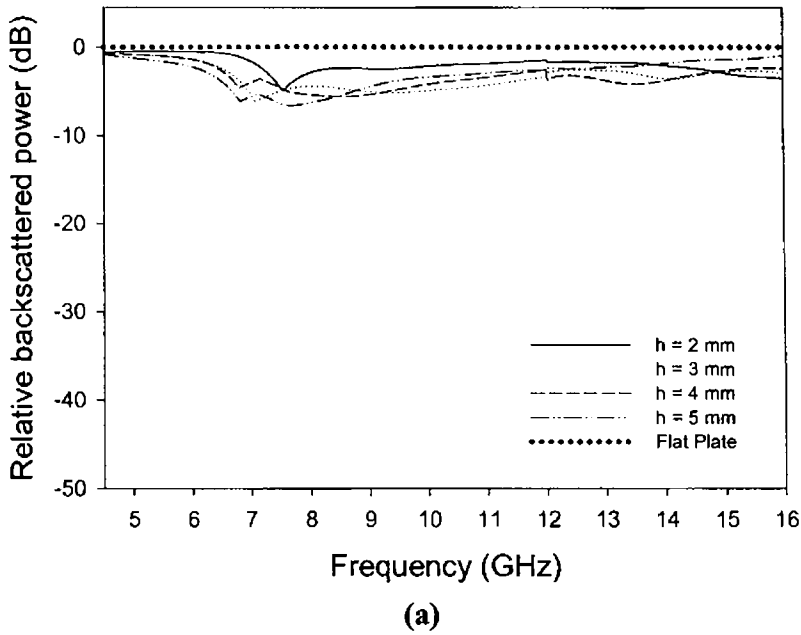


Figure 4.26 (a) & (b) Variation of backscattered power with frequency for the structure with patches of the shape crossed bar fractal tree dipole

4.1.2.9 Sierpinski carpet array

Array of second iterated Sierpinski carpet fractal geometry is shown in figure 4.27.

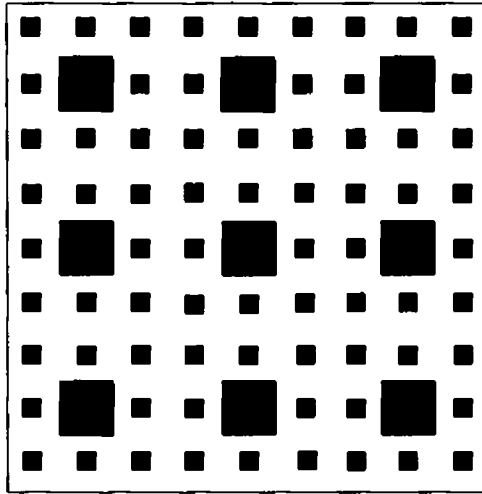
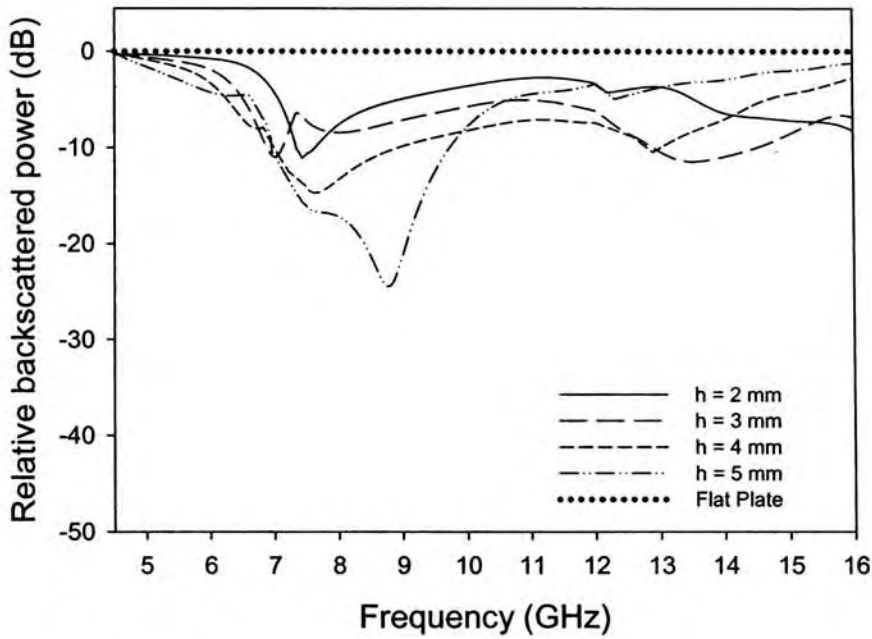


Figure 4.27 Array of second iterated stage of Sierpinski carpet

Results of the scattering measurements for this structure are shown in figure 4.28 (a) and (b). A maximum reduction of backscattered power of -24.5 is obtained at 8.775 GHz for a substrate thickness of 5 mm.



(a)

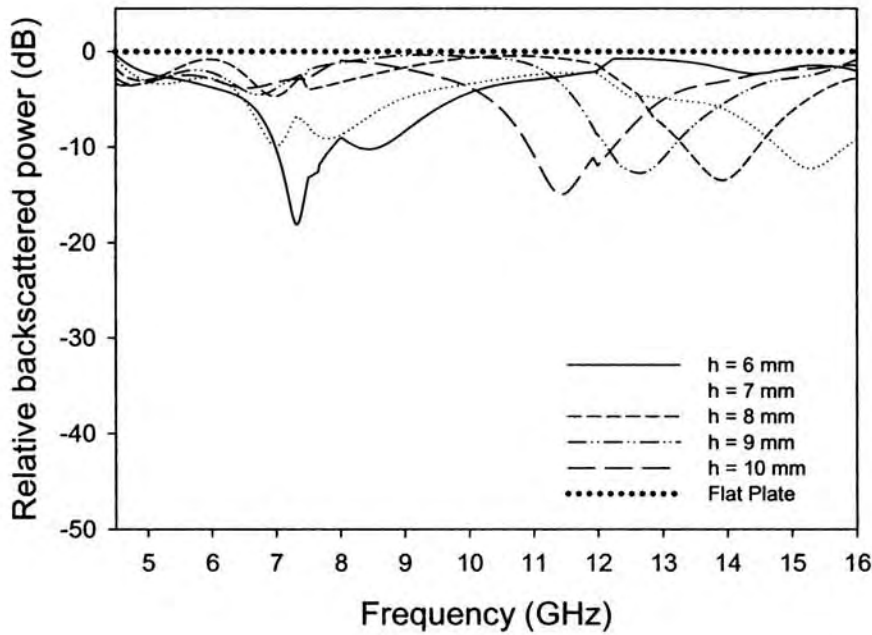


Figure 4.28 (a) & (b) Variation of backscattered power with frequency for the Sierpinski carpet array.

4.1.3 Sierpinski gasket based metallo-dielectric structure

This section describes the use of Sierpinski gasket based metallo – dielectric structure for backscattering reduction. Figure 4.29 shows the metallo-dielectric structure based on Sierpinski gasket.

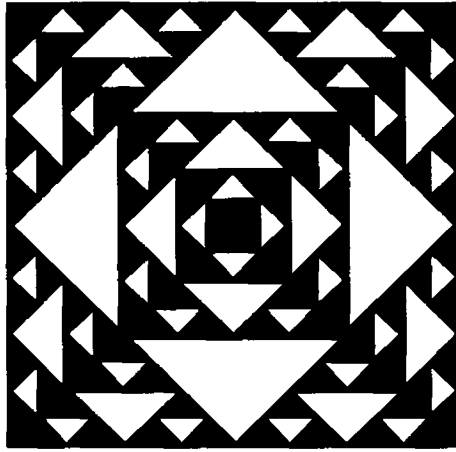
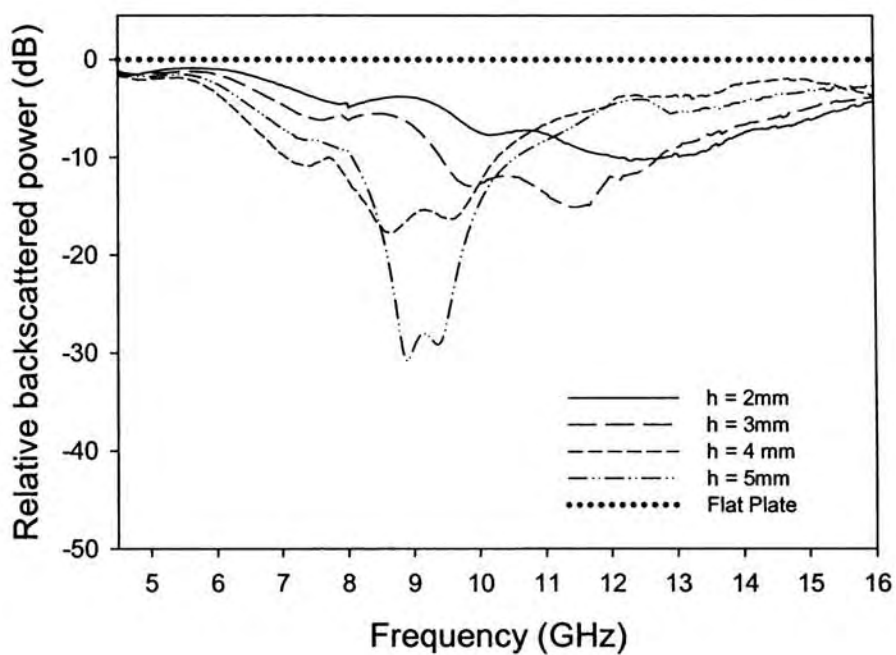
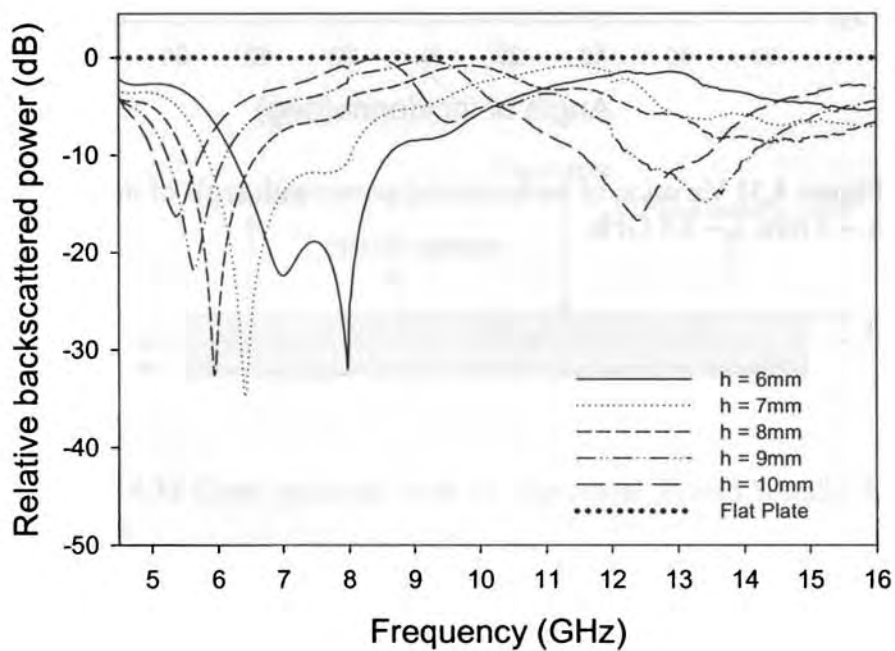


Figure 4.29 Sierpinski gasket based metallo-dielectric structure

Backscattering characteristics of this structure is shown in figure. 4.30 (a) and (b). Here, a reduction of up to -31 dB at 8.8 GHz is achieved for a substrate thickness of 5 mm. Further increase in substrate thickness gives reduction in backscattering at a lower frequency but with less bandwidth.



(a)



(b)

Figure 4.30 (a) & (b) Backscattering characteristics of Sierpinski gasket based metallo-dielectric structure.

Backscattering at different angles of incidence is studied and plotted in figure 4.31. It is observed that a maximum backscattered power of -3.4 dB is obtained for an angle of incidence of 10° .

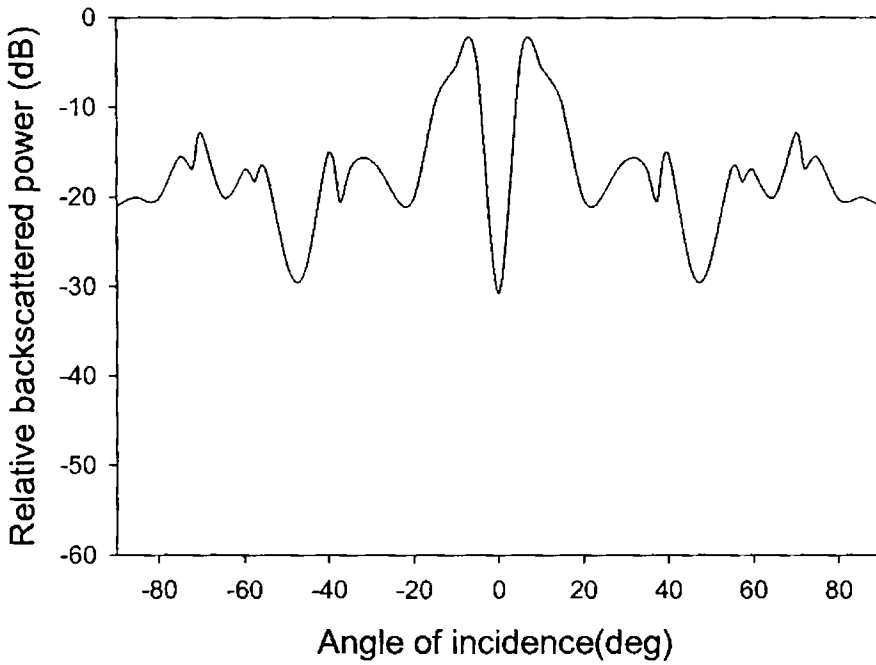


Figure 4.31 Variation of backscattered power with angle of incidence
 $h = 5$ mm, $f = 8.8$ GHz.

4.2 EFFECT OF LOADING SUPERSTRATES

For a given fractal geometry and patch shape, the frequency at which maximum reduction in backscattering is obtained depends on the substrate thickness. Once the structure is constructed, further tuning of the frequency can be achieved by loading superstrates. This section presents the measurement results of superstrate loaded metallo-dielectric structure.

The cross sectional view of superstrate loaded metallo-dielectric structure is shown in figure 4.32. Superstrates of various thickness are loaded over the metallo-dielectric structure and the backscattered power is measured in order to study the frequency tuning effect. It is found that the frequency of minimum backscattering can be tuned to a large range by varying the thickness of the superstrates. Also, the superstrate can act as a radome.

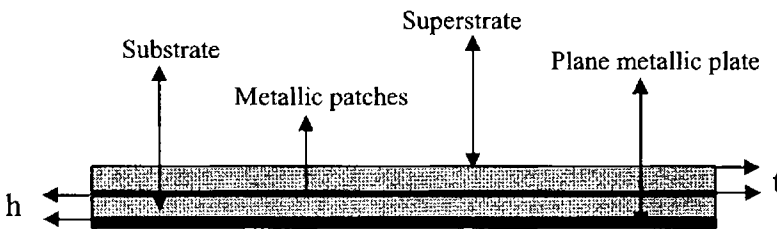


Figure 4.32 Cross sectional view of superstrate loaded metallo-dielectric structure

h = substrate thickness, t = superstrate thickness

4.2.1 Superstrate loading on Sierpinski carpet fractal geometry

The Sierpinski carpet based metallo-dielectric structure is loaded with superstrates of various thickness (t) and the backscattering is measured. This is repeated for the structure fabricated on substrates of different thickness (h).

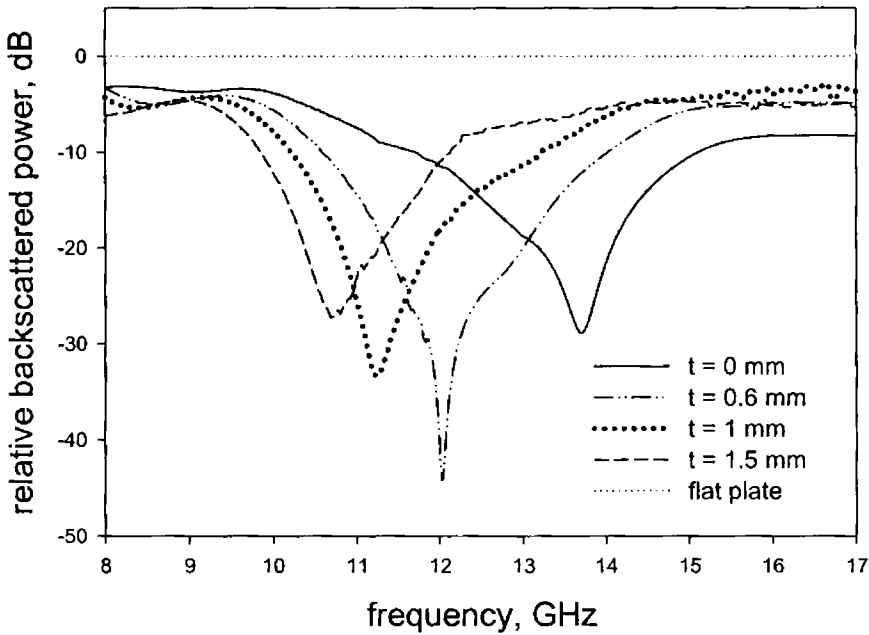


Figure 4.33 Variation of backscattered power with frequency with superstrate loading on Sierpinski carpet structure, $h = 3$ mm.

Results shown in figure 4.33 indicate that as the superstrate thickness is increased, the frequency giving minimum backscattering decreases. The frequency of minimum backscattering at 13.75 GHz without superstrate ($t = 0$) can be shifted upto 10.4 GHz by loading superstrate of thickness $t = 1.5$ mm. Appreciable reduction is obtained at

the 'tuned' frequencies. Further increase in superstrate thickness lowers the frequency but backscattering is found to be increasing.

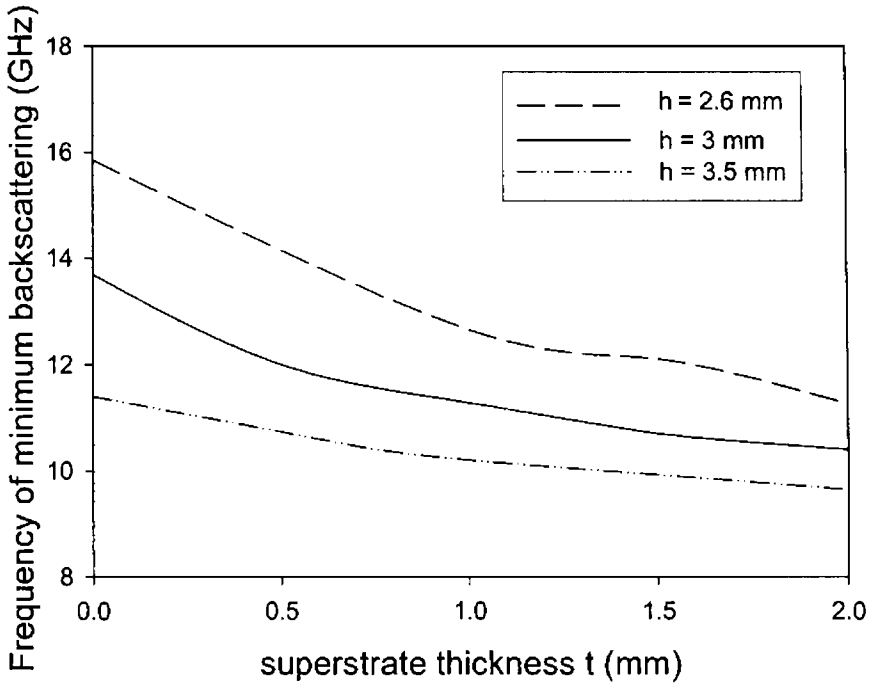


Figure 4.34 Variation of frequency of minimum backscattering with superstrate thickness for third iterated stage of Sierpinski carpet structure

The frequency tunability by superstrate loading is clearly indicated in figure 4.34 Here, superstrates are loaded over metallo-dielectric structure fabricated on substrates of different thickness $h = 2.6$ mm, 3 mm and 3.5 mm.

4.2.2 Superstrate loading on Sierpinski gasket fractal geometry

Effect of superstrate loading is studied on Sierpinski gasket geometry also. As before, when the structure is loaded with superstrate, the frequencies of minimum backscattering are shifted downwards with increase in superstrate thickness as shown in figure 4.35.

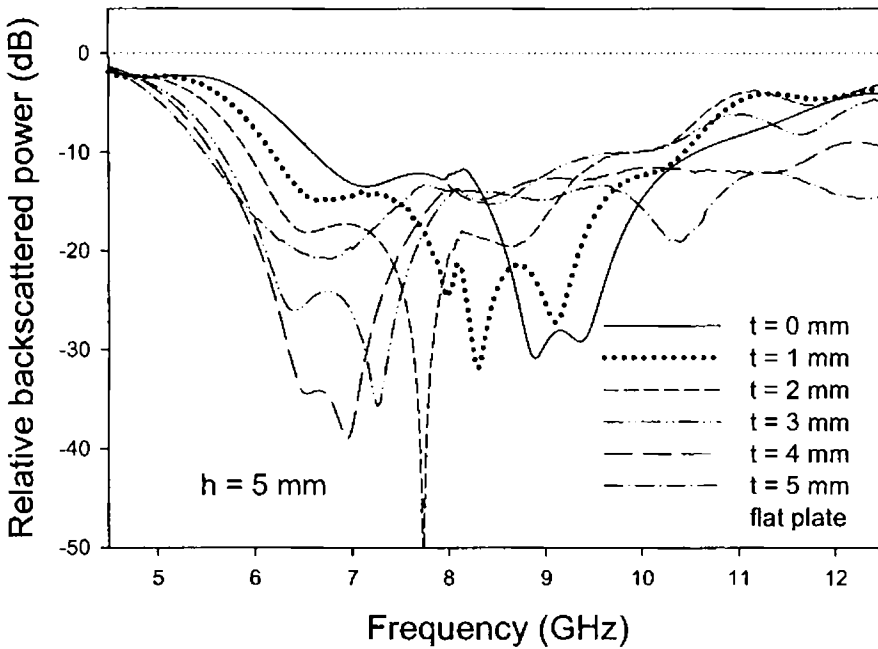


Figure 4.35 Power measured for different superstrate thickness on the Sierpinski gasket structure

Figure 4.36 shows the shift in frequency of minimum backscattering as the superstrate thickness is varied.

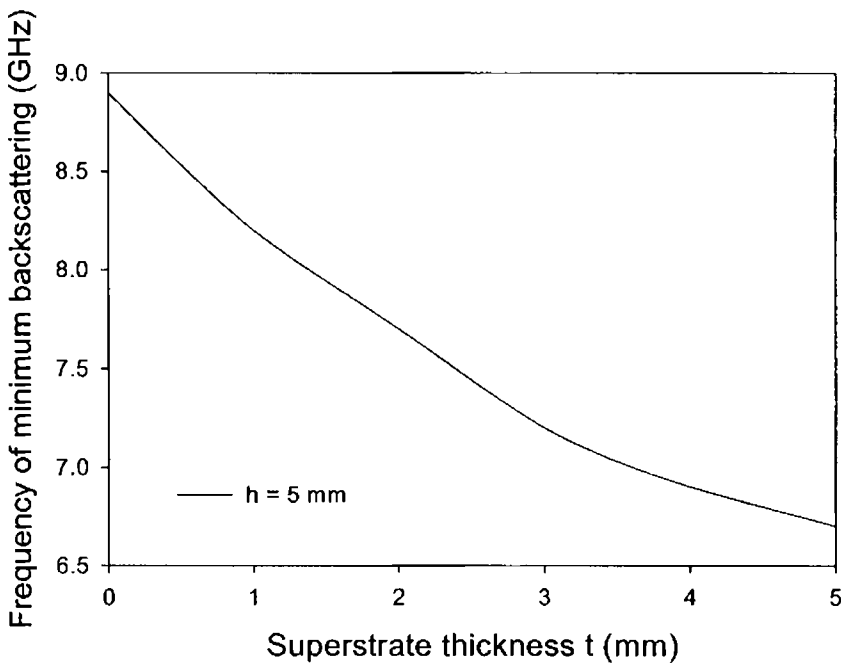


Figure 4.36 Variation of frequency of minimum backscattering with superstrate thickness, for Sierpinski gasket structure

From the experimental results, it is clear that the backscattering reduction can be obtained at a wide range of frequencies by loading superstrate of proper thickness.

4.3 FRACTAL GEOMETRIES WITH VARYING LACUNARITY

Scattering properties of metallo-dielectric structure based on Sierpinski carpet structures having same fractal dimension with different lacunarity values is investigated. Figure 4.37 (L1-L6) shows the Sierpinski carpets with dimension 1.9152 and varying lacunarity.

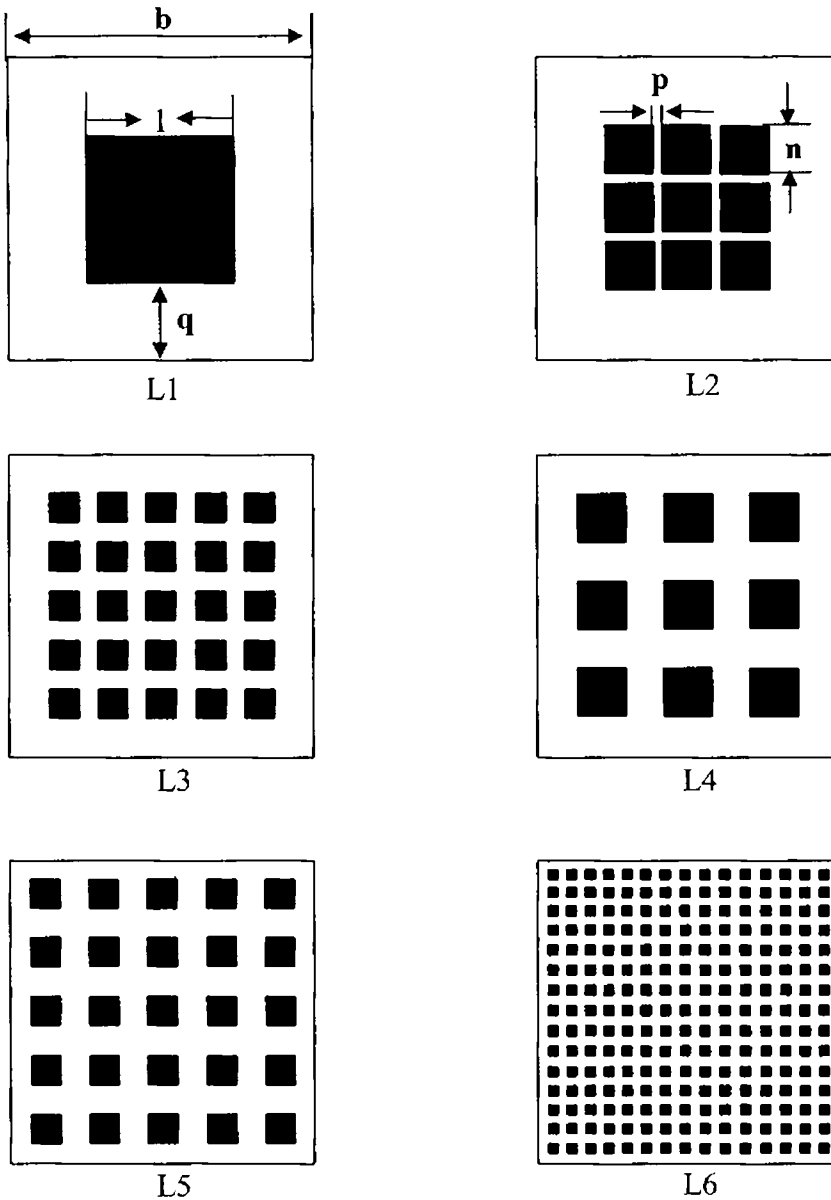


Figure 4.37 Sierpinski carpets with varying lacunarity ($D = 1.915$)

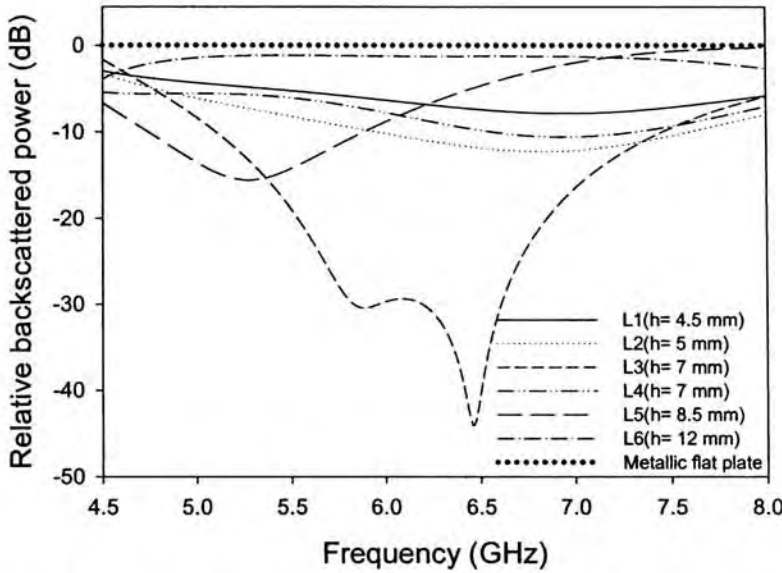


Figure 4.38 Variation of backscattered power with frequency for optimum dielectric thickness for carpets with varying lacunarity in C band

Figure 4.38 shows the variation in relative backscattered power with frequency in C – band for the structures shown in figure 4.37. The substrate thickness is varied for each structure and the thickness giving minimum backscattering in the band is found out. A reduction in backscattered power of 44dB is achieved at 6.46 GHz for a dielectric thickness $h = 7$ mm for the structure L3. It is also noted that the backscattered power is below -20 dB for a wide band of 5.54 GHz to 6.84 GHz. Similarly, the results of the measurements in X and Ku bands, are shown in figure 4.39 and 4.40. The backscattered power is reduced up to -42 dB at 8.34 GHz and -44 dB at 15.22 GHz in X and Ku frequency

bands. It is found that the structure L3 is giving maximum reduction in backscattered power in all the three frequency bands for different values of h . Hence, the reduction in backscattered power can be obtained in any of the three bands by varying the substrate thickness with the same design.

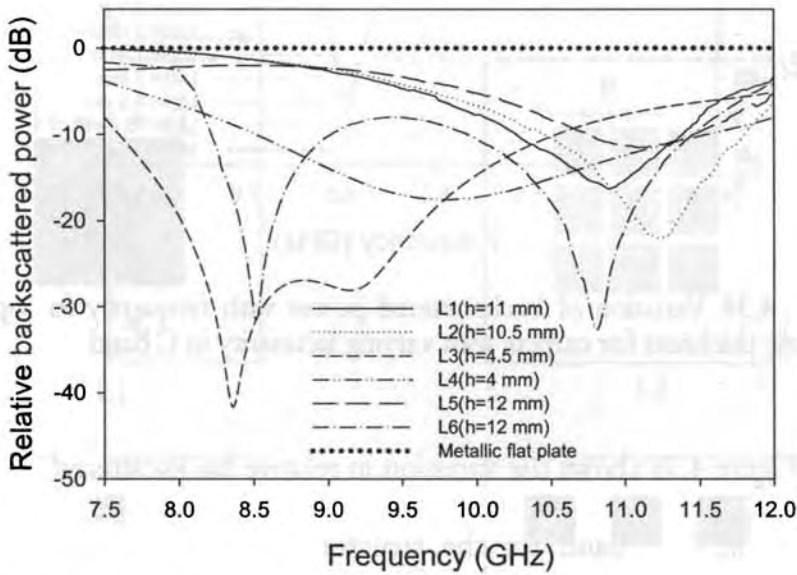


Figure 4.39 Backscattered power variations with frequency for optimum dielectric thickness in X band

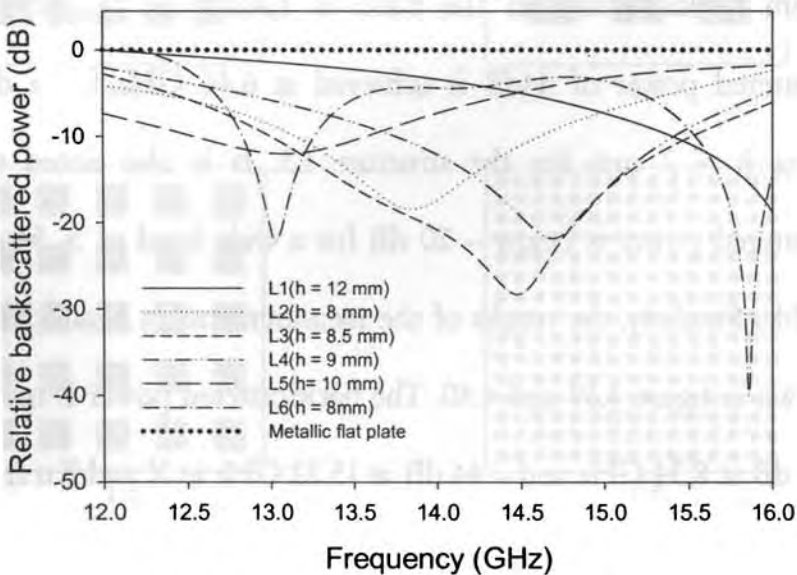


Figure 4.40 Variation of backscattered power with frequency for optimum dielectric thickness in Ku band

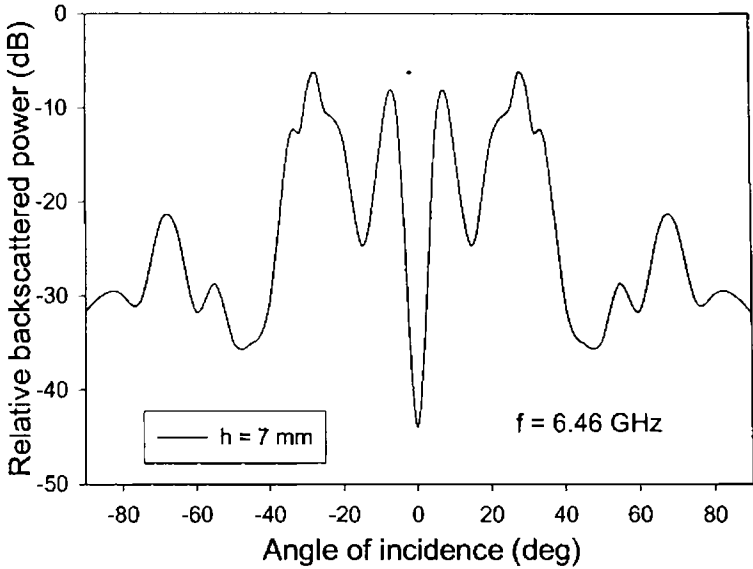


Figure 4.41 Backscattered power variations with angle of incidence for L3 in C band

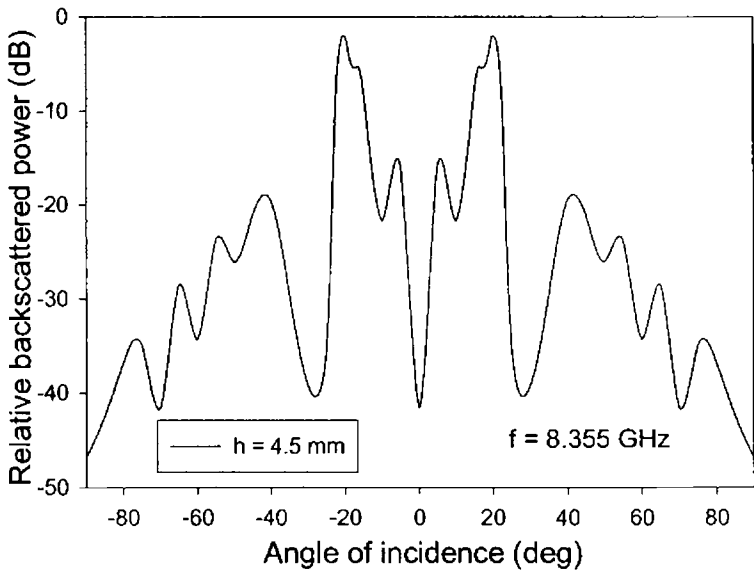


Figure 4.42 Backscattered power variations with angle of incidence for L3 in X band

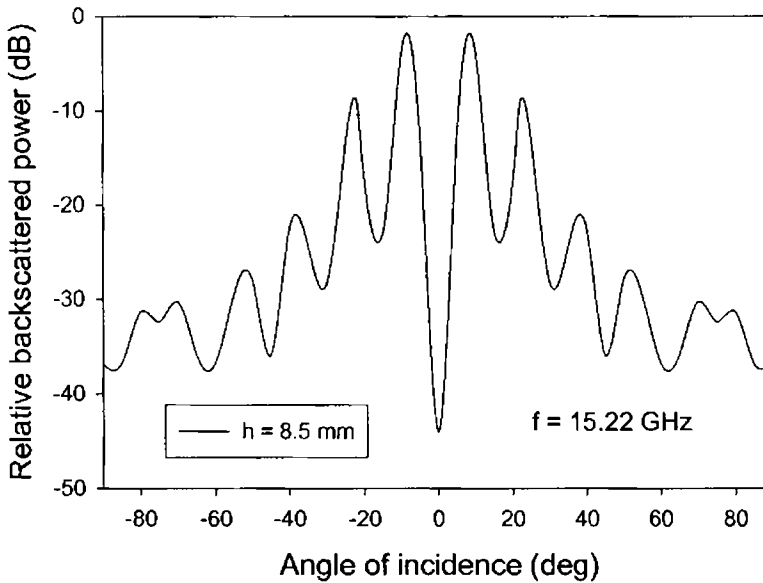


Figure 4.43 Backscattered power variations with angle of incidence for L3 in Ku band

The backscattered power for different angles of incidence for the structure L3 measured in different frequency bands are presented in figures 4.41 - 4.43. The results indicate that the backscattering is minimum at normal incidence and maximum backscattering occurs at the blazing angle. The blazing angles in C, X and Ku bands are 27° , 20° and 11° respectively. Studies also indicated that the backscattered power is distributed symmetrically with respect to the normal in both the azimuth and elevation angular ranges. Since the structures are symmetric, this property is observed for both TE and TM polarizations.

4.4 RCS REDUCTION OF 3D STRUCTURES

As mentioned earlier, basic building blocks of any complex targets are flat plates, cylinders, cones and corner reflectors. Result of loading fractal based metallo-dielectric structure on these objects are described in the next section

4.4.1 METALLIC CYLINDER

A metallic cylinder loaded with the metallo dielectric structure is shown in figure 4.44.

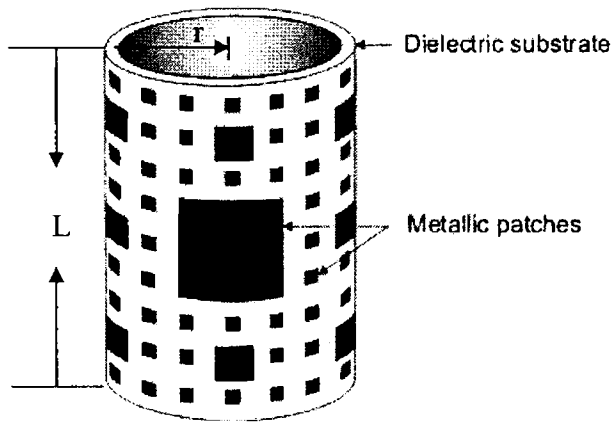


Figure 4.44 Hollow metallic cylinder loaded with fractal based metallo-dielectric structure, $L = 30$ cm, $r = 9.55$ cm

The measurements are done for both TE and TM polarization of the incident field for vertical and horizontal orientation of the cylinder for different angles of incidence.

TE-Polarization

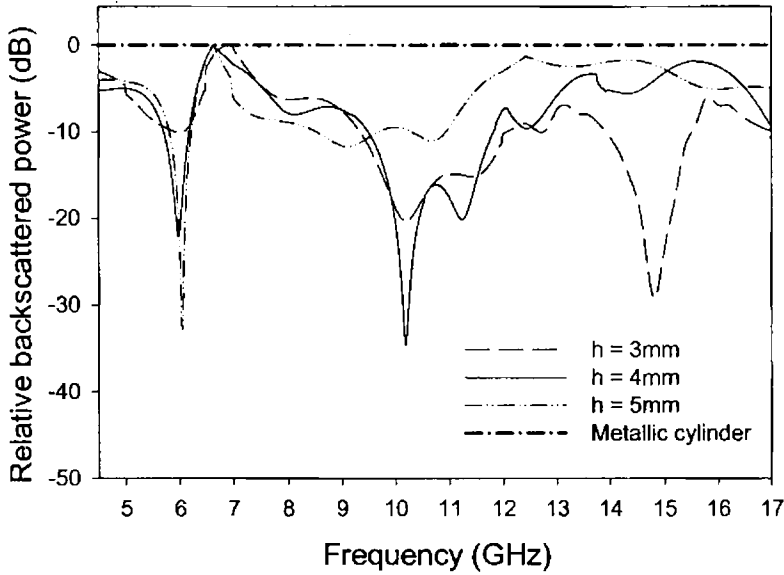


Figure 4.45 Variation of backscattered power from the structure for different dielectric thickness, TE polarization

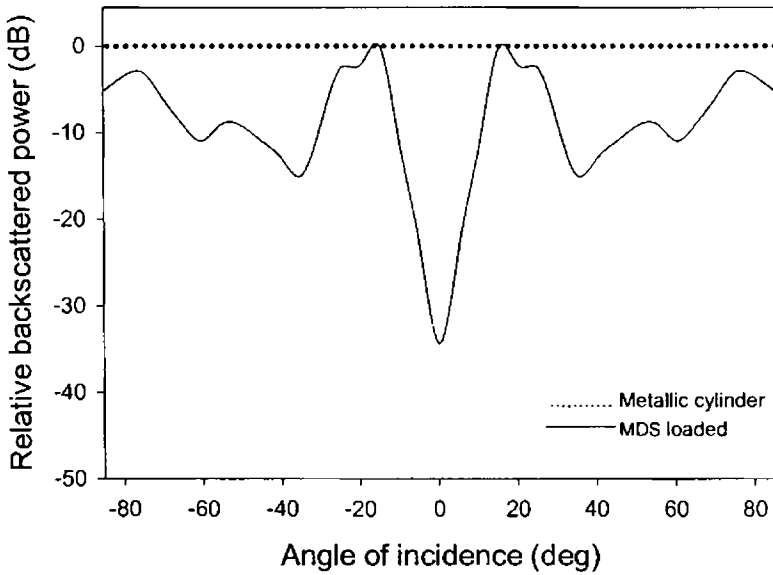


Figure 4.46 Backscattered power variations with angle of incidence, $f = 10.18\text{ GHz}$, $h = 4\text{ mm}$, TE polarization

Figure 4.45 illustrates the variation of the backscattered power with frequency for TE polarization of the incident field for different dielectric thickness. The reduction in backscattering varies with the thickness of the substrate material and a reduction of ~ 35 dB is obtained at 10.18 GHz for a dielectric thickness of $h = 4$ mm. The frequency of minimum backscattered power is also changing with thickness of the substrate.

Backscattered power for different angles of incidence for the configuration giving minimum backscattered power is plotted in figure 4.46. It is found that, at an angle of incidence of 15° , backscattering is maximum. Distribution of scattered power for normal incidence is shown in figure 4.47.

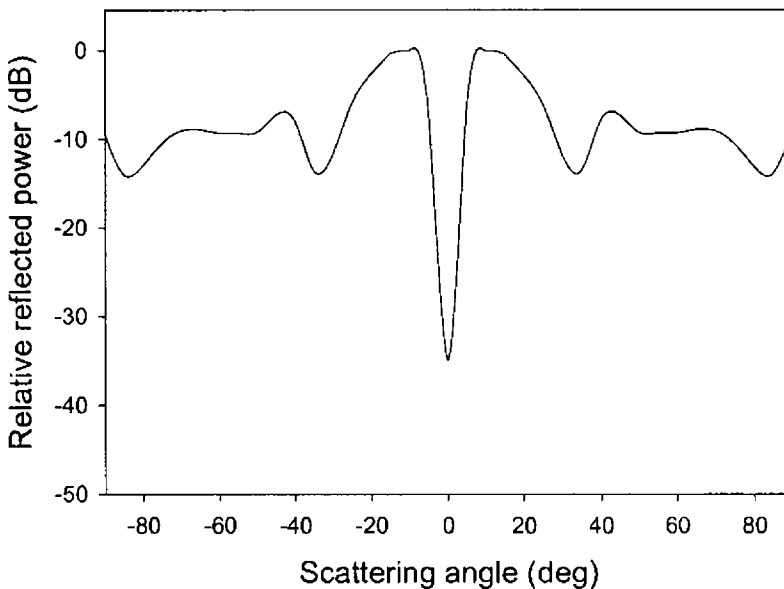


Figure 4.47 Angular distribution of scattered power for normal incidence, TE polarization, $f = 10.18$ GHz, $h = 4$ mm

TM-Polarization

Backscattered power at different frequencies for TM polarization of the illuminated wave is plotted in figure 4.48. Maximum reduction in the backscattered power of -35 dB is obtained at 9.78 GHz for dielectric thickness $h = 4$ mm.

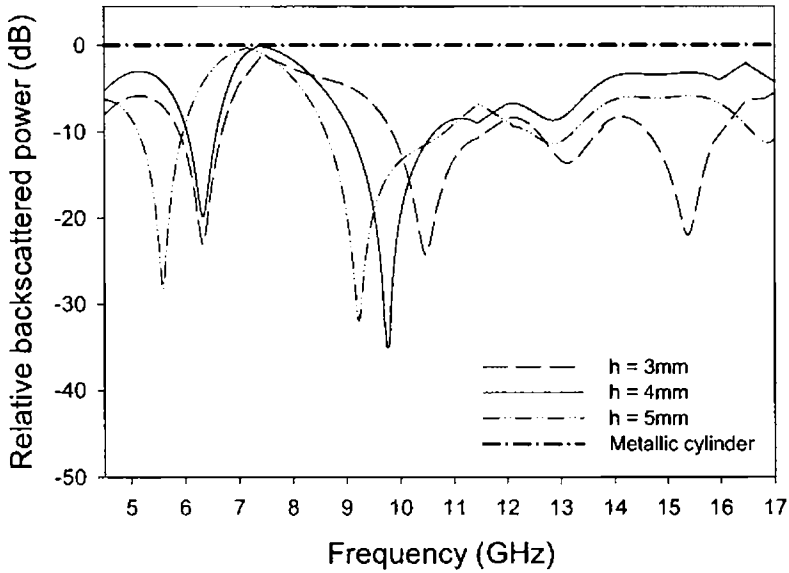


Figure 4.48 Backscattered power variations with frequency for TM polarization

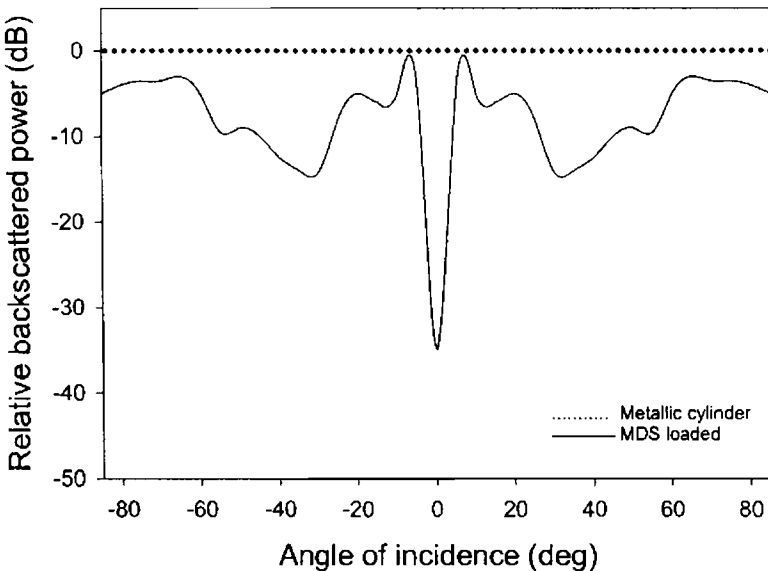


Figure 4.49 Variation of backscattered power with angle of incidence $f = 9.78$ GHz, $h = 4$ mm, TM polarization

In this case also, reduction in backscattered power is obtained at multiple frequency bands. Figure 4.49 shows the backscattered power for different angles of incidence. Maximum backscattered power is obtained at an angle of incidence of 7° .

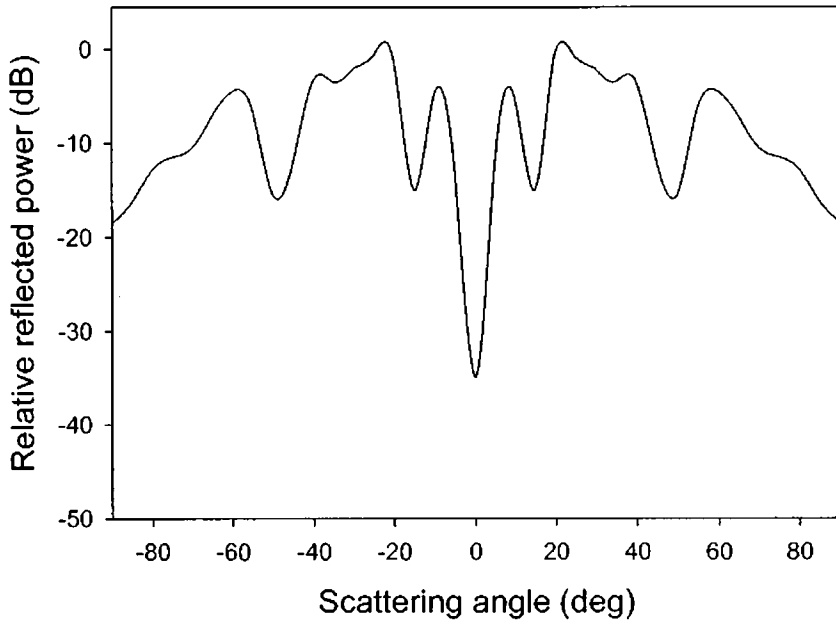


Figure 4.50 Angular distribution of scattered power for normal incidence, TM polarization, $f = 9.78$ GHz, $h = 4$ mm

Distribution of scattered power for normal incidence is shown in figure 4.50. Experimental results obtained for the cylinder oriented horizontally as shown in figure 4.51 for both TE and TM case are given below.

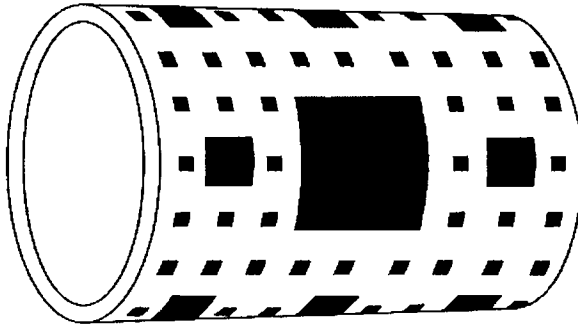


Figure 4.51 Fractal structure loaded cylinder, horizontally oriented

TE-Polarization

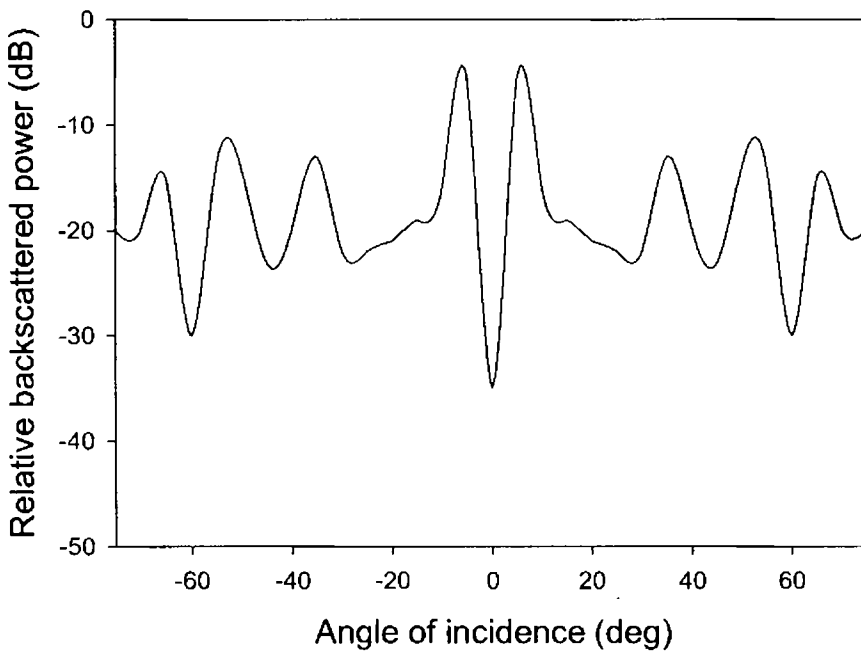


Figure 4.52 Variation of backscattered power with angle of incidence
 $f = 9.78$ GHz, $h = 4$ mm, TE polarization

The graph of variation in backscattered power with angle of incidence for the frequency giving minimum backscattered power and

substrate thickness is shown in figure 4.52. It is seen that a maximum backscattered power of -5.5 dB is obtained at an angle of incidence of 5° . Figure 4.53 shows the distribution of scattered power when the incidence is normal.

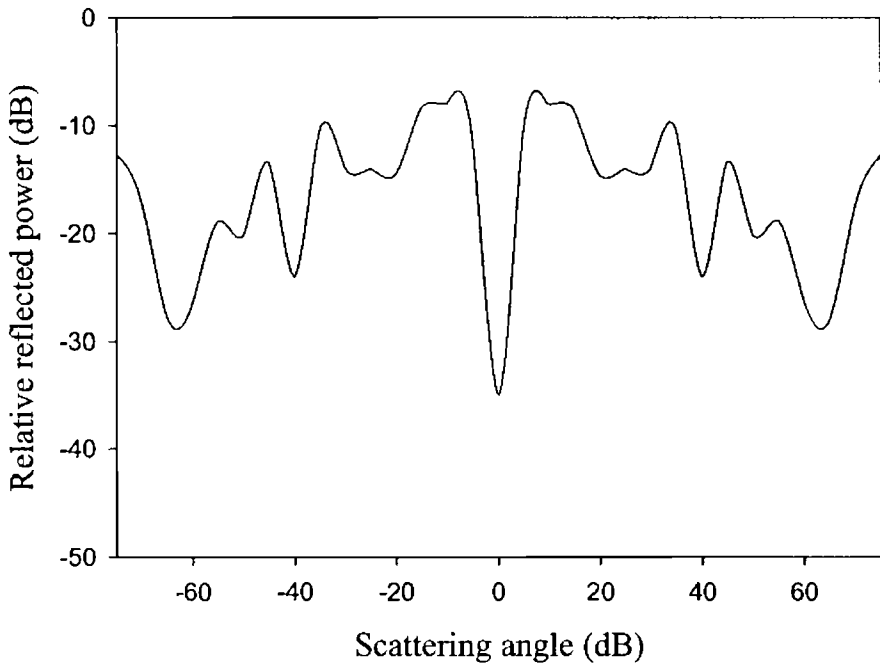


Figure 4.53 Scattered power measured at different angles for normal incidence, $f = 9.78$ GHz, $h = 4$ mm, TE polarization, cylinder horizontal

TM polarization

The variation of backscattered power with angle of incidence for TM polarization is depicted in figure 4.54. A maximum backscattered power of -6.6 dB is obtained at an angle of incidence of 5° .

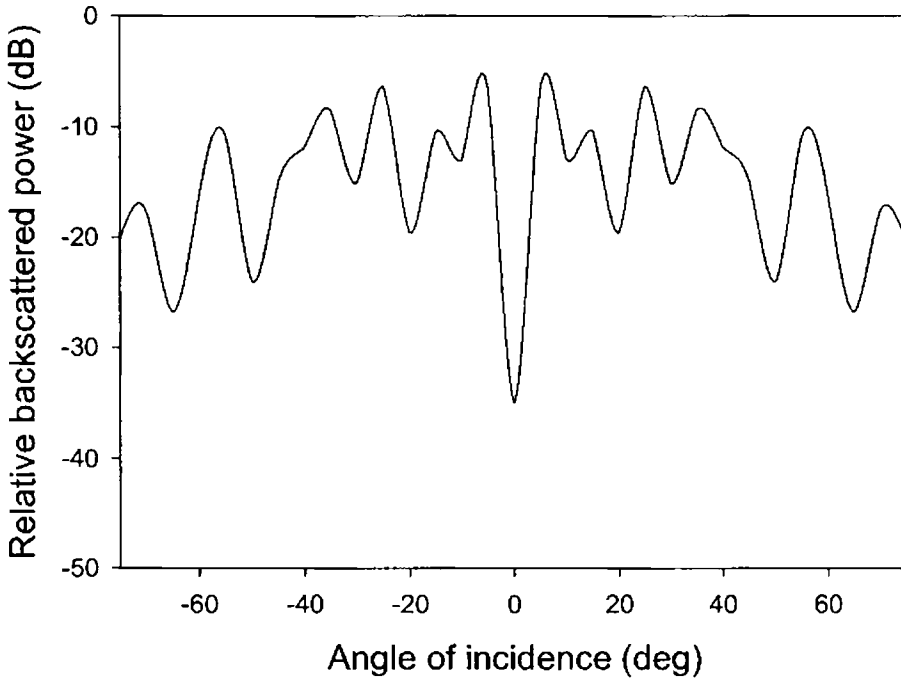


Figure 4.54 Variation of backscattered power with angle of incidence $f = 10.18$ GHz, $h = 4$ mm, TM polarization, cylinder horizontal

Figure 4.55 shows the distribution of scattered power when the incidence is normal.

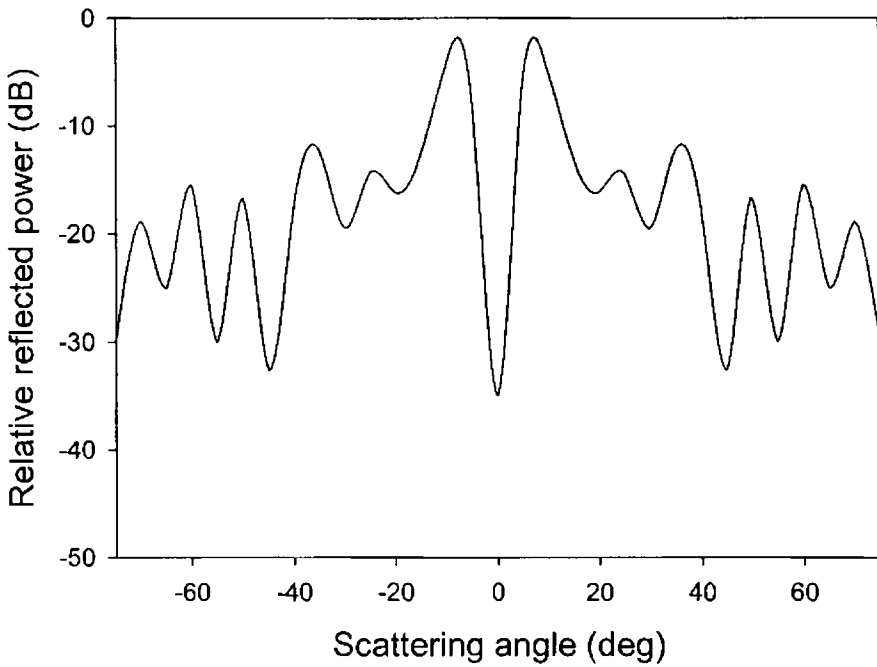


Figure 4.55 Scattered power measured at different angles for normal incidence, $f = 10.18$ GHz, $h = 4$ mm, TM polarization

4.4.2 DIHEDRAL CORNER REFLECTOR

A dihedral corner reflector loaded with Sierpinski carpet based metallo-dielectric structure is shown in figure 4.56.

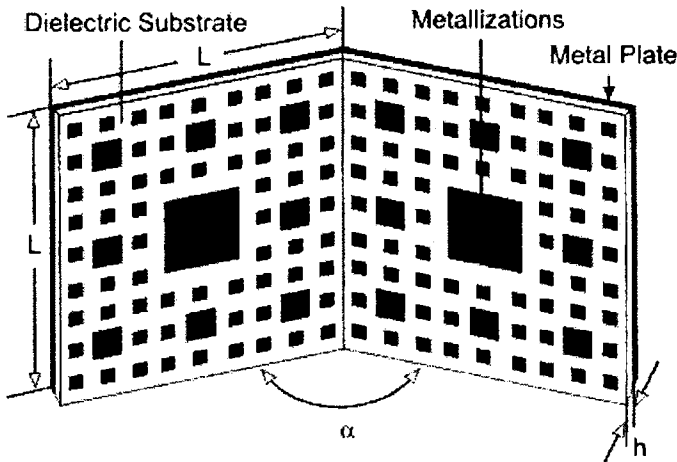
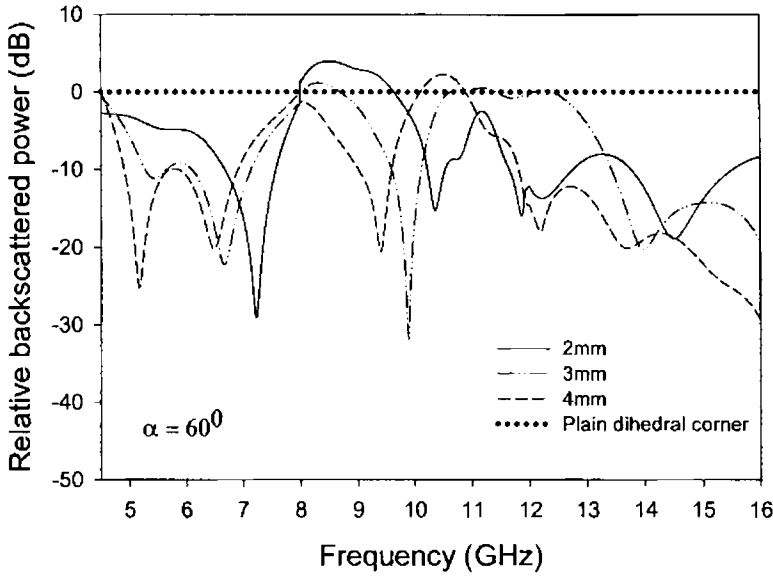


Figure 4.56 Dihedral corner reflector loaded with fractal based metallo-dielectric structure, $L = 30$ cm

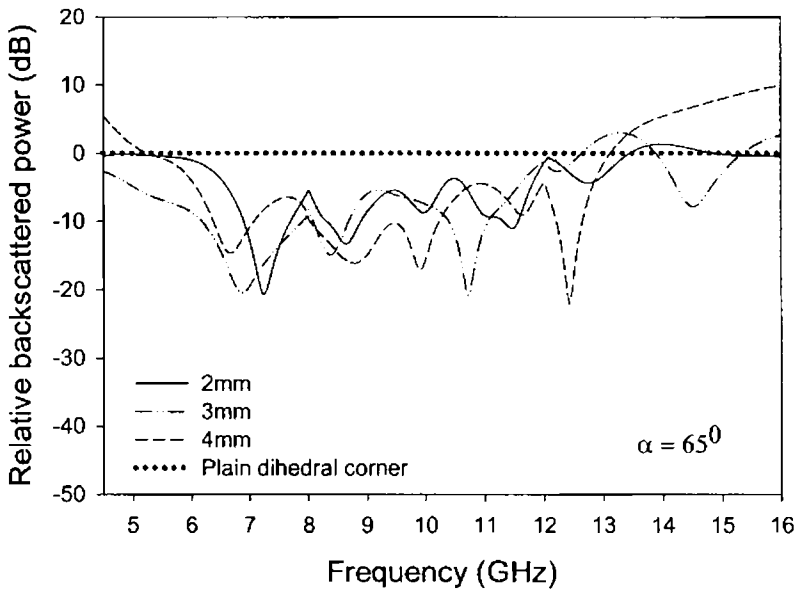
The scattering from a corner reflector is strongly dependent on the corner angle. It gives a large backscattering when the corner angle is 90° and is less at other angles. Hence the measurements are carried out for corner reflectors for a wide range of corner angles (α) from 60° to 175° loaded with metallo-dielectric structures. This is repeated for different substrate thickness for both TE and TM polarizations.

The backscattered power at different frequencies for corner angle $\alpha = 60^\circ$ is plotted in figure 4.57 (a) for different dielectric thickness. As can be observed, compared to a plain corner reflector a reduction in backscattered power of -31.6 dB is achieved at $f = 9.9$ GHz for an

dielectric thickness of $h = 2 \text{ mm}$. It is also observed that there is an increase in backscattering (3.96 dB) at $f = 8.5 \text{ GHz}$ compared to a plane corner reflector. The measurements are repeated for different acute angles of the corner reflector and the results for TE polarization are shown in figures 4.57 (a)-(f).

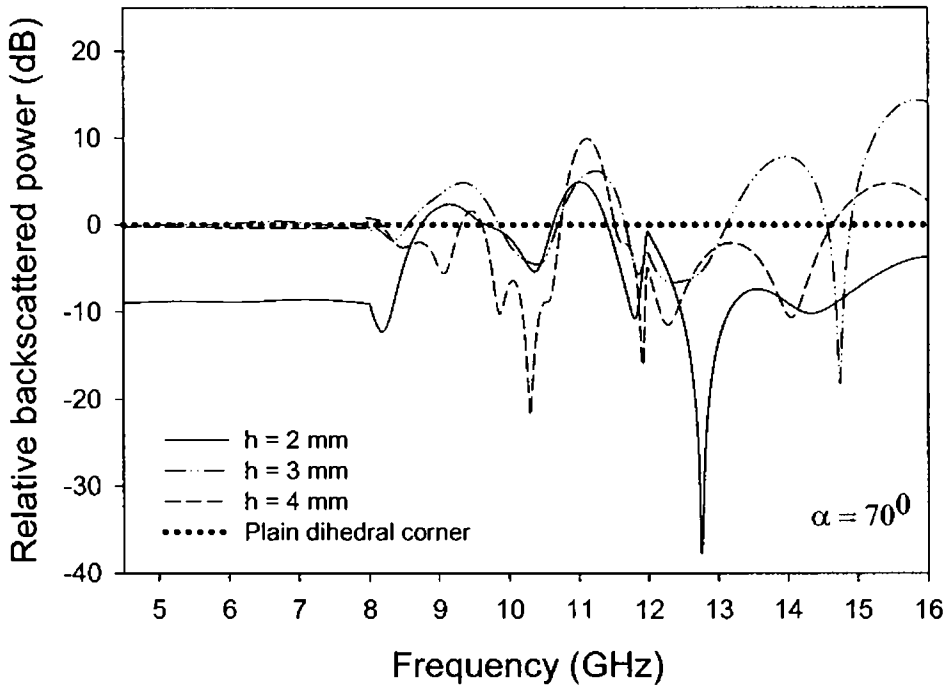


(a)

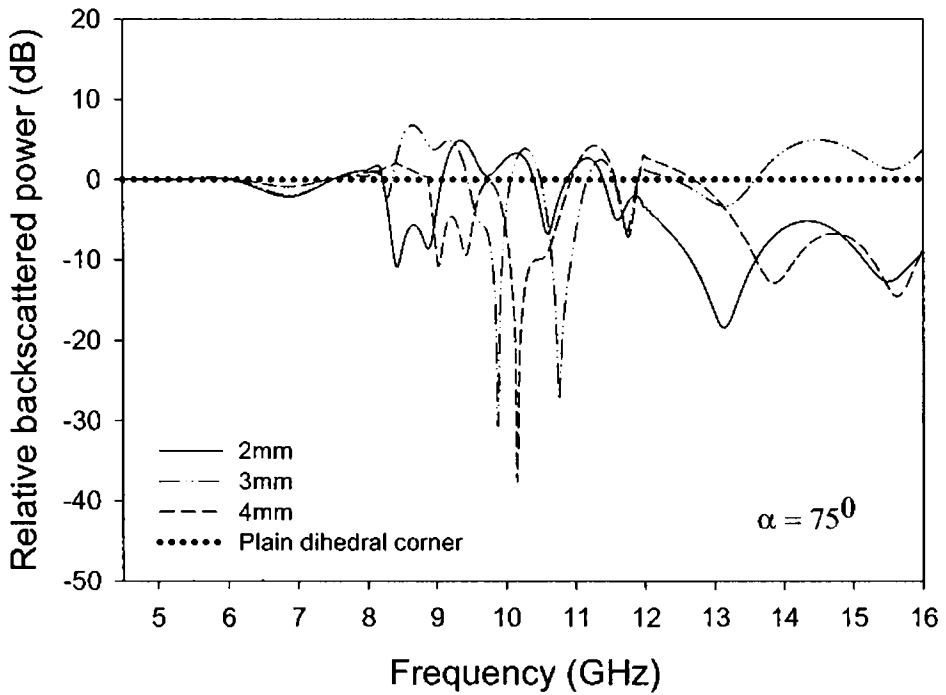


(b)

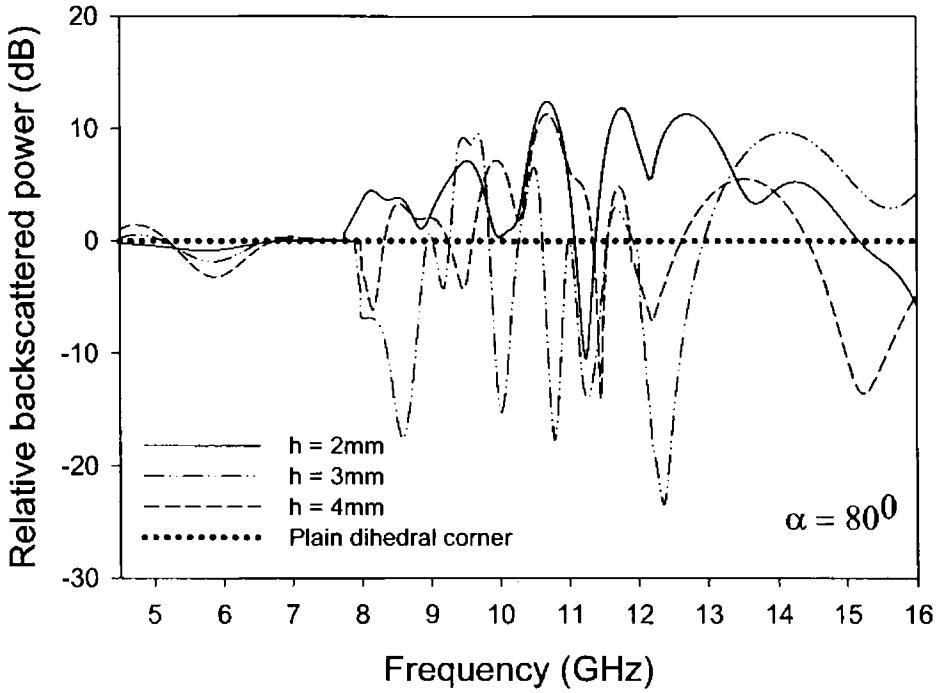
Figure 4.57 Variation of backscattered power against frequency for acute angles of the dihedral corner reflector for TE polarization
 (a) $\alpha = 60^\circ$ (b) $\alpha = 65^\circ$ contd



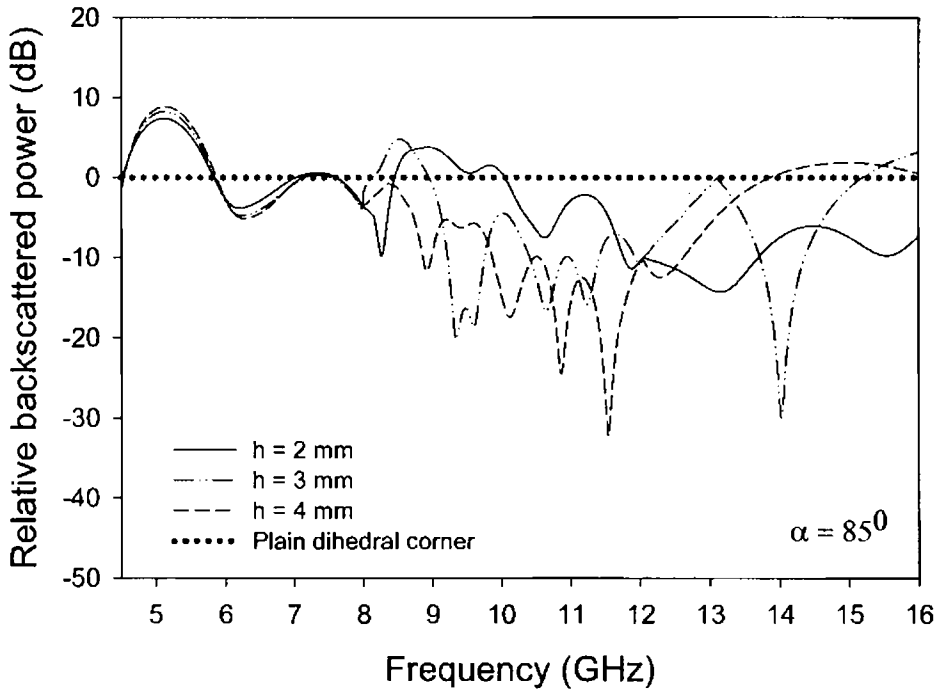
(c)



(d)



(e)



(f)

It is observed from figure 4.57 (a) – (f) that there is an enhancement in backscattering at certain frequencies for corner angles in the range $60^\circ - 85^\circ$.

In the case of 90° plain dihedral corner reflector, a large RCS is obtained due to the multiple reflections from the two mutually orthogonal flat surfaces dominating the backscattered pattern.. This is reduced when the metallo-dielectric structure is loaded over the flat surfaces.

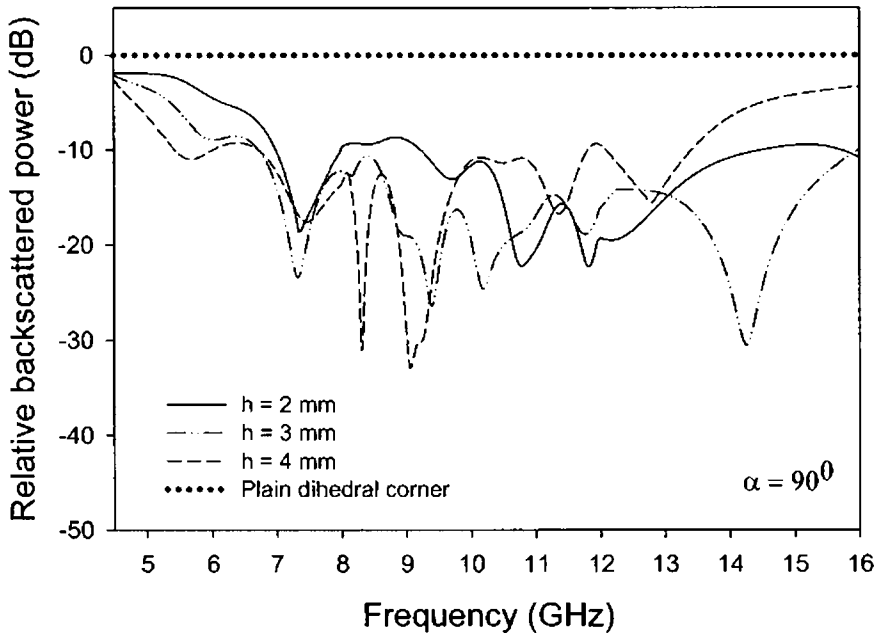


Figure 4.58 backscattered power variations against frequency for a right angled dihedral corner reflector, TE polarization

The variation of backscattered power with frequency for corner angle $\alpha = 90^\circ$ is shown in figure 4.58 for different dielectric thickness. A maximum reduction in backscattered power of -32.8 dB is achieved at $f = 9.05$ GHz for substrate thickness $h = 4$ mm. It is clear that by loading

metallo-dielectric structures, the back scattered power is reduced to a considerable extend for $\alpha = 90^\circ$.

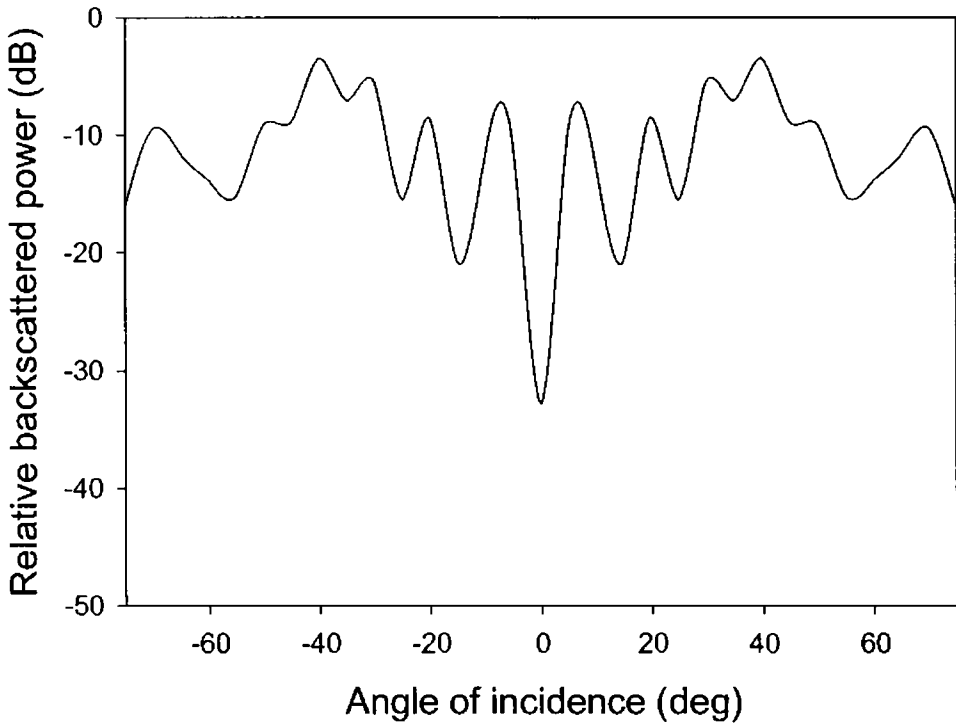
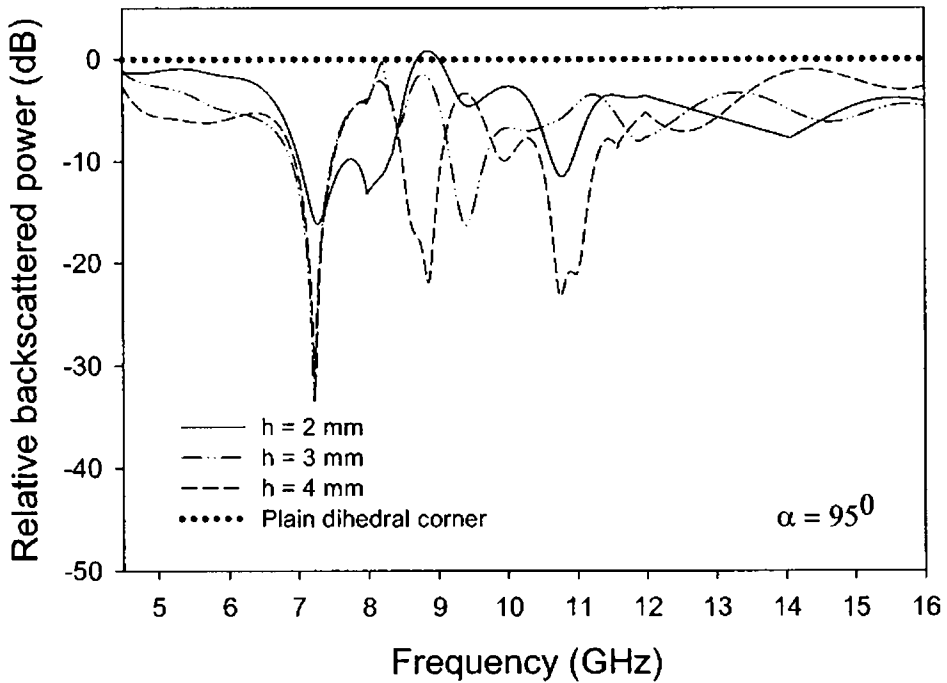


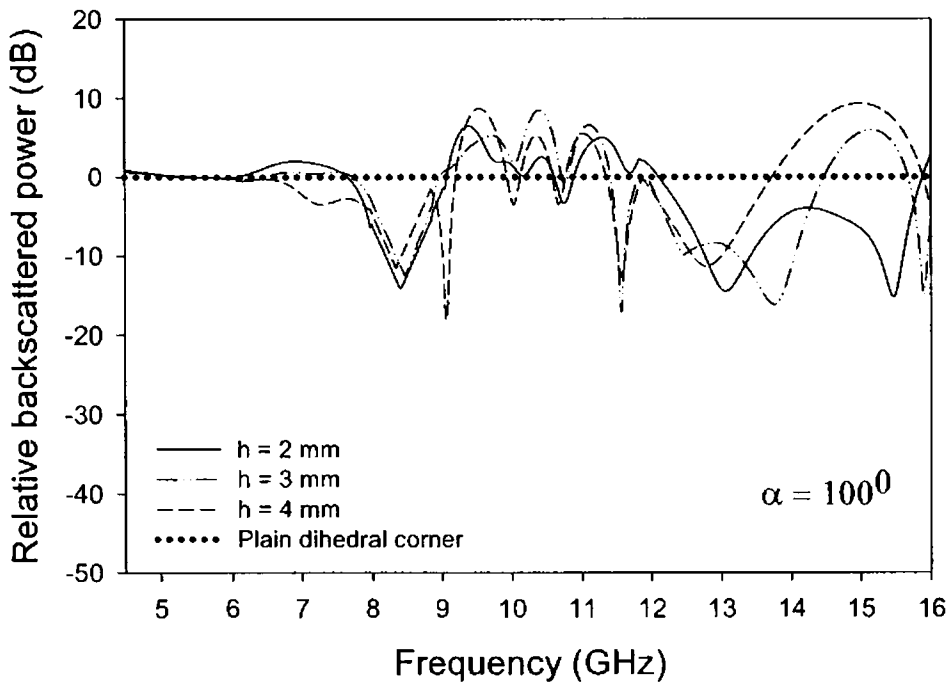
Figure 4.59 Backscattered power variations with angle of incidence for $f = 9.05$ GHz, TE polarization

Backscattered power measured for different angles of incidence for the dihedral corner with corner angle 90° loaded with the metallo-dielectric structure of thickness $h = 4$ mm at $f = 9.05$ GHz is shown in figure 4.58. It is observed a maximum backscattered power of -3.43 is obtained for an angle of incidence of 40° .

The backscattered power measurements for obtuse angles ($\alpha = 95^\circ - 175^\circ$) are shown in figure 4.60 (a) – (q) for different dielectric thickness.

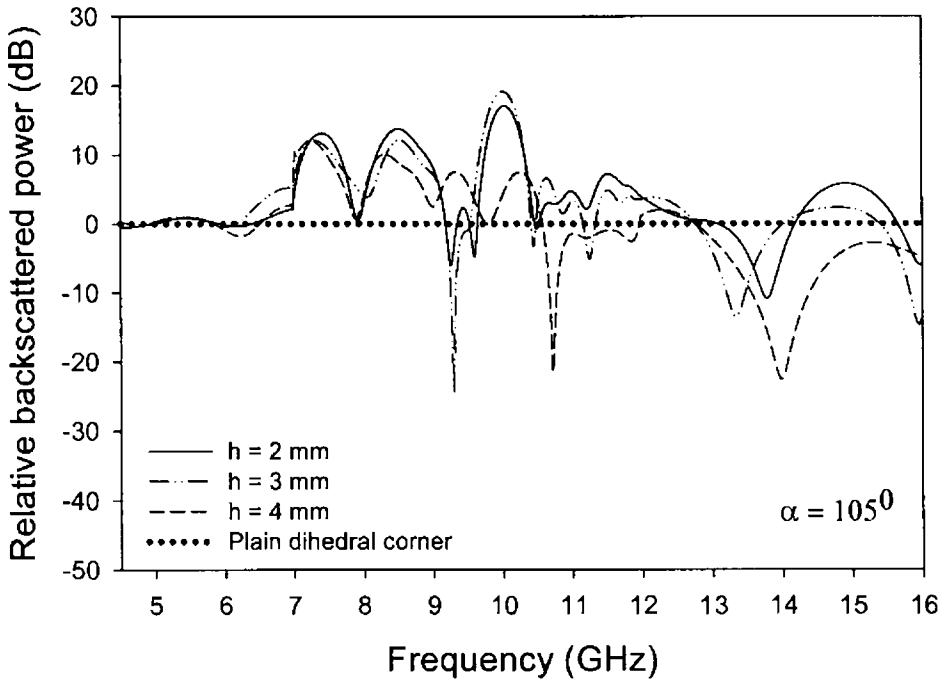


(a)

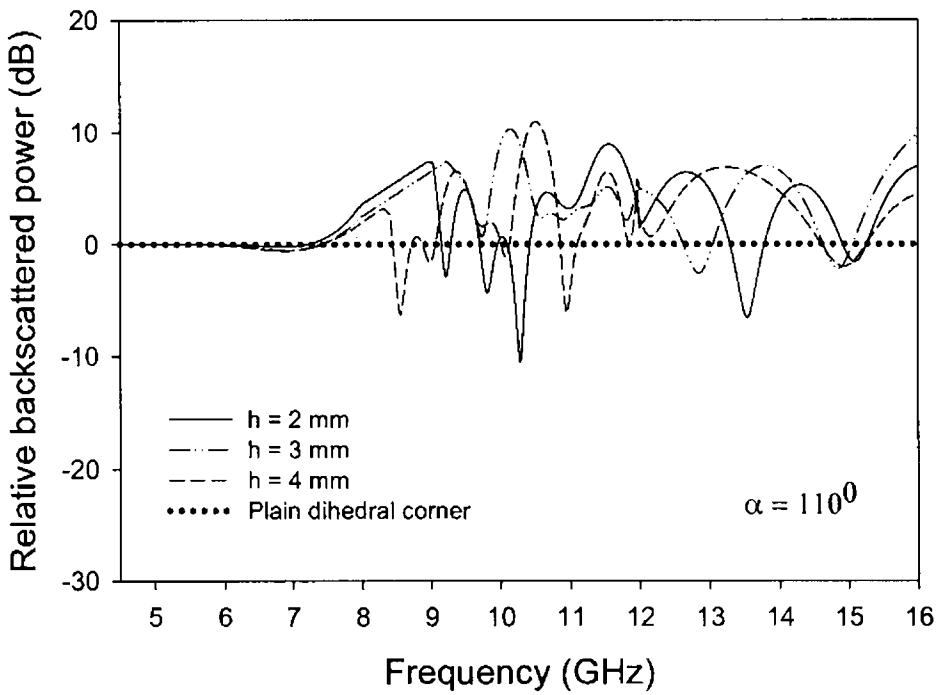


(b)

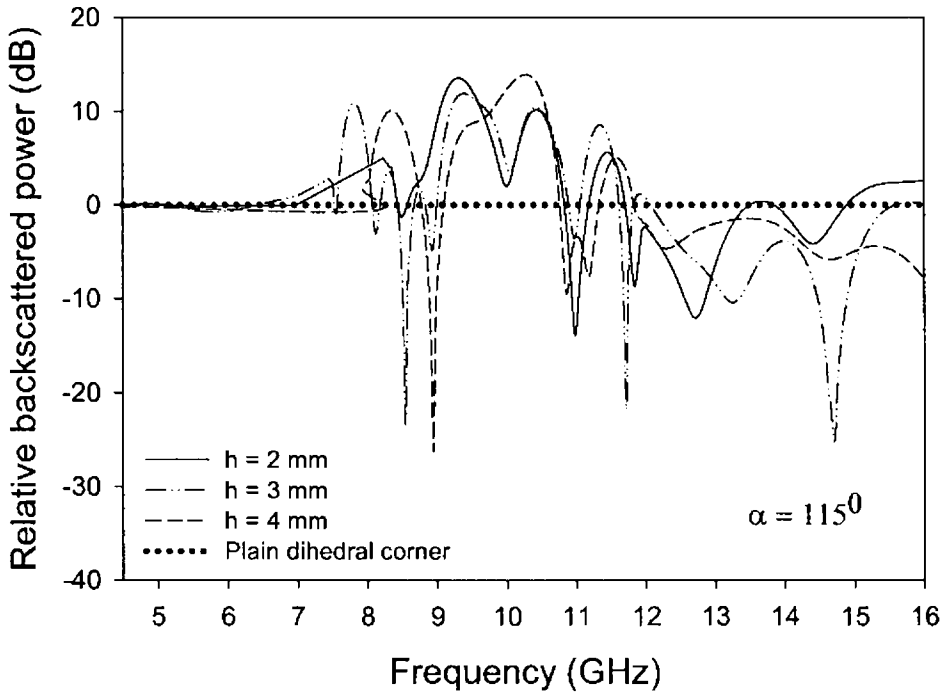
Figure 4.60 Variation of backscattered power against frequency for obtuse angles of the dihedral corner reflector for TE polarization
 (a) $\alpha = 95^\circ$ (b) $\alpha = 100^\circ$ contd



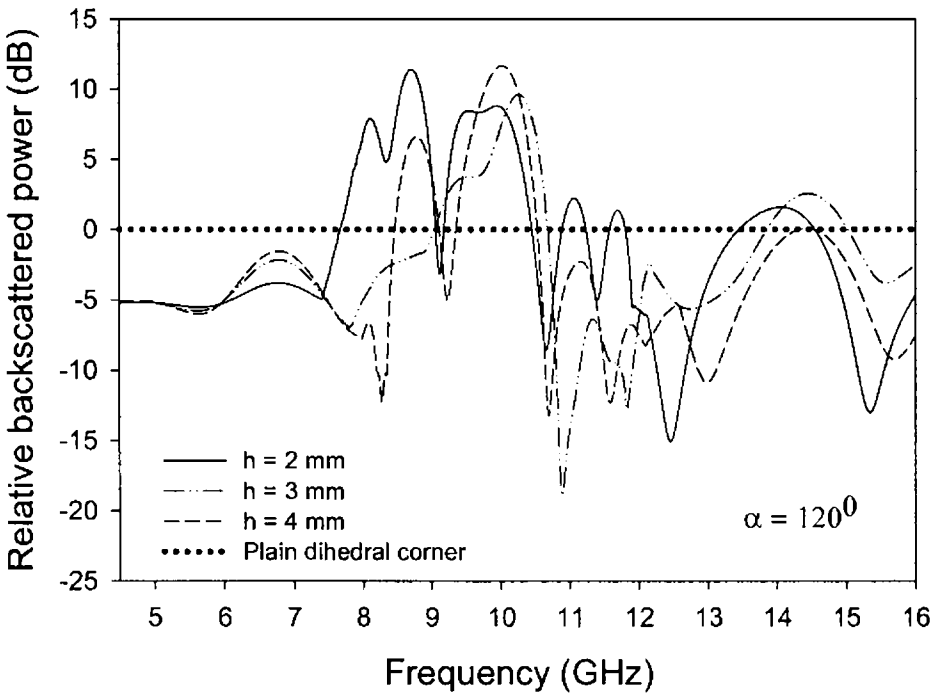
(c)



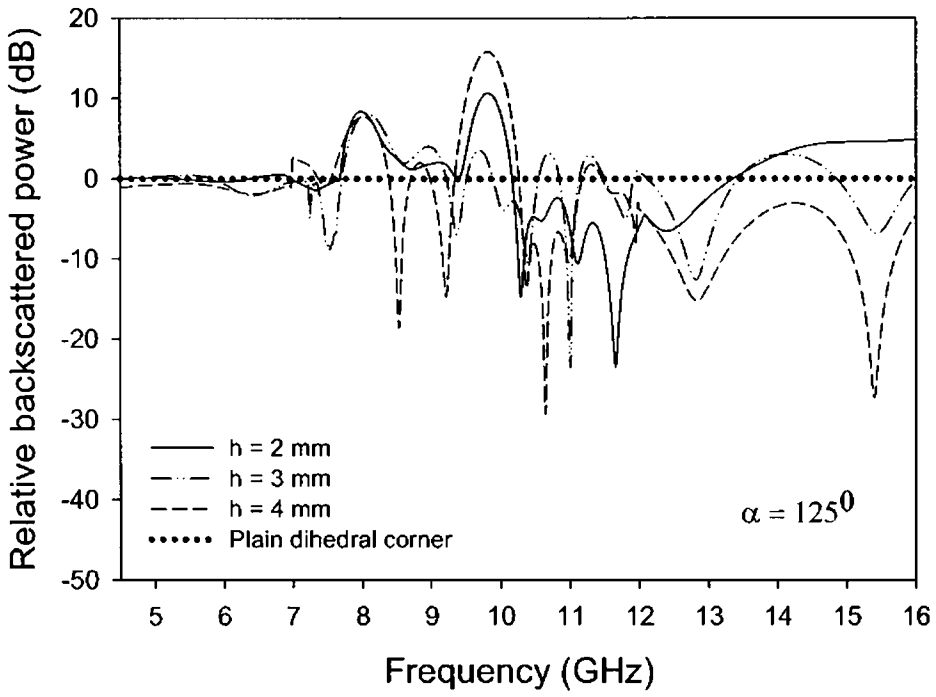
(d)



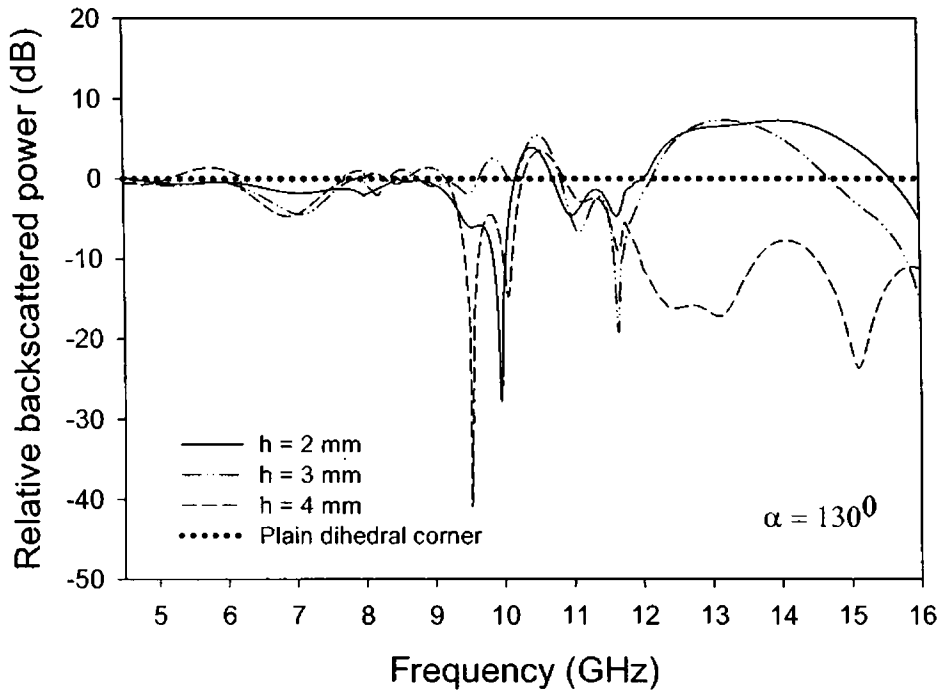
(e)



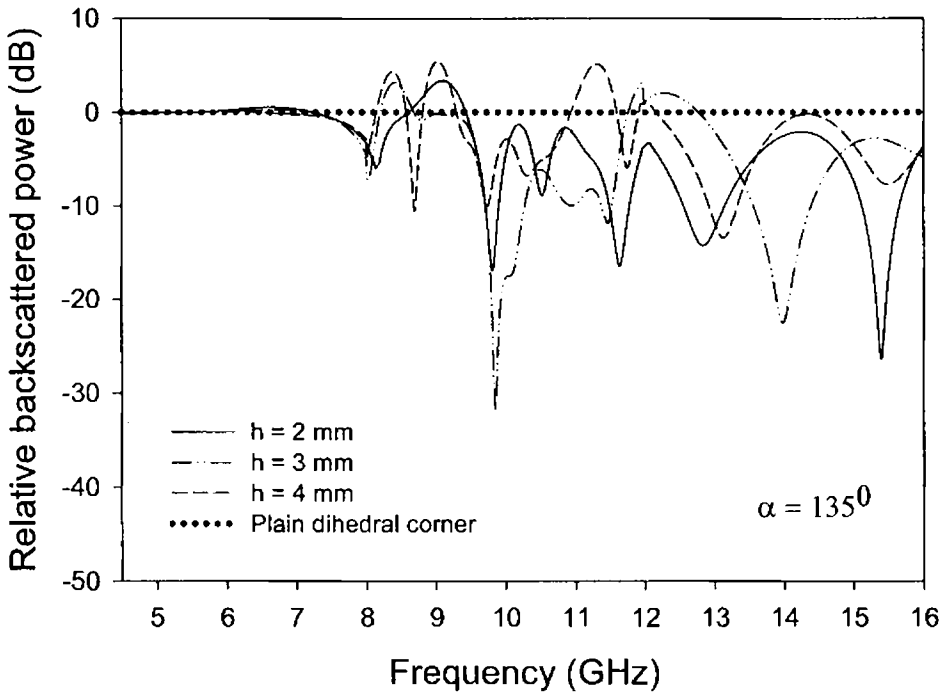
(f)



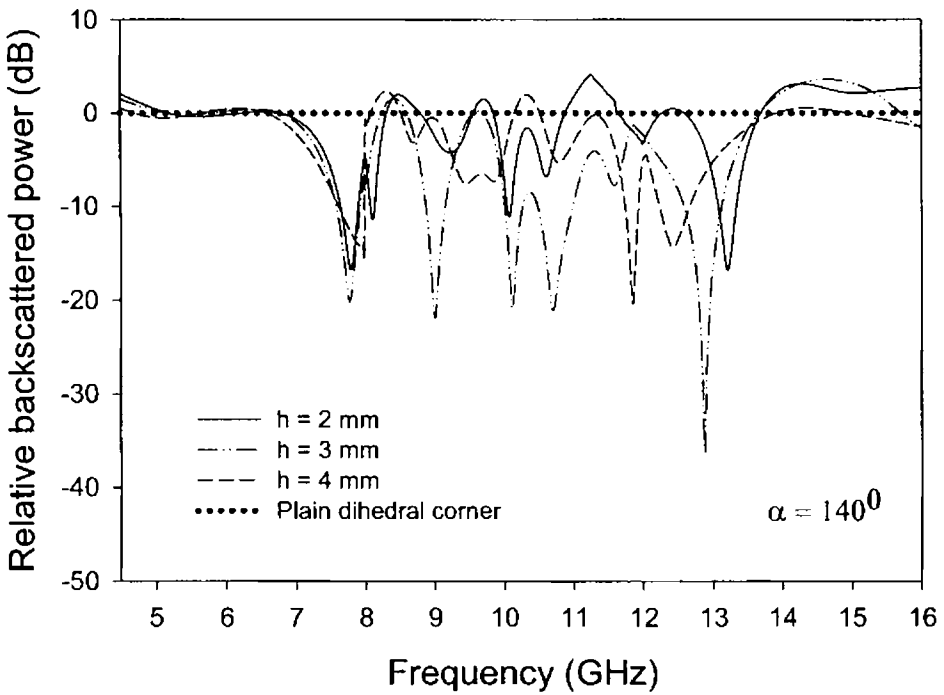
(g)



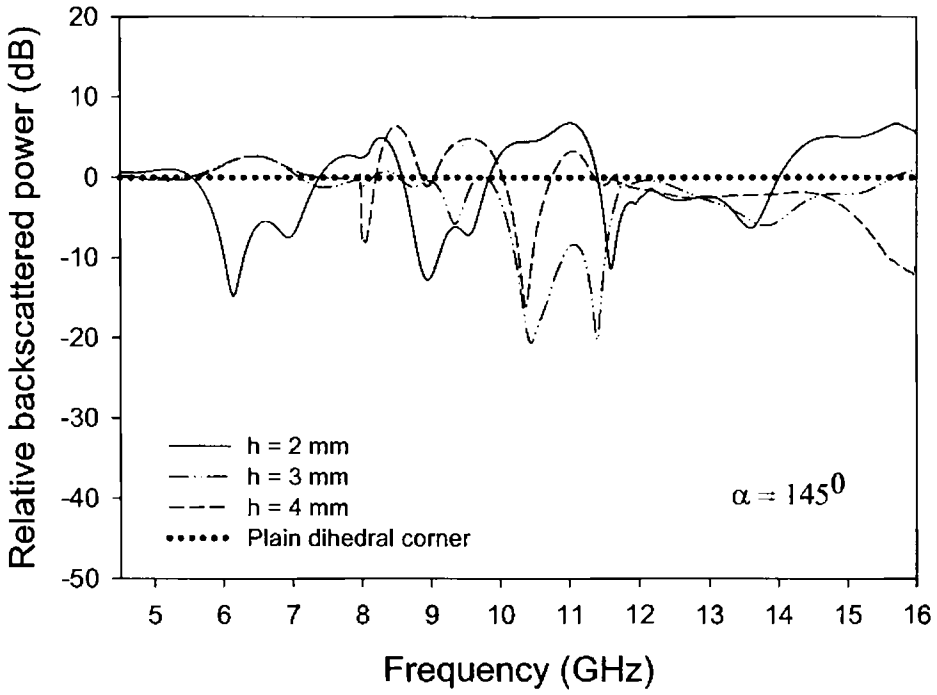
(h)



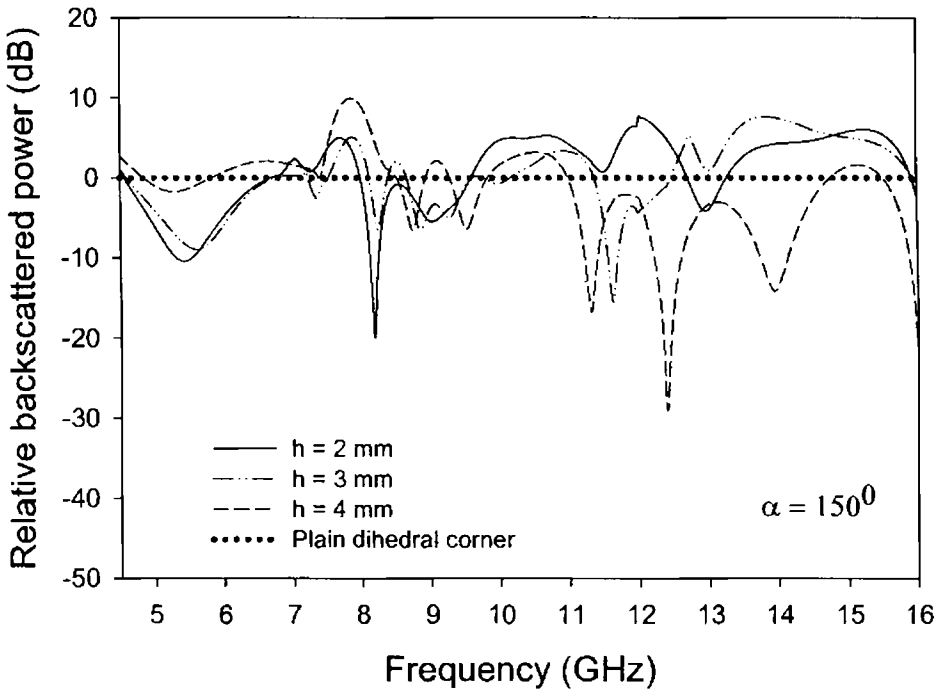
(i)



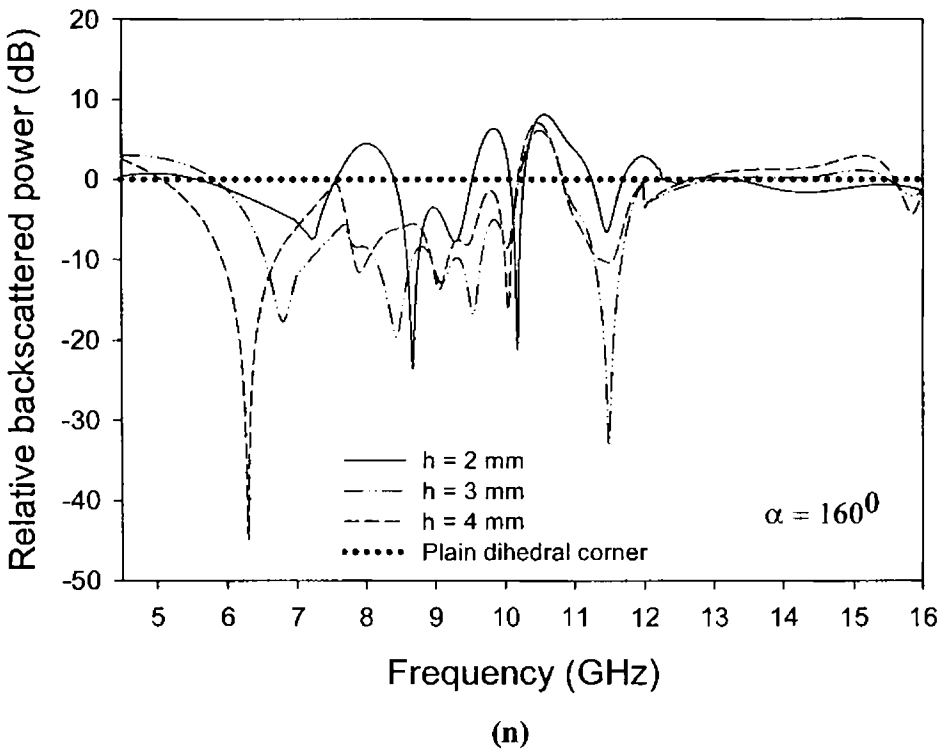
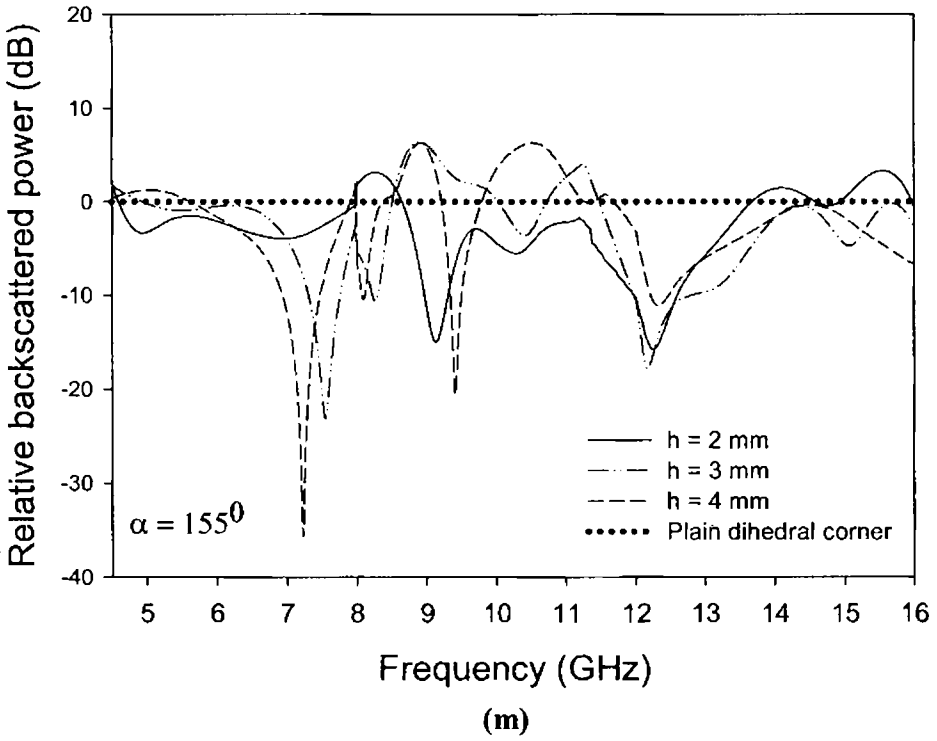
(j)

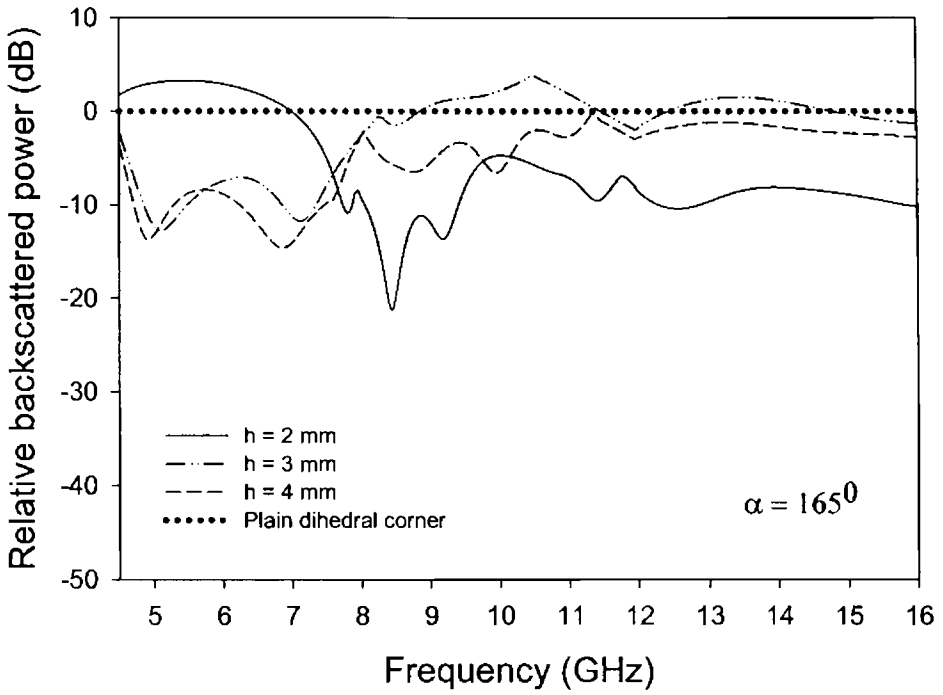


(k)

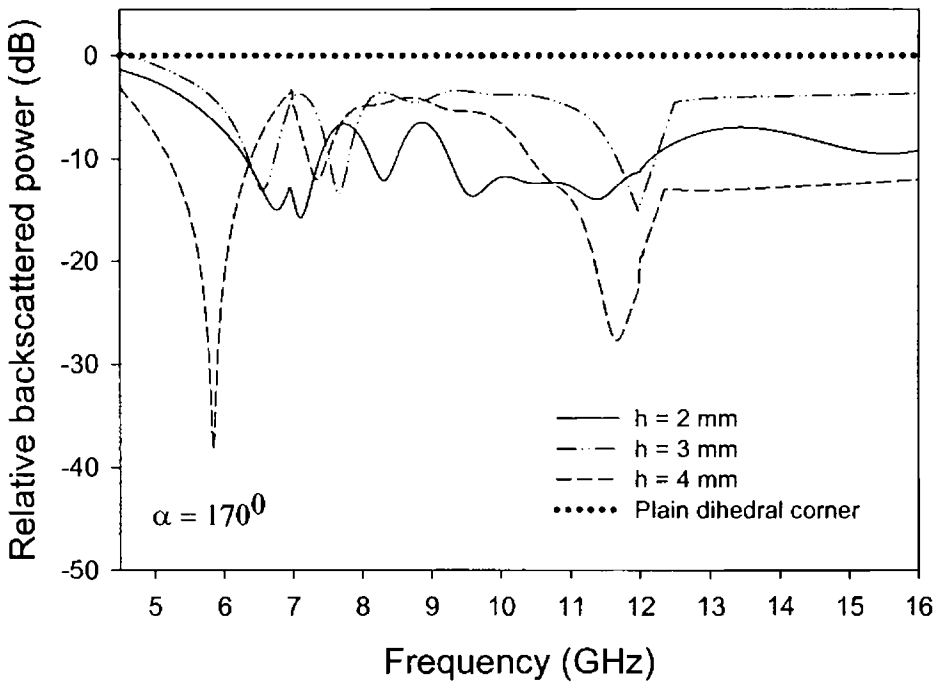


(l)

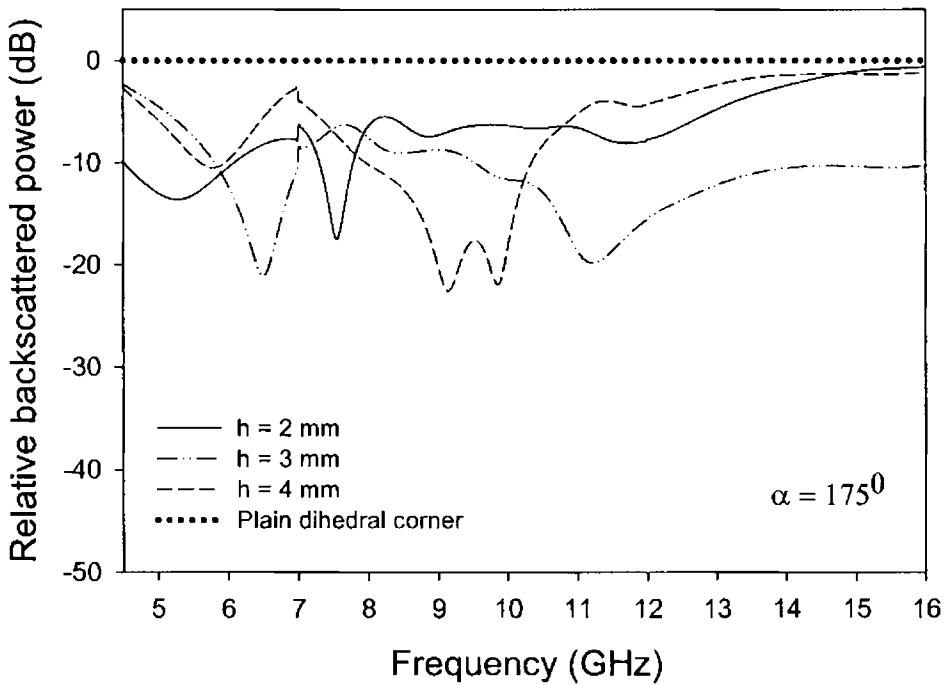




(o)



(p)

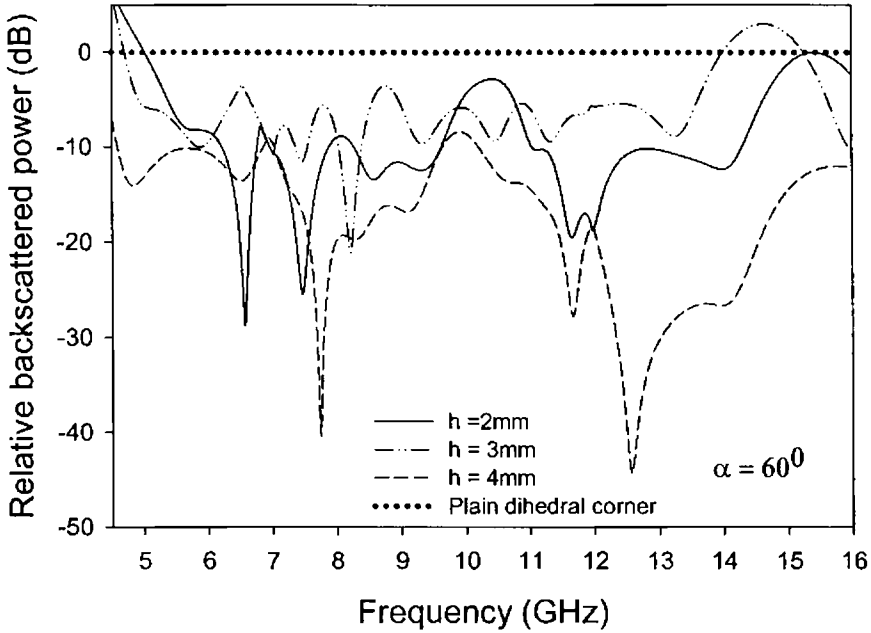


(q)

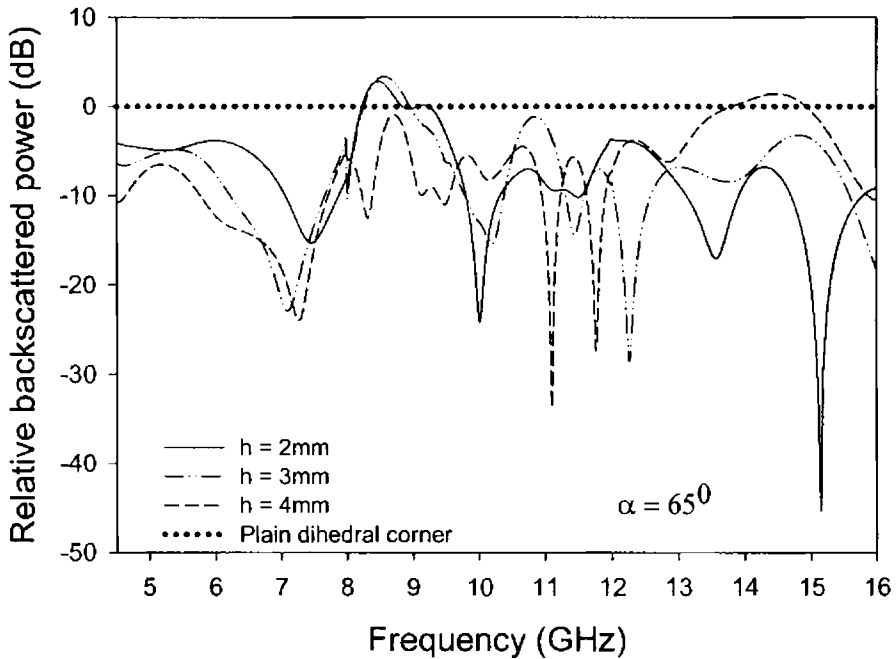
From the observations it is found that loading fractal based metallo-dielectric structure reduces the backscattering from a corner reflector of corner angle 90° . For other angles, an enhancement in backscattered power is observed compared to a plain corner reflector. The backscattered power is maximum for certain acute and obtuse angles. An enhancement in backscattered power of around 20 dB is obtained for corner angles $\alpha = 80^\circ$ and 105° .

TM polarization

The measurement results for acute angles of the corner reflector for TM polarization are shown in figures 4.61 (a) - (f).

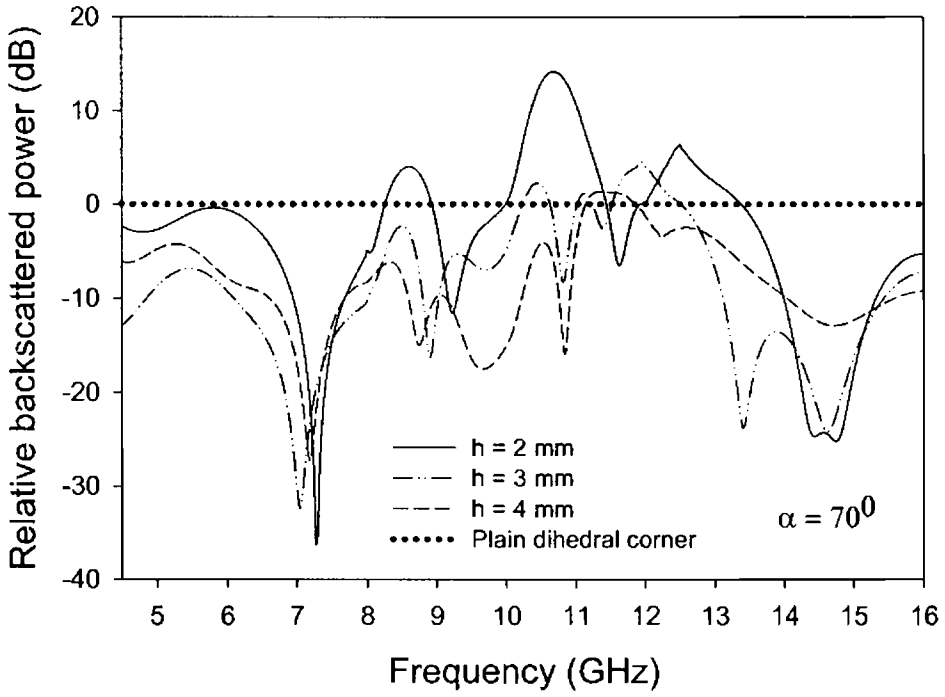


(a)

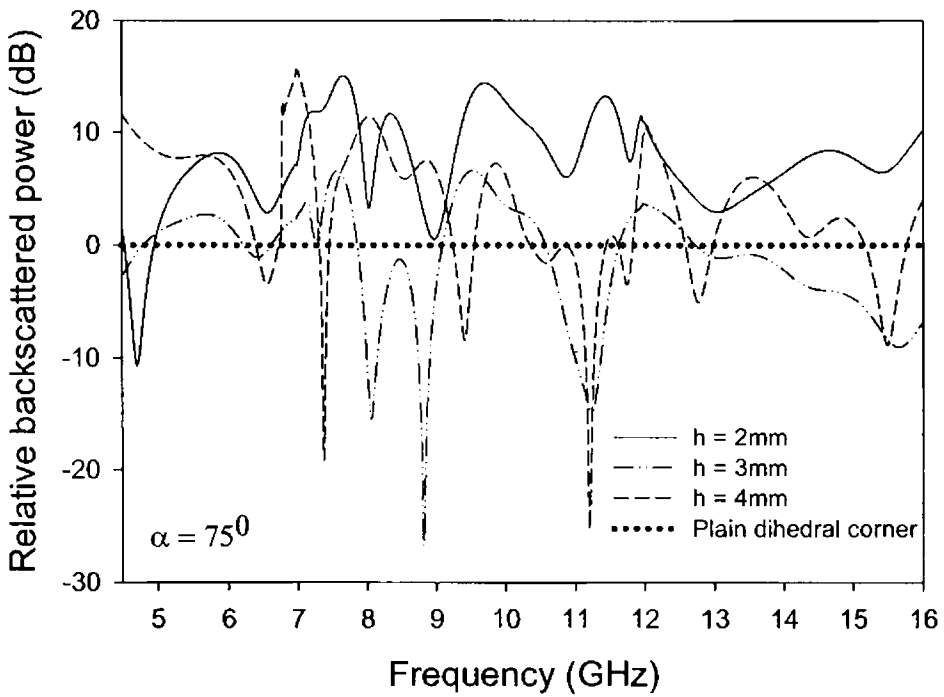


(b)

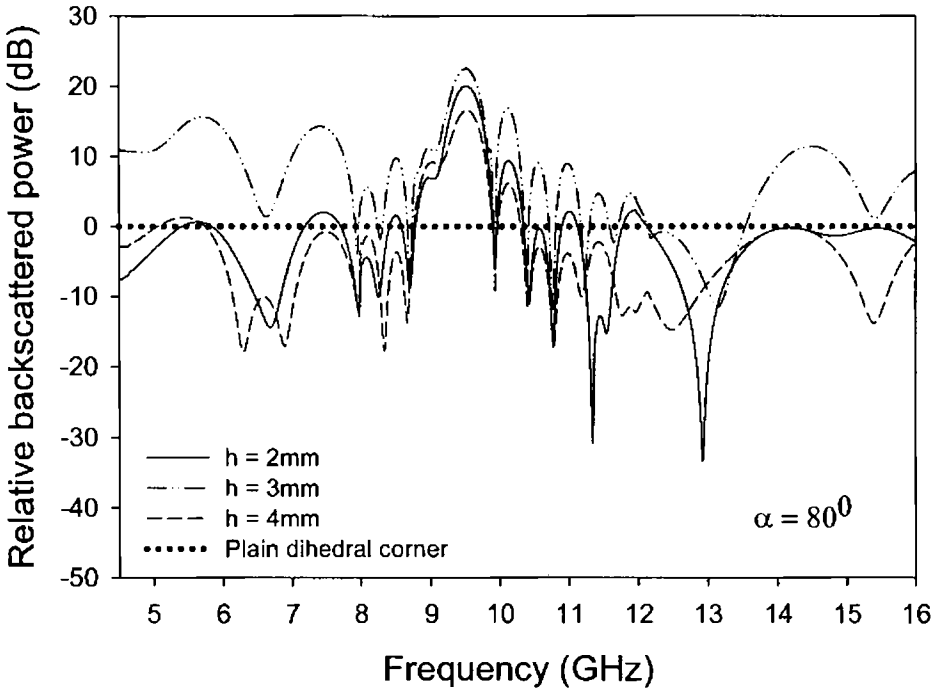
Figure 4.61 Variation of backscattered power against frequency for acute angles of the dihedral corner reflector for TM polarization
(a) $\alpha = 60^{\circ}$ (b) $\alpha = 65^{\circ}$ contd



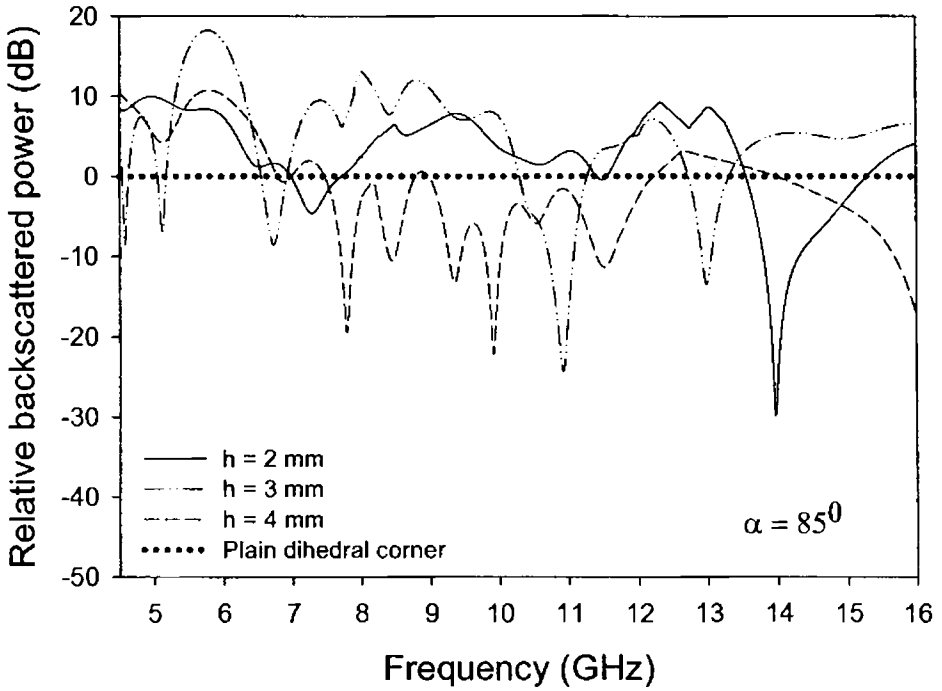
(c)



(d)



(e)



(f)

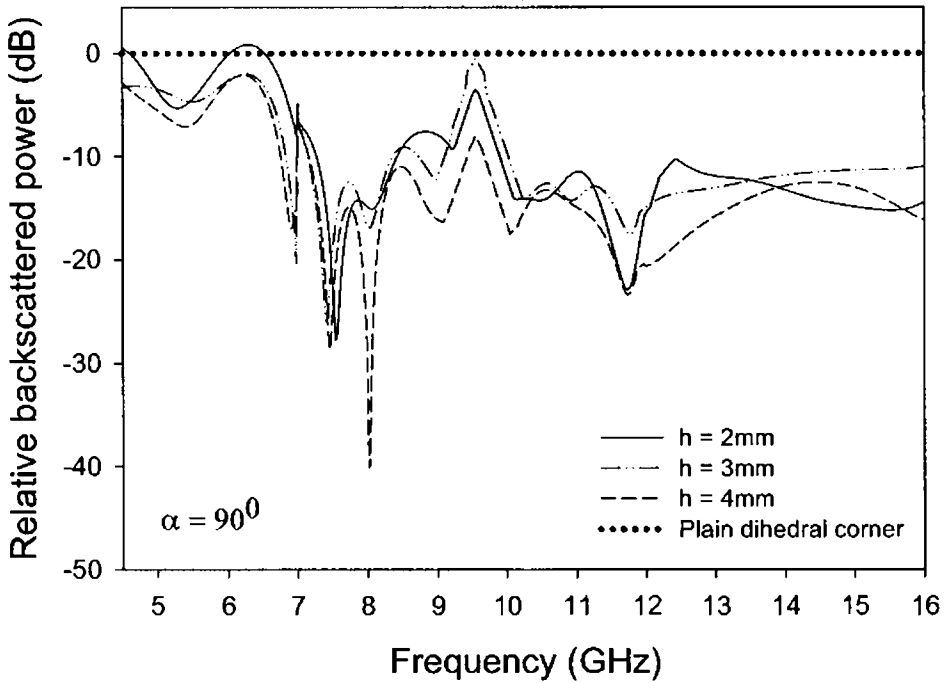


Figure 62 Backscatter power variations against frequency for a right angled corner reflector for TM polarization

As in the case of TE polarisation, 90° corner reflector gives backscattering reduction when loaded with metallo-dielectric structures. Results plotted in figure 62 indicates a reduction of ~ 40 dB at 8.03 GHz for $h = 4$ mm.

Backscattered power measured for different angles of incidence for TM is given in figure 4.63. It is observed a maximum backscattered power of -12.27 dB is obtained for an angle of incidence of 15° .

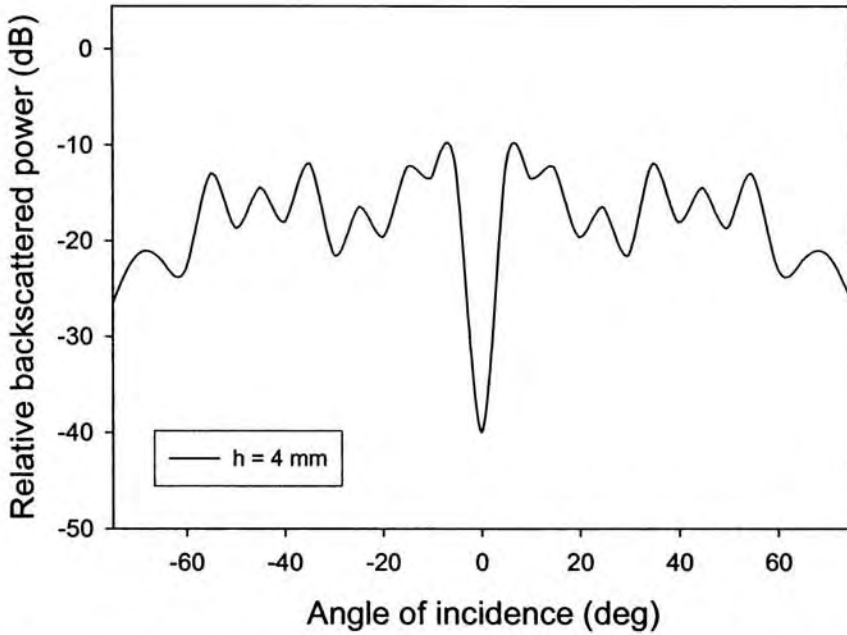
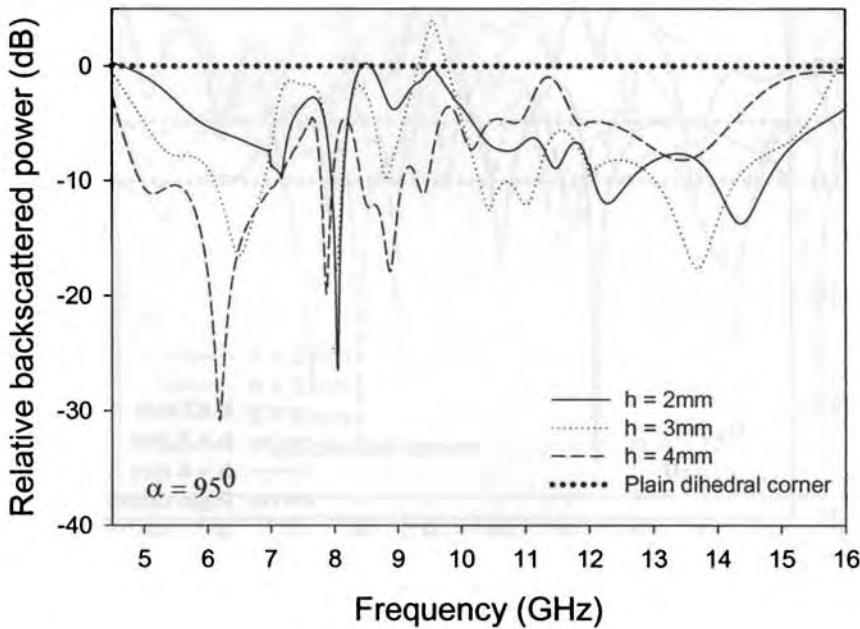


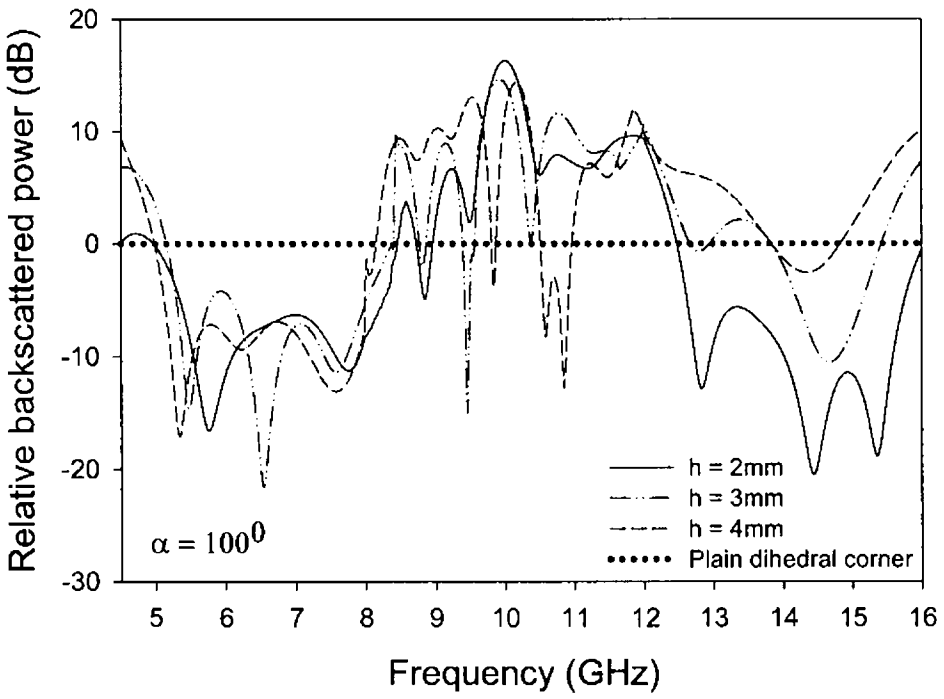
Figure 4.63 Variation of backscattered power with angle of incidence for $f = 8.03$ GHz for TM polarization

The backscattered power measurements for obtuse angles ($\alpha = 95^\circ - 175^\circ$) are shown in figures 4.64 (a) – (q) for different dielectric thickness.

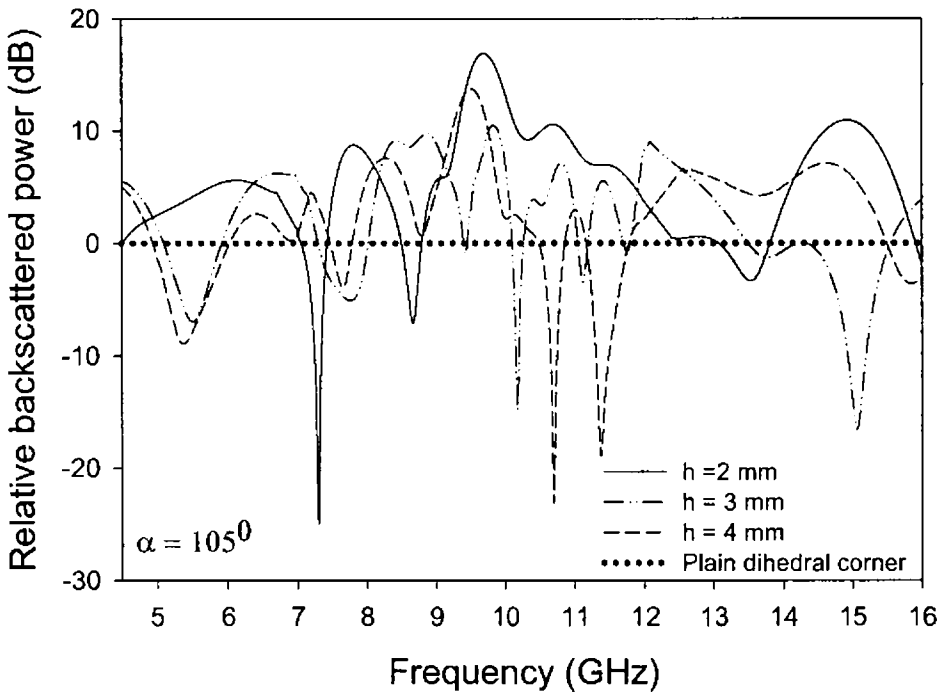


(a)

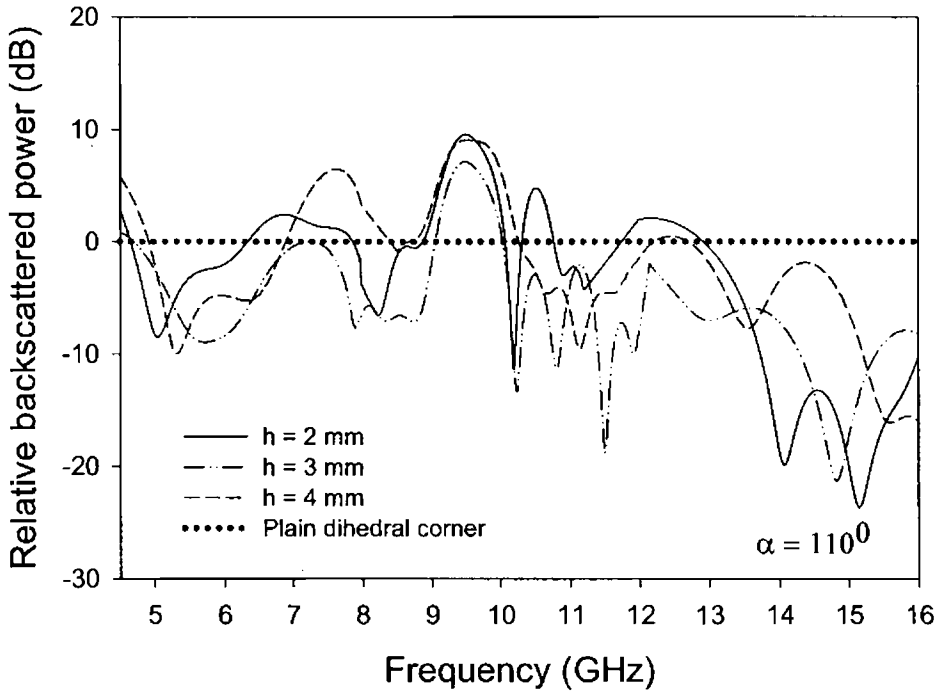
Figure 4.64 Variation of backscattered power against frequency for obtuse angles of the dihedral corner for TM polarization
(a) $\alpha = 95^\circ$ contd



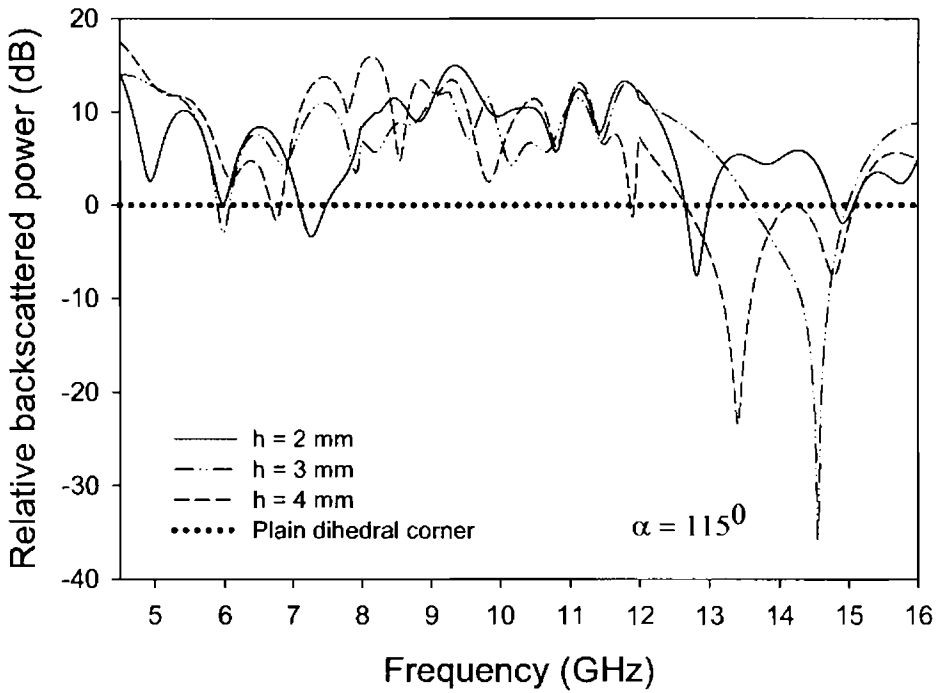
(b)



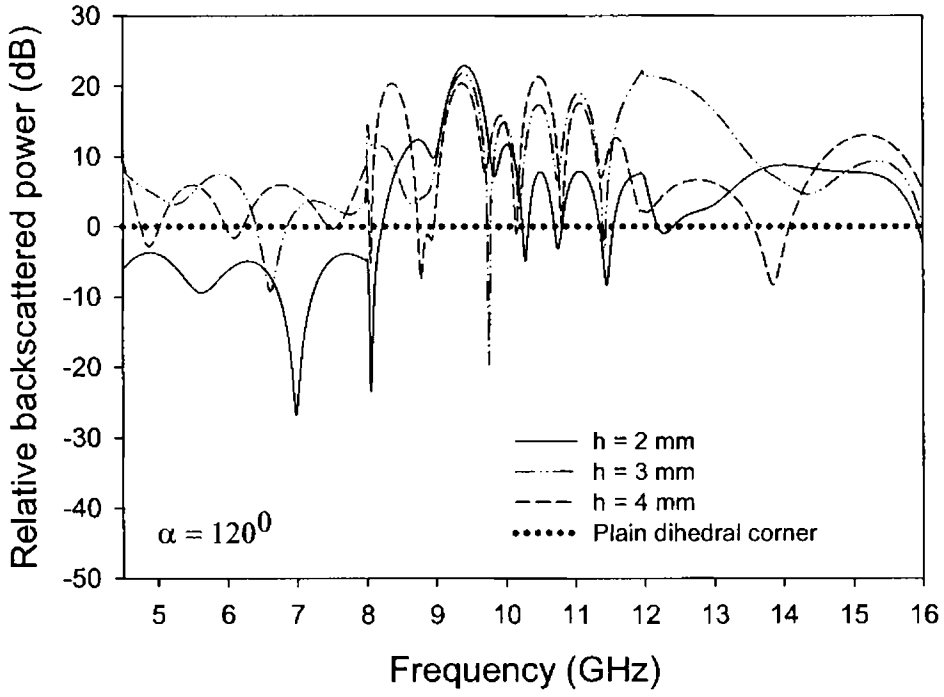
(c)



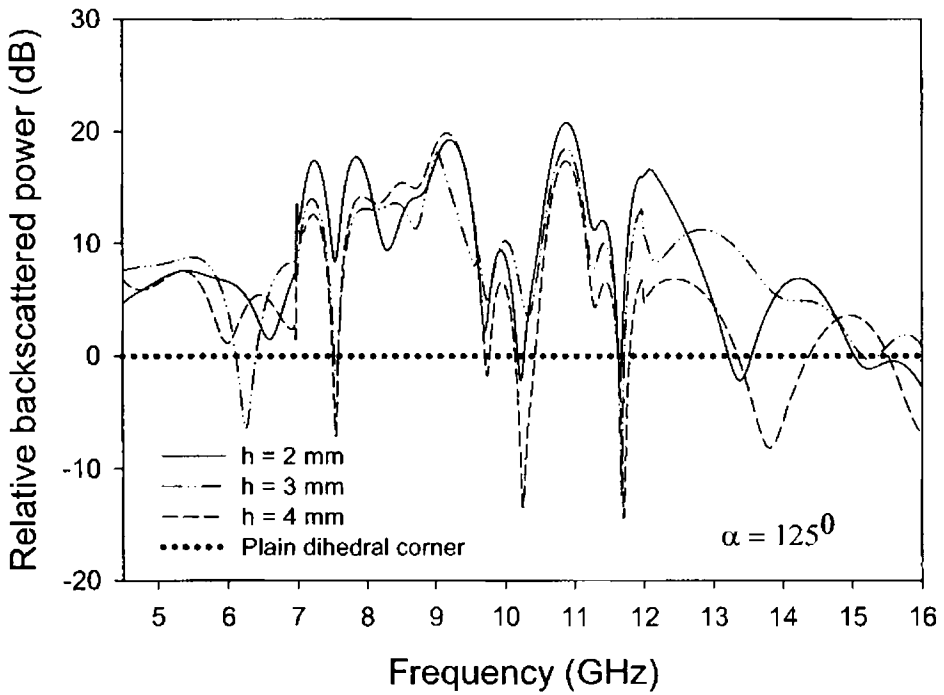
(d)



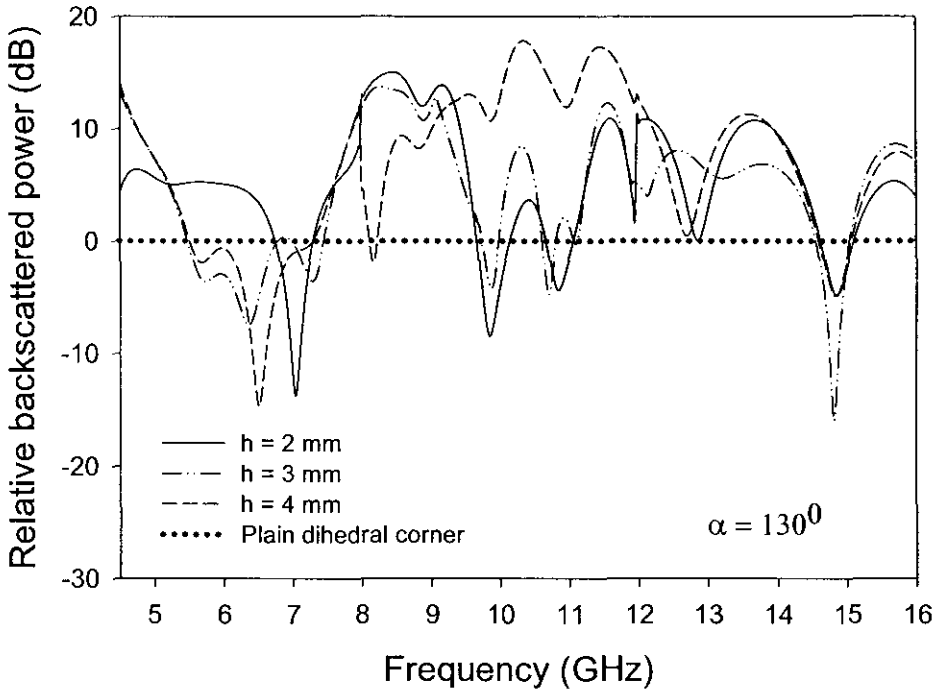
(e)



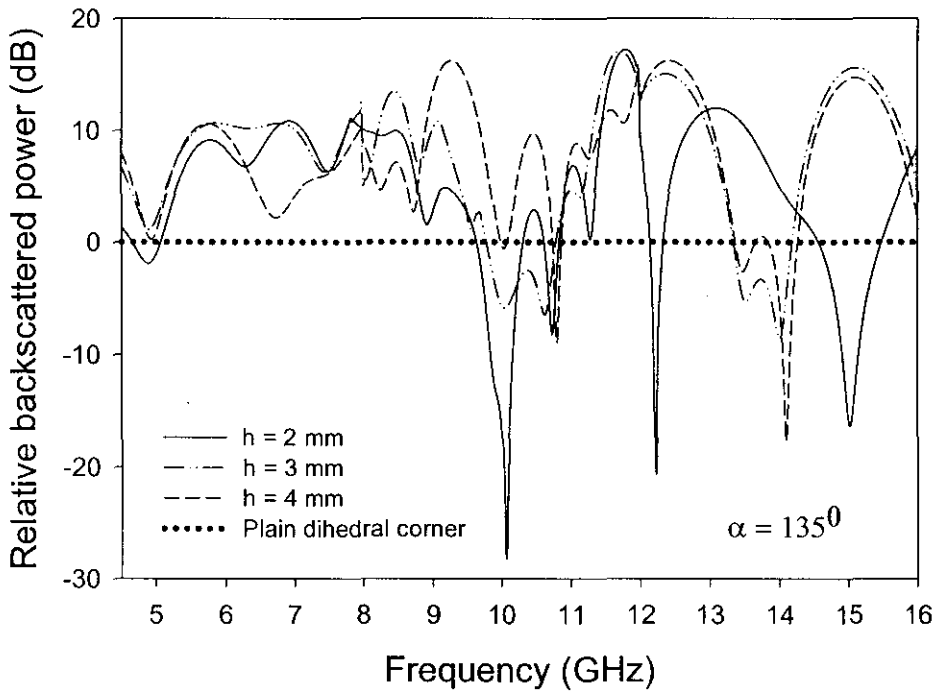
(f)



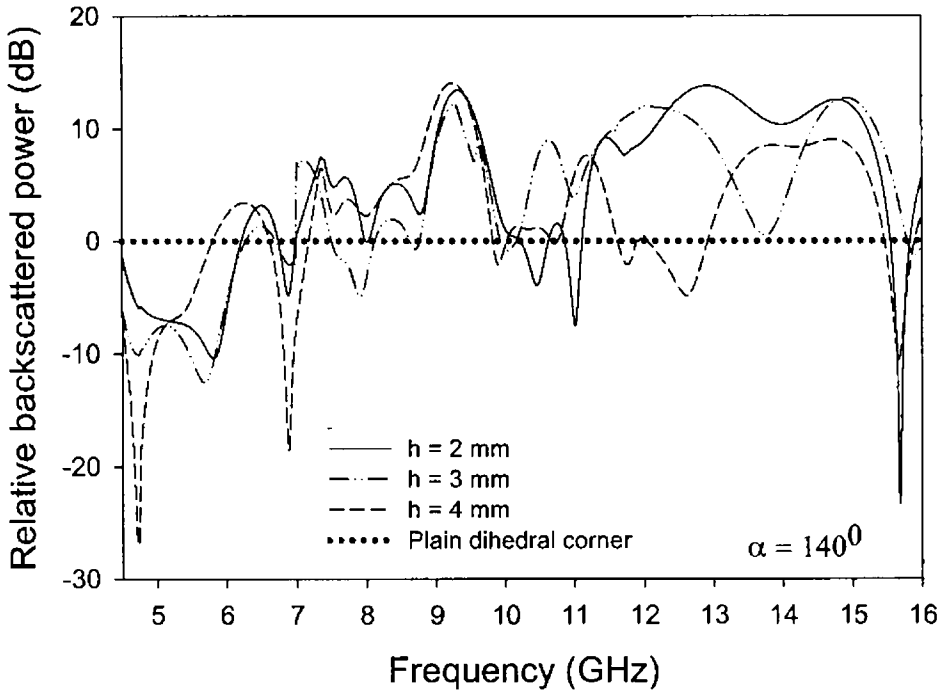
(g)



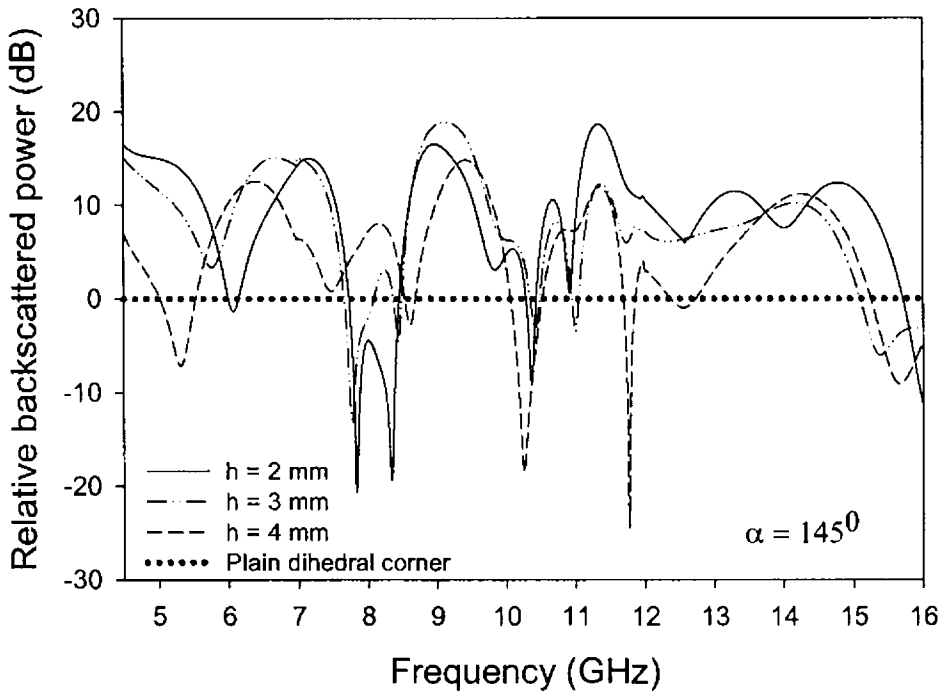
(h)



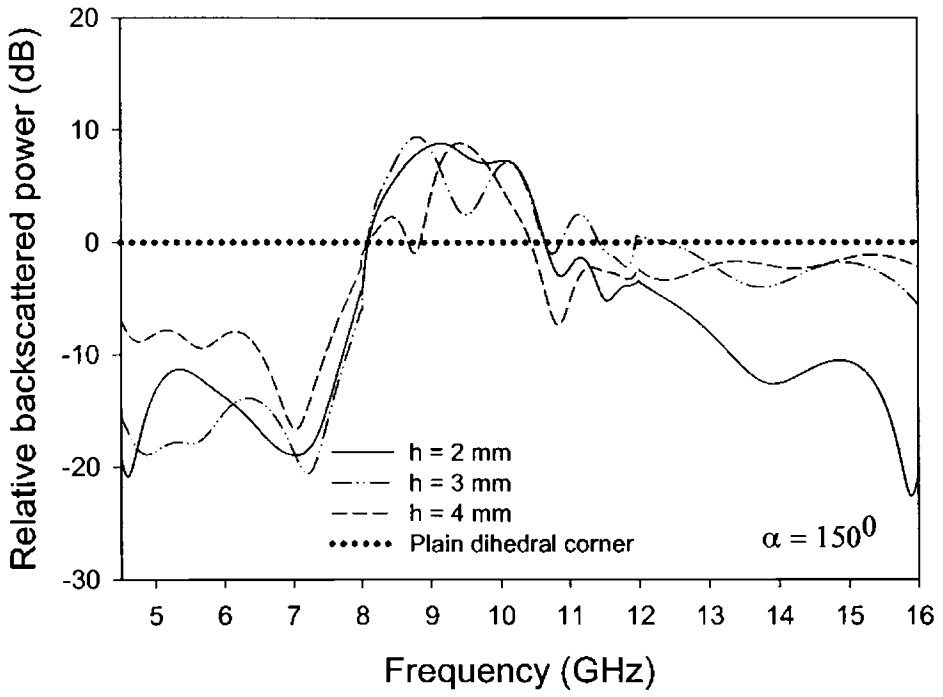
(i)



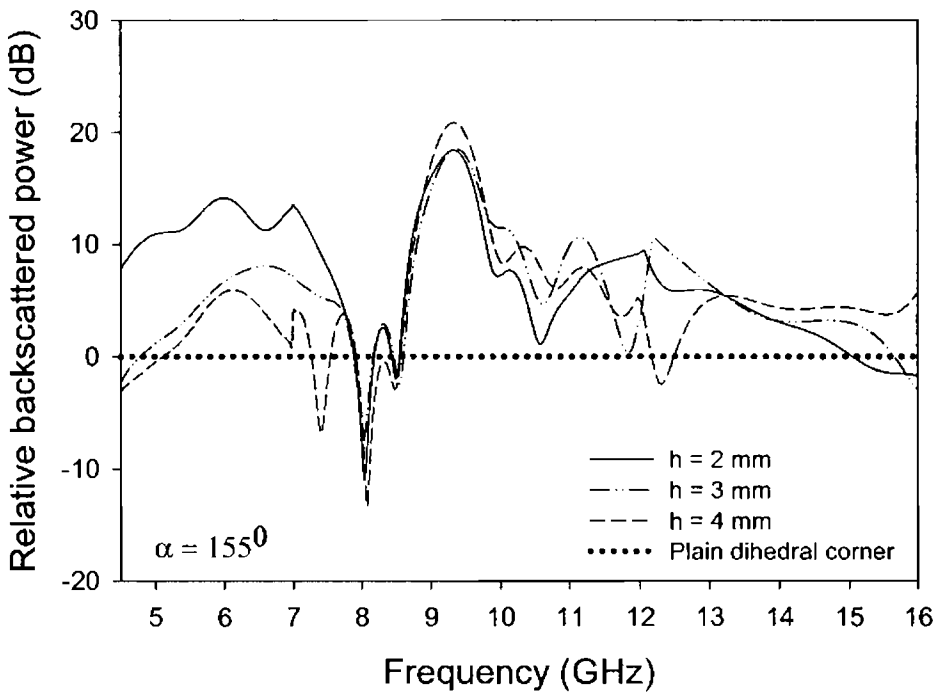
(j)



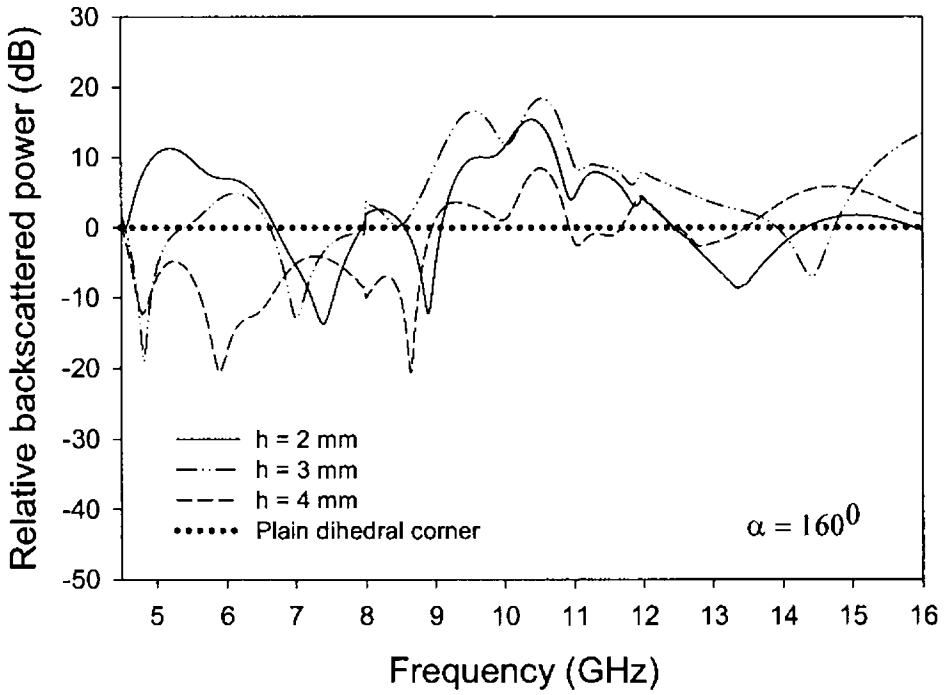
(k)



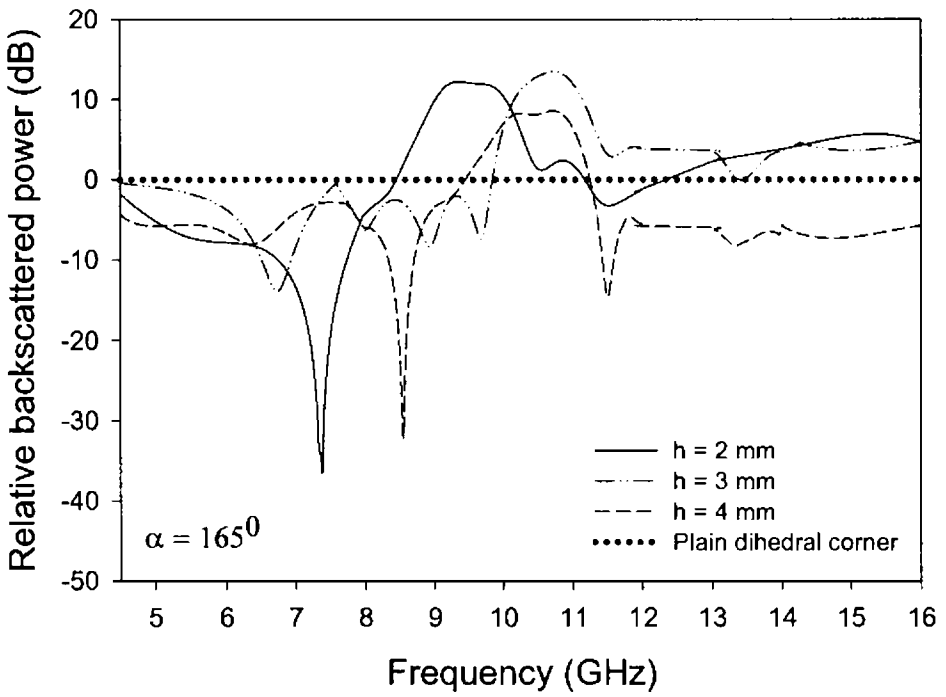
(l)



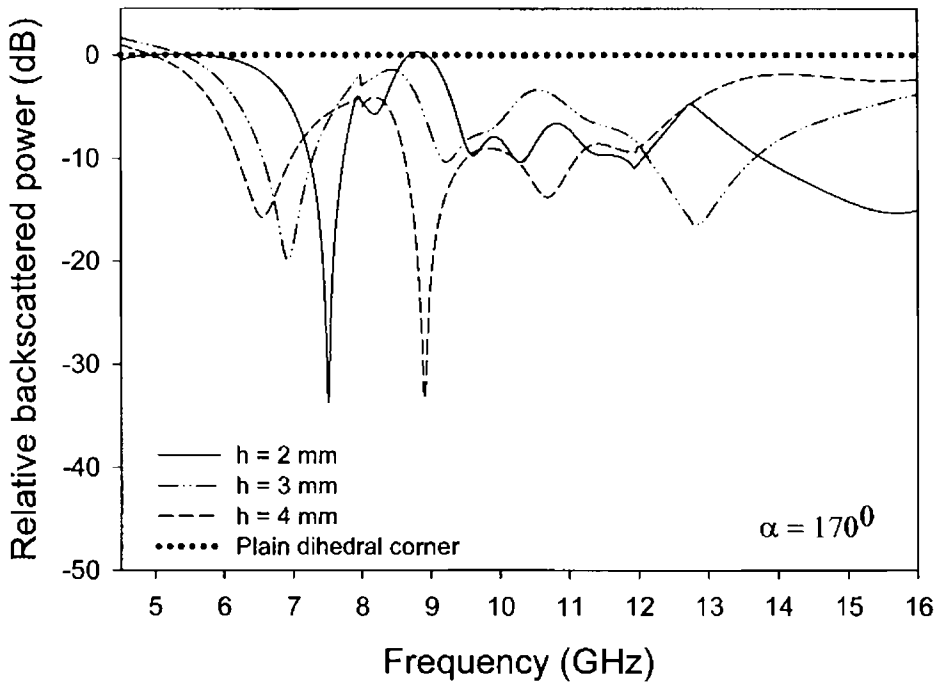
(m)



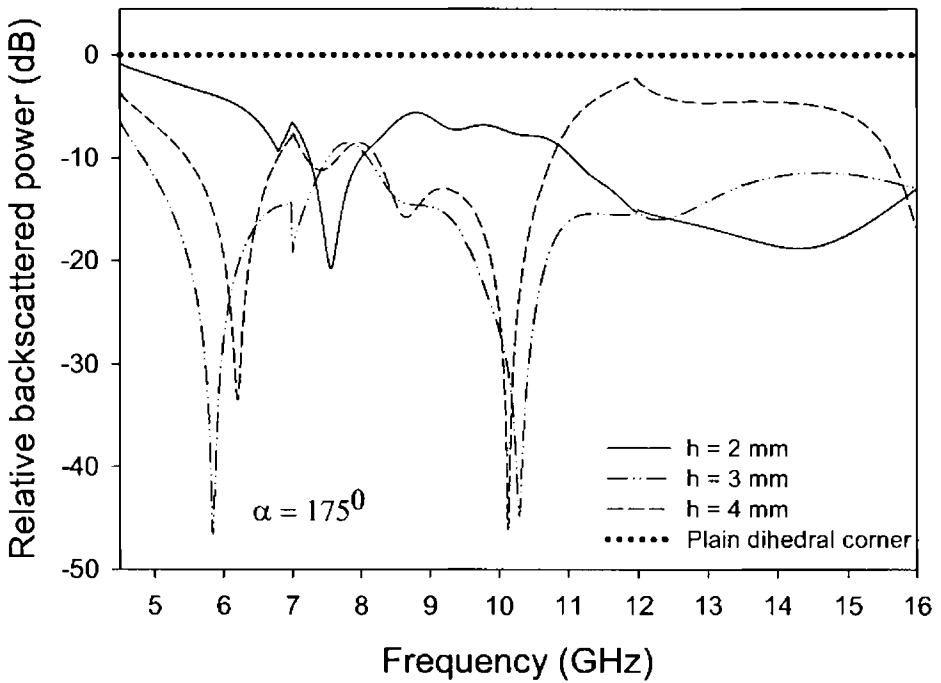
(n)



(o)



(p)



(q)

In the case of TM polarizations also it is found that loading fractal based metallo-dielectric structure reduces the backscattering from a corner reflector of corner angle 90° . There are enhancements in backscattered power for certain acute and obtuse angles. Maximum increase in backscattered power is observed for corner angles $\alpha = 80^\circ$ and 120° .

4.4.3 CIRCULAR CONE

The scattering characteristic of a circular metallic cone loaded with metallo-dielectric structure based on the array of Sierpinski carpet fractal geometry is described in this section. A schematic of the structure is shown in figure 4.65.

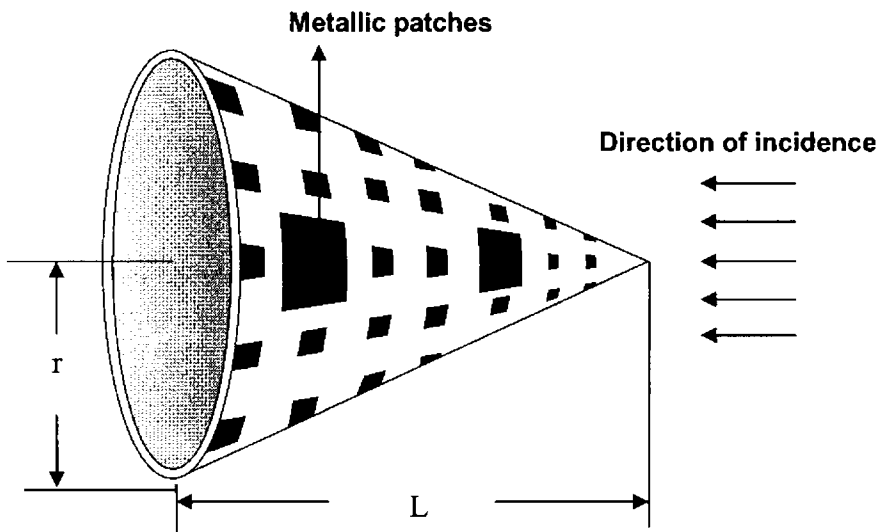


Figure 4.65 Metallic circular cone loaded with array of Sierpinski carpet fractal geometry, radius = 11 cm, $L = 22$ cm.

The variation of backscattered power with frequency for different substrate thickness is shown in figure 4.66. A plain metallic plate having the same area as that of the base of the cone is used as the reference target. The measured results indicate that by loading fractal based structure over the cone the backscattered power can be reduced to a considerable extent. A maximum reduction in backscattered power of 25.5 dB with respect to metallic cone is obtained at $f = 8.1275$ GHz for a dielectric thickness $h = 1.2$ mm.

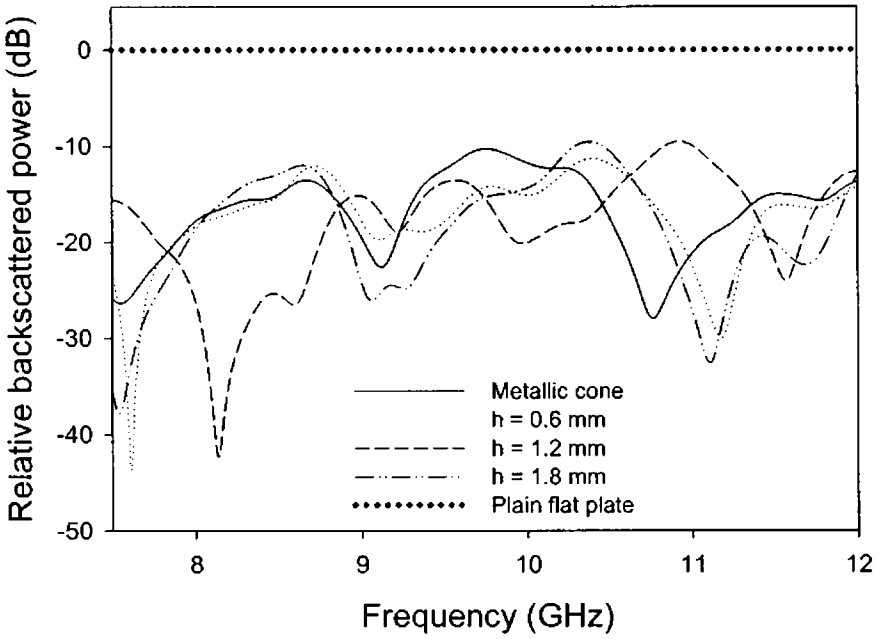


Figure 4.66 Variation of relative backscattered power with frequency for different dielectric thickness

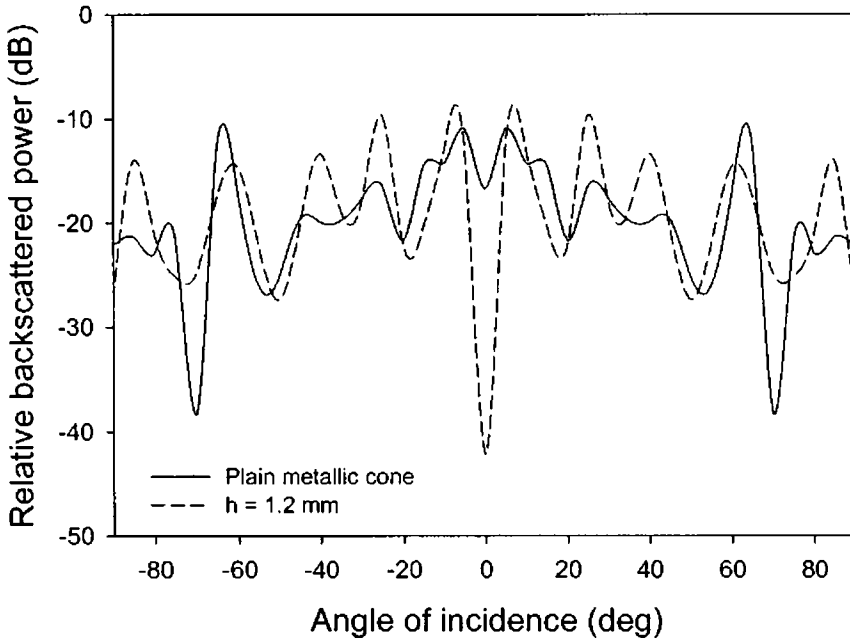


Figure 4.67 Variation of relative backscattered power with angle of incidence, $f = 8.127$ GHz

The variation of backscattered power with angle of incidence at $f = 8.127$ GHz is shown in figure 4.67. A reduction of backscattered power of ~ 25 dB is obtained with respect to a metallic cone for normal incidence. Maximum backscattered power of -10.92 dB is obtained for an angle of incidence of 5° . Scattered power distribution for normal incidence is shown in figure 4.68. It is seen that the distribution is symmetric with respect to normal due to the symmetry in the nature of the structure.

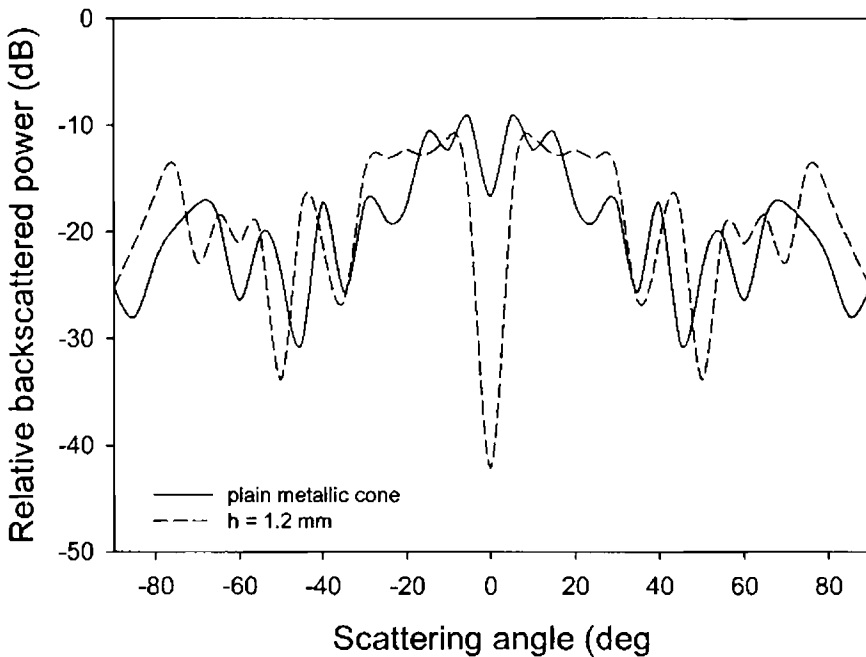


Figure 4.68 Backscattered power received at different scattering angles for $f = 8.127$ GHz

Chapter 5

SIMULATION STUDIES AND ANALYSIS

Comparisons of the backscattering properties of different structures are presented in this chapter. The results of the experimental studies are validated by analyzing the structures using electromagnetic simulation software. The simulation and experimental results are compared for different structures.

5.1 BACKSCATTERING CHARACTERISTICS OF STRUCTURES WITH PATCHES OF DIFFERENT SHAPES

Sierpinski carpet structures with third iterated stages were fabricated with generators of different shapes and their characteristics were studied in detail in the previous chapter.

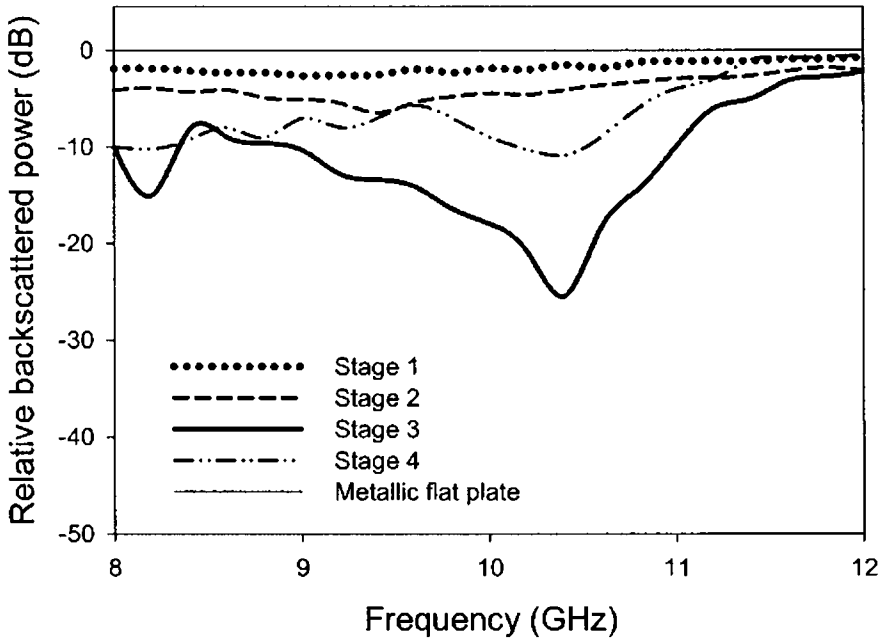
Table 1 presents the comparison of backscattering characteristics of different structures in C, X and Ku frequency bands. From the table, it is clear that by using fractal structures the reduction in backscattered power can be obtained at different bands. Sierpinski carpet with circular patch as the generator is giving backscattering reduction over a bandwidth of 3 GHz (below -10 dB) in the C band. A bandwidth of 3.37 GHz is obtained for the structure with hexagonal patch as the generator in the X band. In Ku band, 3.1 GHz bandwidth is obtained for square Sierpinski carpet structure.

Table 1 Comparison of backscattering properties of different fractal structures

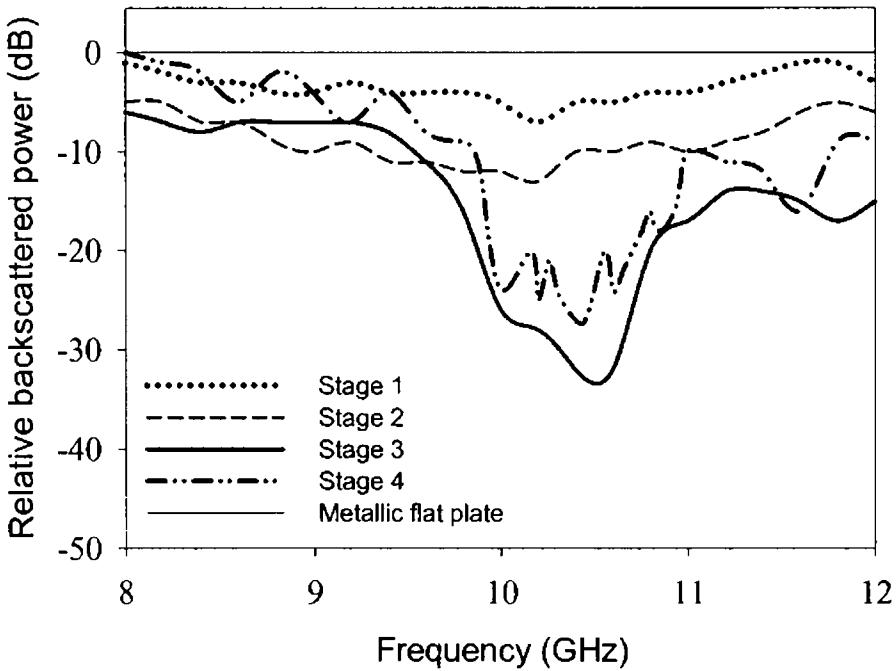
Fractal structures	-10 dB Bandwidth (GHz)		
	C-band	X-band	Ku-band
Sierpinski carpet Square TE & TM	0.46	2.4	3.1
Cross TE & TM	0.21	1.15	1.48
Octagon TE & TM	0.6	1.95	2.52
Hexagon TE-polarization	1.03	1.14	1.44
Hexagon TM-polarization	0.7	3.37	1.64
Circle TE & TM	3	1.71	2.8
Diamond TE & TM	-	1.22	1.64
Purina square TE & TM	0.7	2.66	3
Star TE - polarization	-	1.6	0.13
Star TM - polarization	-	1.25	-
Sierpinski carpet Array TE & TM	1.05	1.05	1.12
Sierpinski gasket TE and TM	2.58	2.6	1.8

5.2 SIMULATED RESULTS

The different iterated stages of Sierpinski carpet (shown in figures 4.1 – 4.4) were studied for the structures fabricated on substrates of different thickness. The optimum thickness giving minimum backscattered power in the band is found out. Simulation using CST Microwave Studio showed that the structure with the third iterated stage of Sierpinski carpet gives maximum reduction in backscattered power. The simulated results are shown in figure 5.1 (a). Experimental results shown in the previous chapter is repeated in 5.1 (b) for comparison.



(a)



(b)

Figure 5.1 Backscattered power variations with frequency for different iterated stages of the Sierpinski carpet structure
(a) Simulated
(b) Measured

Figures 5.2 (a) to 5.2 (g) shows the comparison of the experimental and simulated results of the backscattering from structures with generators of different shapes. In all these cases, the experiment results are found to be in good agreement with the simulation results.

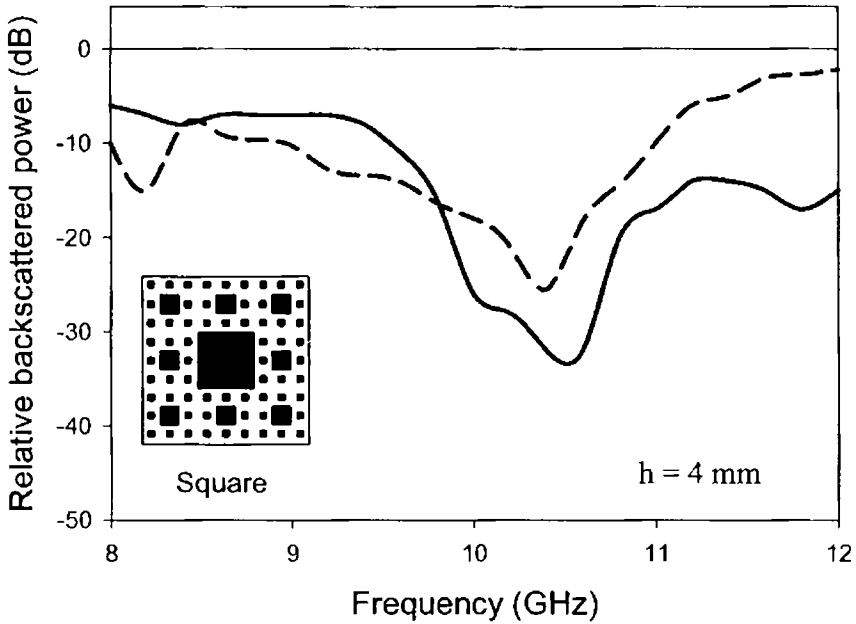


Figure 5.2 (a) Variation of backscattered power against frequency for the structure with square patch as the generator

- Simulation
- Experiment
- Flat plate

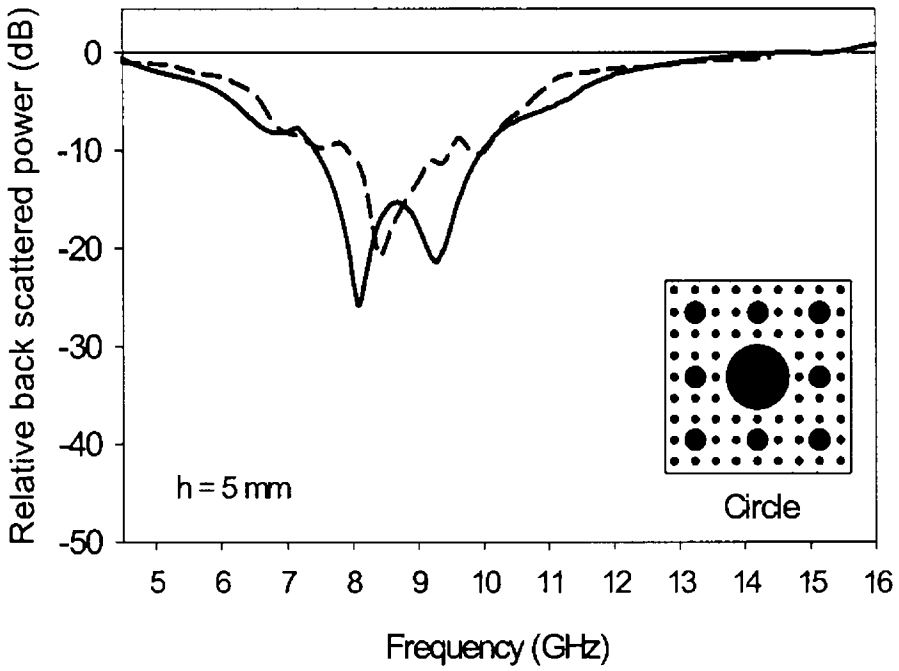


Figure 5.2 (b) Backscattered power variations with frequency for the structure with circular patches

- Simulation
- Experiment
- Flat plate

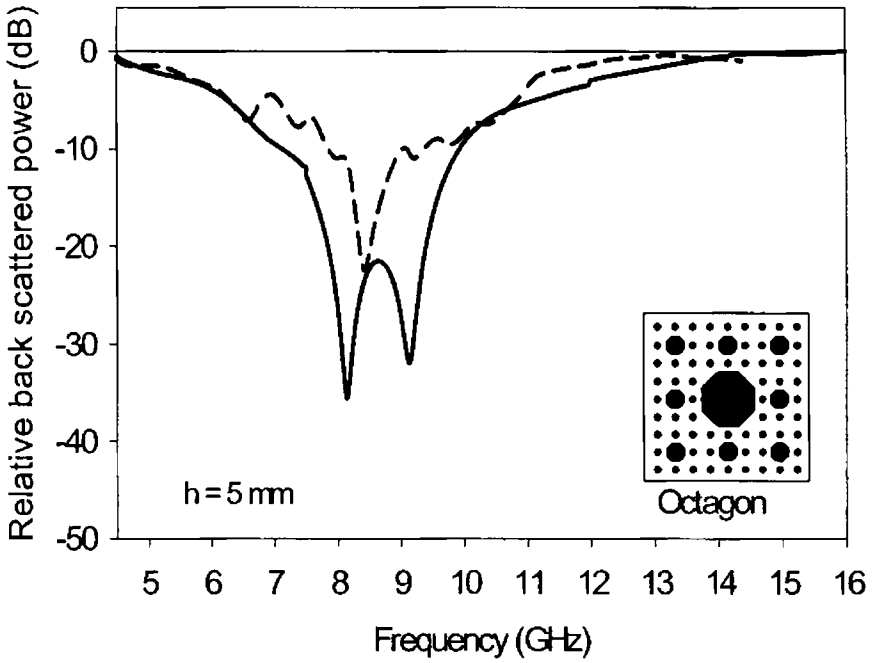


Figure 5.2 (c) Variation of backscattered power with frequency for the structure with octagonal patches

- Simulation
- Experiment
- Flat plate

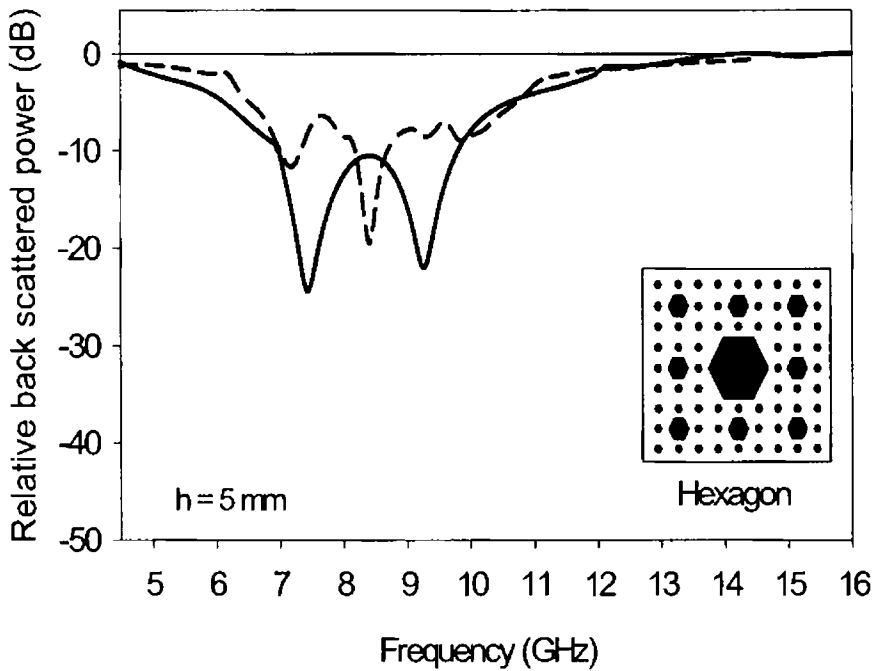


Figure 5.2 (d) Backscattered power variations with frequency for the structure with hexagonal patches, TE polarisation

- Simulation
- Experiment
- Flat plate

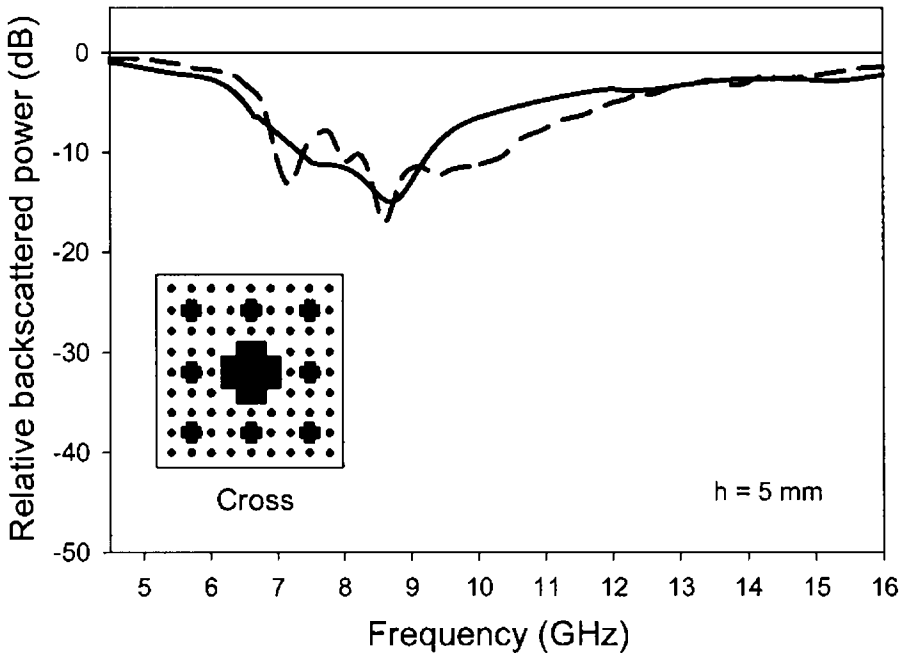


Figure 5.2 (e) Backscattered power variations with frequency for the structure with generator of the shape of cross

- Simulation
- Experiment
- Flat plate

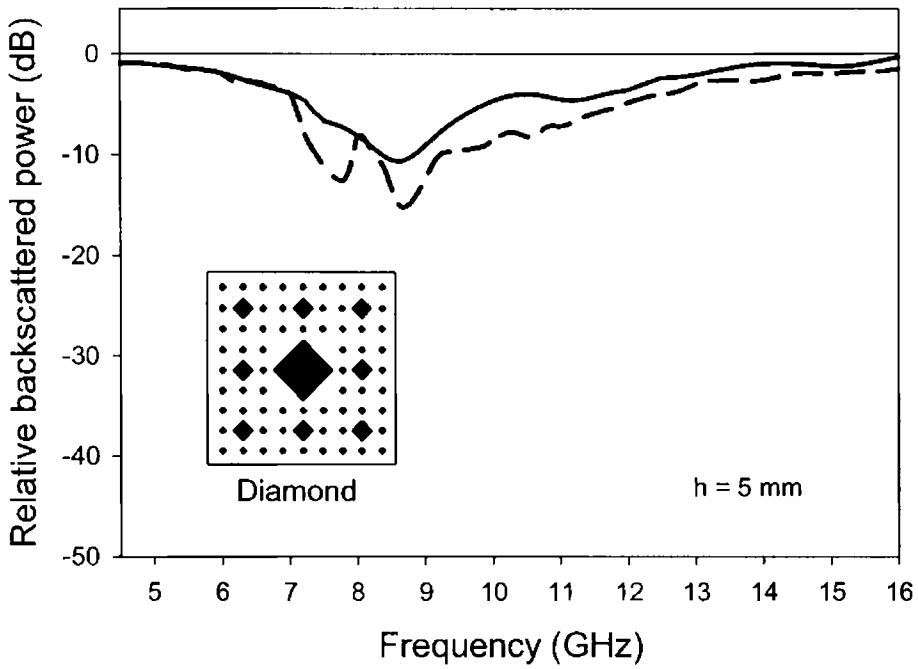


Figure 5.2 (f) Variation of backscattered power with frequency for the structure with generator of the shape of diamond

- Simulation
- Experiment
- Flat plate

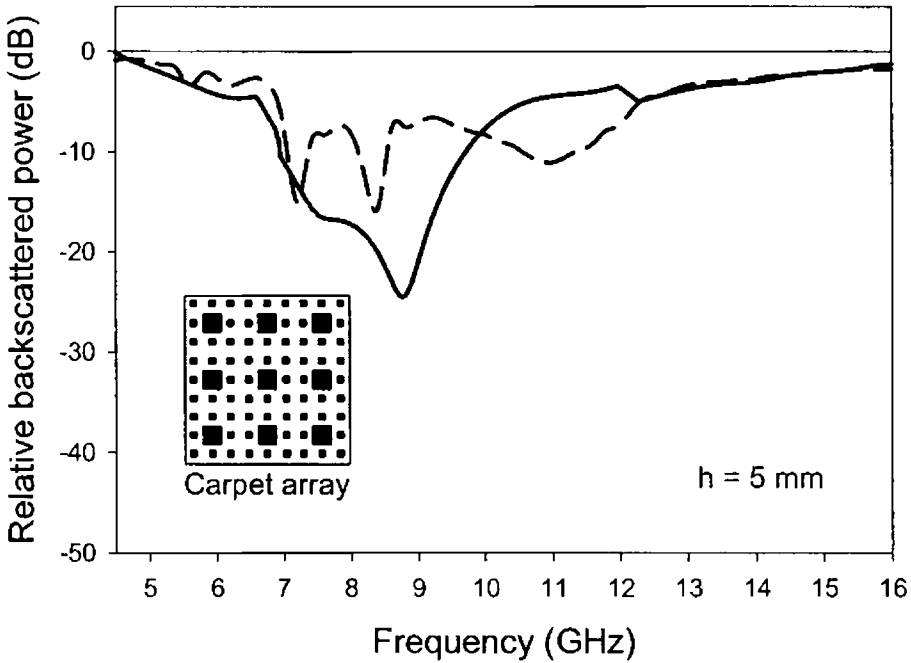


Figure 5.2 (g) Variation of backscattered power against frequency for the structure with array of second iterated stage of Sierpinski carpet

- Simulation
- Experiment
- Flat plate

From the observations it can be concluded that the reduction in backscattered power depends on the area occupied by the patch. The backscattered power obtained is high for Sierpinski carpet fractal structure with diamond, cross bar fractal tree, Purina square and star as generators. This is due to the fact that the patch area occupied by this geometry is less compared to other geometries such as Square, octagon, hexagon, circle, array of Sierpinski carpet. It is also noted that the central patch plays an important role in the reduction of backscattered power.

5.3 RCS ENHANCEMENT OF DIHEDRAL CORNER REFLECTOR

Backscattering property of dihedral corner reflector greatly depends on the corner angle. For a plane right angled dihedral corner reflector, the RCS is large. In chapter 4 it is shown that embedding metallo-dielectric fractal structures reduces the backscattering which means a reduction in RCS. Also low RCS of corner reflectors with acute and obtuse corner angles can be increased by applying metallo-dielectric structures. Studies were conducted on dihedral corner reflectors with corner angles in the range of 65° - 175° for both TE and TM polarizations to verify the dependence of corner angle on RCS reduction/enhancement.

Figure 5.3 presents the variation of RCS against frequency with and without loading MDS, for a dihedral corner reflector with 80° corner angle. Compared to an unloaded corner reflector, a large value of RCS (above 20 dBsm) is obtained in the frequency range 9.15 - 10.33 GHz for substrate thickness of $h = 3$ mm, the peak (31 dBsm) being at 9.55 GHz. The backscattered cross section as a function of angle of incidence at this frequency is shown in Fig. 5.4.

Large enhancement in RCS is obtained for a corner angle of 120° also. The plot of RCS against frequency with and without loading MDS for 120° corner angle is shown in figure 5.5. A maximum RCS is obtained for 9.4 GHz for a dielectric thickness $h = 2$ mm. RCS variations with angle for this configuration is shown in figure 5.6. RCS variations with corner angles at $f = 9.55$ GHz and 9.4 GHz for TM and TE polarizations are shown in figures 5.7 and 5.8 respectively.

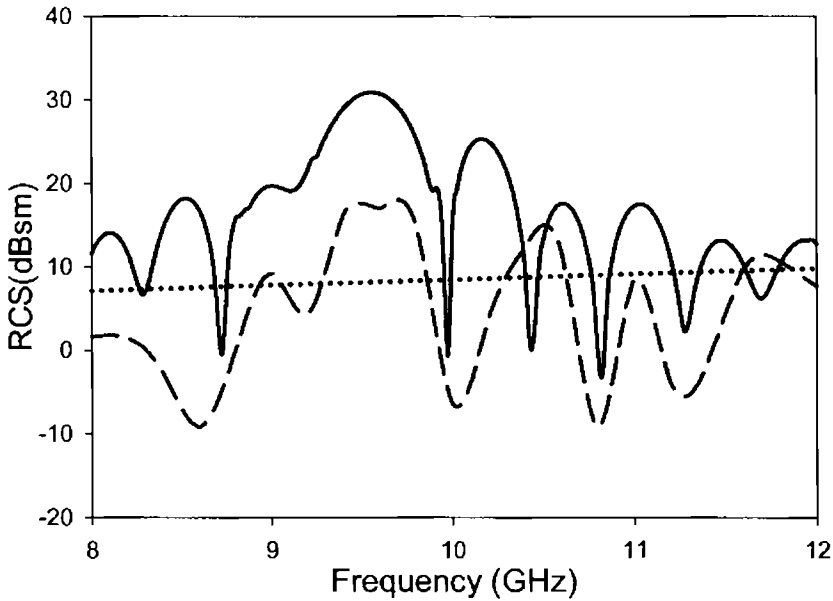


Figure 5.3 Variation of RCS against frequency for normal incidence ($h = 3 \text{ mm}$)
 — MDS loaded, TM polarization - - - MDS loaded, TE Polarization
 80° plain dihedral corner reflector

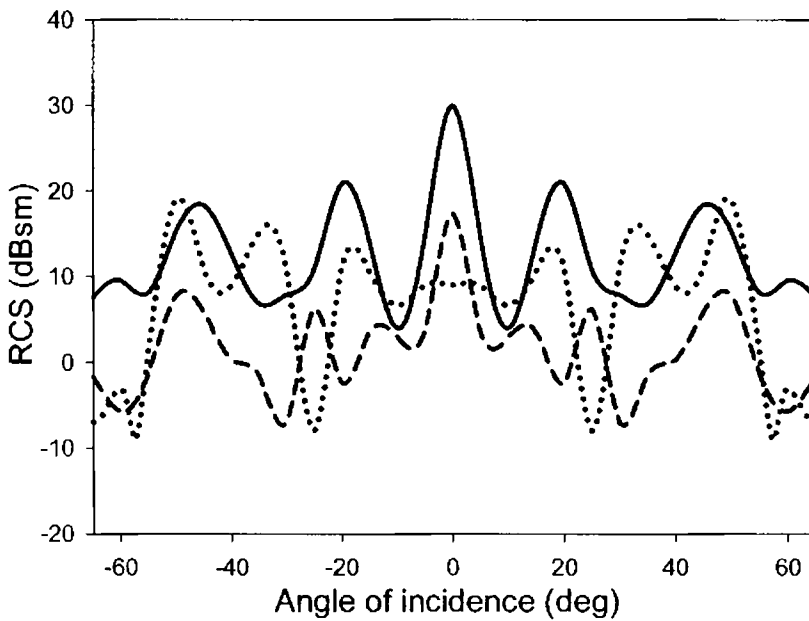


Figure 5.4 Variation of RCS against angle of incidence, $h = 3 \text{ mm}$
 — MDS loaded, TM polarization - - - MDS loaded, TE polarization
 80° plain dihedral corner reflector

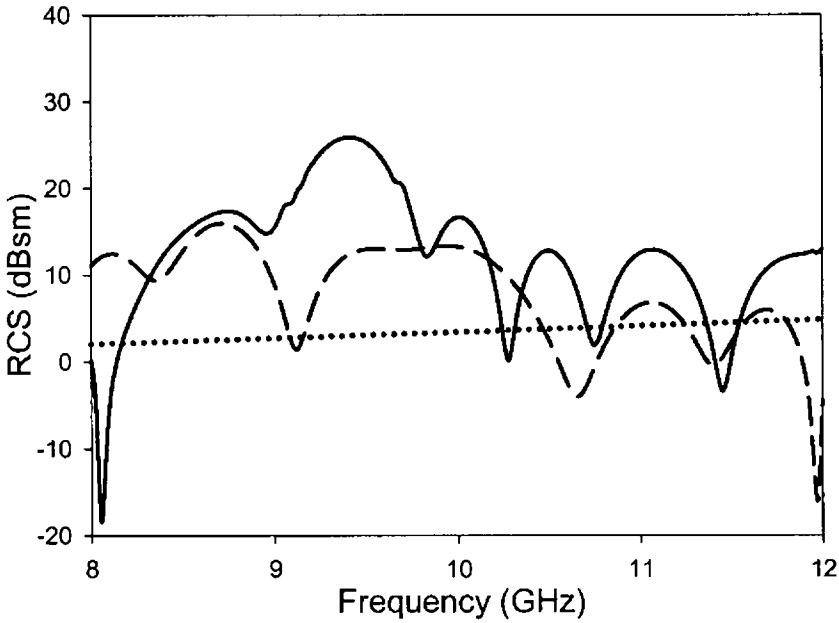


Figure 5.5 Variation of RCS against frequency for normal incidence $h = 2 \text{ mm}$

- MDS loaded, TM polarization
- - - MDS loaded, TE polarization
- 120° plain dihedral corner reflector

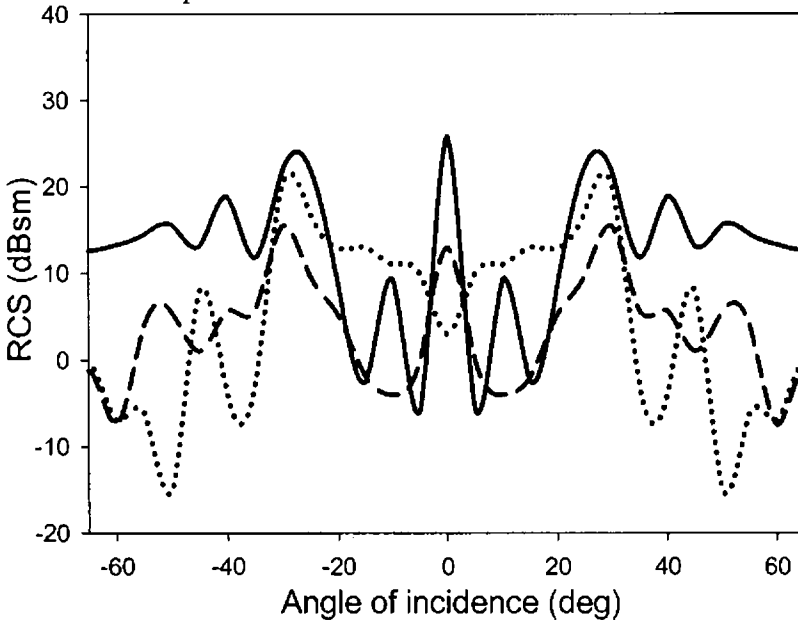


Figure 5.6 Variation of RCS against angle of incidence, $h = 2 \text{ mm}$

- MDS loaded, TM polarization
- - - MDS loaded, TE polarization
- 120° plain dihedral corner reflector

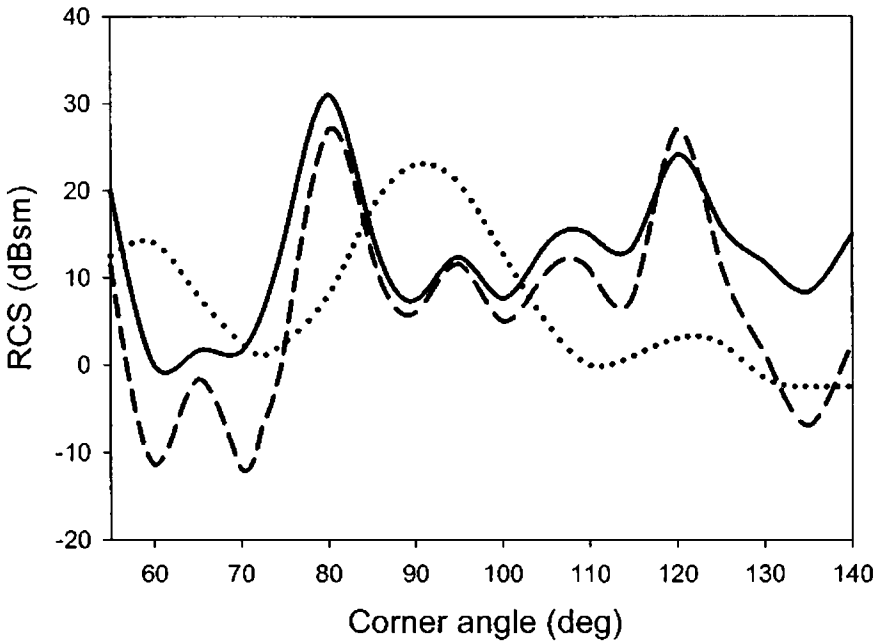


Figure 5.7 Variation of RCS with corner angle for TM polarization

- Plain dihedral corner
- MDS loaded, 9.55 GHz, h = 3 mm
- - - MDS loaded, 9.44 GHz, h = 2 mm

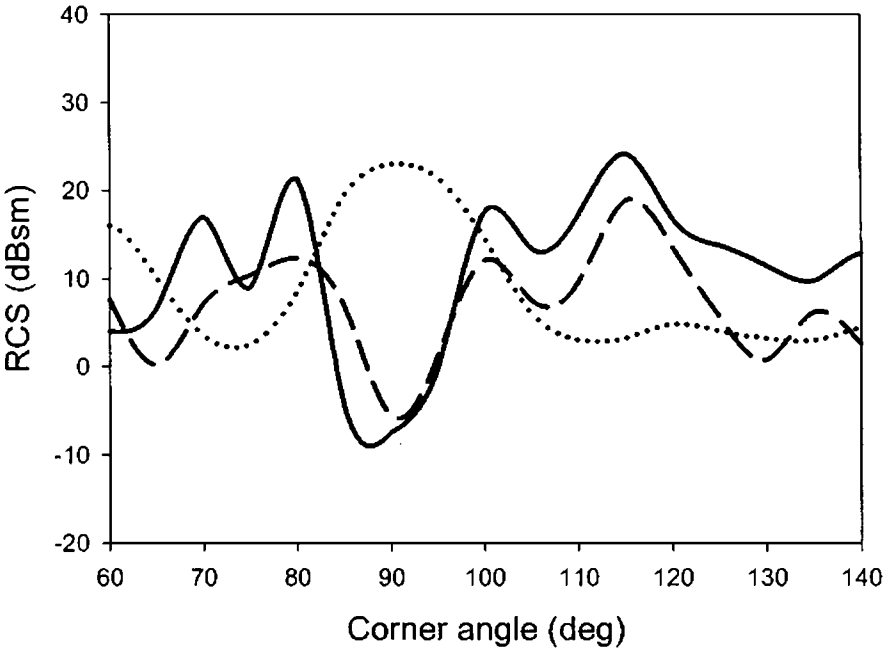


Figure 5.8 Variation of RCS with corner angle for TE polarization

- Plain dihedral corner
- MDS loaded, 9.55 GHz, h = 3 mm
- - - MDS loaded, 9.44 GHz, h = 2 mm

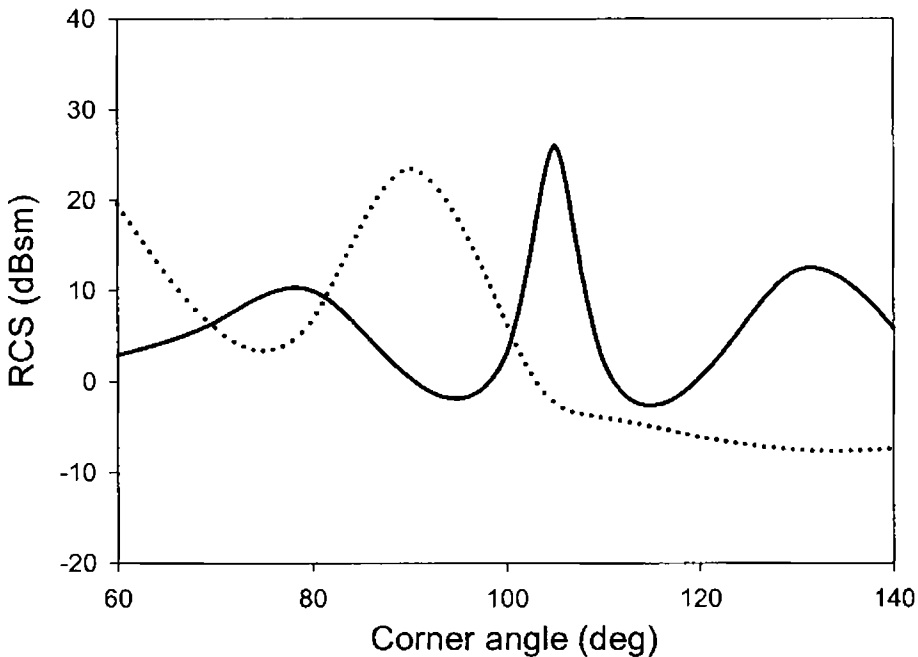


Figure 5.9 RCS variations with corner angles for TE polarization
 Plain dihedral corner
 — MDS loaded, 10.03 GHz, $h = 3$ mm

In chapter 4, it is observed that a large enhancement in RCS in the case of TE polarization is obtained by loading MDS over a corner reflector with corner angle $\alpha = 105^\circ$. The variation of RCS with corner angles at $f = 10.03$ GHz and $h = 3$ mm is shown in figure 5.9. The results of the investigation indicate that the RCS of dihedral corner reflector can be enhanced by loading MDS based on Sierpinski carpet fractal geometries for both TE and TM polarization.

Table 2 shows the frequency of minimum RCS and the frequency of maximum RCS enhancement for dihedral corner reflectors of various corner angles. The results obtained for both TE and TM polarizations are listed. Maximum reduction of backscattered power of 45 dB is obtained

for a corner angle $\alpha = 160^\circ$ in the case of TE polarizations and 47 dB for corner angle $\alpha = 175^\circ$ for TM polarization. Maximum enhancement is observed for corner angle $\alpha = 105^\circ$ in the case of TE polarization and $\alpha = 120^\circ$ in the case of TM polarization.

Table 2 Frequencies of RCS reduction/ enhancement for various corner angles for TE and TM polarizations

Corner angle (α)	Frequency of Maximum RCS Reduction				Frequency of Maximum RCS Enhancement			
	TE (GHz)	dB	TM (GHz)	dB	TE (GHz)	dB	TM (GHz)	dB
60	9.9	-31.6	12.6	-43.3	8.47	4.0	4.5	6.7
65	12.43	-22.1	15.15	-45.3	16	9.9	8.55	3.4
70	12.75	-37.5	728	-36	15.8	14.4	10.68	14.2
75	10.15	-37.7	8.83	-26.7	8.65	6.8	7	15.6
80	12.38	-23.4	12.93	-33.4	10.7	12.4	9.55	22
85	11.55	-31.6	13.95	-29.6	5.15	8.9	5.78	18.2
90	9.05	-32.8	8.03	-40	-	-	6.3	0.9
95	7.24	-31.7	6.19	-30.8	8.85	0.8	9.55	4.0
100	9.08	-18	6.53	-21.6	15	9.3	10	16.3
105	9.3	-24.3	9.75	-25	10.03	19.1	9.98	13.7
110	10.28	-10.5	15.15	-23.7	10.5	10.9	9.53	9.6
115	8.95	-26.1	14.55	-35.6	10.28	14	4.5	17.5
120	10.9	-18.8	6.9	-26.8	10.03	11.7	9.4	22.9
125	10.65	-29.1	11.7	-14.2	9.85	15.8	10.9	20.7
130	9.53	-33	14.83	-15.9	14	7.2	10.35	17.8
135	9.85	-32	10.08	-28.2	9.03	5.4	11.78	17.2
140	12.88	-36.5	4.72	-26.9	11.25	4.1	9.25	14.1
145	11.43	-20.1	11.77	-24.5	11.05	6.8	9.13	18.9
150	12.36	-28.5	15.9	-22.6	7.87	9.9	8.8	9.4
155	7.23	-35.2	8.08	-13.3	8.9	6.4	9.33	20.9
160	6.3	-45	5.9	-20.5	10.58	8.1	10.53	18.4
165	8.4	-21.2	7.39	-36.4	10.48	3.8	10.7	13.5
170	5.85	-38.2	7.5	-33.7	-	-	-	-
175	9.15	-22	5.85	-46.6	-	-	-	-

5.4 EFFECT OF SUPERSTRATE LOADING

A structure is optimised to get a minimum RCS at a particular frequency by adjusting the substrate thickness. Experiments have proved that the frequency can be tuned by applying superstrates of different thickness. The frequency of tuning effect of the structures based on Sierpinski carpet and Sierpinski gasket are shown in tables 3 and 4 respectively.

Table 3 Effect of loading superstrates on Sierpinski carpet structure

Substrate thickness h (mm)	Superstrate thickness, t (mm)	Frequency of minimum backscattering, f (GHz)
3	0	13.7
	0.6	12.03
	1	11.24
	1.5	10.7

Table 4 Effect of loading superstrates on Sierpinski gasket structure

Substrate thickness h (mm)	Superstrate thickness, t (mm)	Frequency of minimum backscattering, f (GHz)
5	0	8.9
	1	8.29
	2	7.74
	3	7.26
	4	6.94
	5	6.74

5.5 EFFECT OF DIELECTRIC CONSTANT

The effect of dielectric constant on the frequency giving minimum backscattering is studied for a particular structure. Table 5 shows the simulated results for different dielectric constant with a substrate thickness of 5 mm.

Table 5 Effect of dielectric thickness on the resonance frequency

Dielectric constant	Frequency of minimum backscattering (GHz)
2.2	8.6
2.56	8.4
4.4	8.0
10.2	5.0

Chapter 6

CONCLUSIONS

This chapter presents the conclusions drawn from the investigations carried out in lowering the RCS of targets. Studies conducted by embedding fractal based metallo-dielectric structures on targets such as metallic flat plate, cylinder, dihedral corner reflector and circular cone conducted for both TE and TM polarizations are found to be very effective in reducing the RCS of targets over a wide frequency band. Scope for further work related to this field is also discussed.

6.1 INFERENCES FROM EXPERIMENTAL INVESTIGATIONS

6.1.1. Fractal Based Metallo-Dielectric Structures Loaded Flat Plate

The results of the backscattering characteristics for various iterated stages of Sierpinski carpet fractal based metallo-dielectric structures loaded flat plates were presented in section 4.1.1. It is observed the third iterated stage is giving a maximum reduction in backscattered power when measured for normal incidence. Also there is an optimum thickness for the dielectric substrate giving maximum backscattering reduction in a particular band. A reduction of backscattered power of 28.6 dB ($h=3$ mm), 32 dB ($h=4$ mm) and 28.8 dB ($h = 3$ mm) in C, X and Ku bands respectively is obtained compared to a flat plate of same physical dimension. The backscattered power measurement with angle of incidence shows that the reduction is obtained for other incident angles also, with large backscattering at the blazing angles. The reduction is obtained for due to the power scattered in different directions and the measurements indicated that the scattered power is distributed symmetrically with respect to normal in both azimuthal and elevation angular ranges. This is true for both TE and TM polarizations, due to the symmetry in the nature of the geometry.

Scattering results of Sierpinski carpet with generators of different shapes are described in section 4.1.2. Patches of different shapes are applied to the third iterated stage of the Sierpinski carpet, as this configuration is giving minimum backscattering. From the observations it is found that Sierpinski carpet with hexagonal patches is giving maximum

reduction in backscattered power of 45 dB at $f = 13.04$ GHz. The optimum substrate thickness giving maximum reduction in backscattered power is $h = 10$ mm. It is also observed that the backscattered power obtained is high for Sierpinski carpet fractal structures with patches of the shape of cross bar fractal tree. This is due to the fact that the patch area occupied by this geometry is less compared to other geometries. It is inferred that the backscattering depends on the area occupied by the patches.

Backscattering reduction to an appreciable range of frequencies is obtained for the Sierpinski carpet structure with square patches. A bandwidth (below -10 dB) of 2.83 GHz is obtained for a substrate thickness $h = 5$ mm compared to other structures.

From the observations it is seen that the backscattering characteristic for TE and TM polarizations are different for Sierpinski carpet structures with patches of the shape Star and Hexagon. This is due to non symmetry in its shape.

Loading superstrates on Sierpinski carpet fractal geometry and Sierpinski gasket fractal geometries are found to be effective in shifting the frequency of minimum backscattering to the desired frequency. Superstrates loading over Sierpinski carpet structure in a shift in the frequency of minimum backscattering from Ku to X band, as the superstrate thickness is increased. A reduction of -28 dB at 13.7 GHz is shifted to 10.7 GHz giving -27 dB by increasing the superstrate thickness by 1.5 mm, while Sierpinski gasket structure shifts the frequency of

minimum backscattering from X to C band. Here a reduction of -31 dB at 8.9 GHz is shifted to 6.76 GHz giving - 21 dB by increasing the superstrate thickness by 5 mm.

The results of the scattering behaviour of Sierpinski carpet fractal geometries with same fractal dimension and varying lacunarity is presented in chapter 4.3. Reduction in backscattered power in all the three frequency bands (C, X and Ku) is obtained for the structure with medium lacunarity.

6.1.2. Experiments with 3D structures

(a) Metallic Cylinder

Scattering studies conducted on metallic cylinder by loading Sierpinski carpet based metallo-dielectric structure is presented in section 4.4. It is observed that loading fractal based structures is effective in reducing the backscattered power for both TE and TM polarizations of the incident field.

Maximum reduction of ~ 35 dB in backscattering for TE polarization is obtained at $f = 10.18$ GHz, for a substrate thickness $h = 4$ mm compared to a metallic cylinder of same physical dimensions. Maximum backscattered power is obtained for an angle of incidence of 15° .

In the case of TM polarization, a maximum reduction of -35 dB is obtained at $f = 9.78$ GHz for a substrate thickness $h = 4$ mm. In this case, maximum backscattered power is obtained for an angle of incidence of 7° . Similar results are obtained for the horizontally oriented cylinder also.

(b) Dihedral Corner Reflector

Studies on the scattering characteristics of dihedral corner reflector loaded with fractal structures have given some interesting results. Here RCS reduction is obtained for a 90° corner reflector while the RCS is enhanced for acute and obtuse corner angles.

Experiments conducted using a corner reflector with adjustable corner angle yielded the following results. In the case of TE polarization, a maximum reduction in backscattered power of 33 dB at $f = 9.05$ GHz is obtained for $h = 4$ mm for 90° corner reflector when compared to metallic dihedral corner reflector of same physical dimension. For TM polarization, reduction is 40 dB at $f = 8.03$ GHz for the same thickness $h = 4$ mm.

For acute and obtuse angles, the backscattered power is more than that of a plane corner reflector. So, this technique is suitable for enhancing the RCS of dihedral corner reflectors. An RCS enhancement of ~ 30 dBsm is observed for corner reflector with angle $\alpha = 80^\circ$ and 120° corner angle.

(c) Circular Cone

Backscattering studies of metallic circular cone loaded with Sierpinski carpet based metallo-dielectric structure is presented in section 4.6. It is observed that this technique reduces the backscattering from the cone for both TE and TM polarizations of the incident field.

A maximum reduction in backscattered power of 25.5 dB with respect to metallic cone, at $f = 8.1275$ GHz is obtained for a dielectric thickness of $h = 1.2$ mm. Maximum backscattered power of -10.92 dB is obtained for an angle of incidence of 5° . The results obtained are identical for both TE and TM polarizations.

6.2 CONCLUSIONS FROM SIMULATION STUDIES AND ANALYSIS

From the experimental results, it is observed that backscattering reduction over a wide range of frequencies is obtained by loading Sierpinski carpet based fractal structure on a metallic plate. Embedding this structure on a dihedral corner reflector gives RCS enhancement at certain acute and obtuse corner angles.

Simulations studies were conducted for Sierpinski carpets with different iterated stages and also for Sierpinski carpets with generators of different shapes. It is concluded that the experimental results are in good agreement with the simulations results.

It is also observed that the frequency of minimum backscattering can be tuned by loading superstrate of different thickness over the metallo-dielectric structure.

6.3 SCOPE FOR FURTHER WORK IN THIS FIELD

Application of fractal based metallo-dielectric structures in real time targets like models of aircrafts, ships, vehicles and missiles for reducing the RCS is an important work to be carried up in this area. This requires more

careful analysis and attention. More detailed investigation could be carried out in this direction.

Backscattering reduction of flat plates, cylinder, dihedral corner reflectors and circular cone are carried out in the present work. Scattering studies could be extended to more targets like trihedral corner reflectors, ellipsoids and bruderhedral.

The study on the scattering characteristics of the metallo- dielectric structures with temperature, the scattering behaviour of non deterministic fractal shapes and other deterministic shapes other than Sierpinski carpet and Sierpinski gasket can be taken up as a further study.

Development of techniques for reducing the backscattering for a wide angular and wide frequency range requires further detailed investigation. A suitable theoretical model to different fractal loaded targets leaves much scope for future work in the field.

Appendix I

DESIGN OF A BANDPASS FILTER USING CANTOR BAR BASED METALLO-DIELECTRIC STRUCTURE

Development of a filter in rectangular waveguides using metallo-dielectric inserts based on Cantor bar fractal geometry is reported. The structure consisting of an array of cantor bars placed inside introduces a higher cutoff frequency for the waveguides which results in a bandpass response. The cutoff frequency depends on the parameters of the array.

INTRODUCTION

Waveguide filters usually require a complex and expensive process of manufacture; but they are very useful in applications where high power handling is desired. Various techniques are reported in the literature for the design of waveguide filters. Many of these designs are based on the use of short circuited stubs about half a wavelength long as discussed by Matthaei et al. [1]. Fin lines are also extensively used for constructing microwave filters [2, 3]. Left handed coplanar waveguide bandpass filters based on split ring resonators and microstrip bandpass filters are discussed in [4, 5]. A technique for constructing a bandstop waveguide filter containing multiple-coupled cavities has been proposed in [6]. Seager et.al. A bandpass type response in a waveguide using a two sided array of close-coupled resonant aperture FSS is presented in [7]. A waveguide filter employing several conducting cylindrical posts that have a bow-tie shape is synthesized and investigated in [8]. In this paper we discuss the use of Cantor bar based fractal structure for designing a waveguide filter.

Mandelbrot described a family of complex objects or shapes as 'fractal' [9]. Fractals are structures that possess inherent characteristics such as self similarity and space filling property. The application of fractal geometries in electromagnetics in radiating, propagation and scattering problems has gained much interest recently [10 - 12]. In the present work, dielectric sheet with metallization pattern in the form of an array of cantor bars is inserted in the waveguide. The transmission characteristic is studied by varying different parameters of the cantor bar geometry.

DESIGN OF THE CANTOR BAR FILTER

The cantor bar is formed by a line segment whose middle third is repeatedly removed. The initiator is defined as a line segment of unit length and the generator is defined as an excise line segment of length one-third. The bar is formed by repeated application of the generator and its scaled replica to the middle third of the initiator or the previous stage of growth. When the thickness of the cantor bar becomes vanishingly small, the resultant fractal becomes cantor dust. The first iterated stage of a cantor bar fractal geometry is shown in figure I 1. Here the middle $1/3^{\text{rd}}$ of the initiator (l) is removed. The fractal dimension of this general cantor bar is given by

$$D = \ln(2) / \ln(3) \\ = 0.6309$$

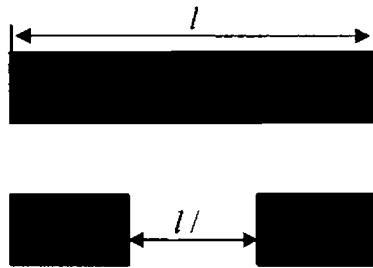


Figure I 1 First iterated stage of cantor bar fractal

A typical cantor bar array with two unit cells with first iteration is shown in figure I 2. The width and height of an element in a unit cell are ' w ' and ' h '. The distance between the elements in a unit cell is d_1 and the unit cells are spaced at a distance d_2 . The gap width inside a unit cell is ' g '.

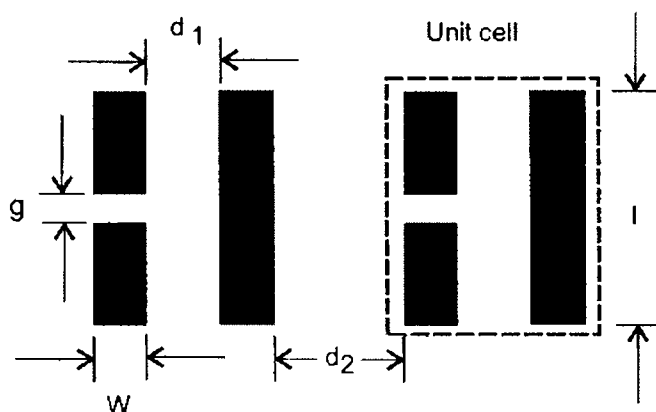


Figure I 2 Cantor bar array of two unit cells

The metallo-dielectric structure based on cantor bar array of fourteen unit cells is photo etched on a FR4 substrate having a thickness $t = 1.6$ mm and dielectric constant, $\epsilon_r = 4.4$. Cantor arrays of unit cells with $l = 7$ mm, $w = 2$ mm, $d_1 = 2$ mm, $d_2 = 2$ mm with different gap width (g) 0.05 mm, 1 mm, 1.5 mm and 2.3 mm are fabricated and studied. The structure is inserted in a X band waveguide as shown in figure I 3.

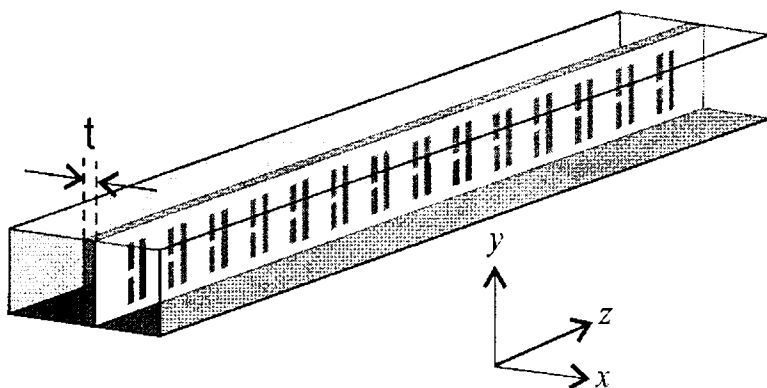


Figure I 3 X - band waveguide with Cantor bar based metallo-dielectric insert

The measurements are performed using Rohde and Schwarz ZVB 20 vector network analyzer. The transmission characteristics are studied by

inserting the structure in the waveguide at different positions (x) along the X-axis. The measurements are also conducted by varying the spacing of the array elements, spacing of the elements in the unit cell and the number of unit cells. Ansoft HFSS V10 simulation software is used to validate the experimental results.

RESULTS AND DISCUSSIONS

The transmission characteristics of the waveguide with cantor bar array unit cells inserted at different position along the width of the waveguide is plotted in figure I 4. It is observed that the response is maximum at the centre of the waveguide.

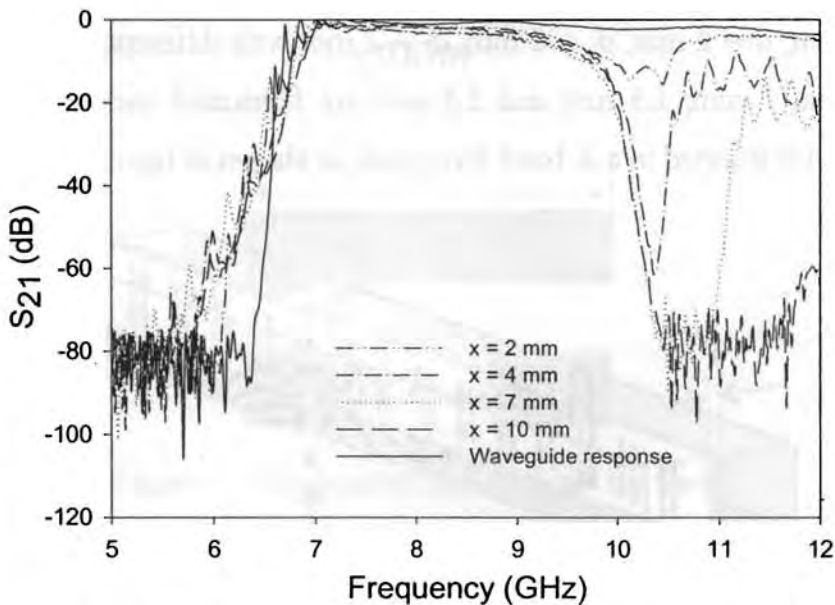


Figure I 4 Transmission characteristic of a waveguide loaded with arrays of cantor bar at different positions ($g = 0.5$ mm, $d_1 = 2$ mm, $d_2 = 2$ mm, $w = 2$ mm, $l = 7$ mm, $N = 14$)

Simulated results of the response of the TE_{10} mode waveguide with different number of unit cells (N) of the cantor bar, kept at the field maximum is shown in figure I 5. It is observed that as the number of unit cell is increased, a bandpass filter response is achieved.

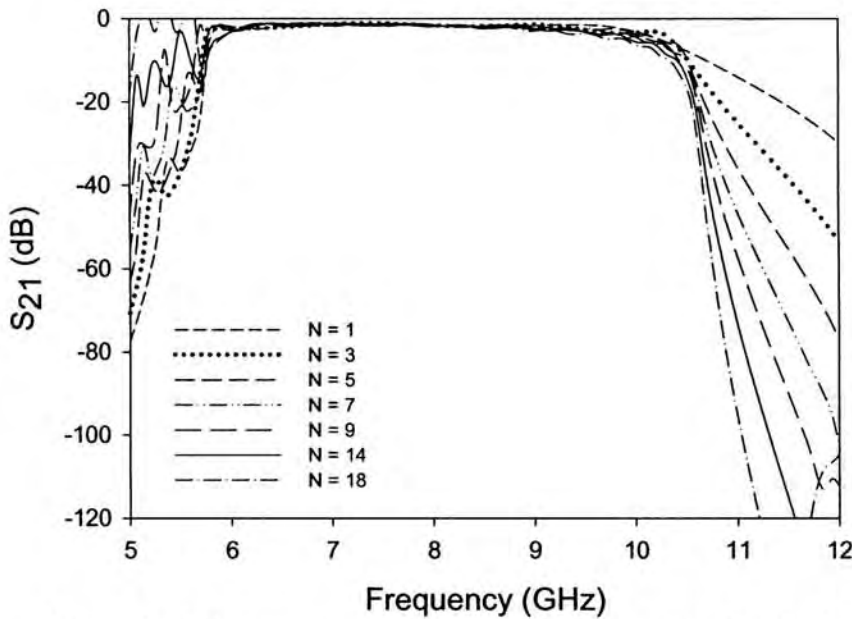


Figure I 5 Transmission characteristic of a waveguide loaded with different number cantor bar unit cells ' N ' ($d_1 = 2$ mm, $d_2 = 2$ mm, $w = 2$ mm, $l = 7$ mm)

The effect of gap width on the transmission characteristic of the waveguide is studied and the measured results are shown in figure I 6. It is observed that as the gap width is decreased the width of the passband is increased. It is also found that the insertion loss is minimum when the gap width is 0.5 mm.

Figure I 7 shows the transmission characteristics of the waveguide loaded with arrays of cantor bar with different period's d_1 and d_2 . It is found that the bandwidth is decreased as the period d_1 or d_2 is increased. It

is also seen that the upper cutoff frequency of the waveguide can be varied by changing either d_1 or d_2 .

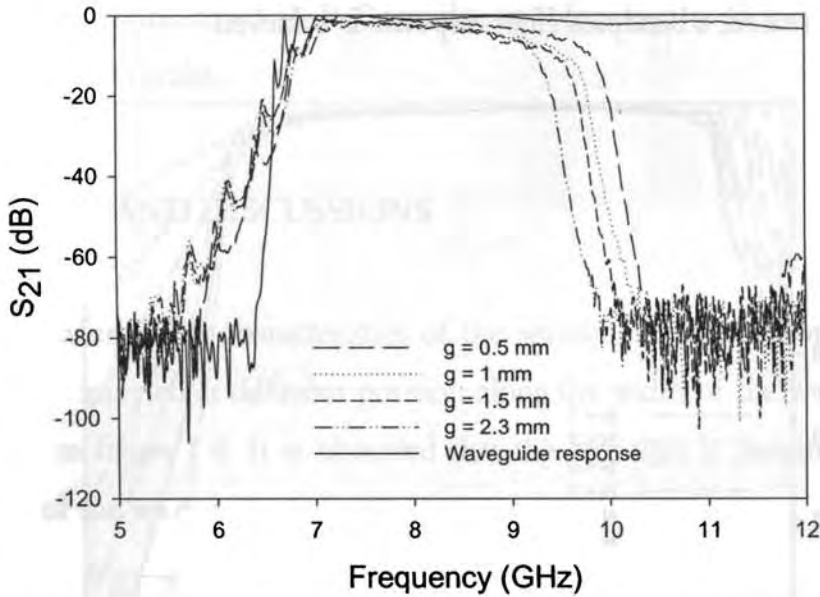


Figure I 6 Transmission characteristic of a waveguide loaded with arrays of cantor bar having different gap width ' g ' ($d_1 = 2$ mm, $d_2 = 2$ mm, $w = 2$ mm, $l = 7$ mm, $N = 14$)

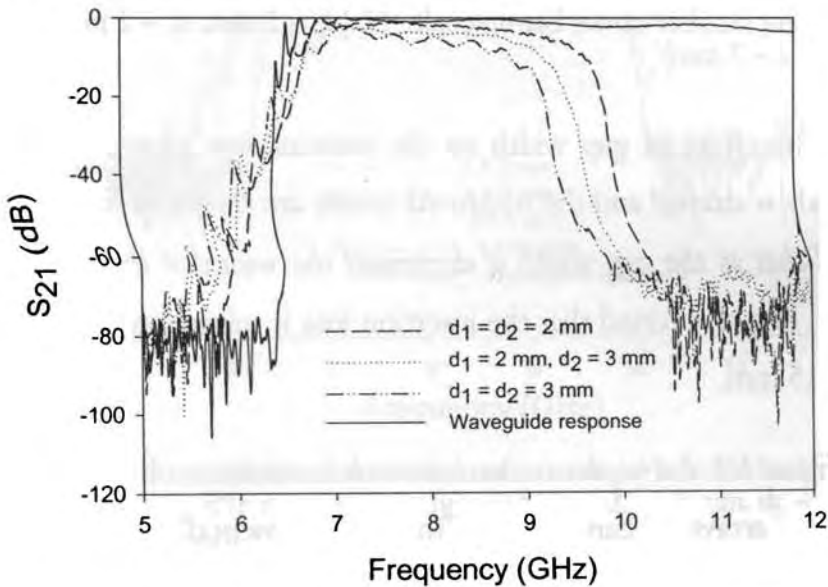


Figure I 7 Transmission characteristic of the waveguide with array spacing variation ($g = 0.5$ mm)

Figure I 8 shows the results in a C-band waveguide. Here also the Cantor bar array introduces a higher cutoff frequency in the waveguide which can be controlled by varying the parameters of the array.

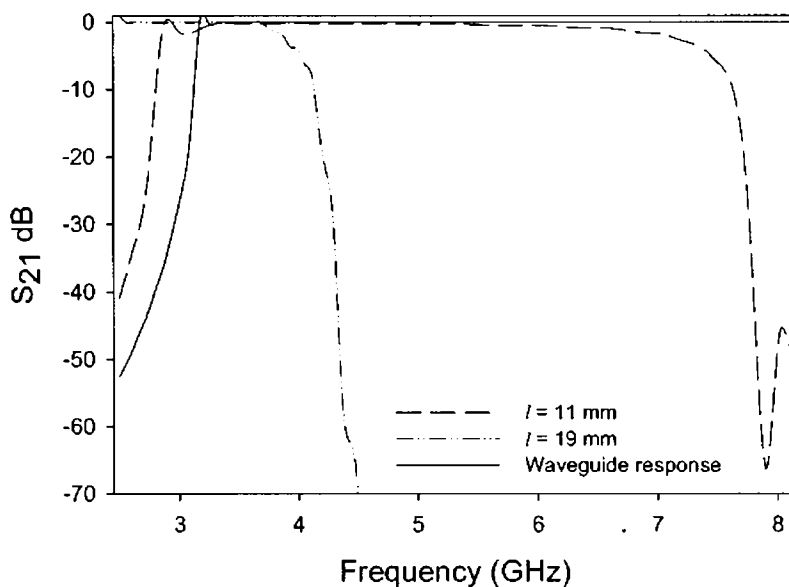


Figure I 8 Transmission characteristic of a C-band waveguide loaded with array of cantor bar ($g = 0.5$ mm, $d_1 = 2$ mm, $d_2 = 4$ mm, $w = 2$ mm, $x = 10$ mm, $N = 14$)

From the observations it can be concluded that the upper cutoff frequency of the waveguide can be controlled by varying either of the parameters l , g , d_1 or d_2 . So that a bandpass response is obtained in the waveguide.

CONCLUSION

Metallo-dielectric structure based on arrays of cantor bar fractal geometry is useful in bringing in an upper cutoff frequency in a waveguide. The higher cutoff frequency depends on the gap width, height of the unit

cell, spacing between two unit cells and also on the spacing between the elements of the unit cell. A bandpass response is obtained by properly adjusting the upper cutoff frequency. These structures with proper parameters may find use in satellite communications, cellular radio and in military applications etc.

References

- [1] G. Matthaei, L. Young and E.M.T. Jones, *Microwave filters, impedancematching networks, and coupling structures*, Artech house Inc, Dedham, MA, 1980.
- [2] Fritz Arndt, Jens Bornemann, Dietrich Grauerholz and Rudiger Vahldieck, "Theory and design of low - insertion loss fin-line filters", *IEEE Transaction on Microwave Theory and Techniques*, Vol. 30, 1982, pp. 155-163.
- [3] Abdel Megid Kamal Saad, Klaus Schunemann, "A simple method for analysing fin-line structure", *IEEE Transaction on Microwave Theory and Techniques*, Vol. 26, 1978, pp. 1002-1007.
- [4] Francisco Falcone, Ferran Martín, Jordi Bonache, Ricardo Marqués, Txema Lopetegui, "Left Handed Coplanar Waveguide Band Pass Filters Based on Bi-layer Split Ring Resonators" *IEEE microwave and wireless component letters*, Vol. 14. 2004, pp. 10-12.
- [5] Chi-Feng Chen, Ting-Yi Huang, and Ruey-Beei Wu, "Design of Microstrip Bandpass Filters with Multiorder Spurious-Mode Suppression", *IEEE Transaction on Microwave Theory and Techniques*, Vol. 53, 2005, pp. 3788-3793.
- [6] Jing-Ren Qian And Wei-Chen Zhuang, "New Narrow-Band Dual-Mode Bandstop Waveguide Filters", *IEEE Transactions On Microwave Theory And Techniques*, Vol. MTT31, No. 12, December 1983, pp. 1045-1050.
- [7] R. D. Seager, J. C. Vardaxoglou and D. S. Lockyer "Close Coupled Resonant Aperture Inserts for Waveguide Filtering Applications", *IEEE Microwave And Wireless Components Letters*, Vol. 11, No. 3, March 2001, pp. 112-114.

- [8] R. Lech and J. Mazur, "Tunable waveguide filter with bow-tie metallicposts", *IEE Proc.-Microw. Antennas Propag.*, Vol. 151, No. 2, April 2004, pp. 156-160.
- [9] B. B. Mandelbrot, *The Fractal Geometry of nature*, New York, W. H. Freeman, 1983.
- [10] D. H. Werner and S. Ganguly, "An overview of fractal antenna engineering research", *IEEE Antennas and propagation Magazine*, 2003, pp. 38-57.
- [11] J. Romeu and Y. Rahmat-Samii, "Fractal FSS: A novel dual-band frequency selective surfaces", *IEEE Transaction on Antennas and propagation*, Vol.40, 2000, pp. 1097 – 1105.
- [12] A. R. Chandran, T. Mathew, C. K. Aanandan, P. Mohanan and K. Vasudevan, "Low Backscattered Dual-Polarised Metallo-Dielectric Structure Based on Sierpinski Carpet", *Microwave and Optical Technology Letters.*, Vol. 40. No.3. February 2004, pp. 246 – 248.

Appendix II

DEVELOPMENT OF AN RCS MEASUREMENT FACILITY AND ITS AUTOMATION

The development of a setup for measurement of Radar Cross Section of different types of targets and its automation are presented in this appendix. Both monostatic and bistatic measurements of RCS can be done using this facility.

MEASUREMENT SETUP AND ITS AUTOMATION

The setup consists of a semicircular wooden frame (Arch) that allows the transmitting and receiving antennas to be fixed at a constant distance from the target, for a variety of subtended angles. The radius of the arch is ~92 inch cm and its circumference is ~288 inch. The target is mounted on a stepper motor based turntable placed at the centre of the arch. The transmitting antenna is mounted on a wooden carriage is placed just outside the arch which can be moved parallel to the arch. The receiver antenna support is mounted on a stepper motor assembly unit that can be moved on the arch. The target rotation as well as the receiving antenna movement is controlled by two separate stepper motors driven by a microcontroller based unit, interfaced to a PC. Rhode & Schwarz network analyzer ZVB 20 is also interfaced to the PC. The measurements can be taken with an accuracy of one degree, using this set up. The photograph of the measurement setup is shown in Figure II. 1.

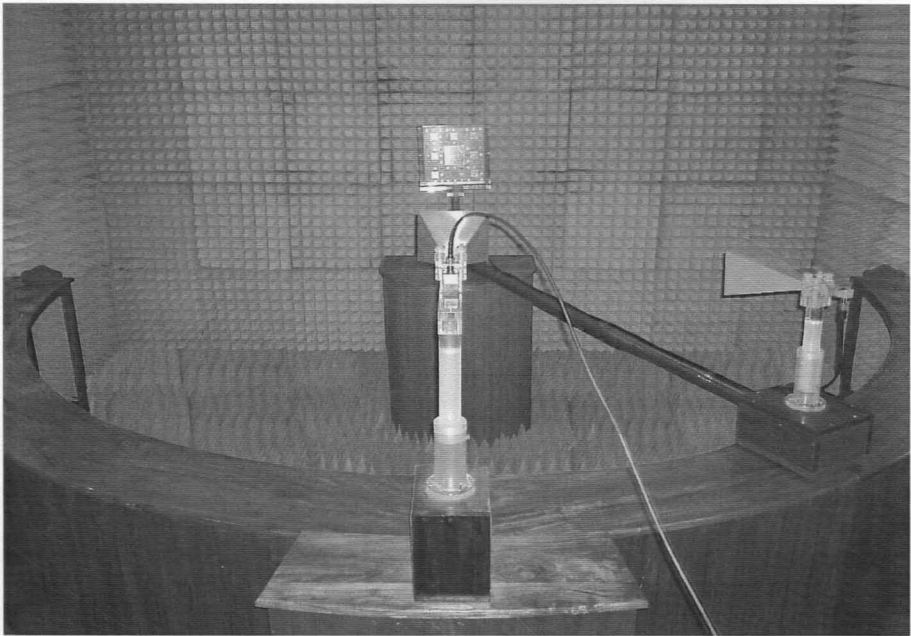


Figure II.1 The arch method

The target mount is driven by a stepper motor of 9 Kg torque with voltage and current ratings of 6 V and 1.4 A. The receiving antenna is rotated using a heavy duty motor of 20 Kg torque with 6 V and 3.3 A rating. The stepper motors are controlled by a microcontroller based unit. The microcontroller used is ATMEL 89C2051 having the following features:

Features of the microcontroller

- 2Kbytes of reprogrammable flash memory
- 2.7V to 6V operating range
- Fully static operation: 0 Hz to 24 MHz

- Two level program memory lock
- 128 x 8 bit internal RAM
- 15 Programmable I/O lines
- Two 16 bit timer/counters
- 6 interrupt sources
- On-chip analog comparator
- Low power idle and power down modes

Maximum ratings

Operating temperature	-----	-55°C to +125°C
Storage temperature	-----	-65°C to +150°C
Voltage on any pin with respect to GND	-----	1.0V to +7.0V
Maximum operating voltage	-----	6.6V
DC output current	-----	25.0mA

A driver circuit consisting of TIP 142 NPN power transistors in monolithic Darlington configurations are used for driving the motors. The driver unit is interfaced to a PC using MAX 232 (serial port communication IC). So that the rotation of the motor can be controlled using a PC. The input for controlling the motor, such as delay, number of steps, step size and the direction (clockwise and anticlockwise) of rotation of the motor can be set through a program written in MATLAB.

Measurements are done using Rohde & Schwarz ZVB 20 Network Analyzer.

The analyzer is interfaced to the PC via RSIB (Rohde & Schwartz Interfacing Bus) interface. The RSIB interface is a R&S defined protocol that uses the TCP/IP protocol for communication with the instrument. It consists of a set of I/O functions very similar to the National Instruments NI-488.2 interface for GPIB. With the use of the RSIB interface, the instruments can be controlled over the LAN. RJ 45 jack is used to connect between the LAN cards of the PC and network analyzer. The measurements made using the analyzer are stored in the PC. The sidewalls and the floor are covered with microwave absorbing materials.

The whole arrangement of the measurement setup is shown in Figure II.2

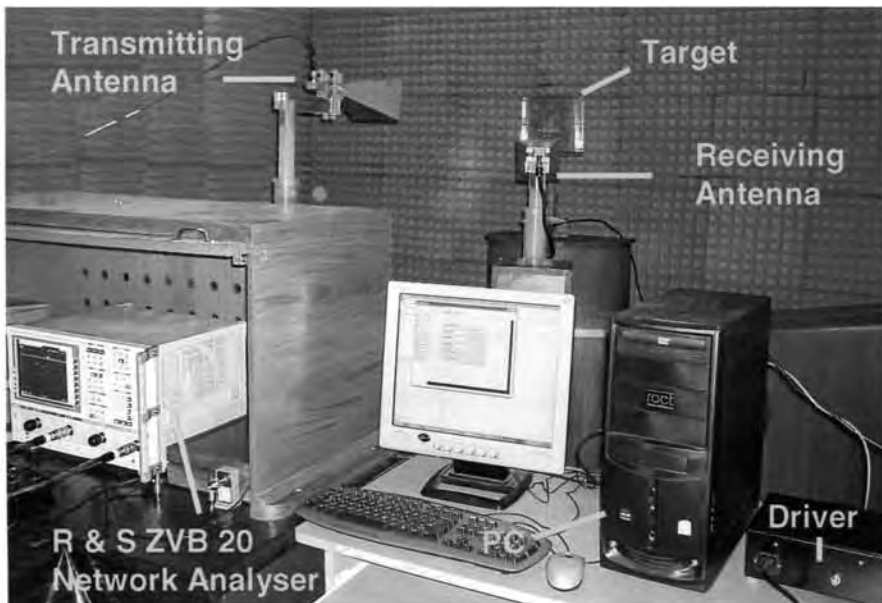


Figure II.2 The automated RCS measurement setup

CONCLUSION

An automated setup is developed and used for measurement of Radar Cross Section using the Rohde & Schwarz vector network analyzer. This automated setup can also be used for the measurement of antenna radiation patterns at multiple frequencies with less time effort.

References

- 1) Muhammad Ali Mazidi & Janice Gillispie Mazidi, "The 8051 Microcontroller and embedded systems", Pearson education, Sixth edition, 2003
- 2) Kenneth.J.Ayala, "The 8051 Microcontroller", Penram international publishing Pvt.Ltd, Second edition, 1998
- 3) Ajay.V.Deshmukh, "Microcontrollers-Theory and Applications", Tata McGraw Hill, Second edition, 2005
- 4) Eugene.F.Knot John.F.Shaeffler Michael.T.Tuley "Radar Cross Section Its Prediction Measurement and Reduction", Artech House, 1985
- 5) Rohde & Schwarz ZVB20 Vector Network Analyzer Reference Manual

REFERENCES

1. George T. Ruck, "Radar Cross Section handbook" Vol. I & II, Plenum Press, New York, 1970.
2. M. I. Skolnik, "Introduction to Radar systems", Mc Graw Hill, 1989.
3. Eugene F. Knott, John F. Shaeffer, and Micheal T. Tuley, "Radar Cross Section" Artech House Inc., Dedham, M. A, 1989
4. Nicholas C. Curie, "Techniques of Radar reflectivity measurements" Artech House Inc., Dedham, M. A, 1989.
5. Y.Y. Hu, "Backscattering cross section of a center loaded cylindrical antenna," *IRE Trans. Antennas & prop.*, Vol. AP-36, No. 1, pp 140-148, Jan 1958.
6. W. J. Bow, A. S. King and C. E. Lee, "Scattering from finite array of microstrip patches on uniaxial substrate", *IEE Electron. Lett.*, Vol. 28, No. 2, pp. 126 - 127. January 1992.
7. E. H. Newman and D. Forria, "Scattering from microstrip patches", *IEEE Trans Antennas Propagat* , Vol. 35, No. 3, pp. 245 -251, March 1987.
8. D. Pozar, "Radiation and Scattering from a Microstrip Patch on a Uniaxial Substrate", *IEEE Trans Antennas Propagat* , Vol. 35, No. 6, pp. 613 -621, June 1987.
9. D. R. Jackson, "The RCS of a rectangular Microstrip patch in a substrate-superstrate geometry", *IEEE Trans Antennas Prop.*, Vol. 38, No. 1, pp. 2 - 8, January 1990.

10. A. Taflove and K. Umashankar, "Radar Cross Section of General Three – Dimensional Scatterers", *IEEE Trans Antennas Prop.*, Vol. 25, No. 4, pp. 433 - 440, Nov. 1983.
11. D. Colak, A. I. Nosich and A. Altintas, "Radar Cross Section study of cylindrical cavity backed Apertures with Outer or Inner Material Coating: The Case of H-Polarization", *IEEE Trans Antennas Prop.*, Vol. 43, No. 5, pp. 440 - 447, May 1995.
12. C. –G. Park, N. –H. Myung and S. –D. Choi, "Efficient solution for backscattered field of a dihedral corner reflector" *IEE Electron. Lett.*, Vol. 31, No. 9, pp. 706 – 707, April 1995.
13. D. A. Edward, R. A. McCulloch and W. T. Shaw, "Variational estimation of radar cross section", *IEE proceedings*, Vol. 137, No. 4, Aug. 1990.
14. C. W. Harrison and R.O. Heinz "On the radar cross section of rods, tubes and strips of finite conductivity " *IEEE Trans. Antennas & prop.*, Vol. AP-11, No. 4, pp 459-468, July 1963.
15. Charles M. Knop "On the Radar Cross Section of a coated plate" *IEEE Trans Antennas & prop.*, "Vol AP-11, No.6, pp 719-721, Nov 1963.
16. W. E. Blore, "The radar cross section of ogives, double backed cones, double rounded cones and cone spheres", *IEEE Trans. Antennas and prop.*, Vol AP-12, No. 5, pp 582-590, Sept 1964.
17. John Rheinstein, " Scattering of electromagnetic waves from dielectric coated conducting spheres", *IEEE Trans. Antennas & prop.*, Vol. AP-12, No. 3, pp 334-340, May1964.

18. T.B.A. Senior, "A survey of analytical techniques for cross section estimation", *Proc. of IEEE*, Vol.53, pp 822-832, Aug 1965.
19. P. Blacksmith, R.E. Hiatt and R.B. Mack. "Introduction to radar cross section measurements", *Proc. of IEEE*, Vol. 53, pp 901-920, Aug 1965.
20. J. W. Crispin and A. L. Maffet, "Radar cross section estimation of simple shapes", *Proc. of IEEE*, Vol.53, pp 833-848, Aug 1965.
21. J. W. Crispin and A. L. Maffet, "Radar cross section estimation of complex shapes" *Proc. of IEEE*, Vol. 53, pp 972-982, Aug 1965.
22. R. G. Kouyoumijian and L. Peters, "Range requirement in the radar cross section measurements," *Proc. of IEEE*, Vol. 53, pp 920-928, Aug 1965.
23. C.C. Freeny, "Target support parameters associated with radar reflectivity measurements", *Proc. of IEEE*, Vol. 53, pp 929-936, Aug 1965.
24. V. V. Liepa and T. B. A. Senior, "Modification of the scattering behaviour of a sphere by loading", *Proc. of IEEE*, Vol. 53, pp. 1004-1011, Aug 1965.
25. H. A. Corriher and Berry O. Pyron, "A bibliography of articles on radar reflectivity and related subjects 1957-1964", *Proc. of IEEE*, Vol. 53, pp 1025-1058, Aug 1965.
26. A.V. Alongi, R.E. Kell and D. J. Newton, "A high resolution X-band FM/CW radar for RCS measurements", *Proc. of IEEE*, Vol. 53, pp 1072-1076, Aug 1965.
27. C. R. Millin, R. Sandburg and C. O. Velline, "A numerical technique for the determination of scattering cross section of infinite cylinders

- of arbitrary cross section”, *IEEE Trans. Antennas and prop.*, Vol AP-13, No. 5, pp 141-149, Jan 1965.
28. R.A. Ross, “Radar cross section of rectangular flat plate as a function of aspect angle”, *IEEE Trans. Antennas prop.*, Vol. AP-14, pp. 329-335, May 1966.
29. E.K. Miller, G.J. Burke, B.J. Maxum, G.M. Pjerrou and A.R. Neureuthev. “Radar cross section of a long wire”, *IEEE Trans. Antennas prop.*, Vol. AP-17, No. 3, pp. 381-383, May 1967.
30. Nicholas C. Alexopoulos, “Radar cross section of perfectly conducting sphere coated with certain class of radially inhomogenous dielectrics”, *IEEE Trans. Antennas prop.*, Vol. AP-17, No. 5, pp. 667-669, Sept 1969.
31. E. K. Miller and J.B. Morton, “ The RCS of a metal plat with resonant slot”, *IEEE Trans. Antennas prop.*, Vol. AP-18, No. 2, pp. 290-292, March 1970.
32. Jiunn S. Yu, “ Radar cross section of a thin plate near grazing incidence”, *IEEE Trans. Antennas prop.*, Vol. AP-22, No. 15, pp. 711-713, Sept. 1970.
33. Y. Rahmat-Samii and Raj Mittra, “Integral equation solution and RCS computation of a thin rectangular plate”, *IEEE Trans. Antennas prop.*, Vol. AP-22, No. 4, pp. 608-610, July 1974.
34. J.L. Lin, W.L. Curtis and M.C. Vincent, “Radar cross section of a rectangular conducting plate by wire mesh modeling” *IEEE Trans. Antennas prop.* Vol. AP-22, No.5, pp. 718-720, Sept. 1974.
35. W.B. Weir, L.A. Robinson and Don Parker, “Broadband automated radar cross section measurements”, *IEEE Trans. Antennas prop.*, Vol. AP-22, No.6, Nov. 1974.

36. Joseph R. Mautz and Roger F. Harrington, "Radiation and scattering from large polygonal cylinders, Transverse Electric Fields", *IEEE Trans. Antennas prop.*, Vol. AP-24, No.4, pp. 469-477, July 1976.
37. P. Corona, G. Ferrara and C. Gennaralli, "Backscattering by loaded and unloaded dihedral corners", *IEEE Trans. Antennas prop.*, Vol. AP-35, No.10, pp. 1148-1153, Oct 1987.
38. Timothy Griesser and Constantine A. Balanis, "Dihedral corner reflector backscatter using higher order reflections and diffractions", *IEEE Trans. Antennas prop.*, Vol. AP-35, No. 11, pp.1235-1247, Nov. 1987.
39. Ercument Arvas and Tapan K. Sarkar, "RCS of two dimensional structures consisting of both dielectric and conductors of arbitrary cross section", *IEEE Trans. Antennas prop.*, Vol. AP-37, No.5, pp. 546-554, May 1989.
40. Eugene F. Knott, "RCS reduction of dihedral corners", *IEEE Trans. Antennas prop.*, Vol. AP-25, No.3, pp. 406-409, May 1977.
41. Leonard L. Tsai, "Radar cross section of a simple target: A three dimensional conducting rectangular box", *IEEE Trans. Antennas prop.*, Vol. AP-25, No.6, pp. 882-884, Nov. 1977.
42. Randy K. Jones and Thomas H. Shumpert, "Surface currents and RCS of a spherical shell with circular aperture", *IEEE Trans. Antennas prop.*, Vol. AP-28, No.1, pp. 128-132, Jan 1980.
43. J. L. Volakis, A. Alexanian and J. M. Lin, "Broadband RCS reduction of rectangular patch by using distributed loading", *IEE Electron. Lett.*, Vol. 28, No. 25, pp. 2322 - 2323 Dec. 1992.

44. Keith M. Keen, "New technique for evaluation of scattering cross section of radar corner reflectors", *IEEE Proc. H*, Vol. 130, No.5, pp. 322-326, Aug 1983.
45. C.C. Huang, "Simple formula for RCS of a finite hollow circular cylinder", *IEE Electron Lett.*, Vol. 19, No. 20, pp. 854, Sept. 1983.
46. David M. Le. Vine, "The radar cross section of dielectric disks", *IEEE Trans. Antennas prop.*, Vol. AP-32, No.1, pp 6-12, Jan. 1984.
47. Subrata Sanyal and Asoke K. Bhattacharyya, "Electromagnetic scattering by a curved -plate -Solution by uniform asymptotic theory of diffraction", *IEEE Trans. Antennas and prop.*, Vol. AP-32, No.2, pp. 187-189, Feb. 1984.
48. Asoke K. Bhattacharyya and S.K. Tandon, "Radar cross section of a finite planar structure coated with lossy dielectric", *IEEE Trans. antennas prop.*, Vol. AP-32, No. -9, pp. 1003-1007, Sept 1984.
49. Bernhard Rembold, "Radar cross section of long wires", *IEEE Trans. Antennas prop.*, Vol. AP-32, No. 10, pp. 1124-1126, Oct. 1984.
50. Asoke K. Bhattacharyya, S.K. Tandon, Subrata Sunyal and D .R. Sarkar, "A CW radar cross section facility in X-band", *IETE Technical review*, Vol. I, No.5, pp. 59- 64, 1984.
51. P. Corona, G. Ferrara and G. Gennarelli, "A simple and practical reference target for RCS measurements", *Alta Frequenza*, Vol. LIV No.4, pp. 261-267, 1985.
52. Robert B. Dybdal, "Radar cross section measurements", *Proc. IEEE*, Vol. 75, No. 4, pp. 498-516, April 1987.
53. Choon S. Lee and Shung Wu Lee, "RCS of a coated circular

- waveguide terminated by a perfect conductor”, *IEEE Trans. Antennas prop.*, Vol. AP-35, No.4, pp.391- 398, April 1987.
54. W.C. Anderson, “Consequences of non-orthogonality on the scattering properties of dihedral comer reflectors”, *IEEE Trans. antennas prop.*, Vol. AP-35 , No. 10, pp. 1154-1159, oct. 1987.
 55. Byron Welsh and Jon N. Link, “Accuracy criteria for RCS measurements of targets consisting of multiple independent scatterers”, *IEEE Trans. Antennas prop.*, Vol AP- 36, No. 11, pp. 1587-1593, Nov 1988.
 56. Jerome I. Glaser, “Some results in the bistatic radar cross section of complex objects”, *Proc. of IEEE*, Vol. 77, No.5, pp. 639-648, May 1989.
 57. Nazeh N. Youssef, “Radar cross section of complex targets”, *Proc. of IEEE*, Vol. 77, No.5, pp. 722-734, May 1989.
 58. Te-Kao Wu, “Radar cross section of arbitrarily shaped bodies of revolution”, *Proc. of IEEE*, Vol. 77, No.5, pp. 735-740, May 1989.
 59. Louis N. Medgyesi-Mitschang and Dav-sing Wang, “Hybrid methods for analysis of complex scatterers”, *Proc. of IEEE*, Vol. 77, No.5, pp. 770-779, May 1989.
 60. Tapan K. Sarkar and Ercument Arvas, “Scattering cross section of composite conducting and lossy dielectric bodies”, *Proc. of IEEE*, Vol. 77, No.5, pp. 788-795, May 1989.
 61. Timothy Griesser, Constantine A. Balanis and Kefeng Liu, “RCS analysis and reduction for lossy dihedral comer reflectors”, *Proc. of IEEE*, Vol. 77, No.5, pp. 806-814, May 1989.
 62. Egon Marx, “Scattering by an arbitrary cylinder at a plane interface:

- Broadside incidence”, *IEEE Trans. Antennas prop.*, Vol. AP-37, No.5, pp. 619-628, May 1989.
63. Prabhakar H.Pathak and Robert J.Burkholder, “Modal, Ray and Beam techniques for analysing the EM scattering by open-ended waveguide cavities”, *IEEE Trans. Antennas prop.*, Vol. AP-37, No.5, pp. 635-647, May 1989.
64. Asoke K. Bhattacharyya, “Electromagnetic scattering from a flat plate with rim loading RAM saving”, *IEEE Trans. Antennas prop.* Vol. AP-37, No.5, pp 659-663, I May 1989.
65. Robert P. Penno, Cary A. Thiele and Krishna M. Pasala, “Scattering from a perfectly conducting cube”, *Proc. of IEEE*, Vol. 77, No.5, pp. 815-823, May 1989.
66. Thomas E. Tice, “An overview of radar cross section measurement techniques”, *IEEE Trans. Instrum & meas.*, Vol. 39, No.1, pp. 205-207, Feb 1990.
67. Jaehoon Choi, Nan Wang, Leon Peters Jr. and P-Levy, “Near axial backscattering from finite cones”, *IEEE Trans. Antennas prop.*, Vol. AP-38, No.8, pp. 1264-1272 Aug. 1990.
68. C. Y. Shen, “Application of DFT method to non-orthogonal dihedral reflectors”, *IEEE Trans. Antennas prop.*, Vol. AP-38, No.12, pp. 1913-1919, Dec. 1990.
69. Tai-Mo Wang, Alfonso Cuevas and Hao Ling, “RCS of a partially open rectangular box in the resonant region”, *IEEE Trans. Antennas prop.*, Vol. AP-38, No.9, pp. 1498-1504, Sept. 1990.
70. Dennis J. Blejer. “Physical optics polarisation scattering matrix for a Top Hat reflector”, *IEEE Trans. Antennas prop.*, Vol. AP-39, No.6,

pp. 857-858, June 1991.

71. P.M. Goggans and T .H. Shumpert, "Backscatter RCS for TE and TM excitations of dielectric filled cavity backed apertures in two dimensional bodies", *IEEE Trans. Antennas prop.*, Vol. AP-39, No.8, pp. 1224-1227, Aug 1991.
72. John Baldauf, Shung Wu-Lee, Luke Lin, Shyk-Kaang Jang and Steven McScarborough, "High frequency scattering from Trihedral comer reflectors and other benchmark targets: SBR versus experiment", *IEEE Trans. Antennas prop.*, Vol. AP-39, No.9, pp. 1345-1351, Sept. 1991.
73. R.K. Mongia, C.L.Larose, S.R. Mishra and P. Bhartia, "Measurement of RCS of cylindrical and rectangular dielectric resonators", *IEE Electron Lett.*, Vol. 28, No. 21, pp1953-1955, oct 1992.
74. T .L. Yang and S.S. Bor, "Monostatic radar cross section spectra of a rotating fan array with tilted plate metal blades, in the PQ/PTD approximation" *IEE proc.H*, Vol. 139, No.6, pp. 495-499, Dec. 1992.
75. C.W. Trueman, S.R. Mishra, S.J. Kubina and C.L Larose, "RCS of resonant scatterers with attached wires" *IEEE Trans. Antennas prop.*, Vol. AP-41, No.3, pp. 351-354, March 1993.
76. S.R. Mishra, C.L. Larose and C.W. Trueman, "Precision radar cross section measurements for computer code validation", *IEEE Trans. Instrum. meas.*, Vol. 42, No.2, pp. 179-185, April 1993.
77. Juan M. Rius, Miguel Ferrando and Luis Jofre, "High frequency RCS of complex radar targets in real time", *IEEE Trans. Antennas*

- prop.*, Vol. AP-41, No.9, pp. 1038-1019, Sept. 1993.
78. Hung-Yu Yang, Jesse A. Castaneda and N.G. Alexopoulos, "The RCS of a microstrip patch on an arbitrarily biased ferrite substrate", *IEEE Trans. Antennas prop.*, Vol. AP-41, No. 21, pp. 1610-1614, Dec. 1993.
79. Craig R. Birtcher, Constantine A. Balanis and V.J. Vokurka, "RCS measurements, Transformations and comparisons under cylindrical and plane wave illumination", *IEEE Trans. Antennas prop.*, Vol. AP-42, No.3, pp. 329-334, March 1994.
80. G.G. Cook and S.K. Khamas, "Control of radar cross sections of electrically small high temperature super conducting antenna elements using a magnetic field", *IEEE Trans. Antennas prop.*, Vol. AP-42, No.6, pp. 888-890, June 1994.
81. Mohsine Khaliadi, Juan A. Morente and Jorge A. Forti, "RCS of arbitrarily shaped targets with TLM method", *IEEE Trans. Antennas prop.*, Vol. AP-42, No.6, pp. 891-893, June 1994.
82. W.E. Groves, "Transmission of electromagnetic waves through pairs of parallel wire grids", *Jour. Appl. Phys.*, Vol. 24, No.7, pp. 845-854, July 1953.
83. James R. Wait, "Reflection from a wire grid parallel to a conducting plane", *Canad Jour. Phys.*, Vol. 32, pp. 571-579, 1954.
84. Robin I. Primich, "some electromagnetic transmission and reflection properties of a strip grating" *IRE Trans. Antennas prop.*, Vol. AP-5, pp. 176-182, April 1957.
85. M. Takada and M. Shinji, "An application of the diffraction grating to the 11 GHz microwave systems," *IEEE Trans. Antennas prop.*,

Vol. AP-13, No.4, pp. 532-541, July 1965.

86. Rubens A. Sigelmann, "Surface waves on a grounded dielectric slab covered by a periodically slotted conducting plane", *IEEE Trans. Antennas prop.*, Vol. AP-15 No.5, pp. 672-676, Sept. 1967.
87. Johannes Jacobson, "Analytical, numerical and experimental investigation of guided waves on periodically strip loaded dielectric slabs", *IEEE Trans. Antennas prop.*, Vol. AP-18, No.8, pp. 379-388, May 1970.
88. Robert B. Green, "Diffraction efficiencies for infinite perfectly conducting gratings of arbitrary profile", *IEEE Trans. Microwave Theory & Tech.*, Vol. MTT-18, No. 6, pp. 313-318, June 1970.
89. Shung-Wu Lee, "Scattering by dielectric loaded screen", *IEEE Trans. Antennas prop.*, Vol. AP-19, No.6, pp. 656-665, Sept. 1971.
90. J. P. Montgomery, "Scattering by an infinite periodic array of thin conductors on a dielectric sheet" *IEEE Trans. Antennas prop.*, Vol. AP-23, No.1, pp. 70-75, Jan. 1975.
91. J. P. Montgomery, "Scattering by an infinite periodic array of microstrip elements", *IEEE Trans. Antennas prop.*, Vol. AP-26, No.6, pp. 850-853, Nov. 1978.
92. J.P. Montgomery, "Scattering by an infinite parallel array of multiple parallel strips", *IEEE Trans. Antennas prop.*, Vol. AP-27, No.6, pp. 798-807, Nov. 1979.
93. K.C. Chang, K.T. Tam and T. Tamir, "Simplified approach to surface wave scattering by blazed dielectric gratings", *Appl. Opt.*, Vol. 19, pp. 282-288, 1980.
94. A. Gruss, K. T. Tam, and T. Tamir, "Blazed dielectric gratings with

- high beam coupling efficiencies”, *Appl. Phys. Lett.*, Vol. 36, No.7, pp. 523- 525, April 1980.
95. K.C. Chang, V. Shah and T. Tamir, “Scattering and guiding of waves by dielectric gratings with arbitrary profile”, *J. Opt. Soc. Am.*, Vol. 70, No.7, pp. 804-813, July 1980.
96. R. Petit, “Electromagnetic theory of gratings”, Springer Verlag, New York, 1980.
97. Hassan A. Kalhor and Mohammad Ilyas, “Scattering of plane electromagnetic waves by a grating of conducting cylinders embedded in a dielectric slab over a ground plane”, *IEEE Trans. Antennas prop.*, Vol. AP-30, No.4, pp. 576-579, July 1982.
98. M.J. Archer, “Periodic multielement strip gratings”, *IEE Electron Lett.*, Vol. 18, No. 22, pp. 958-959, Oct. 1982.
99. Xu-Jeandong and Chen Guorui, “Microwave characteristics and applications of a planar metallic grating systems”, *J. China Inst. Comm.*, Vol. 5. pp. 83-87, April 1984.
100. K. Kobayashi, “Diffraction of a plane wave by a thick strip grating” *Proc. of IEEE AP-S Int. Symp.*, Canada, pp. 553-556, 1985.
101. K. Kobayashi, “Diffraction of a plane electromagnetic wave by a parallel plate grating with dielectric loading: The case of transverse incidence”, *Canad. Jour. Phys.*, Vol. 63, No.4, pp. 453-465, 1985.
102. K. Kobayashi, “Diffraction of Electromagnetic waves by a parallel plate grating with dielectric loading”, *The 1000th anniversary Bulletin of Chuo University*, pp. 473-524, 1985.
103. K.A. Jose and K.G. Nair, “Reflector backed perfectly blazed strip

- gratings simulate corrugated reflector effects”, *IEE Electron Lett.*, Vol. 23, No.2, pp. 86-87, Jan 1987.
104. Te-Kao Wu, “Fast convergent integral equation of strip gratings on dielectric substrate”, *IEEE Trans. Antennas prop.*, Vol AP-35, No.2, pp. 205-207, Feb,1987.
105. K.A. Jose, C. K. Aanandan and K.G. Nair, “Low backscattered TM- polarised strip gratings”, *IEE Electronic Lett.*, Vol. 23, No. 17, pp. 905- 906, Aug. 1987.
106. Hassan A. Kalhor, “Electromagnetic scattering by a dielectric slab loaded with a periodic array of strips over a ground plane”, *IEEE Trans. Antennas prop.*, Vol. 36, No.1, pp. 147-151, Jan. 1988.
107. P .S. Kildal, “Definition of artificially soft and hard surfaces for electromagnetic waves”, *IEE Electronic Lett.*, Vol. 24, No.3, pp. 168-170, Feb. 1988.
108. Hassan A. Kalhor, “Plane metallic gratings of finite number of strips”, *IEEE Trans. Antennas prop.*, Vol. 37, No.3, pp. 406-407, March 1989.
109. T .H. Wu and K.S. Chen, “Analysis of scattering and guidance of a two dimensionally periodic metal grating structure by spectral domain method”, *Int. Jour. of Infrared and millimeter waves*, Vol. II, No.3, pp. 451-461, 1990.
110. Jian-Ming Jin and John Volakis. “Electromagnetic scattering by a perfectly conducting patch array on a dielectric slab”, *IEEE Trans. Antennas prop.*, Vol. AP-38, No. 38, pp. 556-563, April 1990.
111. S. Sohail H. Naqvi and N.C. Gallagher, “A general solution to the scattering of electromagnetic waves from a strip grating”, *Jour. of*

- Modern optics*, Vol. 37, No10, pp, 1629-1643, 1990.
112. John Andes Aas, "Plane wave reflection properties of two artificially Hard surfaces", *IEEE Trans. Antennas prop.* Vol. AP-39, No.5, pp. 651- 656, May 1991.
 113. Stephen D. Gedney and Raj Mittra, "Analysis of the electromagnetic scattering by thick gratings using a combined FEM/MM solution", *IEEE Trans. Antennas prop.*, Vol. AP-39, No. 11, pp. 1605-1614, Nov. 1991.
 114. V.G. Borkar, V.M. Pandharipande and E. Ethiraj, "Millimeter wave twist reflector design aspects", *IEEE trans. Antennas prop.*, Vol. AP-40, No. 11, Nov 1992.
 115. B. Gimeno, J.L. Cruz, E.A. Navarro and V. Sueh, "A polariser rotator system for three dimensional oblique incidence", *IEEE Trans. Antennas prop.*, Vol. AP-42, No. 7, pp. 912-914, July 1994.
 116. K.A. Jose, P. Mohanan, and K.G. Nair, "Reduction of radar cross section of metallic cylinders", *IEEE AP-S Int. Symp. Digest* 1990, pp. 1284-1287, 1990.
 117. V. Ajaikumar, K.A. Jose, C. K. Aanandan, P. Mohanan and K.G. Nair, "Backscattering reduction corner reflectors using SCS technique", *Microwave & Opt. Tech. Lett.*, Vol. 5, No. 11, pp. 557-559, Oct.1992.
 118. W. Hong and Z. Zhu, "Radar cross section of dielectric coated conducting cylinder loaded with periodic metallic strips using mixed SDM, CGM, FFT : TE incidence", *IEE proc. H*, Vol. 140, No.5, pp. 373-376, Oct. 1993.
 119. R. E. Kell and N. E. Pedersen, "Comparison of experimental radar

- cross section measurements”, *Proc. of IEEE*, Vol. 53, Aug. 1965, pp. 1092-103.
120. E. F. Knott, “Radar Cross Section reduction using cylindrical segments”, *IEEE Trans. Antennas & Prop.*, Vol. 24, No. 6, Nov, 1976, pp. 882-884.
121. Gordon R. Ebbeson, “TM polarized electromagnetic scattering from fin-corrugated periodic surfaces”, *J. of Opt. Soc. Am.*, Vol. 66, No.12, Dec. 1976, pp. 1363-1367.
122. John F. Hunka, Robert E. Stovall and D. J. Angelakos, “A technique for the rapid measurement of bistatic radar cross section”, *IEEE Trans. Antennas & Propagat.*, Vol. 25, No. 2, march 1977, pp. 243-248.
123. E.V. Jull and G.R. Ebbesson, “The reduction of interference from large reflecting surfaces”, *IEEE trans. Antennas & Propagat.*, Vol. 67, No. 6, march 1977, pp. 565-570.
124. E.V. Jull, J.W. heath and G.R. Ebbesson, “Gratings that diffract all incident energy”, *J. of Opt. Soc. Am.*, Vol.67, No.4, April 1977, pp. 557-560.
125. J.W. Heath and E.V. Jull, “Total backscatter from conducting rectangular corrugations”, *IEEE trans. Antennas & Propagat.*, Vol. 27, No. 1, march 1977, pp. 95-97.
126. L. Cai, E.V. Jull and R. Deleui, “Scattering by pyramidal reflection grating”, *Proc. of IEEE Ap-S Int. Symp.*, 1984, pp. 45-47.
127. E.V. Jull, D.C.W. Hui and P. Facq, “Scattering by dual blazed corrugated conducting strips and small reflection gratings”, *J. of Opt. Soc.Am.*, Vol.2, July 1985, pp. 205-207.

128. Robert B. Dybdal, "Radar cross section measurements", *Proc. IEEE*, April 1987, pp. 498-516.
129. T. Mathew, D.S. Stephen, C.K. Aanandan, P. Mohanan and K.G. Nair, "Wideband trapezoidal strip grating for elimination of specular reflection", *IEE Electron. Lett.*, Vol. 30, pp.1037-1039. June 1994.
130. D.S. Stephen, T. Mathew, P. Mohanan and K.G. Nair, "A modified strip grating with dual periodicity for RCS reduction", *Microwave Opt. Technol Lett.* Vol. 7, No.7, pp. 315 – 317, May. 1994.
131. D.S. Stephen, T. Mathew, K. A. Jose, C. K. Aanandan, P. Mohanan and K.G. Nair, "New simulated corrugated scattering surface giving wideband characteristics", *IEE Electron. Lett.*, Vol. 29, No. 4, pp. 329- 331. Feb 1993.
132. T. Mathew, D.S. Stephen, K. A. Jose, C. K. Aanandan, P. Mohanan and K.G. Nair, "The performance of a novel simulated corrugated surface for reduction of radar cross section", *Microwave Opt. Technol Lett.* Vol. 6, No.10, pp. 615 – 617, Aug. 1993.
133. Kathleen L. Virga, and Yaliya Rahmat-Samii, "RCS Characterization of a Finite Ground Plane with Perforated Apertures: Simulations and Measurements", *IEEE Trans Antennas Prop.*, Vol. 42, No. 11, pp. 1491 - 1501, Nov 1994.
134. D.S. Stephen, T. Mathew, C. K. Aanandan, P. Mohanan, K. A. Jose, and K.G. Nair, "Analysis of a dual periodic strip grating", *Microwave Opt. Technol Lett.* Vol. 13, No.3, pp. 173 – 175, Oct. 1996.
135. J. D. Silverstein and R. Bender, "Measurements and Predictions of

- the RCS of Bruderhedrals at Millimeter Wavelengths”, *IEEE Trans Antennas Propag.*, Vol. 45, No. 7, pp. 1071 - 1079, July 1997.
136. J. A. Porti, J. A. Morente, H. Mag’an, and D. P. Ruiz, “RCS of Low Observable Targets with the TLM Method”, *IEEE Trans Antennas Propagat* , Vol. 46, No. 5, pp. 741 - 743, May 1998.
137. S. Y. Wang and S. K. Jeng, “A compact RCS formula for a dihedral corner reflector at arbitrary aspect angles”, *IEEE Trans Antennas Propagat* , Vol. 46, No. 7, pp. 1112 - 1113, July 1998.
138. M. O. White, “Radar cross-section: measurement, prediction and control”, *Electronics & Communication Engineering Journal*, pp. 169 – 180, August 1998.
139. H. Mosallaei and Y. Rahmat-Samii, “RCS Reduction in Planar, Cylindrical, and Spherical Structures by Composite Coatings using Genetic Algorithms”, *IEEE Int. Symposium on Antennas and Propagation*, Vol. 1, pp 438 – 441, July 1999.
140. Y.T.Chan, K.C.Ho and S.K.Wong, “Aircraft identification from RCS measurement using an orthogonal transform”, *IEE Proc. Radar, Sonar Navig.* Vol. 147, No. 2, pp. 93 – 102, April 2000.
141. F.C. Smith, “Measurement of diffraction radar crosssection (RCS)”, *IEE Electron. Lett.*, Vol. 36, No. 9, pp. 830- 831. April 2000.
142. P. Corona, F. D. Agostino, G. Riccio and G. Toso, “Scattering from dihedral corner reflectors with sinusoidally deformed faces”, *Microwave Opt. Technol Lett.* Vol. 25, No.4, pp. 246 – 251, May. 2000.
143. F. L. Penaranda-Foix and M. Ferrando-Bataller, “Inhomogeneous

- corrugations to improve RCS measurements”, *IEE Electron. Lett.*, Vol. 38, No. 15, pp. 769 – 771, July 2002.
144. V. Losada, R. R. Boix, and F. Medina, “Radar Cross Section of Stacked Circular Microstrip Patches on Anisotropic and Chiral Substrates”, *IEEE Trans Antennas Propagat* , Vol. 51, No. 5, pp. 1136 - 1139, May 2003.
145. Richard Norland, “Multipath of Flat Plate Radar Cross Section Measurements”, *Proceedings of Int. Radar conference 2003*, pp. 152 – 155, Sept. 2003.
146. N. Misran, R. Cahill and V.F. Fusco, “RCS reduction technique for reflectarray antennas”, *IEE Electron. Lett.*, Vol. 39, No. 23, pp. 1630-1632, Nov 2003.
147. Andriy E. Serebryannikov and Alexander I. Nosich, “TE-Case RCS Analysis of Finite-Thickness Slotted Circular Cylinder Loaded With Lossy Filling”, *IEEE Trans Antennas Propagat.*, Vol. 53, No. 4, pp. 1426 - 1434, April 2005.
148. G. G. Peixoto, A. L. de Paula, L. A. Andrade, C. M. A. Lopes and M. C. Rezende, “Radar Cross Section Reduction of Dihedral Corners”, *Proceeding of the 2005 SBMO/IEEE MTT-S Int. Conf. on Microwave and Optoelectronics*, pp. 460-463, July 2005.
149. D.L. Jaggard, “On fractal electrodynamics”, Recent advances in Electromagnetic theory, H.N. Kritikos and D.L. Jaggard (Editors.), Springer-Verlag, New York, 1990, 183 – 224.
150. Benoit. B. Mandelbrot, “The fractal geometry of nature,” W.H. Freeman and company, New York, 1977.

151. D. H. Werner and R. Mittra, "Frontiers in Electromagnetics", Wiley - IEEE press, 1999.
152. J. Romeu and Y. Rahmat-Samii, "Fractal FSS: A novel Dual-band Frequency Selective Surfaces," *IEEE Trans Antennas Propagat.*, Vol. 48, No. 7, pp. 1097-1104, July 2000.
153. C. Peunte, J. Romeu, R. Pous, and A. Cardama, "On the behaviour of the Sierpinski multiband antenna", *IEEE Trans Antennas Propagat.*, Vol. 46, pp. 517-524, April 1998.
154. D. H. Werner, R. L. Haupt and P. L. Werner, "Fractal Antenna Engineering: The Theory and Design of Fractal Antenna Arrays", *IEEE Antennas Propagat Mag*, Vol. 41, No. 5, (1999), 37 - 59.
155. C. T. P. Song, P. S. Hall, H. Ghafouri-Shiraz and D. Wave, "Fractal stacked monopole with very wide bandwidth", *IEE Electron. Lett.*, Vol. 35, No. 12, pp. 945 - 946. June 1999.
156. G. J. Walker and J. R. James, "Fractal Volume Antennas", *IEE Electron. Lett.*, Vol. 34, No. 16, pp. 1536 - 1537. August 1998.
157. Z. Du, K. Gong, J. S. Fu and B. Gao, "Analysis of microstrip fractal patch antenna for multi-band", *IEE Electron. Lett.*, Vol. 37, No. 13, pp. 805 - 806 June 2001.
158. D. H. Werner and D. Lee, "Design of dual-polarised multiband frequency selective surfaces using fractal elements", *IEE Electron. Lett.*, Vol. 36, No. 6, pp. 487 - 488 March 2000.
159. D. H. Werner and P. L. Werner, "On the Synthesis of Fractal Radiation Pattern", *Radio Science*, Vol. No. 30, No. 1, pp. 29-45, Jan-Feb 1995.
160. D. L. Jaggard and A. D. Jaggard, "Cantor Ring Arrays",

- Microwave Opt. Technol Lett.* Vol. 19, No.2, pp. 121 – 125, Oct. 1998.
161. Y. Kim and D. L. Jaggard, “The Fractal Random Array”, *Proceedings of IEEE*, Vol. 74, No. 9, pp. 1278-1280, Sept. 1986.
162. A. Lakhtakia, N.S. Holter, V.K. Varadan and V.V. Varadan, “Self similarity in diffraction by a self similar fractal screen,” *IEEE Trans Antennas Propagat*, Vol. AP-35, (1987), 236 - 239.
163. C. Peunte-Baliarda and R. Pous, “Fractal Design of Multiband and Low Side-Lobe Arrays”, *IEEE Trans Antennas Propagat* , Vol. 44, No. 5, pp. 730 -739, May 1996.
164. X. Sun and D.L. Jaggard, “Wave interactions with generalized cantor bar fractal multilayers,” *J. Appl. Phys.* 70 (1991), 2500 - 2507.
165. D. H. Werner, K. C. Anushko and P. L. Werner, “*Microwave Opt. Technol Lett.* Vol. 22, No.1, pp. 54 – 57, July. 1999.
166. M. Lehman and M. Garavaglia, “Beam reflection from multilayers with periodic and fractal distributions”, *Journ. of modern Optics*, Vol. 46, No. 11, pp. 1579 – 1593, 1999.
167. D. L. Jaggard and Y. Kim, “Diffraction by band limited fractal screens”, *Opt. Soc. Am. A*, Vol. 6, (1987), 1055-1062.
168. D. L. Jaggard and X. Sun, “Fractal Surface Scattering: A generalized Rayleigh Solution”, *J. Appl. Phys.*, Vol. 68, No. 11, Dec 1990.
169. E. Jakeman, “Scattering by a corrugated random surface with fractal slopes”, *J. Phys. A. Math Gen.*, Vol. 15, pp. L55-L59, 1982.

170. Y. -W. Wu and B. Hu, "Phase transitions on complex Sierpinski carpets", *Phy. Rev. A*, Vol. 35, No. 3, pp. 1404 – 1411, Feb 1987.
171. A. D. Jaggard and D. L. Jaggard, "Scattering from fractal superlattices with variable lacunarity", *J. Opt. Soc. Am. A*, Vol. 15, No. 6, pp 1626 – 1635, June 1998.
172. D. L. Jaggard and X. Sun, "Reflection from fractal multilayers", *Optics Lett.* Vol. 15, No. 24, Dec. 1990, pp 1428 – 1430.
173. E. Troncet, G. Ablart and L. Allam, "Microwave characterization and modeling of the surface impedance of fractal structure copper films", *IEEE Trans Antennas Propagat* , Vol. 46, No. 3, pp. 434 - 441, March 1998.
174. C. Puente Baliarda, C. Borja Borau, M. Navarro Rodero and J. Romeu Robert, "An iterative model for fractal Antennas: Application to the Sierpinski Gasket Antenna", *IEEE Trans Antennas Propagat.*, Vol. 48, No. 5, pp. 713 - 719, May 2000.
175. D. H. Werner and S. Ganguly, "An overview of fractal antenna engineering research", *IEEE Antennas Propagat. Mag.*, Vol. 45, No. 1, pp. 38 -57, Feb. 2003.
176. J. P. Gianvittorio, J. Romeu, S. Blanch and Y. Rahmat-Samii, "Self-Similar Prefractal Frequency Selective Surfaces for Multiband and Dual-Polarised Applications", *IEEE Trans Antennas Propagat.*, Vol. 51, No. 11, pp. 3088 - 3096, Nov. 2003.
177. F. Chiadini, V. Fiumara, I. M. Pinto and A. Scaglione, "Self-Scaling properties of the reflection coefficient of cantor prefactal multilayers", *Microwave Opt. Technol Lett.* Vol. 37, No.5, pp. 339 – 343, June 2003.

178. L. Zhou, W. Wen, C. T. Chan and P. Sheng, "Reflectivity of planar metallic fractal patterns", *Applied Phy. Lett.* Vol. 82, No. 7, Feb. 2003.
179. C. T. P. Song, P. S. Hall and H. G. Ghafouri-Shiraz, "Multiband Multiple Ring Monopole Antennas, "*IEEE Trans Antennas Propagat* , Vol. 51, No. 4, pp. 722 - 729, May 2000.
180. D. H. Werner, M. A. Gingrich and P. L. Werner, "A self similar fractal radiation pattern synthesis technique for reconfigurable multiband arrays", *IEEE Trans Antennas Propagat* , Vol. 51, No. 7, pp. 1486 - 1498, July. 2003.
181. D. H. Werner, D. Baldacci and P. L. Werner, "An efficient Recursive procedure for evaluating the impedance matrix of linear and planar fractal arrays", *IEEE Trans Antennas Propagat* , Vol. 52, No. 2, pp. 380 - 387, Feb. 2004.

INDEX

A

Aanandan · 207, 229, 230, 232
 Active cancellation · 5, 7, 81
 Ajaikumar · 42, 230
 Anderson · 31, 223
 Anechoic · 58, 59, 61, 62, 63, 76
 Aspect angle · 3, 30, 220
 Automation · 19, 209
 Azimuth · 61, 88, 124

B

Backscattering reduction · 65, 88, 98,
 112, 119, 152, 169, 191, 195
 Balanis · 28, 32, 221, 223, 226
 Bhattacharyya · 30, 32, 222, 224
 Bistatic · 18, 31, 34, 43, 58, 59, 62,
 209, 223, 231
 Blore · 25, 218

C

Circle · 98, 170
 Cone · 17, 18, 25, 65, 75, 77, 78, 79,
 81, 163, 165, 189, 194, 195, 196,
 218
 Corner angle · 28, 76, 134, 138, 139,
 148, 162, 180, 184, 194
 Corner reflector · 17, 18, 24, 29, 30,
 42, 46, 65, 76, 79, 81, 134, 138,
 148, 149, 152, 162, 180, 184, 189,
 194, 195, 218, 233
 Corona · 28, 30, 46, 221, 222, 233
 Cross · 2, 3, 7, 23, 24, 25, 26, 27, 28,
 32, 43, 44, 45, 46, 47, 76, 115, 179,
 180, 192, 217, 218, 219, 220, 221,
 222, 223, 224, 225, 226, 230, 231,
 232, 233
 Crossed bar fractal · 108
 CW · 26, 43, 57, 219, 222

Cylinder · 17, 18, 24, 29, 32, 33, 35,
 42, 53, 75, 76, 79, 125, 129, 189,
 193, 196, 222, 223, 230

D

Dimension · 11, 12, 13, 25, 33, 47, 49,
 51, 65, 66, 67, 70, 71, 74, 76, 77,
 83, 120, 191, 193, 194, 200
 Dybdal · 30, 222, 231

E

Electrodynamics · 18, 21, 48, 234
 Electromagnetics · 15, 48, 199
 Elevation angle · 45

F

Flat plate · 17, 18, 47, 53, 65, 67, 79,
 83, 189, 191, 220, 224
 Fractal · 7, 8, 9, 11, 12, 13, 14, 17, 18,
 19, 21, 48, 49, 50, 51, 52, 64, 65,
 66, 67, 68, 69, 70, 71, 75, 76, 79,
 81, 82, 83, 84, 89, 91, 95, 105, 108,
 110, 115, 116, 118, 120, 125, 148,
 162, 163, 169, 179, 180, 181, 189,
 191, 192, 193, 194, 195, 196, 197,
 199, 200, 205, 207, 234, 235, 236,
 237, 238
 Frequency selective · 15, 48, 49, 52,
 64, 207, 235

G

Geometric theory of diffraction · 27

H

Harrington · 27, 221
 Harrison · 25, 218
 Heinz · 25, 218

Hexagon · 93, 170, 192
 Huang · 29, 206, 222

I

Ilyas · 38, 228

J

Jacobson · 37
 Jaggard · 48, 49, 50, 51, 234, 235,
 236, 237
 Jose · 39, 42, 228, 229, 230, 232

K

Kalhor · 38, 39, 40, 228, 229
 Kildal · 40, 229
 Knot · 28, 43, 215
 Kobayashi · 39, 228
 Kouyoumijian · 25, 219

L

Lacunarity · 12, 49, 51, 65, 71, 82,
 120, 193, 237
 Le Vine · 29
 Leipa · 26
 Lin · 27, 220, 221, 225

M

Mandelbrot · 7, 11, 12, 48, 199, 207,
 234
 Mathew · 45, 207, 232
 Mautz · 27, 221
 Microstrip · 23, 36, 38, 47, 49, 199,
 217, 226, 227
 Miller · 26, 27, 220
 Mittra · 27, 41, 48, 220, 230, 234
 Mode matching technique · 24, 40, 45
 Mohanan · 207, 230, 232
 Moment method · 24, 27, 36

N

Nair · 39, 228, 229, 230, 232
 NETWORK ANALYSER · 60

O

Octagon · 91, 170
 Optical region · 4, 65

P

Passive cancellation · 5, 6, 81
 Pathak · 32, 224
 Petits · 25
 Physical optics · 25, 26, 27, 28, 30, 31,
 33, 34, 35
 Puente · 48, 51, 237
 Purina · 103, 170, 179

R

Radar · 1, 2, 3, 5, 6, 7, 14, 15, 23, 24,
 25, 26, 28, 30, 33, 35, 44, 45, 46,
 47, 57, 58, 65, 76, 81, 218, 219,
 220, 222, 223, 224, 225, 226, 230,
 231, 232, 233
 RADAR CROSS SECTION · 2, 23
 Rahmat Samii · 27
 Rayleigh region · 4
 RCS enhancement · 184, 194, 195
 RCS REDUCTION · 5, 125
 Resonance region · 4
 Ruck · 217

S

Sarkar · 28, 32, 221, 222, 223
 Scattered field · 35
 Self similarity · 9, 17, 48, 199
 Senior · 25, 26, 219
 Shumpert · 29, 34, 221, 225
 Sierpinski carpet · 9, 10, 48, 49, 65,
 66, 67, 68, 69, 71, 75, 76, 78, 82,

83, 84, 89, 98, 103, 105, 108, 110,
116, 120, 134, 163, 169, 170, 171,
179, 181, 186, 191, 192, 193, 194,
195, 196
Sierpinski gasket · 9, 49, 52, 65, 66,
70, 82, 112, 118, 170, 186, 192,
196
Simulated Corrugated Surface · 16
Skolnik · 217
Space filling · 17, 52, 199
Specular reflection · 16, 39, 44, 45,
232
Square · 3, 10, 12, 44, 48, 49, 70, 71,
76, 78, 103, 169, 170, 179, 192
Stephen · 45, 230, 232
Strip grating · 16, 37, 38, 39, 41, 42,
45, 52, 226, 228, 229, 232
Sun · 50, 51, 236, 237

T

Tandon · 30, 222
TARGET POSITIONER · 61

V

Volakis · 29, 40, 221, 229

W

Weir · 220

Y

Yang · 34, 36, 225, 226
Yousef · 31

List of publications of the author

International Journal

1. **A. R. Chandran**, M. Gopikrishna, C.K. Aanandan, P. Mohanan and K.Vasudevan, "Radar Cross Section enhancement of dihedral corner reflector using fractal based metallo-dielectric structures" **IEE Electronics Letters.**, Vol. 42. No.2. September 28, 2006. pp. 1135-1136.
2. **A. R. Chandran**, T. Mathew, C.K. Aanandan, P. Mohanan and K.Vasudevan, "Frequency tunable metallo-dielectric structure for backscattering reduction" **IEE Electronics Letters.**, Vol. 40. No.20. September 30, 2004.pp. 1245-1246.
3. **A. R. Chandran**, T. Mathew, C. K. Aanandan, P. Mohanan and K. Vasudevan, "Low Backscattered Dual-Polarised Metallo-Dielectric Structure Based on Sierpinski Carpet", **Microwave and Optical Technology Letters.**, Vol. 40. No.3. February 2004, pp. 246 - 248.
4. **A. R. Chandran**, M. Gopikrishna, C.K. Aanandan, P. Mohanan and K.Vasudevan, "Scattering behaviour of fractal based metallo-dielectric structures" **Progress in Electromagnetic Research, PIER 69**, 2007, pp. 323 - 339.
5. M. Gopikrishna, D. D. Krishna, **A. R. Chandran** and C. K. Aanandan, "Band notched planar square monopole Antenna for UWB systems" **Journal of Electromagnetic waves and applications (JEMWA)**, Vol 21, No. 11, 2007, 1525 - 1537.

International Conference

1. **A. R. Chandran**, T. Mathew, C. K. Aanandan, P. Mohanan and K. Vasudevan, "Low Backscattered Dual polarized Metallo-Dielectric Structure Based on Fractal Geometry", **IEEE APS 2003** Int Symp USNC/CNC/URSI, North Amer. Radio Sci. Mtg, Columbus, OH, **USA**. Vol.4, June 2003, pp. 315 - 318.
2. **A. R. Chandran**, Thomaskutty Mathew, C. K. Aanandan, P. Mohanan and K. Vasudevan, "Backscattering Reduction Using Fractal Based Metallo-

- Dielectric Structure*", **Proc. PIERS 2003**, Honolulu, Hawaii, **USA**, Oct 2003, Pp. 663.
3. Shynu S.V, Rohith K. Raj, **A. R. Chandran**, C. K. Aanandan, P. Mohanan and K. Vasudevan, "*Single-Feed Dual-Frequency Dual Polarized Microstrip Antenna with Hexagonal Slot*", **IEEE APS 2004** Int. Symp USNC/CNC/URSI, Monterey, California, **USA**, June 2004, pp. 4380-4383.
 4. **Anupam R. Chandran**, Thomaskutty. Mathew, Sona O. Kundukulam, C. K. Aanandan, P. Mohanan and K. Vasudevan, "*Multi-band Characteristic of a Fractal Based Metallo-dielectric Structure for Backscattering reduction*," **Proc. of Asia Pacific Microwave Conference (APMC-04)** Int. Symp. New Delhi, **INDIA**. 15-18 December, 2004. pp. 580-581(APMC/04/C/66).
 5. **A. R. Chandran**, Thomaskutty. Mathew, C. K. Aanandan, P. Mohanan and K. Vasudevan, "*Metallo-Dielectric Structures for backscattering reduction*", **IEEE APS 2005** Int Symp USNC/CNC/URSI, North Amer. Radio Sci. Mtg, Washington DC, **USA**, July 2005, pp. 7803-8883.
 6. **Anupam R. Chandran**, Thomaskutty. Mathew, C. K. Aanandan, P. Mohanan and K. Vasudevan, "Superstrate Loaded Metallo-Dielectric Structure Based On Fractal Geometry" **Proceeding on The 5th International Conference on ITS Telecommunications (itst 2005)**, , Brest, **FRANCE**, 27-29 June.
 - 7 **Anupam R. Chandran**, Gopikrishna M, C.K. Aanandan, P. Mohanan and K.Vasudevan , "Sierpinski gasket based fractal structure for Radar Cross Section reduction with frequency tunability" International Conference on Microwaves, Antennas, Propagation and Remote Sensing (**ICMARS-2006**) 20-22 December, Jodhpur, **India**.
 8. D. D. Krishna, **A. R. Chandran** and C. K. Aanandan, "A Compact Dual Frequency Antenna with Sierpinski Gasket Based Slots" **European Microwave conference 2007 (EURAD 07)** accepted.
 9. **A. R. Chandran**, M. Gopikrishna, C. K. Aanandan, P. Mohanan and K. Vasudevan, "*Filter design using Cantor bar based Metallo-dielectric Structure*," **Proc. of Asia Pacific Microwave Conference (APMC-07)** Int. Symp. **Thailand**, December 11-14, 2007 (communicated).

National Conference

1. **Anupam R. Chandran**, Thomaskutty Mathew, C. K. Aanandan, P. Mohanan and K. Vasudevan, "*Scattering Behaviour of Metallo-Dielectric Structure Based On Fractal Geometry*", **Proceedings of National Symposium on Antennas and Propagation (APSYM-2002)**, 9-11 December, Cochin, **India**, pp.148-151, 2002.
2. **Anupam R. Chandran**, Thomaskutty Mathew, C.K. Aanandan, P. Mohanan K.Vasudevan and K.G. Nair, " *On the effect of loading superstrate on a Metallo-Dielectric Structure based on Sierpinski Gasket*", **Proceedings of National Symposium on Antennas and Propagation (APSYM-2004)**, 21-23 December, Cochin, **India**, pp .94-97, 2004.
3. M. Gopikrishna, D. D. Krishna, **A. R. Chandran** and C. K. Aanandan, "*5 GHz WLAN band notched square monopole antenna for UWB systems*" **Proceedings of National Symposium on Antennas and Propagation (APSYM-2006)**, 14 - 16 December, Cochin, **India**, pp. 47-50, 2006.

Resume of the author

Anupam R. Chandran

Senior Research Fellow

Centre for Research in Electromagnetics and Antennas

Department of Electronics

Cochin University of Science and Technology

Kochi-22, Kerala, India

Tel: +91-484-2576418, Mob: +91-9447475614

Fax: +91-484-2575800

Email: anupamrc@gmail.com , anupamrc@yahoo.com

OBJECTIVE

To pursue research activities in the field of Radar Cross Section studies, frequency selective surfaces and microstrip antennas.

EDUCATION

M. Sc Applied Electronics (2001)

PSG College of Arts and Sciences

Bharathiar University

Coimbatore

Tamil Nadu

India

Class: First Class

B. Sc Applied Electronics (1998)

College of Applied Sciences

Mavelikkara

Kerala University

Kerala

India

Class: First Class

PROJECTS/TRAINING

1. Actively involved in development of an RCS measurement facility and its automation at Dept. of Electronics, Cochin University, Cochin, Kerala.
2. Successfully completed a project entitled "Development of Multi-functional single chip telephone" done at BPL Telecom Ltd. Palakkad, Kerala India.

3. Successfully completed a project entitled "Interfacing 12-bit Serial ADC with 16C84 PIC microcontroller" done at PSG College of Arts and Science, Coimbatore India.
4. Attended State level workshop on "Recent Trends in Biomedical Instrumentation" held at PSG College of Arts and Science, Coimbatore, India from March 27 to March 29, 2000.
6. Attended National conference on Antennas and Propagation (APSYM 2002 held at Cochin, India) and presented paper.
7. Attended National conference on Ocean Electronics (SYMPOL 2003 held at Cochin, India)
8. Attended National conference on Antennas and Propagation (APSYM 2004 held at Cochin, India) and presented paper.
9. Attended National conference on Ocean Electronics (SYMPOL 2005 held at Cochin, India)
10. Attended workshop on LabVIEW conducted by National Instruments at Sophisticated Test and Instrumentation Centre, Cochin University, Kochi, India.
11. Attended National conference on Antennas and Propagation (APSYM 2006 held at Cochin, India)

COMPUTER SKILLS

Languages

C++, FORTRAN

Assembly language programming 8085, 8051, PIC 16F84

Operating Systems

Windows 9x, Windows 2000, Windows XP, Macintosh.

RF Tools

Zealand IE3D, Ansoft HFSS, Ansoft Designer

Scientific Applications

Matlab, Mathematica, Sigma plot, LabVIEW 8

Computer Hardware

Certification in Diploma in Computer Hardware Engineering with 'A' grade from Drishna Technologies, Cochin, India.